



2

7th International Cryocooler Conference



Cryocoolers 7

17-19 November 1992
Santa Fe, New Mexico

Part 1 of 4

April 1993

Conference Proceeding

DTIC
ELECTE
AUG 09 1993
S A D

APPROVED FOR PUBLIC RELEASE; DISTRIBUTION IS UNLIMITED.

93-18217



PHILLIPS LABORATORY
Directorate of Space and Missiles Technology
AIR FORCE MATERIEL COMMAND
KIRTLAND AIR FORCE BASE, NM 87117-5776

This final report was prepared by the Phillips Laboratory, Kirtland Air Force Base, New Mexico, under Job Order 11050502. The Laboratory Project Officer-in-Charge was Marko M. Stoyanof (VTPT).

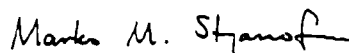
When Government drawings, specifications, or other data are used for any purpose other than in connection with a definitely Government-related procurement, the United States Government incurs no responsibility or any obligation whatsoever. The fact that the Government may have formulated or in any way supplied the said drawings, specifications, or other data, is not to be regarded by implication, or otherwise in any manner construed, as licensing the holder, or any other person or corporation; or as conveying any rights or permission to manufacture, use, or sell any patented invention that may in any way be related thereto.

This report has been authored by employees and contractors of the United States Government and Foreign Governments. Accordingly, the United States Government retains a nonexclusive royalty-free license to publish or reproduce the material contained herein, or allow others to do so, for the United States Government purposes.

This report has been reviewed by the Public Affairs Office and is releasable to the National Technical Information Service (NTIS). At NTIS, it will be available to the general public, including foreign nationals.

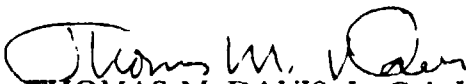
If your address has changed, or if your organization no longer employs the addressee, please notify PL/VTPT, Kirtland AFB, NM 87117-5776 to help maintain a current mailing list.

This conference proceeding has been reviewed and is approved for publication.


MARKO M. STOYANOF
Project Officer

FOR THE COMMANDER


ROBERT M. VACEK, GM-14, DAF
Chief, Thermal Management Br


THOMAS M. DAVIS, Lt Col, USAF
Acting Director of Space & Missile
Technology

DO NOT RETURN COPIES OF THIS REPORT UNLESS CONTRACTUAL
OBLIGATIONS OR NOTICE ON A SPECIFIC DOCUMENT REQUIRES THAT
IT BE RETURNED.

REPORT DOCUMENTATION PAGE			Form Approved OMB No. 0704-0188	
<small>Public reporting burden for this collection of information is estimated to average 1 hour per response, including the time for reviewing instructions, searching existing data sources, gathering and maintaining the data needed, and completing and reviewing the collection of information. Send comments regarding this burden estimate or any other aspect of this collection of information, including suggestions for reducing this burden, to Washington Headquarters Services, Directorate for Information Operations and Reports, 1215 Jefferson Davis Highway, Suite 1204, Arlington, VA 22202-4302, and to the Office of Management and Budget, Paperwork Reduction Project (0704-0188), Washington, DC 20503.</small>				
1. AGENCY USE ONLY (Leave blank)		2. REPORT DATE April 1993		3. REPORT TYPE AND DATES COVERED 17-19 Nov 92, Conference Proceeding
4. TITLE AND SUBTITLE 7th International Cryocooler Conference Part 1 of 4			5. FUNDING NUMBERS PE: 62601F PR: 1105 TA: 05 WU: 02	
6. AUTHOR(S) Several authors				
7. PERFORMING ORGANIZATION NAME(S) AND ADDRESS(ES) Phillips Laboratory Kirtland AFB, NM 87117-5776			8. PERFORMING ORGANIZATION REPORT NUMBER PL-CP--93-1001	
9. SPONSORING / MONITORING AGENCY NAME(S) AND ADDRESS(ES)			10. SPONSORING / MONITORING AGENCY REPORT NUMBER	
11. SUPPLEMENTARY NOTES Publication of this report does not constitute approval or disapproval of the ideas or findings. It is published in the interest of scientific and technical information exchange. The established procedures for editing reports were not followed for this report.				
12a. DISTRIBUTION / AVAILABILITY STATEMENT Approved for public release: distribution is unlimited.			12b. DISTRIBUTION CODE	
13. ABSTRACT (Maximum 200 words) The 7th International Cryocooler Conference was held in Santa Fe, New Mexico, on 17-19 November, 1992. Jiri L. Ludwigsen of Nichols Research was the conference chairperson; Capt William Wyche and Marko Stoyanof of Phillips Laboratory served as the program committee chairmen. The topics included Cryocooler Testing and Modeling, Space and Long Life Applications, Stirling Cryocoolers, Pulse Tube Refrigerators, Novel Concepts and Component Development, Low Temperature Regenerator Development, and J-T and Absorption Coolers.				
14. SUBJECT TERMS Absorption, Cryocoolers, Cryogenic, Low Temperature Heat Exchanger, Pulse Tube Refrigerators, Regenerative, Recuperative, Stirling, Thermal Modeling			15. NUMBER OF PAGES 320	
			16. PRICE CODE	
17. SECURITY CLASSIFICATION OF REPORT Unclassified	18. SECURITY CLASSIFICATION OF THIS PAGE Unclassified	19. SECURITY CLASSIFICATION OF ABSTRACT Unclassified	20. LIMITATION OF ABSTRACT SAR	

Chairman

Jill Ludwigsen
 Nichols Research Corporation
 2201 Buena Vista, S.E. #203
 Albuquerque, NM 87106
 (505) 843-7364

Program Committee

Capt. Bill Wyche, Co-Chairman
 Marko Stoyanof, Co-Chairman
 Air Force Phillips Laboratory

Ronald White, WRDC/FIVE

Dodd Stacy, Creare

Ron Ross, Jet Propulsion Lab

Al Johnson, Aerospace Corp.

Peter Gifford, Cryomech

Local Arrangements

Peter Jones, Aerospace Corp.

Accession For	
NTIS CRA&I	<input checked="" type="checkbox"/>
DTIC TAB	<input type="checkbox"/>
Unannounced	<input type="checkbox"/>
Justification	
By	
Distribution	
Availability Codes	
Dist	Avail and/or Special
A-1	

Advisory Board

DTIC QUALITY INSPECTED 3

John Barclay
 University of Victoria

Joseph Smith
 MIT

Stephen Castles
 NASA/GSFC

Michael Superczynski
 DTRC

Ray Radebaugh
 NIST

Klaus Timmerhaus
 University of Colorado

Hiroshi Nagano
 Toyama University, Japan

Paul Sheihing
 DOE

Ralph Longworth
 APD Cryogenics

Peter Kerney
 Janis Research

Martin J. Isenoff
 NRL

George Robinson
 Nichols Research Corp.

FOREWORD

This report contains the proceedings of the Seventh International Cryocooler Conference, held in Santa Fe, New Mexico, on 17-19 November, 1992. Jiri L. Ludwigsen of Nichols Research was the conference chairperson; Capt William Wyche and Marko Stoyanof of Phillips Laboratory served as the program committee chairmen.

The first cryocooler conference held in 1980 was designed to stimulate interest and discussion in the scientific and engineering community about the latest developments and advances in refrigeration for cryogenic sensors and electronic systems. The conference is held every even numbered year and this year over 300 participants attended representing 11 countries.

The technical program consisted of over 100 unrestricted oral and poster presentations. The topics included Cryocooler Testing and Modeling, Space and Long Life Applications, Stirling Cryocoolers, Pulse Tube Refrigerators, Novel Concepts and Component Development, Low Temperature Regenerator Development, and J-T and Absorption Coolers. The proceedings show significant progress in the field of cryocooler technology.

ACKNOWLEDGEMENTS

The Seventh International Cryocooler Conference Board would like to thank the Air Force Phillips Laboratory for sponsoring the conference and publishing these proceedings. The generous supply of manpower and dedication contributed by Phillips Laboratory was key to the success of the 1992 conference.

The Conference Chairperson would like to express her appreciation to Nichols Research Corporation for providing the support, assets and time required for this effort.

CONTENTS

TUESDAY SESSION	1
SDIO AND AIR FORCE CRYOCOOLER TECHNOLOGY DEVELOPMENTS AT USAF PHILLIPS LABORATORYP. J. Thomas	3
JPL CRYOCOOLER DEVELOPMENT AND TEST PROGRAM OVERVIEWR. G. Ross, Jr.	14
NASA/GSFC CRYOCOOLER DEVELOPMENT PROGRAMS. Castles, T. Cygnarowicz, R. Boyle, L. Sparr, R. Cory, F. ConnorsE. James, R. Fink, V. Arillo, J. Marketon, C. Lee, and D. Bugby	26
DEVELOPMENT AND DEMONSTRATION OF A DIAPHRAGM STIRLING 65 K STANDARD SPACECRAFT CRYOCOOLERD. Stacy, J. McCormick, and J. Valenzuela	40
STIRLING SPACE COOLERC. K. Chan, M. Lopez, J. Raab, E. Tward, and G. Davey	50
THERMAL, VIBRATION, AND RELIABILITY TEST RESULTS FOR A BALANCED 80 K CRYOCOOLERR. Boyle, L. Sparr, T. Cygnarowicz, S. Castles,R. G. Fink, and E. F. James	57
SPACECRAFT COOLER CHARACTERIZATIOND. L. Johnson, G. R. Mon, and R. G. Ross, Jr.	73
PERFORMANCE OF A LONG LIFE REVERSE BRAYTON CRYOCOOLERW. Swift and H. Sixsmith	84
SDI CRYOCOOLER PRODUCIBILITY PROGRAMJ. Bruning	98
MINIATURES PULSE TUBE COOLERC. K. Chan, C. B. Jaco, J. Raab, E. Tward, and M. Waterman	113
FLOW PATTERNS INTRINSIC TO THE PULSE TUBE REFRIGERATORJ. M. Lee, P. Kittel, K. D. Timmerhaus, and R. Radebaugh	125
EXPERIMENTAL PERFORMANCE OF MODIFIED PULSE TUBE REFRIGERATOR BELOW 80 K DOWN 23 KY. Ishizaki and E. Ishizaki	140

CONTENTS (Continued)

PULSE TUBE REFRIGERATOR RESEARCH	
....Y. Zhou and Y. J. Han	147
DEVELOPMENT OF PULSE TUBE REFRIGERATOR WITH LINEAR-MOTOR DRIVE COMPRESSOR	
....T. Kuriyama, H. Hatakeyama, Y. Ohtani, H. Nakagome, Y. Matsubara,H. Okuda, and H. Murakami	157
AN EXPERIMENTAL AND ANALYTICAL INVESTIGATION OF 4 K PULSE TUBE REFRIGERATOR	
....Y. Matsubara, J. L. Gao, K. Tanida, Y. Hiresaki, M. Kaneko	166
A NEW CONFIGURATION FOR SMALL-CAPACITY, LIQUID-HELIUM-TEMPERATURE CRYOCOOLER	
....J. A. Crunkleton	187
ANALYSIS OF A MINIATURE TWO-STAGE CRYOCOOLER	
....E. B. Ratts, Dr J. L. Smith, Jr., and Dr Y. Iwasa	197
POWER, EFFICIENCY, AND OPTIMUM DESIGN OF ELECTROCHEMICAL REFRIGERATORS	
....R. T. Ruggeri	213
LINEARIZED PULSE TUBE CRYOCOOLER THEORY	
....H. Mirels	221
VIBROIMPACT RESONANCE APPLICATION FOR THE DISPLACER MOTION PASSIVE CONTROL IN THE SPLIT CRYOGENIC COOLER	
....A. Veprik and N. Pundak	233
A HIGHLY RELIABLE, MINIATURE STIRLING-CYCLE CRYOCOOLER	
....C. S. Keung and G. Esposito	247
PERFORMANCE TEST RESULTS ON A MINIATURE STIRLING CRYOCOOLER FOR USE IN INTEGRATED DEWAR DETECTOR ASSEMBLIES	
....P. Ab-der-Halden	257
VALIDATION OF THE STIRLING REFRIGERATOR PERFORMANCE MODEL AGAINST THE PHILLIPS/NASA MAGNETIC BEARING REFRIGERATOR	
....S. W. K. Yuan and I. E. Spradley	280
THE MS*2 STIRLING CYCLE CODE	
....M. P. Mitchell	290

CONTENTS (Continued)

AN INTRODUCTION TO THE LUCAS AEROSPACE THERMODYNAMIC
COMPUTER MODEL CMOD

...C. S. Brice. 294

THERMOACOUSTIC THEORY FOR REGENERATIVE CRYOCOOLERS: A
CASE STUDY FOR A PULSE TUBE REFRIGERATOR

...J. H. Xiao 305

SOME PRELIMINARY EXPERIMENTAL RESULTS ON OSCILLATORY HEAT
TRANSFER IN A PERIODICALLY REVERSING PIPE FLOW

...X. Tang and P. Cheng 321

THERMOELECTRIC COOLERS FOR THE TWS, SFW, WAM AND SADARM
PROGRAMS, AND ASSOCIATED MANTECH PROGRAM OBJECTIVES...W. L. Kolander, B. Morrison, J. Bierschenk,
...J. Fuhrer, and T. Kottak 332CRYOGENIC ATTACHMENT FIXTURE WITH HIGH STRENGTH AND LOW
THERMAL CONDUCTION

...P. R. Roach 349

HELIUM LIQUID- AND GAS-GAP HEAT SWITCHES

...A. Kashani, B. P. M. Helvensteijn,
...F. J. McCormack, and A. L. Spivak 355A RADIATIVE COOLING SYSTEM FOR THE EOS STRATOSPHERIC WIND
INFRARED LIMB SOUNDER

...D. J. Kuyper 371

NEW MAGNETIC REFRIGERANTS FOR THE LOW TEMPERATURES REGION

...M. D. Kuz'min, A. M. Tishin, and S. Y. Dan'kov 385

WEDNESDAY SESSION 387

EXPERIMENTAL INVESTIGATION OF THE REGENERATIVE MAGNETIC
REFRIGERATOR OPERATING BETWEEN 4.2 K AND 1.8 K

...S. Jeong, J. L. Smith, Jr., Y. Iwasa, and T. Numazawa 389

A 4 K GIFFORD-McMAHON REFRIGERATOR FOR RADIO ASTRONOMY

...R. Plambeck, N. Thatte, and P. Sykes 401

CONTENTS (Continued)

DYNAMIC CHARACTERISTICS OF REGENERATORS USED IN CRYOCOOLERS
B. J. Huang and C. W. Lu 416

REGENERATOR PERFORMANCE AND REFRIGERATION MECHANISM FOR
 4 K GM REFRIGERATOR USING RARE EARTH COMPOUND REGENERATOR
 MATERIALS

....T. Kuriyama, M. Takahashi, H. Nakagome, T. Hashimoto,
T. Eda, and M. Yabuki 429

A STIRLING CYCLE CRYOCOOLER FOR 4 K APPLICATIONS

....D. Stacy, J. McCormick, and P. Wallis 444

SUPERFLUID STIRLING REFRIGERATOR WITH A COUNTERFLOW
 REGENERATOR

....J. G. Brisson and G. W. Swift 460

GRADED AND NONGRADED REGENERATOR PERFORMANCE

....W. Rawlins, K. D. Timmerhaus, R. Radebaugh,
J. Gary, and P. Bradley 471

SPECIFIC HEAT DESIGN AND PROPOSAL OF A NEW CUBIC TYPE MAGNETIC
 MATERIAL FOR A REGENERATOR MATRIX

....Y. Tokai, A. Takahasi, M. Sahashi, and T. Hashimoto 484

A COMPACT 150 GHz SIS RECEIVER COOLED BY 4 K GM REFRIGERATOR

....M. Takahasi, H. Hatakeyama, T. Kuriyama, H. Nakagome, R. Kawabe,
H. Iwashita, G. McCulloch, K. Shibata, and S. Ukita 495

DEVELOPMENT OF A PRECISION, SIX-AXIS LABORATORY DYNAMOMETER

....P. J. Champagne, S. A. Cordova, M. S. Jacoby, and K. R. Lorell 508

DEVELOPMENT AND DEMONSTRATION OF AN ELECTRONIC CONTROLLER
 FOR A DOUBLE-ACTING DIAPHRAGM CRYOCOOLER

....C. Konkell, T. Gibboney, L. Van Allen, K. Ha, and R. Boyle 526

MAGNETIC NOISE PRODUCED BY GM CRYOCOOLERS

....S. Fujimoto, H. Ogata, and H. Kado 560

REGENERATOR TWO-PHASE "SINGLE-BLOW" FOR PERFORMANCE
 EVALUATION AT SMALL VELOCITIES: ORIENTATION INFLUENCE AT "1g"

....K. V. Ravikumar, R. M. Carandang, T. H. K. Frederking,
R. Confair, W. Hong, F. Sherman, and C. Toribio 569

CONTENTS (Continued)

OPTIMIZATION ANALYSIS ON A TWO-STAGE AMR HYDROGEN LIQUEFIERL. Zhang, A. J. DeGregoria, S. A. Sherif, and T. N. Veziroglu	586
SUBMILLIMETER SPACE ASTRONOMY WITHOUT LIQUID HELIUM?C. Hagmann and P. L. Richards	595
RECENT PROGRESS ON APPLICATION OF HIGH ENTROPY MAGNETIC MATERIAL TO THE REGENERATOR IN HELIUM TEMPERATURE RANGET. Hashimoto, T. Eda, M. Yabuki, T. Kuriyama, and H. Nakagome	605
THE EFFECTS OF A LAYERED BED ON ACTIVE MAGNETIC REGENERATOR PERFORMANCES. R. Schuricht, A. J. DeGregoria, and C. B. Zimm	614
LONG LIFE STIRLING CYCLE COOLER DEVELOPMENTS FOR THE SPACE APPLICATION RANGE OF 20 K TO 80 KB. G. Jones and R. C. Peddle	621
STIRLING CRYOCOOLER WITH DUAL OPPOSED DISPLACERS FOR SPACE APPLICATIONSP. Arter, D. Berry, W. Gully, and C. Varner	644
DEVELOPMENT AND SPACE QUALIFICATION TESTING OF A RANGE OF MECHANICAL CRYOCOOLERSC. Weir	656
NOVEL LINEAR FLEXURE BEARINGT. E. Wong, R. B. Pan, and A. L. Johnson	675
NASA/GSFC CRYOCOOLER TEST PROGRAM RESULTSL. Sparr, R. Boyle, R. Cory, F. Connors, E. James,R. Fink, V. Arillo, and J. Marketon	699
PERFORMANCE OF THE SIGNAAL USFA STIRLING COOLING ENGINESD. Verbeek, H. Helmonds, and P. Roos	728
PRESENT LIFE-TESTING STATUS OF "OXFORD TYPE" CRYOCOOLERS FOR SPACE APPLICATIONSC. Jewell, T. Bradshaw, A. Orlowska, and B. Jones	738

CONTENTS (Continued)

DESIGN AND TEST OF A COMPREHENSIVE FACILITY FOR LIFE-TESTING
SPACE CRYOCOOLERS

....R. G. Ross, Jr. and D. L. Johnson 748

SIMULATION PROGRAM FOR MULTIPLE EXPANSION STIRLING MACHINES

....G. Walker, M. Weiss, R. Fauvel, G. Reader, and E. R. Bingham 759

COMPUTER MODELING OF STIRLING CYCLE COOLERS

....T. W. Bradshaw, A. H. Orlowska, and J. Hieatt 772

DESIGN EQUATIONS AND SCALING LAWS FOR LINEAR COMPRESSORS
WITH FLEXURE SPRINGS

....E. Marquardt, R. Radebaugh, and P. Kittel 783

NON-REAL TIME, FEED FORWARD VIBRATION CONTROL SYSTEM
DEVELOPMENT AND TEST RESULTS....R. Boyle, F. Connors, J. Marketon, V. Arillo,
....E. James, and R. Fink 805DEMONSTRATION OF ACTIVE VIBRATION REDUCTION ON A STIRLING-
CYCLE CRYOCOOLER TESTBED....B. G. Johnson, D. B. Eisenhaure, F. J. Flynn, M. S. Gaffney,
....R. L. Hockney, D. L. Johnson, and R. G. Ross, Jr. 820

THURSDAY SESSION 829

EVOLUTION OF THE 10 K PERIODIC SORPTION REFRIGERATOR CONCEPT

....A. L. Johnson and J. A. Jones 831

DEVELOPMENT OF A PERIODIC 10 K SORPTION CRYOCOOLER

....S. Bard, T. Fujita, L. Wade, J. Rodriquez, and J. J. Wu 854

EVALUATION OF A PROTOTYPE HYDRIDE COMPRESSOR FOR PERIODIC
HYDROGEN SORPTION CRYOCOOLERS....R. C. Bowman, Jr., B. D. Freeman, D. Labor, F. E. Lynch,
....R. W. Marmaro, and L. A. Wade 867ASSESSMENT OF A HYDROGEN JOULE-THOMSON EXPANDER AND
VANADIUM HYDRIDE SORPTION BEDS FOR 20 K CRYOCOOLERS....E. L. Ryba, B. D. Freeman, R. C. Bowman, Jr., R. E. Spjut,
....E. A. Liu, P. Budic, and C. Okado 880

CONTENTS (Continued)

DESIGN OF A METAL HYDRIDE SORPTION CRYOCOOLER SYSTEMH. J. Strumpf and R. H. Norman	898
LINEAR COMPRESSOR FOR JT CRYOCOOLERD. T. Kuo	921
PROGRESS REPORT ON THE DEVELOPMENT OF THE BALL J-T CRYOCOOLERR. Levenduski and R. Scarlotti	931
JT CRYOSTAT WITH LIQUID-SOLID CRYOGEN RESERVOIRR. C. Longworth	958
DESIGN AND OPERATION OF A 30 K TWO-STAGE NITROGEN-NEON J-T COOLERW. A. Little, R. Yaron, and C. Fuentes	971
DESIGN CONCEPTS FOR A 10 K SOLID HYDROGEN SORPTION REFRIGERATORJ. R. Phillips, B. D. Freeman, and R. C. Bowman, Jr.	978
EXPERIMENTAL VERIFICATION OF JOULE-THOMSON CRYOCOOLER COOLDOWN PERIOD SIMILARITY RATIOSB-Z. Maytal	996
BI-MATERIAL CONTROLLED DEMAND FLOW JOULE-THOMSON COOLERSG. E. Bonney	1003
CONTAMINATION CONTROL IN CLOSED CYCLE JOULE-THOMSON CRYOCOOLERS AND A NEW J-T VALVEJ. Lester and S. Nieczkoski	1012
PHASE EQUILIBRIA IN CRYOGENIC MIXTURESL. B. Robinson	1025
INCORPORATING A MECHANICAL REFRIGERATOR WITH A REFREEZABLE CRYOGEN IN SPACE APPLICATIONSB. G. Williams and J. C. Batty	1043
APPLICATIONS AND PACKAGING OF SEMICONDUCTOR DEVICES FOR USE AT CRYOGENIC TEMPERATURESK. P. Hyde, J. R. McCoy, and C. S. Naiman	1064

CONTENTS (Concluded)

A METHOD TO ESTIMATE THE PULSE TUBE REFRIGERATOR PERFORMANCES

....M. David, J. Marechal, and Y. Simon 1078

CRYOCOOLER TIP MOTION SUPPRESSION USING ACTIVE CONTROL OF PIEZOELECTRIC ACTUATORS

....R. J. Glaser, R. G. Ross, Jr., and D. L. Johnson 1086

HIGH TEMPERATURE SUPERCONDUCTING SPACE EXPERIMENT CRYOGENIC SYSTEM OVERVIEW

....T. Kawecki 1098

10 K SORPTION CRYOCOOLER FLIGHT EXPERIMENT (BETSCE)

....S. Bard, P. Cowgill, J. Rodriguez, L. Wade, J. J. Wu,
....M. Gehrlein, and W. Von Der Ohe 1107

GAS ATOMIZED Er_3Ni POWDER FOR CRYOCOOLER APPLICATIONS

....I. E. Anderson, M. G. Osborne, H. Takeya,
....and K. A. Gschneidner, Jr. 1120

MAGNETIC NANOCOMPOSITES AS MAGNETIC REFRIGERANTS

....R. D. Shull, R. D. McMichael, J. J. Ritter,
....L. J. Swartzendruber, and L. H. Bennett 1133

ENTHALPY FLOW TRANSITION LOSSES IN REGENERATIVE CRYOCOOLERS

....P. Kittel 1145

NEODYMIUM REGENERATOR TEST RESULTS IN A STANDARD GIFFORD-McMAHON REFRIGERATOR

....J. Chafe, G. Green, and R. C. Riedy 1157

SOLVAY REFRIGERATOR OPERATING AT HELIUM TEMPERATURES

....G. Chen, J. Zheng, F. Zhang, J. Yu, and T. Sun 1165

TUESDAY SESSION

SDIO AND AIR FORCE CRYOCOOLER TECHNOLOGY DEVELOPMENTS
AT USAF PHILLIPS LABORATORY

PETER J. THOMAS
USAF Phillips Laboratory
Kirtland AFB, NM 87117

INTRODUCTION

The multi-year development efforts in cryogenic technology through the Strategic Defense Initiative Organization (SDIO) are coming to first fruition with the completion and initiation of industry contracts for cryogenic refrigerators and peripheral thermal management capabilities. USAF Phillips Laboratory, as primary development agency for Department of Defense cryogenic technology, has planned and implemented a diverse program of research from industry contracts to first principle in-house investigations.

BACKGROUND

As the designated manager for the SDIO Program Management Agreement (PMA) Task 1101.2, Cryocooler Technology, Phillips Laboratory has hosted a multi-year effort to ensure that the SDIO goals of developing long-life reliable space cryogenic refrigerators are implemented.

Several key goals of this effort include the development of the 65 Kelvin Standard Spacecraft Cryocooler, the Single Stage Reverse Turbo Brayton Cryocooler, the Protoflight Spacecraft Cryocooler, the 35 Kelvin Pulse Tube and the 10 Kelvin Cryocooler programs. Our efforts for development of long-life, high reliability, cryogenic refrigeration capabilities are paramount to successful operational deployment of key SDIO space systems.

TECHNICAL PROGRAM

65 Kelvin Standard Spacecraft Cryocooler (65K SSC)

This program, started in late 1989, focuses on development of the first generation of highly producible single stage cryocoolers for medium to low cooling loads (.25 to 5 watts with a nominal 2 watts design point) in the 60 to 80 kelvin temperature range. Emphasis is placed on a technology using standardized interfaces, electronics, heat rejection and cooling load integration techniques and a view toward scalability in design over a variety of user scenarios.

The idea of a truly "standardized" refrigerator is incorporated in order to meet a variety of SDIO sensor cooling requirements both near and far term and to lend an air of flexibility for changing user requirements.

This refrigerator effort sought to better the state-of-the-art in areas such as increased efficiency (a goal of 30 Watts/Watt specific power or less), vibration, and weight and to meet the predicted capability of 95% reliability for 10 years of continuous, unattended operation in space.

Three contracts with industry were let for the conceptual design of the cryocooler. Lockheed Missiles and Space Co.(LMSC) teamed with Lucas Aerospace (UK), Hughes Aircraft Co. and Creare Inc. Both LMSC/Lucas and Hughes Aircraft Co. chose to develop a linear flexure bearing supported Stirling cycle cryocooler similar to pioneering work accomplished earlier by Oxford University and Rutherford Appleton Laboratory.

Creare Inc. (USA) designed and implemented a novel Stirling cycle refrigerator using large bore, small displacement titanium diaphragms as the gas compression and expansion mechanism. This design features a laminar flow recuperative type heat exchanger instead of a displacing screen regenerator matrix.

Both Hughes and Creare were selected by SDIO for fabrication and test of their designs and have now just started the last leg to successful fruition with hardware in initial testing, debugging and characterization. SDIO plans for four prototype cryocoolers (2 each from Creare Inc. and Hughes Aircraft Co.) include performance characterization testing funded through Phillips Laboratory and to be conducted by Jet Propulsion Laboratory. These 6-8 week efforts for each cryocooler will be followed by long-term endurance and performance testing at Phillips Laboratory, Kirtland AFB, New Mexico. These tasks start in October 1992 and will run through 1993.

Single Stage Reverse Turbo Brayton Cryocooler

Through SDIO/Phillips Laboratory sponsorship and with the technical leadership of NASA's Goddard Space Flight Center, this program with Creare Inc., Hanover, NH. has, to-date, proven to be a striking success. Born of several component level research projects funded under both NASA and SDIO Small Business Innovation Research (SBIR) programs, a complete "breadboard" system level demonstration between May and October 1992 illustrated the capability to provide 5 watts cooling at 65 kelvin for less than 200 watts total input power. This was a first ever demonstrated capability for a reverse Brayton turbo cryocooler.

Concurrent investigation showed that scalability to smaller cooling loads of 1 W at 35 kelvin and 2 watts at 65 kelvin may readily be accomplished through use and optimization of select system components. Engineering Development Model (EDM) design and fabrication will culminate with performance testing starting in October of 1993 with a performance goal of 5 W at 65 K for less than 180 watts input power.

As an alternative cryogenic refrigerator to Stirling cycle machines, the work at Creare Inc. has demonstrated a high capacity refrigerator with virtually no vibration imparted to its mounting structure and promises high reliability over time and through many start/stop cycles.

Endurance/Life testing will commence upon successful EDM validation at either Phillips Laboratory or NASA's Goddard Space Flight Center.

Protoflight Spacecraft Cryocooler

The motivation for this multi-year program is to develop through industry, cryocooler designs capable of meeting requirements imposed by a typical space-based surveillance mission and environment. Inherently based on those technology findings developed through the 65 Kelvin Standard Spacecraft Cryocooler and similar industry efforts, the Protoflight Spacecraft Cryocooler program seeks to mitigate reliability and performance degradation factors discovered during these earlier engineering development model (EDM) programs.

As the necessary follow-on to EDM cryocoolers, the PSC refrigerators in both the 60 kelvin and 150 kelvin temperature regimes will be designed, fabricated and tested within an ambitious 16 month schedule in order to accommodate SDIO integration and flight test schedules for the Brilliant Eyes program.

Currently selected for the PSC development are Hughes Aircraft Co. and Lockheed Space and Missiles/Lucas Aerospace, each for the design, build, and test of a 60 kelvin cryocooler, and TRW Inc. for a 150 kelvin capable cryocooler. Electronics control and spacecraft requirements call for stringent adherence to fully qualified electronic topology and parts selection to ensure simple integration and flight capability. Specifically the mission requirements for the PSC are as follows:

Mode	Transport	Storage	Pre-Launch Check	Launch	Orbit
Environment	Ground	Ground	Ground	Launch & Orbit	Space Orbit
Temperature-K	233-328	233-328	233-328	233-328	275-325
Time-hours	72	17,530	1,080	0.5	61,320
Operation	none	Once every 6 months	Once for 32 hours prior to installation, and three 5-minute operations after installation	none	continuous with up to 8,000 stop/start cycles

The 60 kelvin variant of the PSC will be a Stirling cycle refrigerator capable of 2 watts cooling load at $60 \pm .5$ kelvin while rejecting to 275 to 325 kelvin through a conductive interface. Total input power from the spacecraft bus must not exceed 100 watts of 28 ± 6 Vdc when operated at a nominal 300 kelvin rejection temperature and vibration imparted from the cryocooler to the spacecraft body will be less than .02 newtons_{rms}.

Similarly, the 150 kelvin variant of the PSC will be a Stirling cycle cooler capable of 1 watt of cooling load at $150 \pm .5$ kelvin with no greater than 15 watts of total input power to the refrigerator. Operating at a nominal 300 K rejection temperature, this cryocooler will impart no greater than .02 newtons_{rms}.

Quick Cool-Down J-T Cryocooler

As required technology for SDIO interceptor platforms, small, light, efficient and very fast cool-down Joule-Thomson cryostats have been developed by industry with Phillips Laboratory sponsorship. A key attribute of the program was to solicit and award contracts to particularly innovative ideas for these very small cryocoolers.

In September of 1990, with technical management provided by the Naval Air Warfare Center, Weapons Division, China Lake, Ca., three contracts with industry were started to develop and demonstrate answers to this SDIO need. Key to this technology is the use of high cryogen retention methods for high-g environments.

MMR Inc. of Mountain View, CA uses a novel metal foil heat exchanger in their 60 kelvin design and is currently in development fabrication of a 1/3 scale heat exchanger for evaluation.

Alabama Cryogenic Engineering of Huntsville, AL is pursuing a miniature perforated plate heat exchanger for the 10 kelvin requirement. This effort is also in the component fabrication stage.

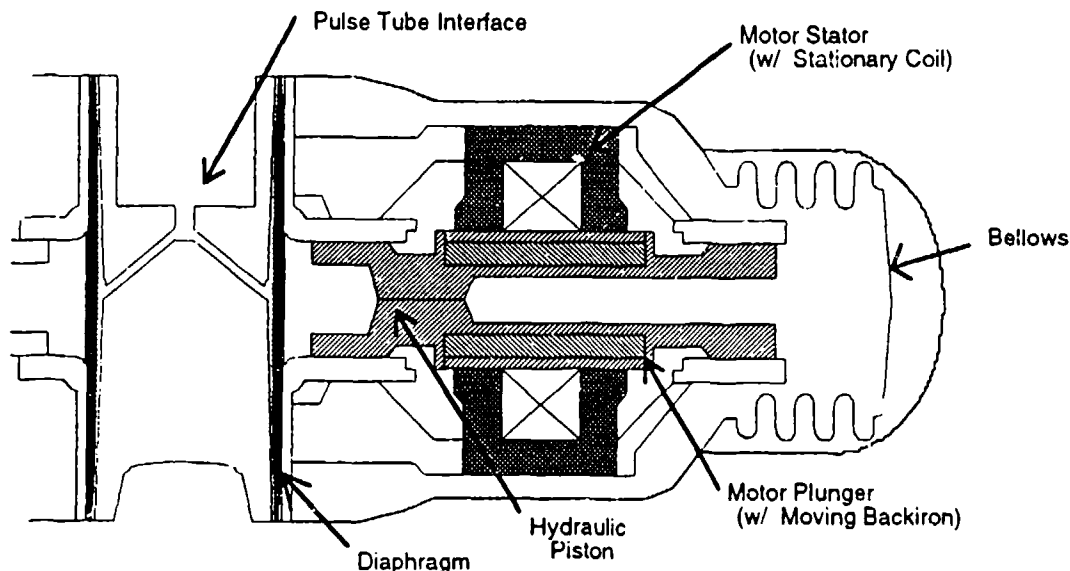
APD Cryogenics Inc. features liquid cryogen reservoirs of helium, neon or oxygen depending on cooling temperature desired. Their 10 kelvin J-T cryocooler has been successfully tested and 30 kelvin and 60 kelvin work continues. In general, cooling objectives for the Quick Cool J-T are as follows:

Environment:	Space	Space	Ground/Space
Operating Temp:	60 K	30 K	10 K
Ambient Temp:	250 K	150 K	213/328 K
Cooldown Time:	5 sec	15 sec	120 sec
Flight Time:	30 min	30 min	3 min
Heat Load:	1 W	1 W	.5 W
Interceptor Mass:	< 100 gm	< 100 gm	< 100 gm

Advanced Compressor

This Phillips Lab sponsored program with Mechanical Technology Inc. of Latham, NY. will develop a two-stage, hermetically-sealed Stirling cycle diaphragm compressor which could provide an alternative to moving piston compressors of the same capacity. In this design, the compressor module housing is flooded with synthetic oil and hydraulic actuation of each diaphragm is achieved by the oscillating piston directly attached to the linear motor plunger.

This hermetically sealed design has the potential benefit of reducing all contaminants: out-gassing, organics, debris or particles, to the working fluid that have been associated with performance degradation in Stirling cycle cryocoolers.

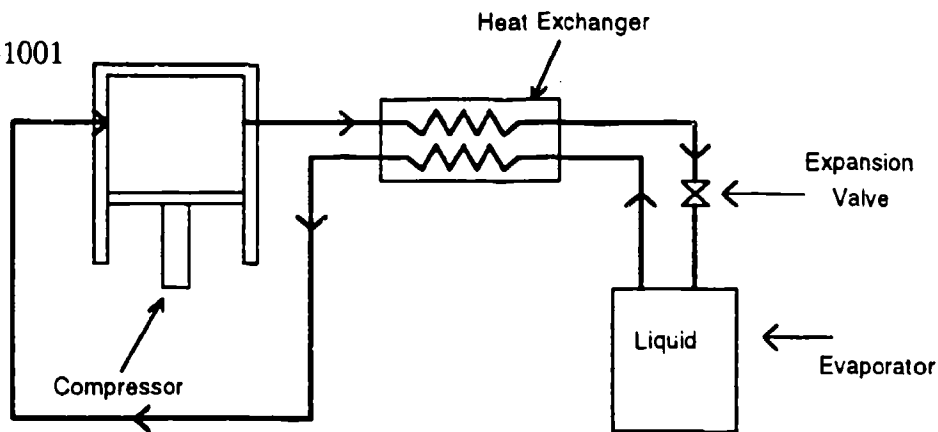


Back to back compressor modules are used for dynamical vibration balancing and provide a common compression volume for use with Stirling or Pulse tube cold end assemblies.

MTI's effort is particularly focused on providing sufficient compression work for pulse tube applications in the 30 - 40 kelvin temperature range. A single engineering model is scheduled for delivery to Phillips Laboratory in April 1993.

Electrochemical Cryocooler

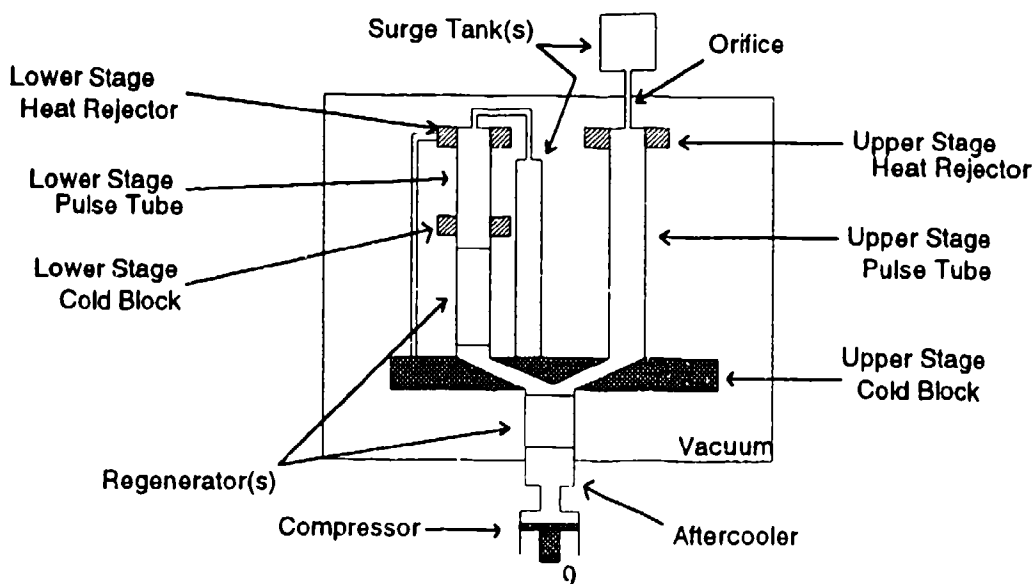
With a no moving parts electrochemical compressor designed for operation in the 60 to 70 kelvin range, this refrigerator concept is based on an innovative method by which oxygen is compressed across ceramic electrolyte membrane. Potentially high pressure ratios are achievable for use with Joule-Thomson expansion cryostats. The demonstrated performance by this contract with The Boeing Co., Seattle, WA. include successful operation of the electrochemical membranes at high temperature (800-1000 kelvin) and high pressure (up to 2000 psi).



The promise of highly reliable, contaminant free oxygen compression for J-T expansion will be explored as an alternative to Stirling cycle machines in the .5 watt range at 65 kelvin. Conceptual design phase of this program is scheduled for completion in October of 1992.

The 35 Kelvin Pulse-Tube Cryocooler

A program for the analysis, validation and demonstration of a two-stage, dual-load, pulse tube cryocooler for SDIO Brilliant Eyes LWIR sensor requirements was awarded to TRW Inc., Redondo Beach, Ca. in September 1992. The pulse-tube design obviates the use of a displacing regenerator mass in the cryocooler cold head and promises a significant reduction in vibration forces imparted to a sensor or spacecraft instrument.



With no moving, contacting parts in the cold finger assembly, this technology may be a solution to many reliability and manufacturing concerns currently associated with "traditional" flexure bearing Stirling cycle machines similar to those under the Protoflight Spacecraft Cryocooler program.

Though pulse tube cryocooler investigations have not yet fully demonstrated the capability for the high efficiency found in Stirling cycle refrigerators, their relative simplicity, ease of manufacturing, and potentially limitless cold assembly operating life combine to promote this technology as a viable alternative cryocooler in several temperature and cooling load areas.

TRW's effort is to analyze and design a two-stage pulse tube for loads at 60-70 kelvin and 30-40 kelvin and to fabricate and optimize a cold head for integration with their existing 20cc displacement, linear flexure bearing "Stirling" compressor.

With the successful demonstration of .25 watts of useful cooling at 35 kelvin, Phillips Laboratory may exercise an option for fabrication, test and delivery of two optimized engineering development models.

Performance characterization and long term endurance testing of these models will be slated to begin in June 1994 at Phillips Laboratory.

10 Kelvin Cryocooler Development

With SDIO/TNS goals as the driver for new technologies in 10 kelvin cryogenic refrigeration, Phillips Laboratory has contracted efforts with 3 industry corporations for a cryocooler capable of meeting continuous and simultaneous cooling loads of .15 watts at 10 kelvin, 2 watts at 35 kelvin and 5 watts at 80 kelvin. Primary programs desires include reduction in weight and spacecraft power penalties relative to other cryocooling systems.

The three contracts, started in October 1992, include TWR Inc. whose selected approach is that of a three stage pulse-tube cryocooler, Aerojet Corporation using hydride sorption for the 10 K and 35 K stages, and the combined team of Lockheed Space and Missiles Co. and Lucas Aerospace whose chosen design is for a 3-stage Stirling cycle refrigerator.

This development consists of 3 stages: (I). Conceptual Design, (II.) Critical Component Development - this phase will fund any or all successful designs from the conceptual design phase and will consist of fabrication, testing and performance mapping of critical subsystem level components sufficient to show advancement to state of the art, and (III.) Engineering Development Model (EDM) - funding of any or all successful designs in phase II to optimize, fabricate and test a system level hardware prototype sufficient to prove legacy to flight hardware.

Phillips Laboratory Thermal Systems Test Facility

With the near completion of the 65 Kelvin Standard Spacecraft Cryocooler, Phillips Lab has been tasked with providing independent long life endurance testing capabilities for SDIO required cryogenic systems. In joint cooperation with the Jet Propulsion Laboratory, Pasadena, CA., Phillips Laboratory has defined and developed the in-house capability for this testing which includes full space operation simulation through thermal-vacuum test stands, vibration isolation and fluid heat rejection temperature control. Endurance testing will include the continuous monitoring of performance characteristics through varying heat rejection temperatures, cooling loads and temperatures and multiple stop/start conditions. Fundamental vibration characteristics will be monitored for correlation with performance parameter variations over long time intervals.

Additionally, Phillips Laboratory has planned a program of separate effects tests and subcomponent evaluations for items of critical importance to cryocooler lifetime performance, reliability, and producibility.

These evaluations will include many facets including flexure bearing fatigue analysis and testing, diaphragm fatigue testing and analysis, linear motor optimization studies, cold sensor integration and regenerator optimization studies.

Long-term interests include advanced electronic control and vibration isolation and cancellation capabilities and non-destructive evaluation of life limiting factors for cryocoolers and thermal support systems.

In-house work at Phillips Laboratory includes analysis and development of a .5 watt, 70 kelvin low penalty sorption cryocooler with goals of 1.5 Kg and 25 watts total weight and total power input, respectively.

Cryogenic Phase-Change Materials

This Brilliant Eyes program office funded development and flight experiment effort focuses on key parameters of phase change material thermal storage devices required for sensor applications in space. The Phillips Laboratory contract with Grumman Aerospace as primary contractor and with ESL Inc. as secondary contractor is a two part program. Conceptual Design Phase includes investigations of phase change materials and physical configurations sufficient for operation at three separate temperature regimes: 65K, 120K and 180K.

Prototypical hardware design and fabrication for each of these temperatures will explore alternative compounds, energy storage, effectiveness, cool/thaw cycling ability and orbital service life. Testing and performance characterization will run from 6/93 through 4/94.

Successful conclusion of phase I will result in the identification of phase change materials and hardware configurations optimized for these temperature ranges. Phase II will then incorporate a 2nd generation fabrication selected from a 120 kelvin capable phase change material.

This device will undergo complete space qualification and performance mapping and conclude with a flight demonstration consisting of a 1 Watt 120 kelvin Stirling cycle cryocooler manufactured by TRW Inc. and a variable dummy sensor heat load. Shuttle-Flight demo will be part of the SDIO SPAS III program.

CONCLUSION

Phillips Laboratory's effort for supporting SDIO space surveillance and thermal management needs is a growing and increasingly important program. Actively seeking new methods and technologies for providing cryogenic refrigeration and storage must carefully balance the need for innovation and originality with that of meeting customer needs. Our carefully planned course for providing answers to our users while fostering growth and exchange of information with industry, academia and government finds its strength in communication with the cryogenic community at large. We invite that dialogue always.

JPL CRYOCOOLER DEVELOPMENT AND TEST PROGRAM OVERVIEW

R. G. Ross, Jr.

**Jet Propulsion Laboratory
California Institute of Technology
Pasadena, California 91109**

ABSTRACT

The growing demand for long-wavelength infrared imaging instruments for space observational applications, together with the emergence of the multi-year-life Oxford University 80 K Stirling-cycle cooler, has led to a rapidly expanding near-term commitment to mechanical cryocoolers for long-life NASA and SDIO space missions. To help ensure the success of these cooler commitments, the Jet Propulsion Laboratory (JPL) has implemented an extensive cryocooler program in cooperation with the Air Force Phillips Laboratory (AFPL), the Air Force Space Division, the Aerospace Corp., and NASA Goddard Space Flight Center. This program is directed at assisting industry in developing advanced cryocoolers that successfully address the broad array of complex performance requirements needed for NASA and SDIO long-life space instruments. The JPL cryocooler program includes extensive characterization and life testing of industry-developed Stirling coolers, development and test of advanced vibration-suppression systems for mechanical cryocoolers, flight tests of advanced low-vibration Stirling-cooler systems, and development and flight testing of advanced sorption cooler systems for detector cooling to 10 K.

INTRODUCTION

Extensive near-term and future space-instrument programs within NASA and the Strategic Defense Initiative Organization (SDIO) depend on the successful development of long-life, low-vibration space cryocoolers. The most demanding near-term programs include a number of science instruments selected for NASA's Earth Observing System (Eos) program, and a number of space reconnaissance instruments associated with the SDIO's Brilliant Eyes and Brilliant Pebbles programs; all of these programs require delivery of similar types of flight coolers in the next few years.

The high level of commonality that exists between the NASA and SDIO cooler requirements has fostered a highly collaborative, cooperative program involving both NASA and DoD laboratories supporting major contractual development efforts within the world-wide aerospace industry. JPL, under a combination of NASA and SDIO funding, is playing an

extensive role in assisting industry in the development of advanced cryocoolers to meet both NASA's and SDIO's needs. The JPL cryocooler program is focused in four areas:

- 1) Active support of flight projects in the selection, application and acquisition of cryocoolers meeting their needs. This activity plays an important role in identifying the key performance and integration requirements that must be addressed by the cryocoolers, and the key cryocooler integration issues that must be addressed by the interfacing science instruments. The major JPL activities in this area are support of the JPL/NASA Eos Atmospheric Infrared Sounder (AIRS) instrument in the acquisition of long-life, low-vibration 1.5-watt 55K Stirling coolers for cooling of longwave infrared focal planes to 60 K, and support to the SDIO Brilliant Eyes program in the development of an advanced cryocooler for periodic cooling to 10 K.
- 2) Extensive characterization testing of industry-developed cryocoolers to provide a consistent database of performance data for use by instrument developers and the cryocooler development community. JPL initiated an extensive cryocooler characterization program in support of the Eos AIRS instrument in 1989, and has expanded the effort under AFPL/SDIO sponsorship to provide a thorough cryocooler performance database for the SDIO/NASA-wide community.
- 3) Flight test of important cryocooler developments to provide reliable flight heritage data, and to insure thorough qualification status and compliance with launch vehicle safety and cryosystem integration constraints. JPL is managing three ongoing cryocooler flight experiments scheduled for launch in the 1994 timeframe: the NASA In-step Hughes Cryosystem Flight Experiment, the Space Technology Research Vehicle (STRV) Cryocooler Vibration Suppression Experiment, and the Brilliant Eyes Ten Kelvin Sorption Cryocooler Experiment (BETSCE).
- 4) Research of advanced cryocooler technologies needed to help the community meet identified short-falls in cryocooler performance. The principal focus of these activities is in the areas of cryocooler vibration suppression and development of advanced vibration-free sorption refrigerators, and the conduct of reliability physics investigations to establish the technology base for achieving and verifying multi-year cryocooler life.

These JPL cryocooler programs are summarized below and described in detail in the cited references. For ease in presentation, the activities are organized programmatically, starting with 55- to 80-K Stirling-cooler activities and ending with 10-K sorption-cooler activities.

STIRLING CRYOCOOLER CHARACTERIZATION

AIRS Cryocooler Development and Characterization

In 1989 JPL initiated an extensive Stirling cryocooler characterization program in support of the JPL Atmospheric Infrared Sounder (AIRS) instrument, which is scheduled to fly on

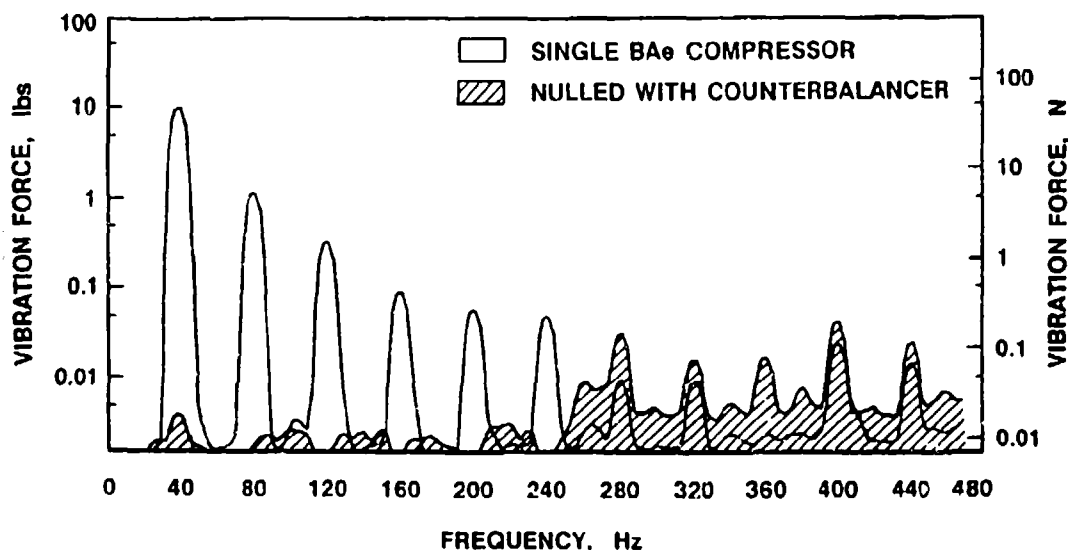


Fig. 1. Reduction of vibration harmonics of BAe 80K cooler coupled with active counterbalancer and SatCon narrowband controller [8,9].

the NASA Eos PM platform in the 1999 timeframe; the AIRS cooler program also supports other JPL and NASA instruments requiring advanced high-capacity (1.5-watt 55K) low-vibration Stirling coolers. To provide the foundation of Stirling-cooler data needed for this program, one of the first British Aerospace (BAe) 80 K "Oxford" coolers was purchased in 1990 and has been extensively characterized [1-5]. Over the past two years the characterization program also led to the design and development of unique and sophisticated cryocooler test facilities. Because the AIRS instrument is particularly sensitive to vibration during operation, an area of special emphasis has been applying advanced vibration control techniques to achieving high levels of vibration suppression. Figure 1 illustrates the 70 dB of vibration suppression achieved using an advanced single-axis narrow-band vibration control system developed under contract with SatCon Technology Corporation [8,9]. Advanced 3-axis vibration suppression systems are also currently under development at JPL and through a contract with the Massachusetts Institute of Technology.

In order to expand the performance of the first generation BAe 80 K cooler to meet the AIRS requirements, JPL's AIRS instrument systems contractor, Loral Infrared & Imaging Systems, Inc. (LIRIS), has contracted with BAe and Lockheed-Lucas for the development-testing of advanced second-generation Stirling coolers with the needed capacity, efficiency and low vibration. This contractual effort has proved the feasibility of achieving the AIRS requirements through the development and test of coolers referred to as AIRS 55K coolers [6,7]. Example performance curves for these coolers are presented in Fig. 2.

SDIO/AFPL Cryocooler Characterization Program

With the recognized need within the space-cooler community for thorough and accurate data on the performance of emerging space cryocoolers, the JPL cryocooler characterization

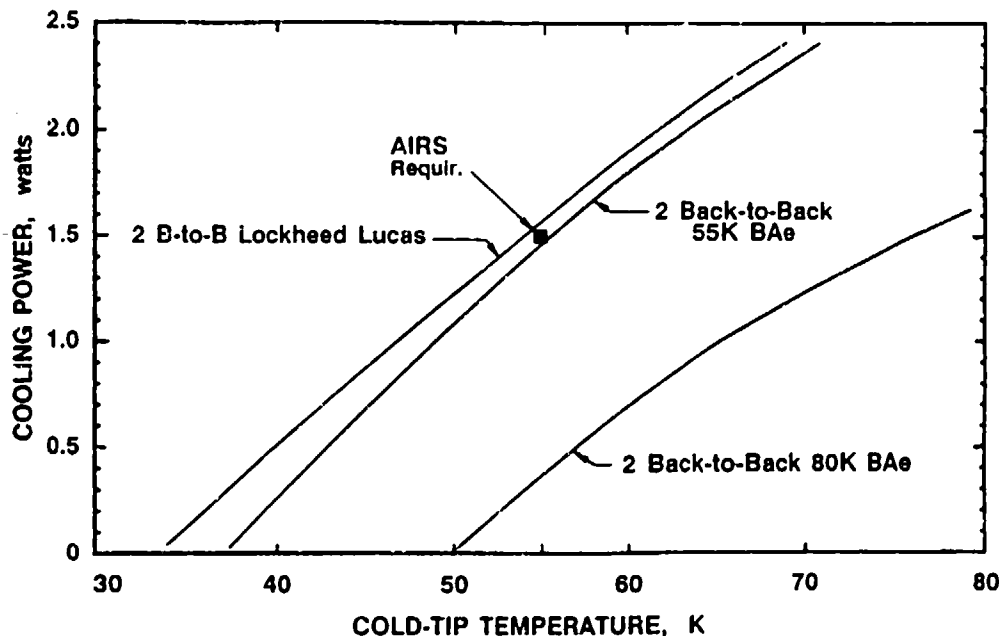


Fig. 2. Thermal performance of prototype AIRS 55K Stirling coolers compared to that of the original BAe 80K cooler.

program was expanded in 1992 under the sponsorship of the Strategic Defense Initiative Organization/Air Force Phillips Laboratory. The objective of the expanded test program is to gather thorough thermal, vibration, electromagnetic interference (EMI) and reliability performance data on space cryocoolers under development by, or of interest to the SDIO Community [10]. Current coolers under test, or about to be tested, include the Hughes and Creare 65 K SSC Stirling coolers -- both under development through AFPL/SDIO funding -- and coolers from BAe, Lockheed-Lucas, Stirling Technology Company, TRW, and Sunpower Corporation; in addition, several other manufacturers are in active discussions relative to testing of their coolers. The test program covers all aspects of cooler performance affecting instrument compatibility including thermodynamic cooling capacity, cold finger off-state parasitics, location and amount of rejected heat, generated vibration, and EMI. The JPL characterization program is designed to provide a comprehensive database obtained using a common set of instrumentation, test procedures, and test facilities. This helps provide standardization of test-result formats and parameter ranges to aid in comparing and interpreting cryocooler performance.

Cryocooler Life-Test Facility Development

With the growing commitment of long-life Stirling cryocoolers to multi-year NASA and SDIO space applications, there is also increasing need for quantitative reliability data verifying the long-term performance of the coolers and identifying any possible time-dependent degradation or wear-out failures. To obtain such data, JPL is designing and fabricating comprehensive life-testing facilities for use by the Air Force Phillips Laboratory (AFPL) and the Jet Propulsion Lab [11]. These life-test facilities are directed at acquiring



Fig. 3. JPL cryocooler lifestest chamber installation overview.

quantitative cooler performance data in three areas: 1) refrigeration performance including thermal efficiency, long-term temperature stability and possible effects of contamination and wear, 2) level and stability of generated vibration including long-term performance of vibration cancellation technologies, and 3) illumination of any wear-out or random failure mechanisms that need to be corrected prior to flight hardware deliveries. To provide these functional capabilities, the developed life-test chambers, shown in Fig. 3, incorporate a number of unique features including thermostatically controlled thermal-vacuum heatsink environments, continuous monitoring of cooler-generated vibration, and active fault detection.

JPL STIRLING COOLER FLIGHT EXPERIMENTS

To provide flight-heritage performance data, and to thoroughly demonstrate flight qualification status and compliance with launch vehicle safety and cryosystem integration constraints, JPL is managing two ongoing Stirling-cooler flight experiments scheduled for launch in the 1994 timeframe: the NASA In-STEP Cryosystem Flight Experiment, and the STRV Cryocooler Vibration Suppression Experiment.

NASA In-STEP Cryosystem Flight Experiment

Under JPL management, the Hughes Aircraft Co. is developing a cryosystem flight experiment [12] to validate and characterize the on-orbit performance of a hybrid cryogenic cooling system integrating three advanced technologies: a 2-watt 65K low-vibration long-life

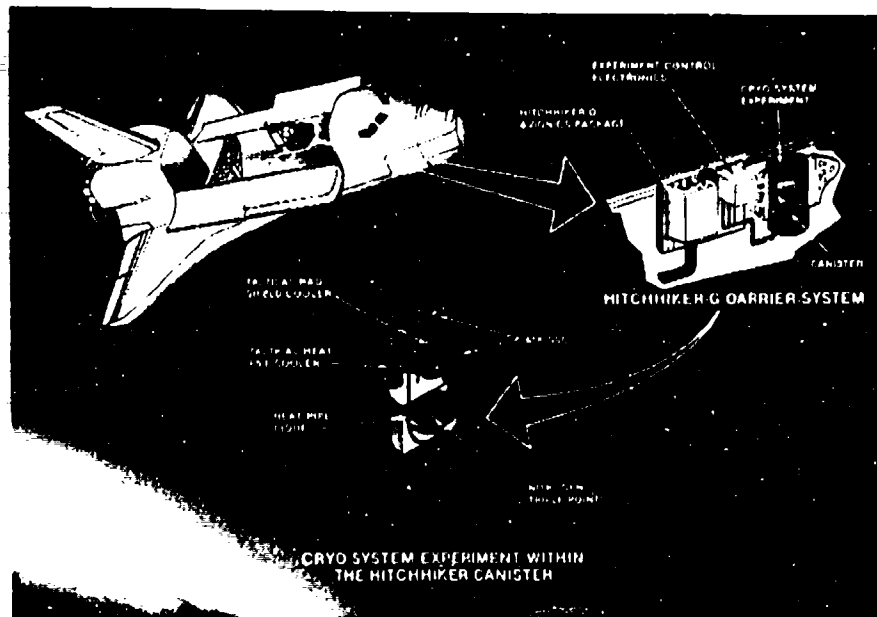


Fig. 4. Hughes In-step Cryo System Experiment (CSE) mounted in Shuttle bay.

Stirling cooler developed by Hughes under AFPL/SDIC sponsorship, a diode oxygen heat pipe thermal switch that also enables physical separation between the cryocooler and the thermal load, and a thermal-energy storage device that provides a stable thermal sink at cryogenic temperatures. A key feature of the experiment is the on-orbit measurement of the vibration generated by the advanced, fully counterbalanced, second-generation Stirling cryocooler in contrast to typical short-life "tactical" coolers, which are also used in the experiment for shield cooling. The NASA-sponsored experiment, illustrated in Fig. 4, is in the final stages of construction and is scheduled for launch aboard the Shuttle in mid-1994.

STRV Cryocooler Vibration Suppression Experiment

Under SDIO sponsorship, JPL is also developing a flight experiment to demonstrate more advanced control technologies for quieting cryocooler tip vibration in three axes [13]. This experiment is scheduled to fly as a small 15-watt payload on the Space Technology Research Vehicle (STRV-1b), a small English satellite scheduled for launch on the Ariane-4 in early 1994. To meet stringent power, weight, and space constraints, the experiment makes use of the tiny 1/5-watt Texas Instruments tactical Stirling cooler, shown in Fig. 5. Two different vibration-cancellation actuator techniques are being demonstrated: 1) applique ceramic piezoelectric actuators that are bonded to the coldfinger and stretch the coldfinger to cancel tip motion, and 2) commercial low voltage piezoelectric translators that similarly cancel tip motion by moving the entire cryocooler in three axes. Motion of the coldfinger tip is measured in all three axes to 10 nanometer accuracy using eddy-current transducers. Two types of control systems are also being demonstrated: 1) an analog control system that uses a bandpass filter to track the drive signal and suppress it, and 2) a unique narrow-band

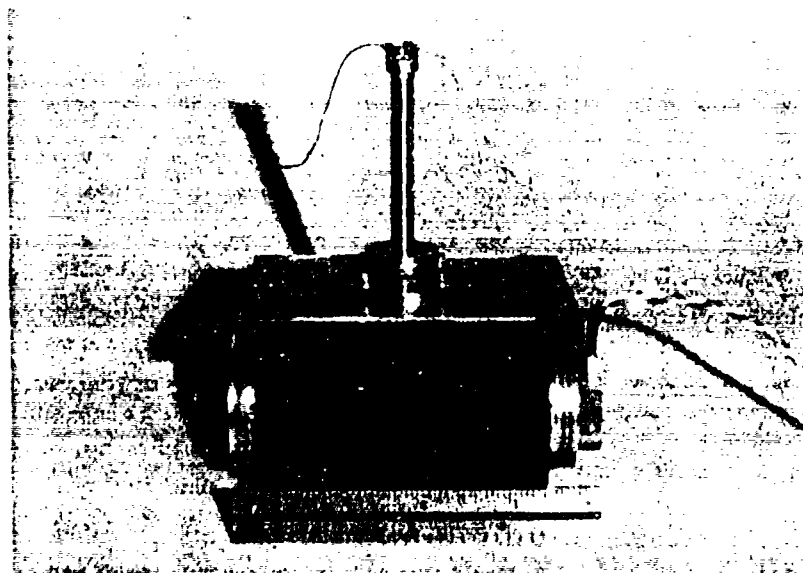


Fig. 5. Texas Instruments 1/5-watt 80K cooler to be flown in JPL STRV cryocooler vibration-suppression flight experiment.

adaptive feed-forward system that continually updates a steady-state command signal to each actuator to cancel the tip vibration. Either control system can be used with either actuator.

TEN KELVIN BRILLIANT-EYES SORPTION COOLER DEVELOPMENT

One of the concepts for the Brilliant Eyes (BE) surveillance satellite system involves a long-wavelength infrared detector focal plane that requires periodic operation at near 10 K. To provide the necessary cryogenic cooling, a novel periodic 10-K sorption cooler concept was invented by Dr. Al Johnson of Aerospace, Inc. in collaboration with Mr. Jack Jones of JPL [14,15]. The basic feasibility of the unique 10-K hydrogen/hydride sorption cryocooler was demonstrated at JPL in a series of proof-of-principal experiments in 1991 [16]. Figure 6 shows the breadboard cooler and the successful demonstration of the ability of the cooler to cooldown to below 10 K in under 2 minutes and maintain a detector heat load of 150 mW for over 30 minutes. Based on this successful demonstration, a comprehensive technology development program is now underway to advance the maturity level and mitigate the risks of utilizing this novel technology for spaceflight systems such as BE. The various elements of the development program include component-level characterization and reliability physics investigations, engineering model and protoflight development by industry, and a JPL BETSCE spaceflight technology demonstration experiment scheduled for launch in 1994.

The Periodic Sorption Cryocooler Concept

The operation of the 10-K periodic sorption cryocooler system is based on alternately heating and cooling beds of metal hydride powders to circulate hydrogen in a closed cycle,

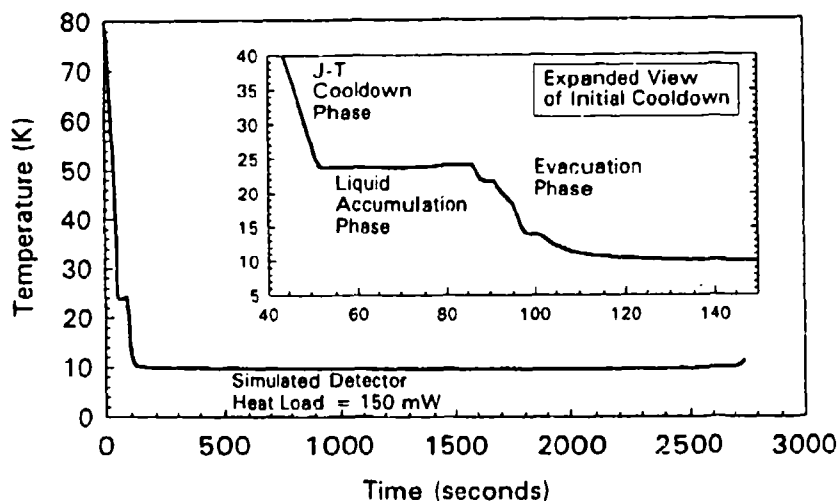
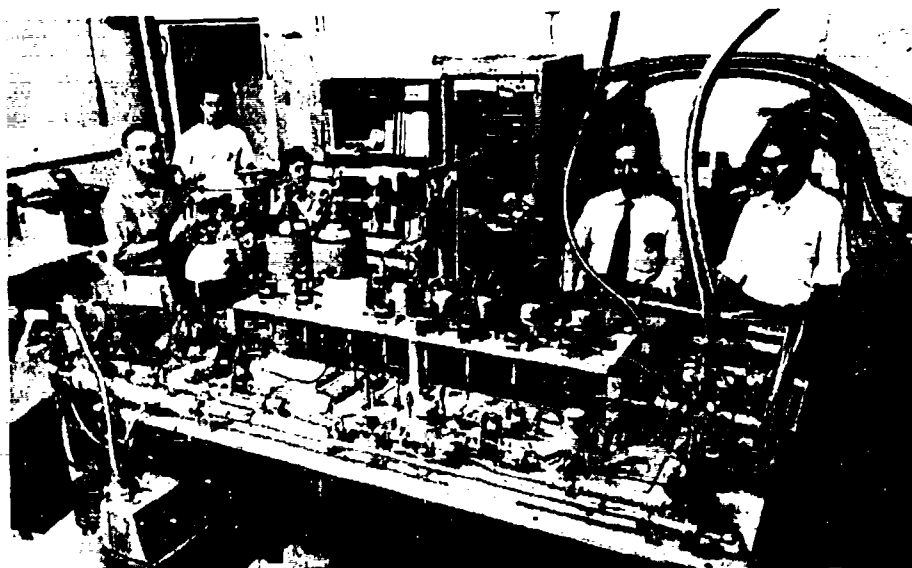


Fig. 6. JPL 10 K sorption proof-of-principle breadboard cooler and test results.

and periodically cool the detector cold head assembly to 10 K on command [14,15,16]. Cooldown to 10 K occurs in two separate steps. First, a valve is opened to release high pressure hydrogen at about 10 MPA (1500 psia) from the storage tank. The hydrogen gas is circulated past a 60-K upper stage -- cooled by second-generation Stirling coolers such as the SDIO SSC coolers or the AIRS coolers -- and then flows through a Joule-Thomson refrigeration loop where it is cooled and partially liquified at 25 to 30 K. The liquid is collected in a wick contained in the cryogen reservoir, and all unliquified hydrogen vapor is absorbed by a hydride sorbent bed. The second cooldown step begins after a sufficient quantity of liquid hydrogen is collected (about 0.5 to 2 g). At this point the J-T flow is stopped and solid H_2 at ≤ 11 K is produced by vacuum pumping the cold head reservoir with a low-pressure sorbent bed. The process is sized to provide sufficient solid hydrogen to absorb the infrared sensor heat load over the required 10- to 30-minute operating period.

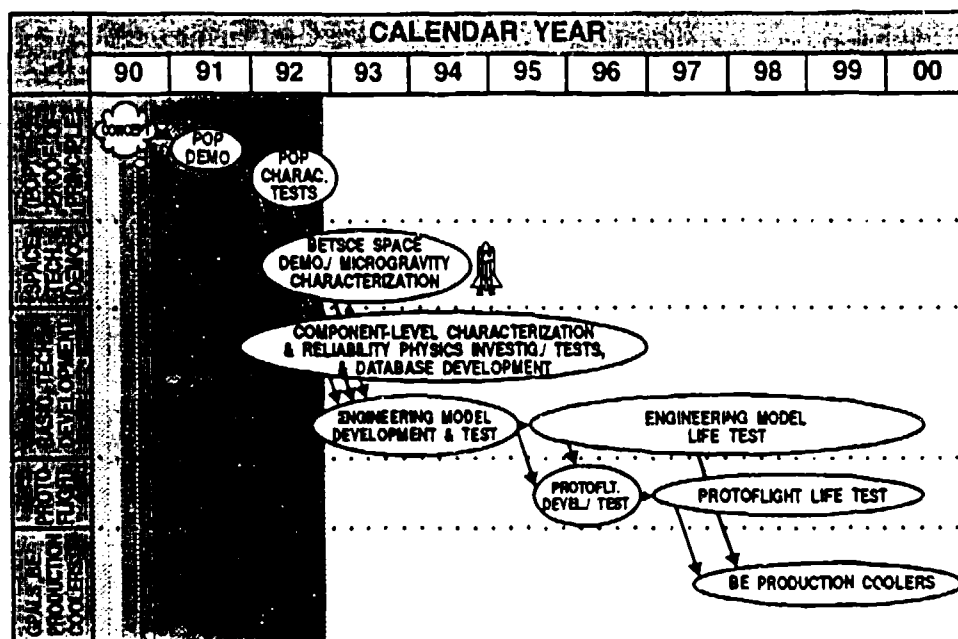


Fig. 7. JPL 10 K sorption cooler development roadmap.

Following the operational period, the cryocooler is recharged by heating the sorbent beds; this drives off the hydrogen and returns it to the storage tank.

JPL 10-K Basic Technology Development Activity

Figure 7 presents a technology development roadmap that shows the evolution from the original periodic 10-K sorption cooler concept, through to BE cooler utilization [16]. The key activities ongoing in 1993 are the Basic Technology Development Activity and the BETSCE Flight Experiment.

Component-Level Characterization and Reliability Physics Investigations. This aspect of the 10-K basic technology development activity is directed at providing the basic technology base required to design and manufacture high reliability 10-K hydride sorption cryocooler stages [16]. A key initial focus is on issues associated with the candidate hydride materials including lanthanum-nickel-tin hydride ($\text{LaNi}_{4.8}\text{Sn}_{0.2}\text{H}_x$) for the upper sorption stage and zirconium-nickel (ZrNiH_x) hydride for the low-pressure sorption stage. Vanadium hydride (VH_x) is also planned to be studied for the upper sorption stage. Specific studies are currently underway to determine the effects of purity and manufacturing techniques on hydride isotherm properties, and to establish requirements for preventing migration and compaction of the hydride power. Other studies are making good progress in characterizing the kinetics and absorption capabilities of fast absorption beds containing phase-change-material (PCM) heatsinks. In addition to the tests associated with the hydride materials, other issues under investigation include the reliability physics of high-strength pressure-vessel container materials, electrical heaters, valves, phase change materials, and candidate cryostat thermal storage materials.

10-K Engineering Model Development. To provide the necessary precursor to eventual flight BE coolers, a flight-like engineering model is scheduled to be contracted to industry in early 1993. The engineering model will be targeted directly to the BE cooling requirements, mission constraints, satellite designs and interfaces. The engineering model effort will include parametric design trade-off studies directed to the performance range needed by system developers. As a result, close cooperation between the BE system developers and the 10-K cooler development team is planned to insure that the engineering model design is faithful to BE needs. Following comprehensive performance characterization testing, the engineering model will be subjected to life testing.

BETSCE 10-K Sorption Flight Experiment

A critical part of the 10-K sorption cooler development effort is the Brilliant Eyes Ten-Kelvin Sorption Cryocooler Experiment (BETSCE) [17]. This Shuttle side-wall-mounted flight experiment, illustrated in Fig. 8, is scheduled for launch in 1994 in conjunction with the Shuttle Pallet Satellite (SPAS III) mission. The BETSCE objectives are to: (1) demonstrate the 10-K sorption cooler technology in a microgravity space environment, (2) advance the enabling technologies and integration techniques by developing an automated, space flightworthy cryosystem, and (3) characterize spaceflight performance and develop the needed flight database to support the planned 10-K flight-cooler development efforts. Key technologies and elements to be characterized include hydride sorbent beds, phase-change materials, heat sinks, heat exchangers and other refrigeration loop components, the cold-

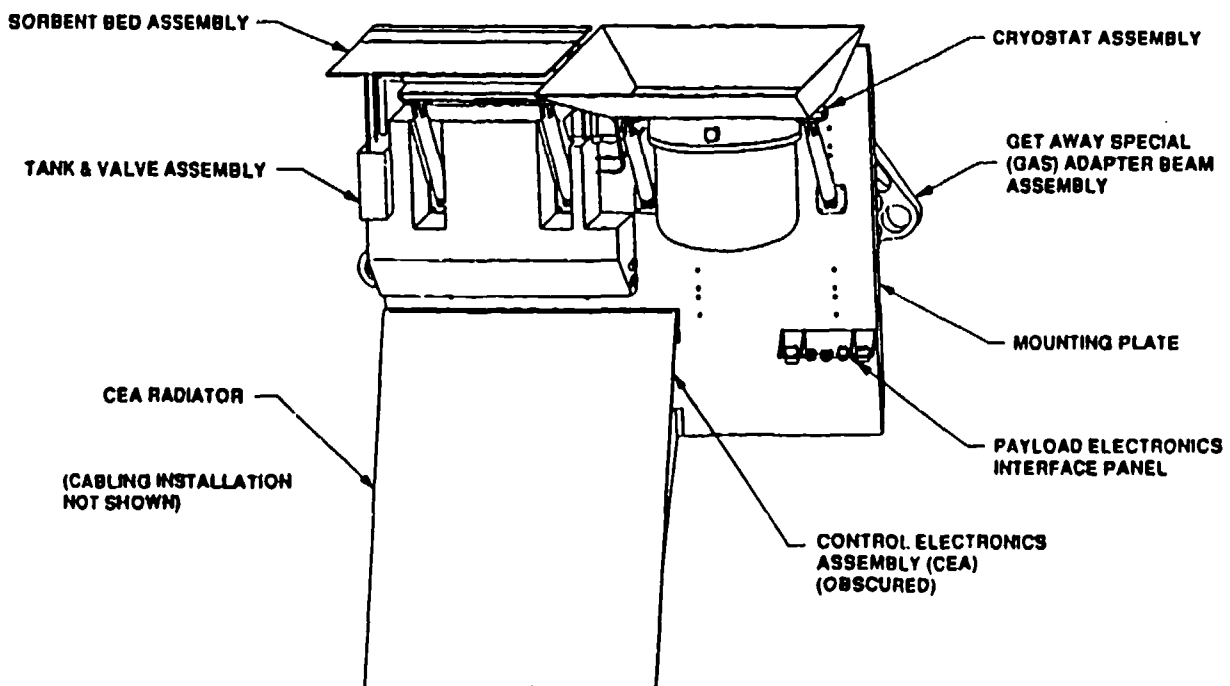


Fig. 8. Brilliant Eyes Ten Kelvin Sorption Cooler Experiment (BETSCE) side-wall mounted in Shuttle bay.

head assembly containing a wicked solid/liquid cryogen reservoir, cycle process controls, and cycle repeatability.

SUMMARY

The growing demand for long-wavelength infrared imaging instruments for space observational applications has led to a rapidly expanding near-term commitment to mechanical cryocoolers for long-life NASA and SDIO space missions. To help ensure the success of these cooler commitments, the Jet Propulsion Laboratory (JPL) has implemented an extensive cryocooler program directed at assisting in the development of advanced cryocooler technologies that successfully address the broad array of complex performance requirements needed. The JPL cryocooler program is making good progress in the characterization and life testing of industry-developed Stirling coolers, the development and test of advanced vibration-suppression systems, the flight test of advanced low-vibration Stirling-cooler systems, and the development and flight test of advanced sorption cooler systems for detector cooling to 10 K.

ACKNOWLEDGEMENT

The work described in this paper was carried out by the Jet Propulsion Laboratory, California Institute of Technology, and was sponsored by the NASA Eos AIRS Project and the Strategic Defense Initiative Organization/Air Force Phillips Laboratory through an agreement with the National Aeronautics and Space Administration.

REFERENCES

1. Ross, R.G., Jr., Johnson, D.L. and Sugimura, R.S., "Characterization of Miniature Stirling-cycle Cryocoolers for Space Application," Proceedings of the 6th International Cryocooler Conference, Plymouth, MA, DTRC-91/002, David Taylor Research Center (1991), p. 27-38.
2. Kotsubo, V., Johnson, D.L. and Ross, R.G., Jr., "Cold-tip Off-state Conduction Loss of Miniature Stirling Cycle Cryocoolers," Adv. Cryo. Engin., Vol. 37B (1991), p. 1037-1043.
3. Ross, R.G., Jr., Johnson, D.L. and Kotsubo, V., "Vibration Characterization and Control of Miniature Stirling-cycle Cryocoolers for Space Application," Adv. Cryo. Engin., Vol. 37B (1991), p. 1019-1027.
4. Johnson, D.L. and Ross, R.G., Jr., "Electromagnetic Compatibility Characterization of a BAe Stirling-cycle Cryocooler for Space Applications," Adv. Cryo. Engin., Vol. 37B (1991), p. 1045-1053.
5. Kotsubo, V.Y., Johnson, D.L., and Ross, R.G., Jr., "Calorimetric Thermal-Vacuum Performance Characterization of the BAe 80 K Space Cryocooler", SAE Paper No. 929037, Proceedings of the 27th Intersociety Energy Conversion Engineering Conference, San Diego, California, August 3-7, 1992, P-259, Vol. 5, pp. 5.101-5.107.

6. Jones, B., "Long Life Stirling Cycle Cooler Developments for the Space Application Range of 20K to 80K", 7th International Cryocooler Conference, Santa Fe, NM, November 17-19, 1992.
7. Hocking, B. and Weir, C., "Development and Space Qualification Testing a Range of Mechanical Cryocoolers", 7th International Cryocooler Conference, Santa Fe, NM, November 17-19, 1992.
8. Johnson, B.G., et al., "Demonstration of Active Vibration Control on a Stirling-cycle Cryocooler Testbed", Proceedings of the American Control Conference, Chicago IL, June 24-26, 1992.
9. Johnson, B.G., et al., "Demonstration of Active Vibration Reduction on a Stirling-cycle Cryocooler Testbed", 7th International Cryocooler Conference, Santa Fe, NM, November 17-19, 1992.
10. Johnson, D.L., Mon, G.R. and Ross, R.G., Jr., "Spacecraft Cooler Characterization", 7th International Cryocooler Conference, Santa Fe, NM, November 17-19, 1992.
11. Ross, R.G., Jr. and Johnson, D.L., "Design and Test of a Comprehensive Facility for Life Testing Space Cryocoolers", 7th International Cryocooler Conference, Santa Fe, NM, November 17-19, 1992.
12. Russo, S. and Sugimura, R., "NASA Cryo System Flight Experiment (CSE)", 7th International Cryocooler Conference, Santa Fe, NM, November 17-19, 1992.
13. Glaser, R., Ross, R.G., Jr. and Johnson, D.L., "Cryocooler Tip Motion Suppression Using Active Control of Piezoelectric Actuators", 7th International Cryocooler Conference, Santa Fe, NM, November 17-19, 1992.
14. Johnson, A.L. and Jones, J.A., "Periodic 10 K Sorption Cooling," USA Patent Pending, 1992.
15. Johnson, A.L. and Jones, J.A., "Evolution of Periodic 10 K Sorption Cooling," 7th International Cryocooler Conference, Santa Fe, NM, November 17-19, 1992.
16. Bard, S., et al., "Development of a Periodic 10 K Sorption Cryocooler", 7th International Cryocooler Conference, Santa Fe, NM, November 17-19, 1992.
17. Bard, S., et al., "10 K Sorption Cryocooler Flight Experiment (BETSCE)," 7th International Cryocoolers Conference, Santa Fe, NM, November 17-19, 1992.

NASA/GSFC CRYOCOOLER DEVELOPMENT PROGRAM

S. Castles, T. Cygnarowicz, R. Boyle, L. Sparr,
R. Cory, F. Connors
NASA/Goddard Space Flight Center
Greenbelt, MD 20771

E. James, R. Fink
McDonnell Douglas Astronautics Corp.
Seabrook, MD 20706

V. Arillo, J. Marketon
Hughes STX, Inc.
Lanham, MD 20706

C. Lee, D. Bugby
Swales and Associates, Inc.
Beltsville, MD 20705

INTRODUCTION

NASA has a number of important earth sciences and astrophysics missions planned that will require long lifetime cryogenic cooling of instruments. Examples include the Earth Observing System (EOS); Thermosphere, Ionosphere, Mesosphere Energetics and Dynamics (TIMED); the Advanced X-Ray Astrophysics Facility (AXAF); High Energy Solar Physics (HESP); INTEGRAL (a gamma-ray astronomy mission); Astromag (a cosmic ray mission); and the Sub-Millimeter Intermediate Mission (SMIM). In addition, new, very long wavelength infrared sensors are under development that will operate at 30 K. One application of such infrared sensors will be used early in the next century on a space-based very long baseline interferometer to search for planets around nearby stars.

To meet the needs of these missions, NASA/Goddard Space Flight Center has established a major program to develop long lifetime, high reliability coolers. The program focuses on contracts with industry to develop space flight coolers. In addition,

an analysis and test program has been established at Goddard to augment the industry development program. This paper will provide a summary of the status of the Goddard contractual efforts and the Goddard analysis and test programs. References are provided to papers that provide more details on particular topics.

CRYOCOOLER DEVELOPMENT CONTRACTS

Three linear Stirling coolers are being developed under contract with industry. A prototype 80 K cooler is under development by the Lockheed/Lucas team and two parallel contracts have been issued to Ball Aerospace and to the Fairchild/Creare team for the development of two-stage, 30 K coolers.

The Lockheed/Lucas 80 K cooler consists of two 15 mm diameter compressors operating on the same compression space and a single 8 mm diameter displacer with a counterbalancer. The cooler incorporates the flexure spring, linear motor configuration originated by Oxford. However, the seals and alignment characteristics are being changed significantly.

At its baseline design point, this cooler will provide 0.8 watts of cooling at 80 K with 30 watts of input power. The cooler is designed to allow a significant variation in the compressor stroke which allows the cooler to operate over a wide range of operating conditions. At the baseline design point, the cooler has a 4.5 mm stroke and operates with a mean working fluid pressure of 6 atmospheres. With a 7 mm stroke and a pressure of 10 atmospheres, the cooler will produce 2.5 W of cooling at 80 K. The cooler has a mass of approximately 13 kg, including electronics. The Lockheed/Lucas team has completed the preliminary design of this cooler. The fabrication of the cooler should be complete by June 1993.

Ball Aerospace has been pursuing the development of Stirling cycle coolers for several years¹ and is now under contract to GSFC to develop a 30 K cooler. This cooler also incorporates the flexure spring, linear motor configuration and is designed to provide no touch contact at the clearance seals. It is a two-stage cooler that has two compressors

¹P. Arter, D. Berry, W. Gully, C. Varner, "Stirling Cryocooler with Dual Opposed Displacers for Space Applications", presented at the 7th International Cryocooler Conference, Santa Fe, NM (1992).

operating on a single compression volume and a single, two-stage displacer with a counterbalancer. The pistons are 21 mm in diameter and the displacer is 16.7 mm in diameter at the first-stage expansion volume and 9 mm in diameter at the second-stage. At its baseline design point the Ball 30 K cooler will provide between 0.3 and 0.4 W of cooling at 30 K with an input power of 75 W. The estimated mass of the machine is 15 kg.

Two-stage coolers are inherently more efficient than single-stage machines at temperatures below 55 K and possibly even at higher temperatures. In addition, a two-stage cooler could provide the same cooling as a single-stage cooler while simultaneously providing cooling to a thermal shield at a higher temperature. Thus, the Ball 30 K cooler could be used over a wide variety of temperatures with only a slight modification to the regenerator. Ball Aerospace has completed the preliminary design of the engineering model cooler and will complete the fabrication of the cooler by May 1993.

The Fairchild/Creare 30 K cooler is a two-stage diaphragm cooler. This cooler is a follow-on to the single-stage Strategic Defense Initiative Office (SDIO)/ Air Force Phillips Laboratories Standard Spacecraft Cooler (SSC) produced by Creare². However, besides being two-stages instead of a single-stage machine, a number of changes have been incorporated. Two are worthy of mention. First, in the SSC design, the two opposed compressors operate on a single compression volume. Creare found that it was difficult to control the motion of the compressor diaphragms at full stroke with this configuration. To eliminate this problem, the 30 K cooler design has two opposed compressors that operate on different working fluid volumes. One compressor is associated with the first-stage expansion volume and one, with the second-stage expansion volume. The Fairchild/Creare team have demonstrated control of compressors with this type of configuration³.

² D. Stacy, J. McCormick, J. Valenzuela, "Development and Demonstration of a Diaphragm Stirling 65K Standard Spacecraft Cryocooler", presented at the 7th International Cryocooler Conference, Santa Fe, NM (1992).

³ C. Konkel, T. Gibboney, L. Van Allen and K. Ha, "Development and Demonstration of an Electronic Controller for a Double-acting Diaphragm Cryocooler, presented at the 7th International Cryocooler Conference, Santa Fe, NM (1992).

The second noteworthy change is in the design of the diaphragm itself. The SSC machine uses a planar diaphragm design while the 30 K cooler uses a half toroid design. The half toroid design has a reduced stiffness and mass for a given stroke. The reduced stiffness and mass can, in principle, reduce the energy losses due to the motion of the diaphragm.

At its baseline design point, the Fairchild/Creare 30 K cooler will produce between 0.3 and 0.4 W of cooling at 30 K with a projected input power of 85 W. The estimated mass of the machine in the flight configuration is between 15 and 20 kg. Fairchild/Creare has completed the design of the engineering model cooler and will complete the fabrication of the cooler by May 1993.

Besides the three Stirling coolers discussed above, Goddard has a contract with Creare, Inc. for the development of a 5 W, 65 K miniature turbo-Brayton cycle cooler. For large Stirling coolers, with a large quantity of heat to reject, the system integration of the cooler within a spacecraft can be problematical. Unless the surface radiating the heat from the spacecraft is located very close to the cooler, either the mass of the thermal link between the cooler and the radiator will be large or the temperature drop through the thermal link will be large. One way around this difficulty is to use a heat pipe. However, a heat pipe can impact system integration and testing. Another possible solution is to use a reverse Brayton cycle cooler in place of a large Stirling cycle cooler. The working fluid of the reverse Brayton cycle cooler can be used to distribute the heat rejected by the cooler. For this reason (and others), large, space-based reverse Brayton cycle coolers have a significant system level advantage over large Stirling cycle coolers.

The development of the Creare reverse Brayton cycle cooler is funded by SDIO and is administered by the Air Force Phillips Laboratories. Details are presented in W. Swift et. al.⁴ An engineering model of this cooler will be completed in 1993.

Table 1 provides a summary of the projected characteristics for these coolers.

⁴ Walter Swift, Herbert Sixsmith, "Performance of a Long Life Reverse Brayton Cryocooler", presented at the 7th International Cryocooler Conference, Santa Fe, NM (1992).

TABLE 1: PROJECTED COOLER CHARACTERISTICS

<u>REQUIREMENT</u>	<u>80 K STIRLING</u>	<u>30 K STIRLING</u>	<u>65 K BRAYTON</u>
TEMPERATURE	80 K	30 K	65 K
COOLING CAPACITY	0.8 W	0.3 - 0.4 W	5 W
INPUT POWER	35 W	75 W	200 W
INDUCED VIBRATION (REQUIREMENT)	.22 NT	0.22 NT	NEGLIGIBLE
VIBRATION GOAL	0.09 NT	0.09 NT	NEGLIGIBLE
MASS (W/O SUPPORT)	13 KG	15 KG	15 KG
LIFE (MINIMUM)	5 YEARS	5 YEARS	5 YEARS
RELIABILITY	0.97	0.97	0.97
DATE AVAILABLE (EARLIEST)	1994	1995	1995

COOLER ANALYSIS AT GODDARD

In reviewing the early efforts by American companies producing coolers, Goddard personnel decided that certain key cooler characteristics deserved detailed analytical studies. The major topics chosen for study by Goddard were the following:

1. The transport of heat from the cooler working fluid to the cooler heat sink.
2. The effect of operating temperature and of temperature gradients within the cooler on the operation of the clearance seals of flexure bearing coolers.
3. The effectiveness of the regenerator for the two-stage diaphragm cooler.
4. The dynamic envelope of the piston and displacer for flexure bearing coolers and the effect of the dynamic envelope on the clearance seal.

These analyses were carried out through a cooperative effort between personnel at Goddard and at Swales and Associates. Many other aspects of the coolers were also studied. However, the areas listed above were chosen for more in-depth study. In the

process, two new analytical tools were created. These two tools and a brief summary of interesting aspects of the analytical results obtained with them are presented below.

Models for Heat Transport within a Cryocooler

The overall efficiency of a cooler can be compromised by a large temperature gradient between the working fluid and the heat sink for the cooler. Thermal analysis programs such as SINDA, a finite element, nodal analysis program, can be used to analyze the thermal conduction through the structure of the cooler. However, it is essential to include the heat distributed by the working fluid in any realistic thermal model of a cooler. Therefore, a coupled thermal/ fluid methodology was developed for building detailed SINDA models of Stirling cycle coolers. The methodology provides the option of using either a steady-state or a transient procedure for simulating the oscillating flow within the cooler, depending upon the modeling precision required. For practical purposes, however, the steady-state procedure is of primary interest because it speeds up SINDA model execution by 1 to 2 orders of magnitude. The steady-state methodology was used to analyze the flexure bearing designs of Hughes, Lockheed/ Lucas, and Ball while the transient procedure was used to analyze the two-stage regenerator in the diaphragm-based cooler design of Fairchild/ Create. The uniqueness of the approach stems from the methods developed to simulate the oscillating flow phenomena.

The first step in the overall procedure is to create a nodal network representing the cooler structure, gas volumes and intervening flow paths. Typically, the structure nodal network involves either a 2-dimensional axisymmetric or a full 3-dimensional discretization. The principle gas volumes are the compression space, the displacer warm end space and the cold expansion space. The main flow path is that which connects the aforementioned gas volumes, although others such as the leakage flow path between the piston and the cylinder can be handled as well. In the steady-state flow modeling procedure, each oscillating flow path is modeled as two separate opposing flow paths in contact with identical structure nodes. The mass flow rate and heat transfer coefficient in each dual flow path are divided by two to ensure mass and energy conservation equivalency to the actual system. The gas nodes in each opposing flow path are connected with "one-way" conductors. In the SINDA code, a one-way conductor is a numerical tool that allows the unidirectional flow of energy between

nodes. The magnitude of the energy flow is $(\dot{m} \cdot C_p \cdot T)$, where \dot{m} is the mass flow, C_p is the gas specific heat and T is the temperature of the upstream gas node. In the transient fluid flow procedure, a single gas node path is used wherein each gas node is connected to the upstream and downstream gas node with two opposing one-way conductors. An approximate mass flow rate calculation procedure is used to determine the flow direction and therefore which of the two one-way conductors is non-zero at each time step during the transient calculation.

To compute the flow conductances between gas nodes, the mass flow rate distribution within the system must be calculated. For the steady-state flow modeling procedure, the average mass flow rate exiting or entering the compression space was computed using the compressor gas temperature, swept volume, minimum and maximum pressures and operating frequency. Obviously these parameters are inputs to the model and must be known beforehand. The mass flow rate distribution is then calculated by assuming isothermal and isobaric conditions along the main flow path up to the warm end of the displacer. Beyond this point, the aforementioned procedure must be modified for the reduction in temperature. For the transient flow modeling procedure, the time-dependent mass flow rates to and from the gas volumes which bound (or intervene) the main flow path are first determined. These mass flow rates represent the flow path boundary conditions. Using mass conservation, the ideal gas law, and the gas node pressure, volume and temperature, the mass flow rate distribution can be computed so that the boundary conditions are satisfied.

The remaining aspects of the methodology involve the calculation of the heat transfer coefficients, the energy dissipation within the system and the coupling of the system to the heat sink boundaries. Due to the dearth of applicable oscillating flow heat transfer data and correlations, the coupling between the gas and structure nodes is based on steady, fully-developed flow correlations that were obtained for geometries which correspond most closely to the cooler flow path geometry being simulated. The energy dissipation involves the allocation of the work of compression, the I^2R heating, the heat from the body being cooled and the parasitic heating (assumed negligible). The cooler interface was modeled by coupling the compressor and expander structures to a constant temperature heat sink boundary based on the contact area and the appropriate contact conductance.

Results of Heat Transport Calculations

Three flexure bearing, Stirling cycle cooler designs were analyzed with the steady-state thermal/ fluid SINDA model. In each case the most interesting results were associated with transferring the heat from the working fluid to the cooler interface with the instrument. In particular, the model was used to study the effectiveness of designs for heat exchangers acting between the working fluid and the cooler structure. It was found that careful design of such heat exchangers could improve the efficiency of coolers.

This thermal/ fluid SINDA modeling technique was also applied to the two-stage Fairchild/ Creare diaphragm cooler. The most interesting analysis was performed on the two-stage counterflow regenerator. A transient analysis produced quasi-steady-state temperature swings at each gas node and structure node within the regenerator. The temperature swings, which provide a measure of the regenerator effectiveness, were acceptably small.

Dynamic Envelope Model

The lifetime and reliability of a flexure bearing cooler is dependent on the proper functioning of the clearance seal at the piston and displacer. The clearances at these seals can be as small as 5 to 10 microns. The dynamic excursions of the piston and displacer can cause the piston or displacer to contact and rub the seal at one or more points during each cycle of the cooler. Such touch contact at the clearance seal during operation of the cooler can decrease the lifetime and reliability of the cooler.

GSFC and Swales and Associates have successfully developed analytical tools to analyze the dynamic envelope of the piston and displacer for a flexure bearing Stirling cooler. In a flexure bearing Stirling cooler design, the piston and displacer are subjected to nonlinear fluid and structural interactions. Specifically, the flexure spring suspension system exhibits nonlinear stiffness and the motion of the piston interacts with the working fluid and exhibits nonlinear squeeze film damping and axial differential pressure forces. To create an effective modeling tool for studying the dynamic envelope on the piston and displacer, mathematical formulations for the fluid dynamics behavior

and the structural dynamics were performed separately. Those formulae were then coupled with a lumped mass dynamics model of the structure to simulate the dynamic response of the moving parts.

In developing the fluid dynamics model we started with the three-dimensional Navier-Stokes equations for laminar, incompressible flow. The parabolic velocity profiles were derived from the momentum equations. By integrating the continuity equation and substituting the velocity profile into this process, a partial differential equation for the pressure was derived as a function of the gap between the piston and cylinder, the lateral velocity of the piston and the position of the flow. The pressure distribution was then integrated circumferentially and axially to obtain the restoring force and moment acting on the piston. To solve the governing partial differential equations requires a numerical solution. Since the solution process is computationally intensive, it is not well suited for incorporation into a structural dynamics model. Therefore, we wrote a program to solve the partial differential equation numerically and then performed regression analysis on the numerical results. This allowed us to model the fluid dynamics with simple algebraic equations. These equations were a function of the motion of the center of gravity of the piston.

In deriving the structural dynamics model we started with a detailed NASTRAN model for the suspension (the flexure spiral springs). We performed a nonlinear static analysis to determine both the axial and lateral stiffness of the spring. The numerical results were then curve fitted with polynomial equations as a function of the axial displacement of the piston. We then derived equations of motion by the force equilibrium method and used variational methods to reduce the multi-degree-of-freedom structure down to a 2 or 3 degree-of-freedom system of linear differential equations. The governing equations of motion incorporate the nonlinear stiffness for the suspension system and the fluid forces as a function of the motion of the piston. The system of differential equations was then solved numerically to determine the response of the structure. The amount of lateral motion of the piston and the reaction forces at the piston interface can then be recovered as a function of time from the transient analysis.

Results from Dynamic Envelope Calculations

This analytical approach allows us to efficiently model the interaction between the fluid and structure. The dynamic envelope of the piston and displacer of several flexure bearing cooler designs has been analyzed. Studies have been performed on the response due to various effects such as unbalanced motor forces; lateral and angular misalignment; suspension stiffness; 1-g field effects; cg location; and various piston designs such as smooth pistons, stepped pistons, and grooved pistons.

Early results indicated that some coolers would have difficulty operating horizontally in a 1-g environment. However, the modeling indicated that, with proper cooler design, clearance seals could be made to operate properly under the influence of 1-g applied horizontally to the cooler.

More recently, the model has been used to study the effects of various initial misalignments between the piston and the cylinder and between the displacer and its surroundings. The model indicates that if the piston or displacer is translated parallel to the centerline of the cylinder (but not tilted relative to the centerline) the effect on the dynamic envelope of the piston and displacer is small. Therefore, the alignment requirement for this type of misalignment is not too severe.

Unfortunately, the effect of angular misalignment on the piston is more severe. Initial tilt misalignment of the piston was studied for three cooler designs. It was found that even with good design practices, the angular misalignment between the centerline of the cylinder and the piston had to be initially aligned to within 10's of microradians. If this alignment is not maintained, the pressure of the working fluid on the reciprocating piston will drive the piston into the surface of the clearance seal. The largest gas forces will occur when the largest pressure gradient exists across the piston, which occurs at the end of the compression stroke. Thus, the largest radial deflections occur during operation at full stroke. The associated angular alignment requirement results in the most severe alignment requirement known for the flexure bearing coolers. Our modeling also indicates that the effect of angular misalignment can be made even worse by improper design of the compressor.

STIRLING COOLER VIBRATION CONTROL SYSTEM

One of the challenges in applying coolers to science instruments has been to reduce the cooler reaction forces to a level that does not degrade the performance of the instrument. The level of force that will be acceptable to a science instrument varies widely with the instrument's design, but has been estimated to be on the order of 0.1 to 1.0 Newtons for many instruments. This level is lower than Stirling cycle coolers produce without a vibration compensation system.

Tests on Stirling coolers indicate that when the operating parameters of the cooler have reached equilibrium, the harmonic content of the cooler vibration is very stable with time. Thus, since cooler operating conditions only change slowly with time, the control system does not need to be fast or operate real-time.

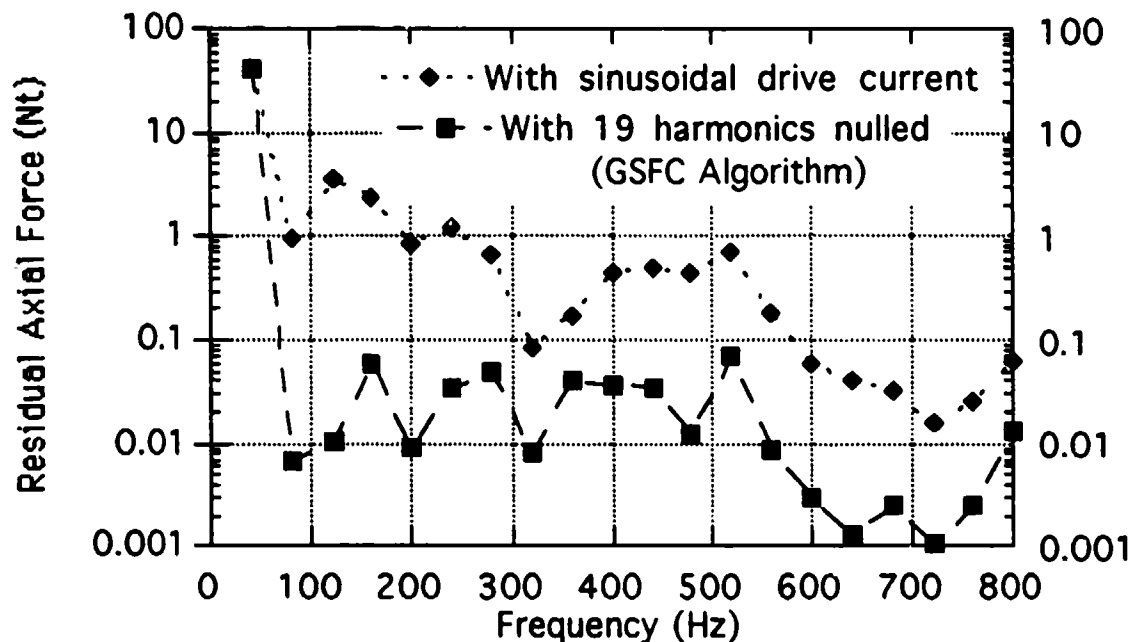
A simple technique using these cooler operating characteristics has been developed by GSFC for vibration control of linear Stirling cycle coolers. This technique takes advantage of the very stable harmonic content of the vibration forces by using simple signal processing and non-real-time control of the harmonic content of the drive signal. Laboratory testing of this technique has shown it to be very effective.

Experimental Results

The control system has succeeded in reducing the cooler reaction force to below our goal of 0.09 NT for each of the coolers to which it was applied. The number of harmonics controlled has varied but control of up to 20 harmonics has been demonstrated. Typical results are presented in Figure 1. Essentially all of the residual vibration occurs at the harmonics of the operating frequency. Therefore, only the response at each harmonic is plotted. The lines connecting the residual vibration at each harmonic are provided only as a guide to the eye. Since essentially all of the residual vibration occurs at the harmonics, the root-mean-square vibrational equivalent to the results shown in Figure 1 is very small. More details of the experimental results and observations are presented in L. Sparr et al.⁵ A description of the theoretical basis

⁵ L. Sparr et. al., "NASA GSFC Cryocooler Test Program Results", presented at the 7th International Cryocooler Conference, Santa Fe, NM (1992).

Figure 1. British Aerospace Compressor
Residual Axial Vibration At Each Harmonic



for the control system is presented in R. Boyle et. al.⁶ The control system is presently implemented on a desktop computer system. However, GSFC has defined a readily available flight-worthy chip set that could be used to implement the control system.

To summarize, a simple control system has been constructed for Stirling cycle coolers that takes advantage of the stable operating characteristics of the machines. Testing has confirmed that axial forces below 0.05 N can be achieved at each of the harmonics for representative coolers.

GSFC STIRLING COOLER TEST PROGRAM

The GSFC has developed a unique cooler test facility that allows for the complete characterization of a Stirling cooler under simulated on-orbit conditions. This facility is incorporated into a large vacuum chamber that is mounted directly to a vibration isolation pad like a bell jar. That is, the coolers to be tested can be mounted directly to

⁶R. Boyle et. al., "Harmonic Vibration Control System for a Cryogenic Refrigerator", presented at the 7th International Cryocooler Conference, Santa Fe, NM (1992).

the isolation pad within the thermal/ vacuum environment. Each cooler is mounted to its own unique 6-axis force dynamometer in this vibrationally quiet environment so that minute changes in the cooler induced vibration can be detected. The "ambient" operating conditions of the cooler can be controlled at any temperature down to approximately 225 K with a chiller system. The heat load on the cold finger of the cooler is controlled with a heater. Thus, the cooler can be operated under a wide variety of environments while precise operating conditions are maintained and measured.

GSFC has performed an extensive series of tests on unbalanced coolers produced by British Aerospace and Lockheed/ Lucas and on balanced coolers produced by Stirling Technology Inc. and Hughes Aircraft. A summary of the results from this test program is presented in Richard L. Sparr et. al.⁵ and G. Fink et. al.⁷ These results include the load curves and power input; the axial and lateral vibration both with and without an active vibration control system; vibration as a function of body temperature; measurements of the stability of cooler parameters over time, including cold finger temperature and residual vibration with a reference waveform; and effects of gas pressure on the load line.

The results from these tests are too extensive to be reproduced herein. However, many features have been observed. One interesting feature is the importance of the DC offset to the operation of flexure bearing coolers. The DC offset controls the axial centering of the piston within the cylinder. The DC offset has been observed to change significantly with time or with a change in the environmental parameters. Also, a change in the DC offset has a significant effect of the cooler operating parameters and its residual vibration.

As a result of this observation, the GSFC has added DC offset control to the electronics used to control the coolers during testing. This addition was found to be necessary to prevent changes in the DC offset from masking the measurement of other interesting but more subtle changes. Such changes may be indicators of changes occurring within the cooler that could effect the lifetime and reliability of the cooler. It is particularly

⁷ Richard G. Fink et. al., "Thermal, Vibration and Reliability Test Results for a Stirling Technology Company 80 K Cryocooler", presented at the 7th International Cryocooler Conference, Santa Fe, NM (1992).

important to be able to observe such changes during a cooler life test. These life tests will be conducted over at least 5 years. It is critical that we be able to observe changes that may occur within the coolers during this life test. Flight programs desiring to use coolers can not wait years before knowing whether or not a cooler is flight-worthy. Therefore, these life tests must be conducted under precisely controlled conditions and with sophisticated thermal and vibration measuring systems.

SUMMARY

NASA/GSFC has on-going contracts for the development of four space-borne coolers: one 80 K and one 30 K flexure bearing Stirling cycle cooler; one 30 K diaphragm-based Stirling cycle cooler; and one 65 K reverse Brayton cycle cooler (funded by SDIO and monitored by AF Phillips Labs). The cooler manufacturers are presently fabricating piece parts for these coolers. All the coolers are engineering models except the Lockheed/ Lucas 80 K cooler, which is a prototype model. The coolers will be fabricated and performance tested at the manufacturer's plant by the summer of 1993. It is anticipated that these coolers will be of sufficient quality that meaningful life tests can be performed on them.

An extensive GSFC cryocooler analysis program has successfully modeled the key structural and thermal characteristics of several linear Stirling cycle coolers that are presently being developed under contract to the US government. In addition, GSFC has developed a simple vibration control system that has demonstrated the capability to reduce the residual vibration from these linear Stirling cycle coolers to less than 0.05 N.

Goddard has performed an extensive series of tests on existing single-stage breadboard coolers to prepare for the life testing of engineering model and prototype model coolers. Sensitive measuring systems will be used during the life tests to detect any degradation within the coolers. When combined with the extensive analysis performed on these coolers, the life test should clearly demonstrate the lifetime and reliability of the coolers.

DEVELOPMENT AND DEMONSTRATION OF A DIAPHRAGM
STIRLING 65 K STANDARD SPACECRAFT CRYOCOOLER

D. STACY, J. McCORMICK, J. VALENZUELA
CREARE INC.
HANOVER, NH 03755

INTRODUCTION

Performance requirements for the SDIO/Air Force 65 K Standard Spacecraft Cryocooler (SSC) focus upon 2 Watts of net cooling capacity at 65 K over 10 years of continuous operation, with 95% system level reliability at the 95% confidence level. Input power requirements are limited to 30 Watts at the 28 volt DC spacecraft bus per Watt of net cooling capacity. Vibration control requirements limit maximum force transmission to the spacecraft to less than 0.02 newtons on any axis and motion of any portion of the cryocooler surface to less than 25 microns. Mass and physical envelope of the SSC system were to be minimized. The 65 K SSC is required to survive the launch vibration environment at qualification test levels as an element of its 95% reliability requirement. Controls are required to provide autonomous operation with temperature stability of 0.1 K over 24 hours following a single operator command to start. Minimum required instrumentation included cold end and warm end temperatures, system mean pressure, vibration, and input and heater power.

The Creare 65 K SSC design employs metal diaphragm displacement volumes in the expander and compressors. This approach eliminates the need for running seals of any kind, provides a passive and robust suspension for reciprocating members, and promotes working volume heat transfer. The regenerator is a simple annular channel geometry which operates always in the laminar flow regime. This design is straightforward to analyze and to fabricate and provides excellent thermodynamic performance. Figure 1 illustrates the gas volume boundary defined by the working volume diaphragms and annular regenerator. The expander diaphragm and attached "flying" regenerator tube, fashioned of Ti-6Al-4V, are shown in Figure 2. The flexible diaphragm web is thickness contoured to smoothly distribute the 90 MPa peak stress incurred from stroking deflection and differential pressure loading.

General design features of the diaphragm type SSC are described in a previous paper [1]. Major components of the SSC are shown in exploded fashion in Figure 3, with 2 fully assembled compressor modules in front of their constituent components. Components wetted

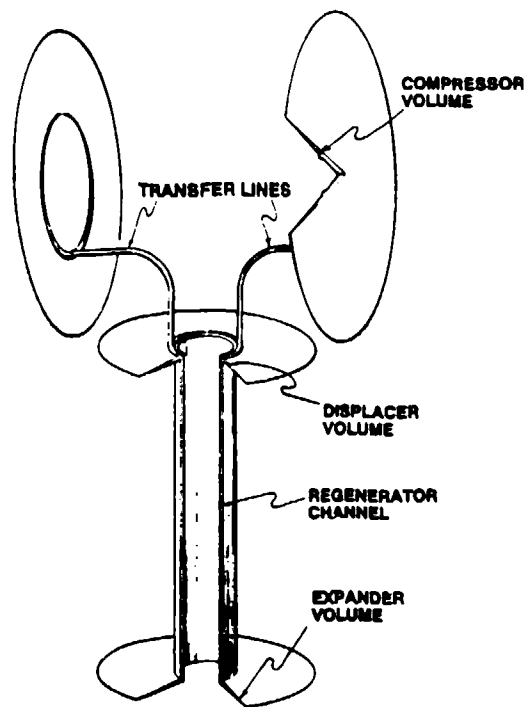


Figure 1. DIAPHRAGM CRYOCOOLER GAS ENVELOPE

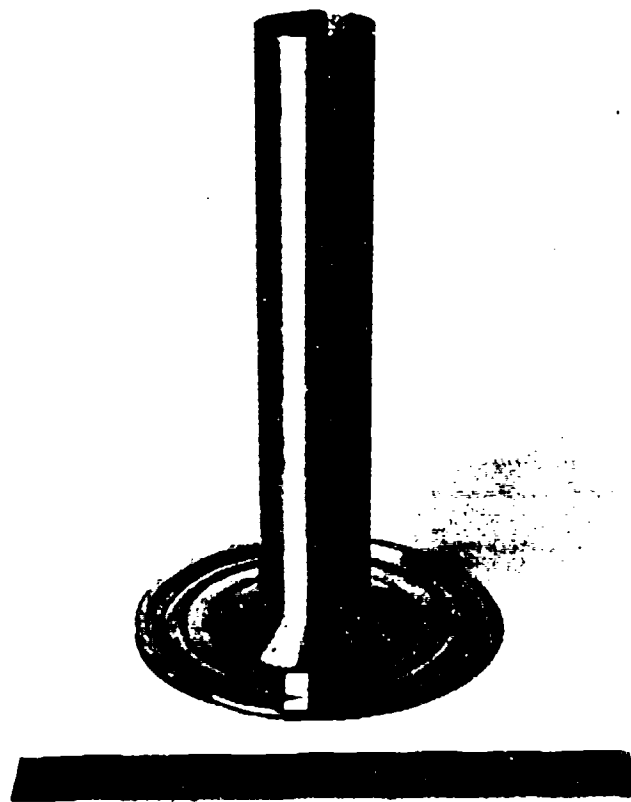


Figure 2. FLYING TUBE/EXPANDER DIAPHRAGM SUB-ASSEMBLY

by the helium working fluid are constructed entirely of titanium alloys or cobalt iron, and the system pressure boundary is hermetically sealed by furnace brazed and e-beam welded joints. The relatively large diameter of the thin walled regenerator tubes results in very high cold finger radial stiffness and strength, with safe loads exceeding 100 Nt. Stator coils for the compressor and displacer linear electromagnet motors are located outside the hermetic gas envelope and may be replaced easily if required by removing the back iron piece from the three piece laminated iron stator core assembly. This construction is shown in Figure 4.

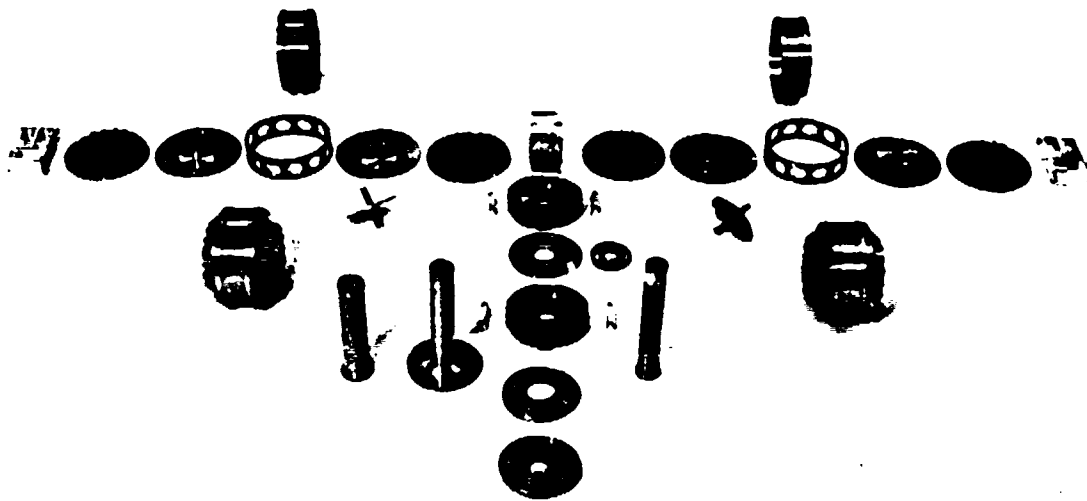


Figure 3. SSC COMPONENTS

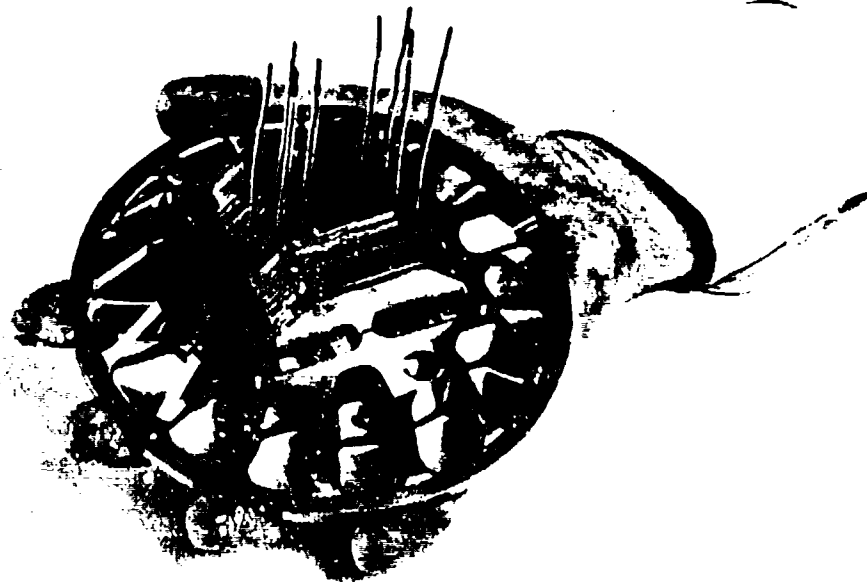


Figure 4. SSC COMPRESSOR HEAD AND MOTOR STATOR

ENGINEERING MODEL SSC

Total mass of the engineering model SSC system is 17.6 Kg. Mechanical cooler mass is 11.9 kilograms as built and fully instrumented. Mass of the electronics module is 5.7 kilograms without an enclosure box. The complete cryocooler system, with cold end vacuum bonnet for stand alone testing, is shown in Figure 5. Electronic interface consists of 28 volt DC supply and ground cables and an RS-232 interface cable to the control computer. All deliverable instruments defined in the performance requirements communicate over the RS-232. Additional instruments such as dynamic pressure transducers, redundant temperature sensors, and auxiliary position sensors employed during shakedown and diagnostic testing are separately cabled to a pc-based data acquisition system. A 3 point soft mount system is used for characterization testing of the engineering model to allow vibration measurement via accelerometers on the compressor and expander axes.

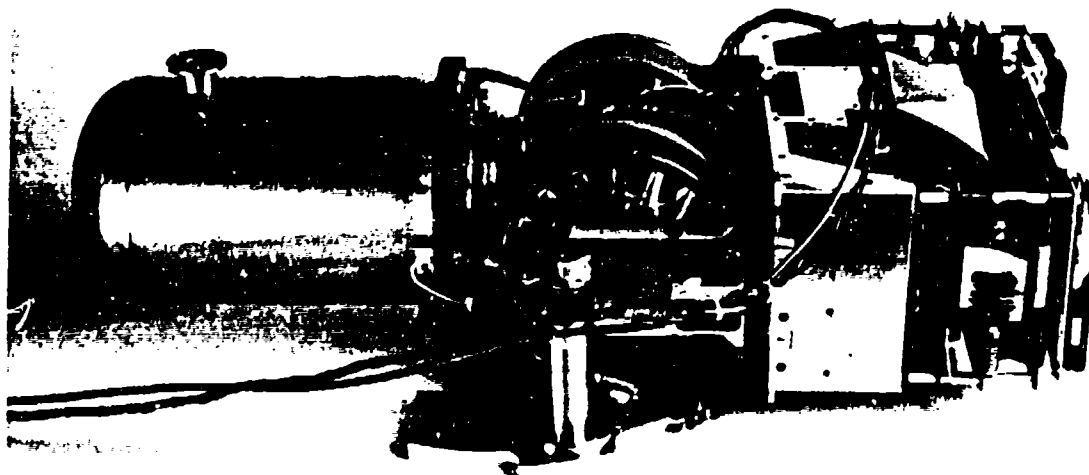


Figure 5. 65 K SSC ENGINEERING MODEL

Waste heat is sunk from the warm end of the cooler system by conduction to thermal straps, with the strap warm ends sandwiched between the mechanical cooler and the electronics base plate. The heat sink for engineering model testing is provided by a copper water-cooled heat exchanger, visible in Figure 5. The conductive thermal interface at the cold end is provided by a flat annular surface on the expander head with a drilled and tapped bolt circle for securing a thermal strap, as shown in Figure 6. During engineering model testing, a copper ring with a DC load heater and embedded silicon diode temperature sensors was bolted to this surface with a thin indium gasket to promote thermal conductance. Pressure and position transducers provided indicator diagram test data.

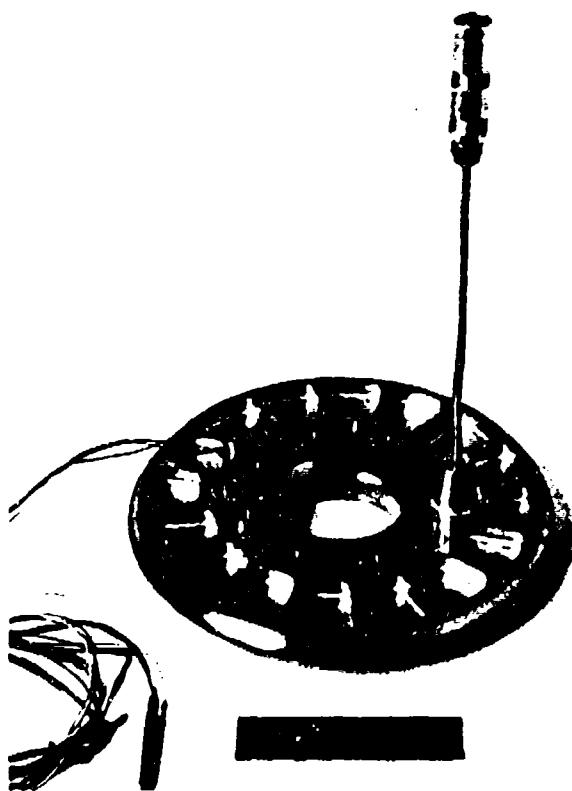


Figure 6. EXPANDER COLD STRAP INTERFACE

Eighteen layers of perforated and crinkled double-aluminized mylar cover the regenerator and expander to shield against radiation parasitics. The expander MLI is closed around the cold end load heater and projecting transducers during engineering model testing, as shown in Figure 7, and would be opened to interface with detector shielding when integrating the cooler with an instrument. An internal shield system prevents radiation heat leak down the open bore of the annular regenerator. A thin walled quarter inch diameter G-10 structural tube on the

regenerator axis supports disks of aluminized mylar to retard radiation down the axis of the regenerator. Electrical leads from cold end instruments and the thermostatically controlled trim heater pass up through the bore of the G-10 tube and through a hermetic pass-through at the warm end of the machine, eliminating the need for instrument lead passthroughs in the vacuum enclosure. Heat leak down these leads is included in the measured parasitics. The engineering model machine was tested both with the vacuum bonnet, as illustrated in Figure 5, and immersed in an environmental vacuum chamber with the bonnet removed. In both cases, parasitic measurement confirmed that radiative heat load to the cold end was less than 50 milliwatts at vacuum levels of 10^{-5} torr.

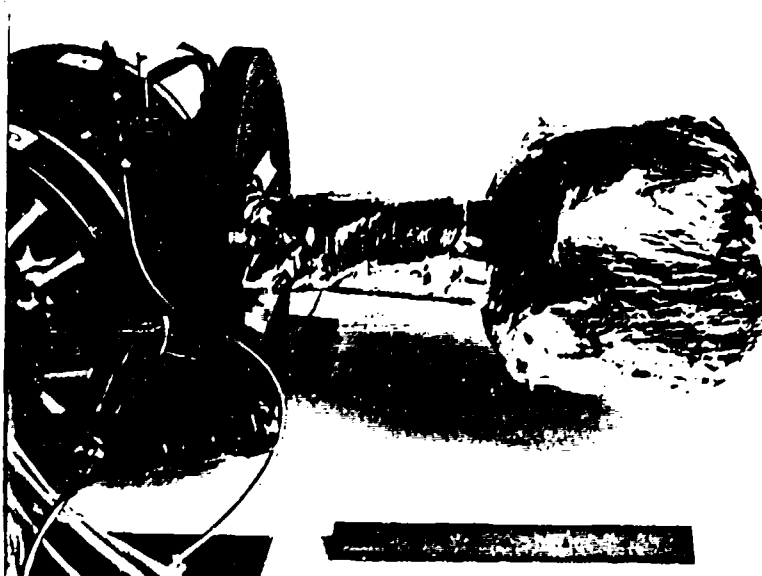


Figure 7. SSC MLI SYSTEM

TESTING

Testing to date has focused upon shakedown and diagnostic testing at the 65 K design point temperature and lower. Cooldown times from 300 to 65 K at no load are about 4 hours. Total parasitics, inferred from the measured power-off warmup rate, are 1.0 Watts at 65 K and are dominated by regenerator conductive heat leak. Figure 8 displays a cooling load curve generated during parametric testing, showing 0.77 Watts of net cooling at 65 K and 0.33 Watts at 55 K.

Shakedown testing uncovered a physical instability mechanism inherent in the machine design and not anticipated in the design of the motor control electronics. The gap⁻¹ force characteristic of the compressor motors is well matched to the volume⁻¹ pressure characteristic

of an isothermal compression process. Two non-linear electromagnet motors compressing a common gas volume however exhibited a coupled system instability, wherein an armature which gets ahead of its mate retards its mate through increased pressure in the shared gas volume and drifts over several cycles to head contact. Design of the controls architecture had not anticipated this mechanism and did not include adequate feedback response to control it. Shakedown testing to date, as typified by Figure 8, has subsequently been constrained to conditions of reduced frequency and discontinuous volume cycles to provide stable operating conditions.

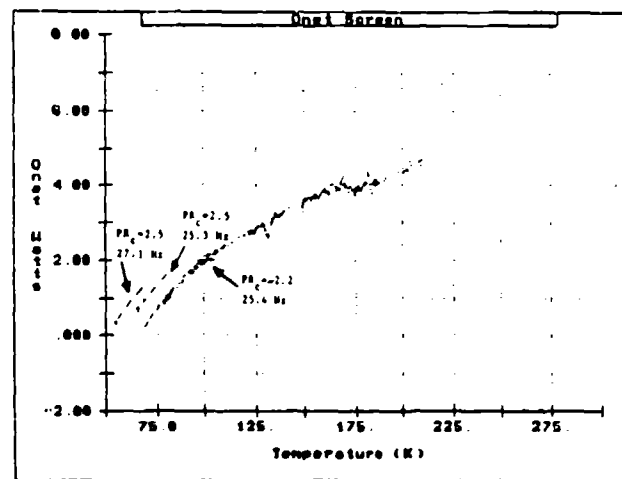


Figure 8. SSC SHAKEDOWN TEST LOAD CURVE

CONTROLS

The reciprocating diaphragm assemblies of the SSC have a fundamental frequency substantially higher than the 30 Hz operating frequency. The electromagnet motors therefore pull as motors from the diaphragm neutral position to top dead center and then act as generators to provide controlled relaxation from top dead center back to neutral. The unidirectional motors are arranged in opposed pairs to provide diaphragm motion on both sides of neutral, with each motor operating on a nominal 50% duty cycle. The motor drive circuit is a capacitive discharge architecture, with MOSFET switching controlled by a timing diagram. MOSFETs are individually timed to allow compensation for variations in as-built motor inductance. A pre-charged drive capacitor is fired through the motor coils to power the pull of the diaphragm mounted armature to top dead center. The coil circuit is then switched to a regenerative capacitor which absorbs the coil current during the quarter cycle of relaxation from top dead center to neutral. Charge thus absorbed by the regenerative capacitor is

subsequently returned through a voltage boost circuit to the drive capacitor during the motor's off-duty cycle. The drive capacitor charge is topped off by a front end power supply which modulates the bus voltage as required. This power supply switches amongst the various drive capacitors and provides buffering such that current demand ripple on the spacecraft power bus is limited to less than 10%. This architecture manages the reactive power or circulating work inherent in Stirling cycle compressors by resonant tuning of the circuit capacitance to the motor inductance rather than by the more conventional mechanical resonance approach.

The engineering model SSC electronics utilized an integrating controller on top dead center position to control the energy supplied to the drive capacitor during each charge cycle. Top dead center position was measured with passive flux sensing coils on each motor stator. This control approach resulted in maintenance of steady pre-charge voltage on the drive capacitors and produced very stable operation of individual compressors right up to gentle contact of the diaphragms against the heads, determined audibly by feeding an amplified accelerometer output through a bass speaker.

Coupled operation of dual compressors at full stroke proved unstable with this relatively slow control system response. Efforts to implement PID controllers with faster response to modulate drive capacitor charge voltage proved unsuccessful. A performance test was therefore run by driving only one of two compressors, with the transfer lines to the inactive compressor valved off. A minimum temperature of 81 K was achieved in this half compressor condition, and the load curve is shown in Figure 9.

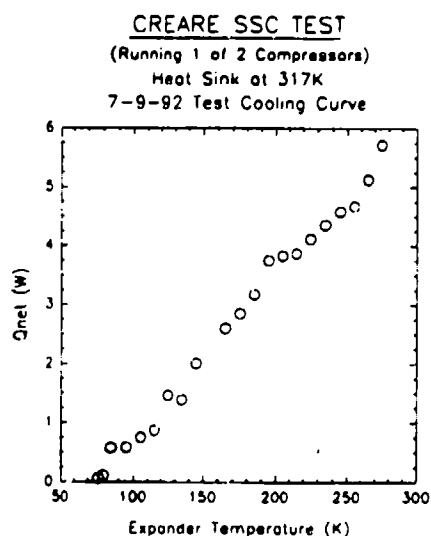


Figure 9. SSC LOAD CURVE WITH 1 (OF 2) COMPRESSOR

Improved controls were developed under IRAD funding to enhance the speed and precision of control of the basic capacitive discharge power circuit. An enhanced position sensor was developed by switching in the coils in the off-duty motor as one element in an oscillator circuit. Variations in the off-duty motor gap altered the inductance coupled to the motor coil and modulated the frequency of the oscillator circuit output around a 10 kHz average rate. From this position signal, a top dead center error signal was generated which in turn closed two control loops. One modulated drive capacitor pre-charge voltage through an integrator control as before to insure adequate voltage to drive the diaphragms slightly beyond the top dead center set point. The second control loop opened the motor drive MOSFET when the diaphragm reached the top dead center set point to prevent overstroking and head contact. The IRAD electronics thus added feedback control of switch timing on top of voltage servocontrol. These electronics were first used to drive a single large breadboard diaphragm compressor plumbed to the SSC expander through temporary transfer lines. Testing in this mode produced 0.50 Watts of net cooling at 65 K.

The IRAD electronics were subsequently employed to drive the dual compressor baseline SSC cryocooler during shakedown testing. Control stability was substantially improved over the engineering model electronics, but stable operation required reducing drive frequency to 25 HZ and introducing discontinuous compressor motion, dwelling briefly at mid-stroke twice during each cycle. This discontinuous motion is reflected in the compressor pressure waves illustrated in Figure 10, recorded by the data system during shakedown testing at 78 K. Maximum performance achieved under these operating conditions was 0.77 Watts of net cooling at 65 K. The architecture of the IRAD electronics did not allow for measurement of a meaningful input drive power during testing.

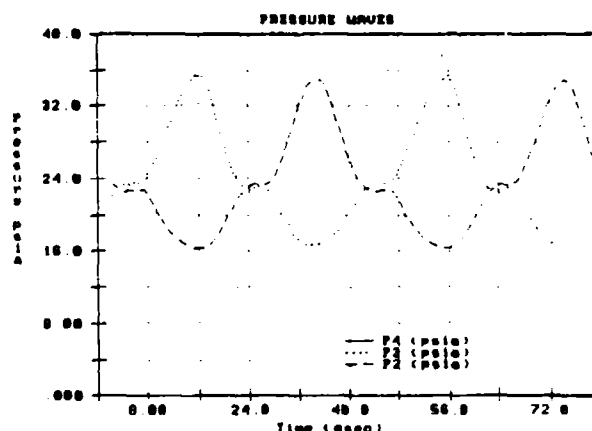


Figure 10. COMPRESSOR PRESSURE WAVES

Development of an alternate drive and control architecture electronics set is currently underway. The capacitive discharge architecture has been replaced by power amplifiers to provide more voltage headroom at TDC for managing the tendency of coupled compressors with electromagnet motors toward system instability. A wide bandwidth position feedback control loop is employed to manage motor force throughout the displacement cycle. Position sensing is based on motor inductance, which varies with the motor gap and hence diaphragm position. Preliminary SSC testing with this electronic set is anticipated in December, 1992.

SUMMARY

The diaphragm 65 K SSC has demonstrated 0.77 Watts at 65 K and 0.33 Watts at 55 K during shakedown testing. Measured parasitics agree well with calculated values. The SSC has proven mechanically robust and trouble free over approximately 100 hours of shakedown and testing. Measured performance data has provided excellent validation of the thermodynamic code used in design of the SSC. Controls development is in progress to allow stable operation at design point test conditions. Delivery of the SSC to JPL for verification testing is expected during the first quarter of 1993.

ACKNOWLEDGEMENTS

Development of the SSC is funded by the Strategic Defense Initiative Organization and managed by the Air Force Phillips Laboratory. We wish especially to express our gratitude to Captain Peter Thomas and Mr. Tim Moran of Phillips Lab for their support and encouragement throughout this program.

REFERENCES

1. Stacy, W.D.; *A 10 Year Life 65 K Stirling Cryocooler for Satellite Sensor Applications*; Proceedings of 6th International Cryocooler Conference, Plymouth MA, Oct. 1990.

STIRLING SPACE COOLER

C.K. CHAN, M. LOPEZ, J. RAAB, E. TWARD

TRW INC.
APPLIED TECHNOLOGY DIVISION
ONE SPACE PARK
REDONDO BEACH, CA 90278

G. DAVEY

UNIVERSITY OF OXFORD
DEPARTMENT ENGINEERING SCIENCE
PARKS ROAD
OXFORD OX1 3PJ

INTRODUCTION

We have designed, built, and tested an engineering model of a miniature integral Stirling cooler intended for long-life space application. The nonwearing design incorporates clearance seals maintained by flexure springs for both the compressor and the drive displacer. The design achieved the performance goal of 0.25 watt at 65 K. A vibrationally balanced engineering model version of this cooler giving 1 watt of cooling at 120 K is now in fabrication intended for the Shuttle Pallet Satellite III (SPAS III) flight experiment and will be flown on the High-Temperature Superconductivity Space Electronics ? (HTSSE 2) flight experiment.

Cryogenic cooling of sensors on spacecraft imposes exceptionally demanding requirements on mechanical coolers due to the high cost associated with launch into space. As a result of these costs, exceptional reliability, long-life, and minimum input power and cooler weight are especially valuable attributes for a space cooler. The potential for very long-life Stirling coolers became a reality at Oxford University^{1,2} with the incorporation of gas clearance seals maintained by flexure bearings into both the compressor and displacer of the Oxford Stirling cooler designed for the NASA/ISAMS instrument on the UARS satellite. This mechanically simple clearance seal technology eliminated wearing parts and hence the need for lubricants in the cooler, removing two major degradation and failure mechanisms found in mass-produced tactical military coolers. In addition to the inherent reliability designed into the cooler, the clearance seal technology results in linear motor driven compressors operating efficiently at the mechanical resonance of the compressor piston on its gas spring. Resonant operation of the compressor minimizes the amount of power required, resulting in a lower weight machine.

A pair of these Oxford Stirling coolers launched on September 26, 1991, on the UARS satellite have performed as designed since that time through a number of on-off cycles both planned and necessitated by instrument problems.

In this paper we describe the next generation of fully vibrationally balanced, miniaturized, low-power space coolers designed for use on small satellites.

DESIGN APPROACH

Small Stirling cryocoolers operating at cryogenic temperatures are thermodynamically inefficient devices. The coefficient of performance of an ideal (Carnot) refrigerator pumping heat from a low temperature, T_L , to a high temperature, T_h , is given by $T_L/(T_h - T_L)$. That is, for W watts of input power one can at best get $WT_L/(T_h - T_L)$ watts of cooling power. Real Stirling cryocoolers are not ideal refrigerators and in fact do not even operate on the Stirling cycle. Typical, small Stirling cryocoolers pumping heat between 80 and 300 K achieve < 7% of Carnot efficiency at the power input terminals to the typical compressor. If one looks at the process efficiency, i.e., the net cooling power relative to the pressure/volume (PV) work delivered by the compressor, an efficiency no better than 9.2% of Carnot for 80 to 300 K heat pumping can typically be achieved. This results from the fact that cryocooler losses dominate performance since 90% of the delivered PV work (or machine shaft power) is lost in the device. As the cooler gets smaller, internal losses use up an increasing fraction of the total gross cooling power.

Miniaturization and efficiency in this small cooler are achieved by using an integral cooler configuration rather than the previous split configuration, resulting in reduced pressure loss and less dead volume between the compressor and cold head. The design required that both the compressor and displacer be colinear, which allowed their motions to be dynamically balanced by a single motor-driven balancer. This design choice removed the need for pair of coolers to vibrationally balance the system on the spacecraft. As a result, system volume and mass drop significantly. System reliability is enhanced by virtue of the reduced number of moving close-tolerance mechanisms. The integral cooler configuration is illustrated in Figure 1. The compressor, displacer, and balancer are each driven by moving coil linear motors. Clearance seals are maintained between the moving compressor cylinder and stationary piston by a paired stack of flexure springs. A clearance seal for the displacer as well as clearance between the displacer and cold finger is maintained by a second paired stack of flexure springs. The balancer's moving mass

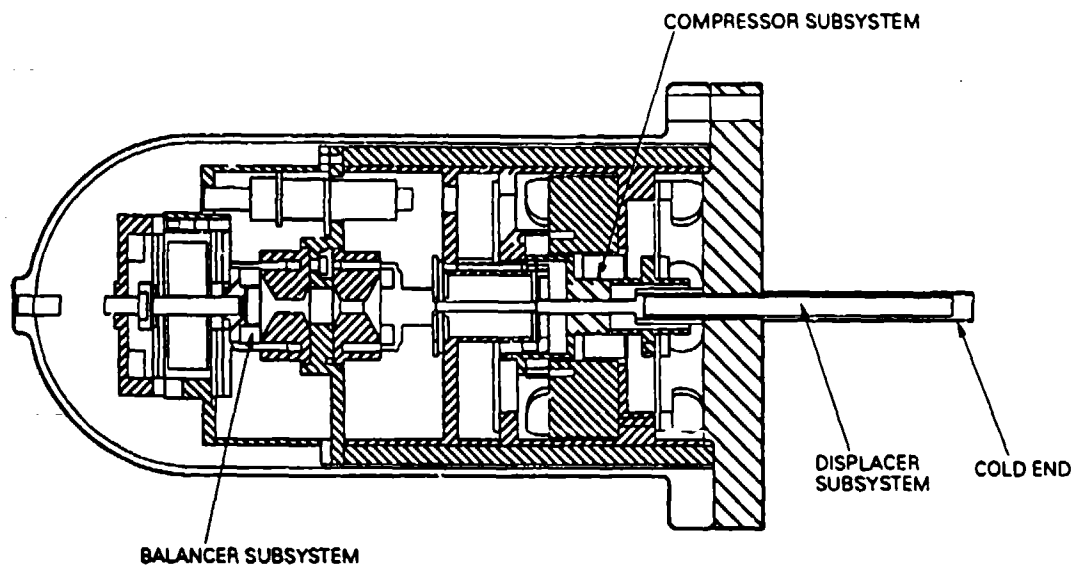


Figure 1. Vibrationally Balanced, Integral Stirling Cooler

incorporates the moving coil, all of which is also suspended from a paired stack of flexure springs mounted to the cooler structure. Cooler materials were chosen to minimize weight and volatile contaminants inside the cooler, which could condense in the cold finger and regenerator and degrade performance. The design goal is for a cooler lifetime of 10 years with 95% confidence.

Figure 2 is a photograph of the engineering model of the cooler, now in fabrication. Shown are the titanium cold finger and the aluminum pressure vessel, which is hermetically sealed by a metal sealing ring to eliminate helium working fluid leakage.

Cooler dimensions are given in Figure 3. Figure 4 lists the cooler specifications as it will be configured for operation in space while cooling a TRW high-temperature superconducting device on the HTSSE 2 flight experiment. The low mass of the mechanical cooler, as well as its small volume, makes the cooler particularly attractive for payloads on small satellites.

PERFORMANCE

Performance of the cooler was evaluated on thermodynamic engineering models that incorporated the compressor and driven displacer and a cold finger modified with additional diagnostic sensors. The performance of the cooler is illustrated in Figure 5, which gives typical cooling power versus



Figure 2. Engineering Model of Pulse Tube Cooler

temperature curves for the thermodynamic engineering model cooler operating about its original 0.25 watt, 65 K design point as well as at temperatures in the 100 to 200 K regime.

Acknowledgement

This work was supported under contract B16045 with the Lawrence Livermore National Laboratory of the University of California.

References

- 1) Bradshaw, T.W., Delderfield, J., Werrett, S.T. and Davey, G. Adv Cryo Eng Plenum Press, New York, USA (1986) 3/ 801-809
- 2) Davey, G. and Orlowska, A.H., Cryogenics (1987) 27 148-151

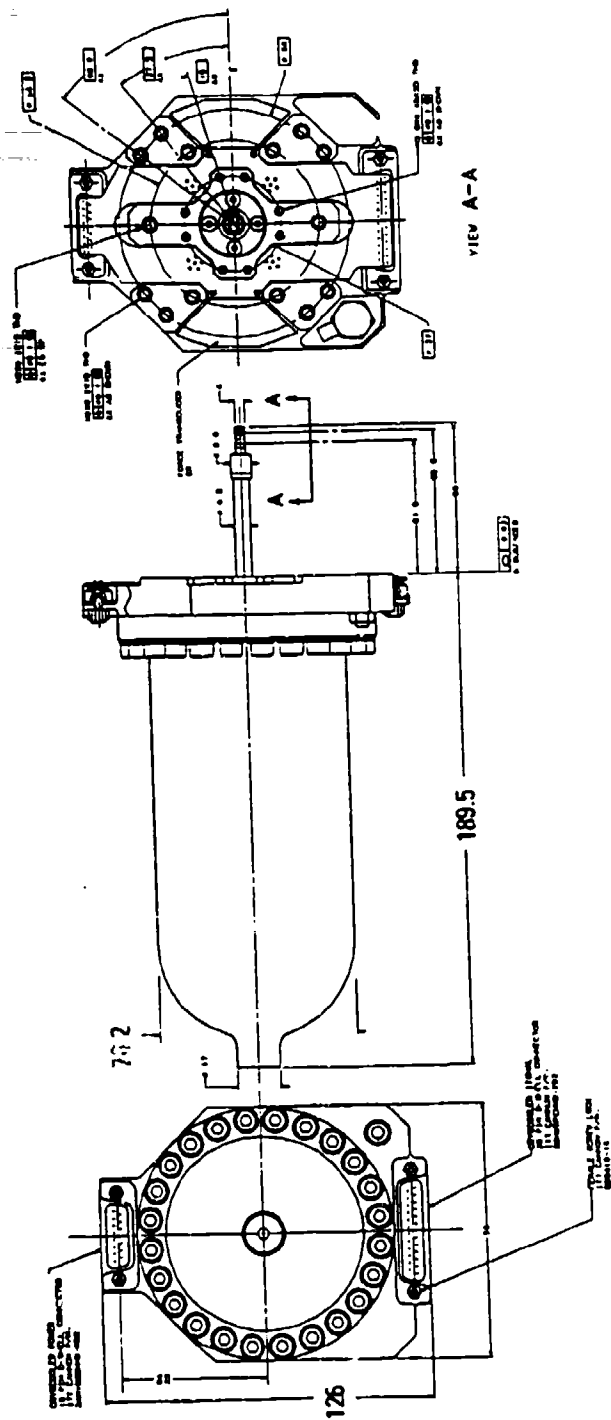


Figure 3. Cooler Dimensions

TOTAL POWER	17.0 W
COOLER POWER	12.2 W
COOLER FOOTPRINT	43.2 cm ²
ELECTRONICS POWER	4.8 W
ELECTRONICS FOOTPRINT	147.1 cm ²
VOLTAGE	22-36 Vdc
COMMAND INTERFACE	SERIAL
TOTAL WEIGHT	2400 gr
COOLER WEIGHT	1400 gr
ELECTRONICS WEIGHT	1000 gr
COOLING POWER	0.25 W
COLD HEAT TEMPERATURE (T _C)	<65 K
REJECT TEMPERATURE	<300 K
VIBRATION AT COOLER MOUNT	<0.1 Nrms

R1M 92.0280.03a

Figure 4. Cooler Specifications for HTSSE 2 Flight Experiment

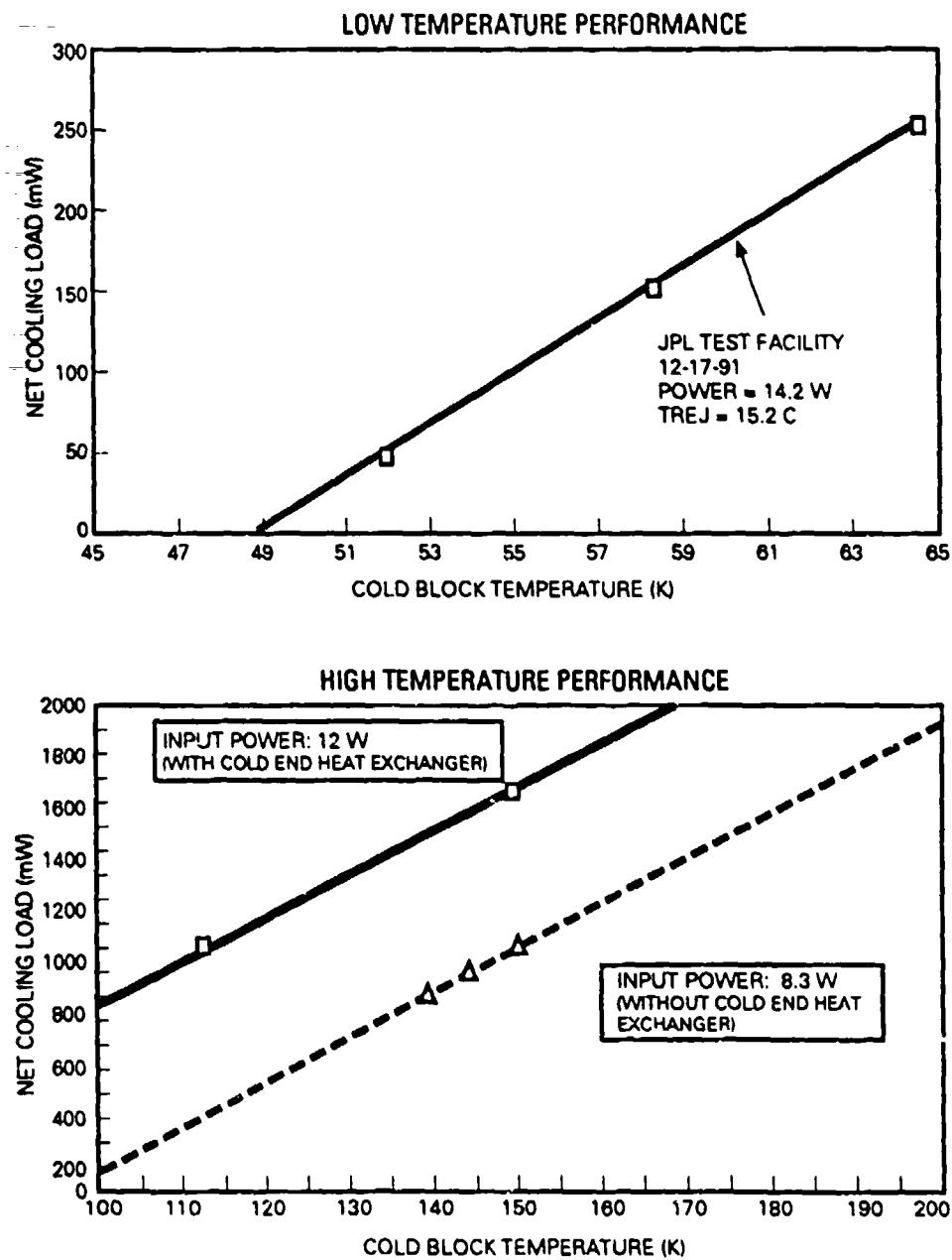


Figure 5. Cooler Performance

THERMAL, VIBRATION, AND RELIABILITY TEST RESULTS FOR A BALANCED 80 K CRYOCOOLER

Robert Boyle, Leroy Sparr, Thomas Cygnarowicz, and Stephen Castles
NASA Goddard Space Flight Center
Greenbelt, MD

Richard G. Fink and Edward F. James
McDonnell Douglas Space Systems Company
Greenbelt, MD

INTRODUCTION

This paper reports the results of a series of tests conducted by Goddard Space Flight Center (GSFC) on an 80 K Technology Demonstration Model (TDM) cryocooler produced by Stirling Technology Company (STC). This Stirling cycle cryocooler is unique in its combination of a free-displacer design, which depends on the pressure wave from the compressor as the sole means of generating displacer motion, with linear flexure bearings and clearance seals. It also provided GSFC with the unique opportunity to measure, and attempt to control, the residual vibration generated by a "balanced" cryocooler assembly. This report contains a summary of the results of the GSFC tests together with conclusions and recommendations for additional tests.

BACKGROUND

The Stirling Technology 80 K TDM Cryocooler was developed in 1990 under a NASA Phase II Small Business Innovation Research (SBIR) contract. This development built upon the results of an earlier Phase I SBIR contract with STC for the design, construction, and testing of long-life axial flexures for Stirling cycle cryocoolers.

The objective of the Phase II contract was to develop a prototype long-life, low-vibration cryocooler which would be capable of providing 2.0 W of cooling at 80 K. STC's approach to meeting the long-life objective was to build a cryocooler whose displacer is driven only by the working gas pressure wave generated by the motor-driven compressor, and transmitted via a copper transfer line. This eliminates the

need for a displacer motor which would otherwise provide several potential failure points. The phase of the displacer motion, which is critical to the Stirling cycle operation, is tuned by adjusting an orifice between the displacer damper space and a working gas buffer volume. This adjustment is made to maximize the cold tip cooling capacity for the nominal compressor operating frequency and stroke.

STC's approach to meeting the low-vibration objective was to integrate a second axial compressor, to operate in opposition with the first, along the same axis of motion. This allows the axial vibration of the first compressor to be partially cancelled by the motion of the second. Similarly, a motor-driven counterbalance mass was assembled with the displacer unit to cancel vibration forces generated by the motion of the displacer. For both the compressor and displacer/counterbalance assemblies, the lateral vibration forces were minimized through the careful alignment of the mating units. The TDM cryocooler, which was delivered to GSFC in 1991, is shown in Fig. 1. The dual-compressor assembly is shown on the left and the displacer/counterbalance assembly is on the right.

The compressor, displacer, and counterbalance pistons use non-contacting clearance seals, and are supported by axial flexure bearings. The compressor and counterbalance pistons are driven by moving-coil linear motors. Their positions, along with that of the displacer piston, are measured using Fast Linear Differential Transformer (FLDT) position sensors. The nominal compressor operating frequency and stroke are 40 Hz and ± 4.8 mm, respectively. The working gas is helium with a nominal fill pressure of 195 psig.

The cold tip is instrumented with a silicon diode temperature sensor and a resistive heating element for the simulation of instrument heat loads. The housings of the compressor, displacer, and counterbalance units are made of aluminum. The dual compressor and displacer/counterbalance assemblies weigh 9.6 and 7.7 kg respectively ¹

Before delivery to GSFC, STC tested the unit for both thermal and vibration performance. In addition, STC developed a conceptual design for a space qualifiable version of the TDM cryocooler. This contract did not include the development of motor drive electronics.

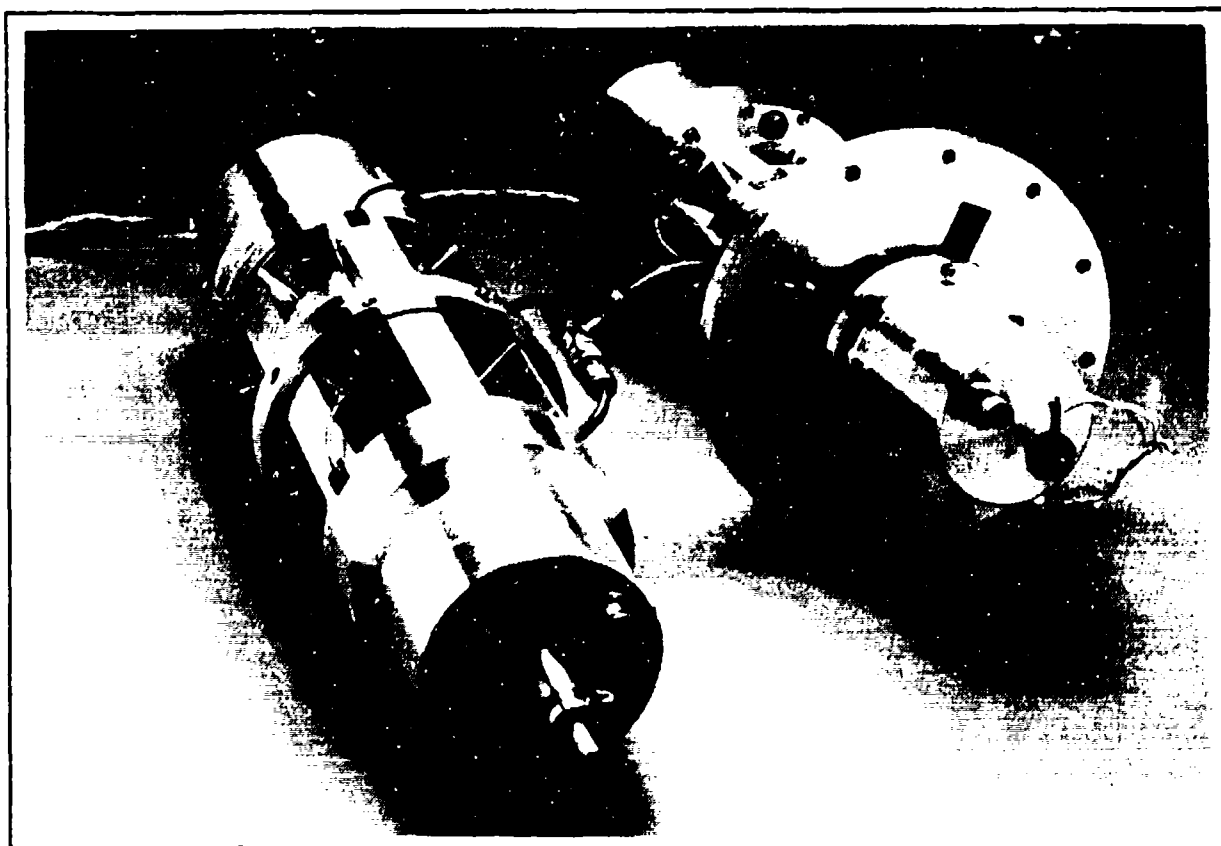


FIG. 1. Photograph of the Stirling Technology Company 80 K TDM Cryocooler (courtesy of STC).

THERMAL PERFORMANCE TEST

The objective of this test was to measure the cold tip temperature as a function of heat load and electrical input power. This test was performed in air with forced convective cooling. The manufacturer's recommended nominal values were used for all operating parameters. Cooldown time and the effects of varying operating frequency, working gas fill pressure, and heat sink temperature were not investigated in these tests.

The motor drive electronics used in these tests were provided by GSFC and consisted of three arbitrary waveform generators and two dual-channel linear power amplifiers. These were used to provide open-loop control of the compressor strokes and offsets.

Because the compressor power was measured at the input to the compressors, the results do not include power losses in the drive electronics or the power required to drive the counterbalance. This should be taken into consideration when comparing these test results with the thermal performance of other cryocoolers.

In this test, the steady-state cold tip temperature was measured with the compressors operating at 100, 90 and 80% of their maximum stroke and the cold tip heater operating at 0, 1, 2, 3 and 4 watts. 100% stroke was taken to be the point of near contact at either physical limit of travel. The manufacturer considers the nominal stroke to be approximately 80% of the maximum stroke.

The estimated uncertainty for all of the test measurements are shown in Table I. Note that the estimated uncertainty for the compressor power and cold tip temperature measurements were found through analysis of their respective measurement apparatus. They do not reflect uncertainties in the measurement of the independent variables which affect the compressor power and cold tip temperature. The test results are shown in Fig. 2.

TABLE I. Estimated uncertainty for thermal performance measurements.

<i>Parameter</i>	<i>Estimated Uncertainty</i>
Cold Finger Vacuum	$\pm 2.2 \times 10^{-8}$ torr
Working Gas Fill Pressure	± 4 psig
Piston Stroke	± 0.13 mm
Cold Finger Heat Load	± 0.005 watts
Compressor Power	± 0.62 watts
Heat Sink Temperature	± 0.6 °C
Cold Tip Temperature	± 0.1 K

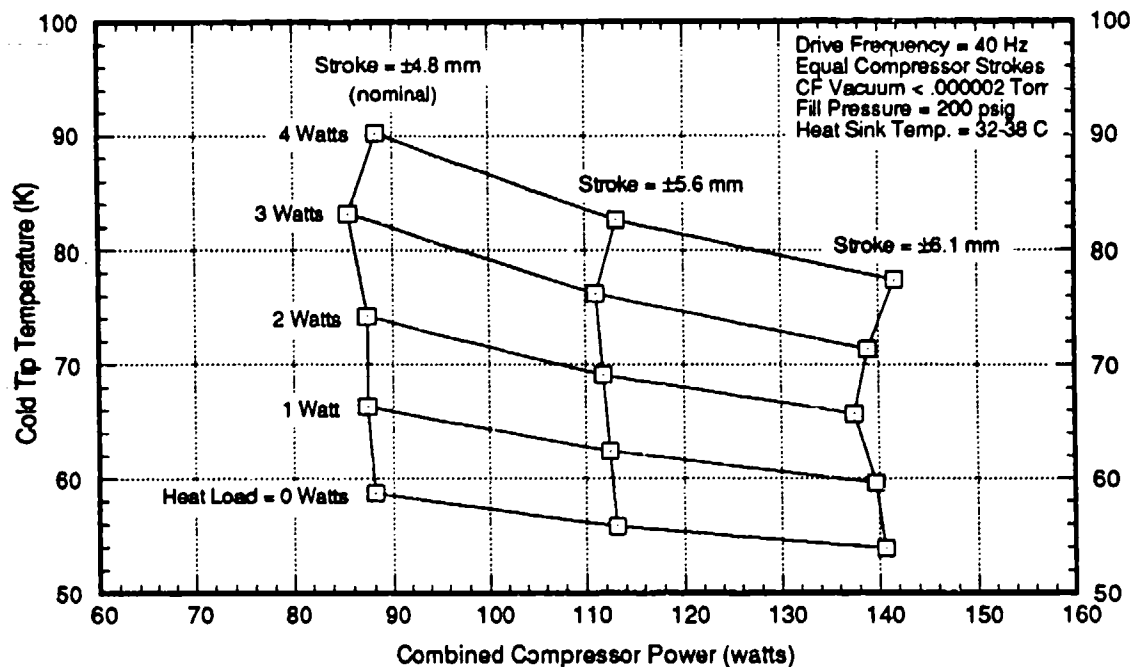


FIG. 2. Nominal Thermal Performance.

STC has produced data which indicates slightly better performance under similar operating conditions¹. This difference may be due to the fact that they were operating the cooler with a working gas fill pressure of 195 psig as opposed to the 200 psig used by GSFC. During the GSFC tests it was noted that small reductions in fill pressure caused a drop in cold tip temperature. No attempt was made to determine the optimum fill pressure or to repeat the tests at 195 psig. Due to this sensitivity of thermal performance to the working gas fill pressure, a more accurate means of measuring the working gas fill pressure should be used in future work with this cooler. An accuracy of ± 1 psig is suggested.

These results show that the TDM cryocooler would satisfy the design goal of maintaining 2.5 watts of cooling at 80 K.

VIBRATION CHARACTERIZATION TESTS

The objectives of this test were to measure the residual vibration forces generated by the cooler while operating under nominal conditions, and to investigate the effect of lateral gravity loading on these vibration signatures. These vibration forces were measured using a six-axis dynamometer and an analog signal mixer which were designed and built by GSFC. The cooler is shown mounted to the dynamometer in Fig. 3. Details regarding the dynamometer design are described by Boyle, et al ².

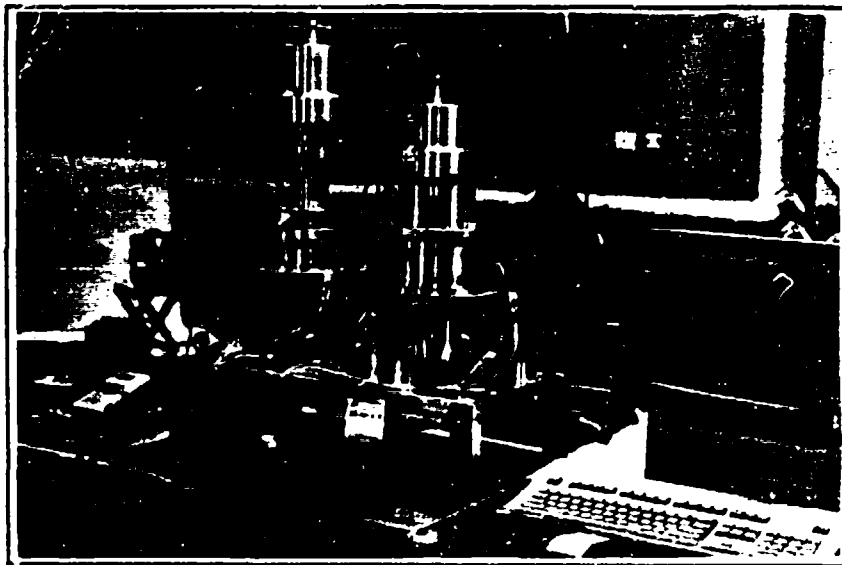


FIG. 3. Photograph of the Stirling Technology Company 80 K TDM Cryocooler mounted in the GSFC STC Dynamometer.

This vibration characterization test was conducted under steady-state no-load conditions with both compressors running with the nominal stroke of ± 4.8 mm. This resulted in a displacer stroke of approximately ± 2.3 mm and a cold tip temperature of approximately 59 K.

Before the vibration measurements were made, the 40 Hz components of the residual axial vibration in the compressor and displacer/counterbalance assemblies were minimized by adjusting the amplitudes and phases of the 40 Hz drive signals for one of the compressors and the counterbalance respectively.

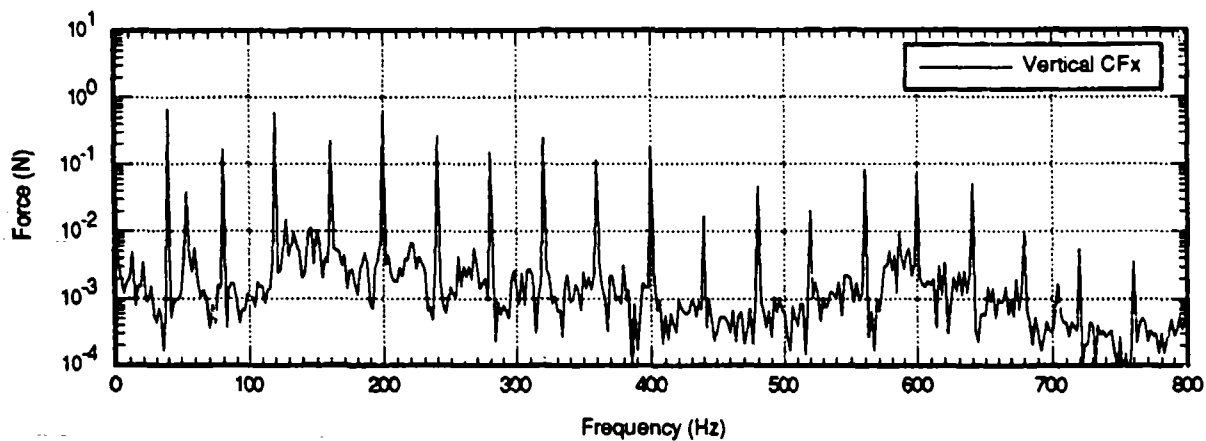
A spectrum analyzer was used to record each force spectrum from 0 to 800 Hz. The moment spectra were not recorded. In addition, two eight-channel A/D converters were used to simultaneously record several cycles of the force and moment time signatures. The test was initially conducted in the vertical orientation, and then repeated in the horizontal orientation to measure the effect of lateral 1-g loading on the axial flexures.

The compressor assembly vibration forces for the vertical orientation are shown in Fig. 4. The displacer/counterbalance vibration forces for the vertical orientation are shown in Fig. 5. In all cases F_z is the force in the direction of piston motion and F_y is the force in the direction between the compressor and displacer/counterbalance assemblies. For the horizontal orientation, F_x is the force in the direction of gravity.

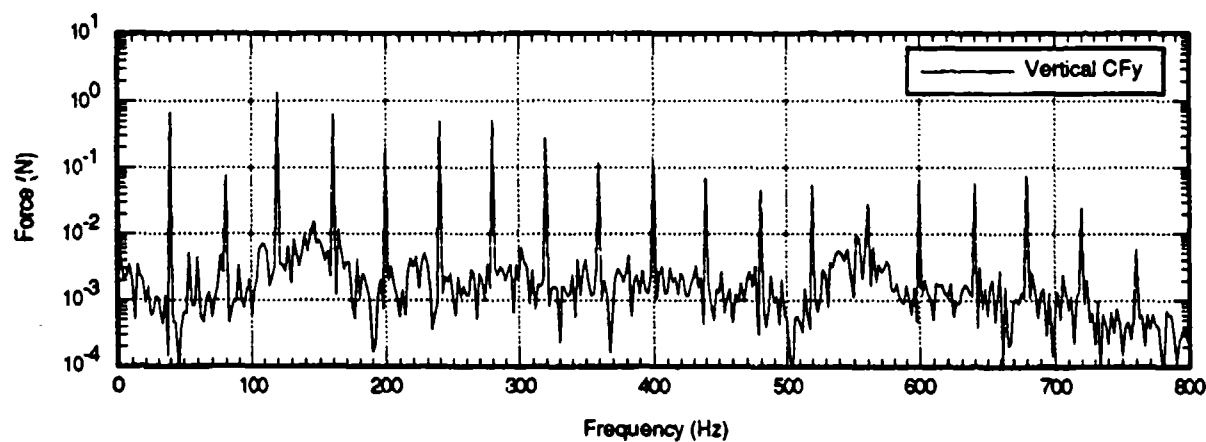
Because the GSFC dynamometer was never calibrated to an absolute standard, the vibration force data is only believed to be accurate to approximately $\pm 10\%$. This conservative estimate is based on the dynamometer force cell specifications and the combination of these errors by the analog signal mixer circuit. This limited accuracy was considered to be adequate for these tests because, for this cryocooler, GSFC was primarily interested in comparative data for different orientations and modes of operation rather than absolute comparison with a vibration specification or other cryocoolers.

It is clear from these graphs that the great majority of the cryocooler vibration force exists only at the harmonics of the operating frequency. As a result, valid comparison between the vibration forces in the vertical and horizontal orientations can be made by considering only the magnitudes at the harmonics. Such a comparison is shown in Fig. 6.

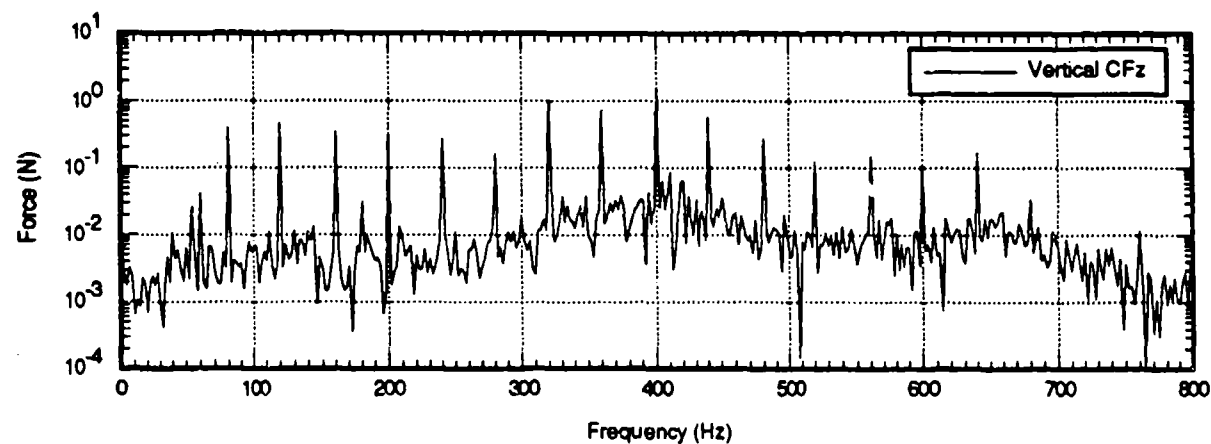
Note that these graphs show only the magnitudes of the vibration forces at the harmonics. The lines between the data points serve only to identify the orientation at which the data was collected.



a) Compressor Assy Fx

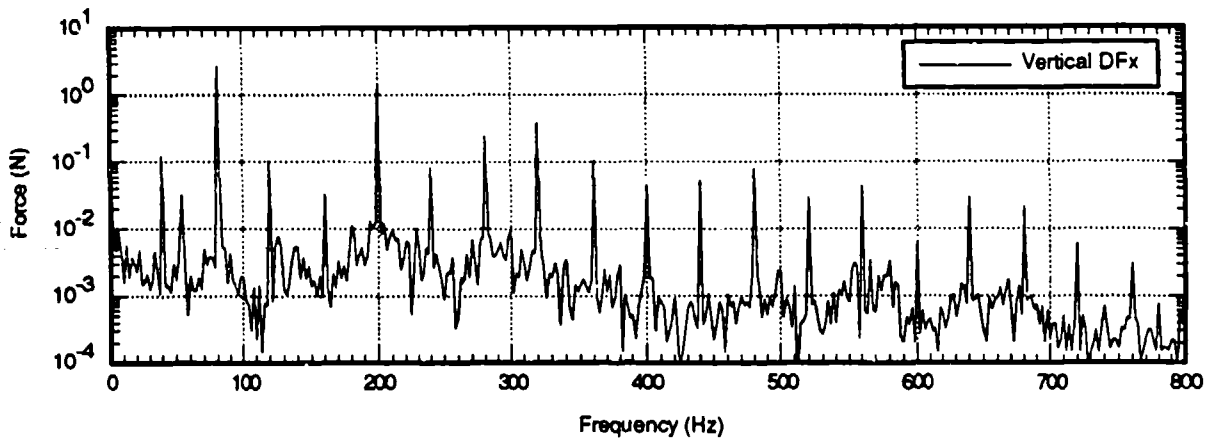


b) Compressor Assy Fy

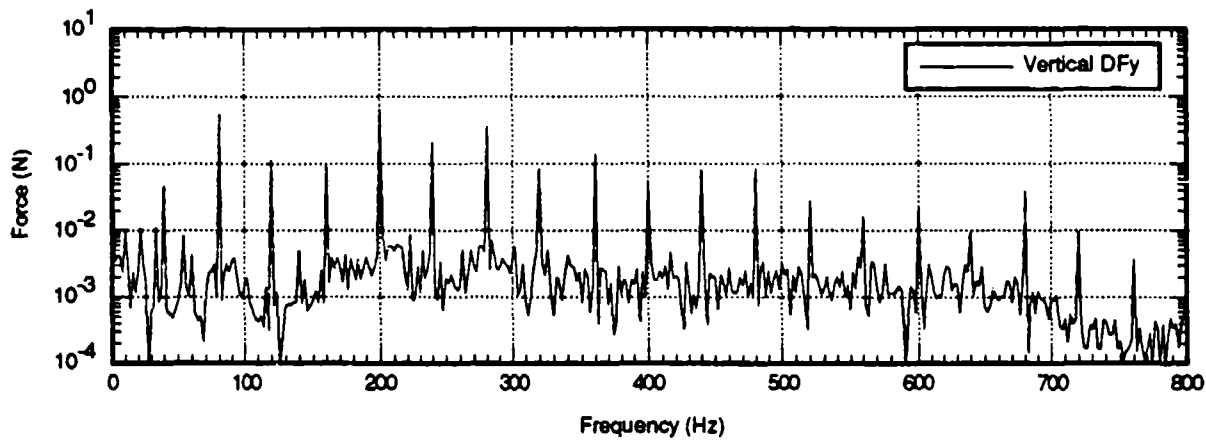


c) Compressor Assy Fz

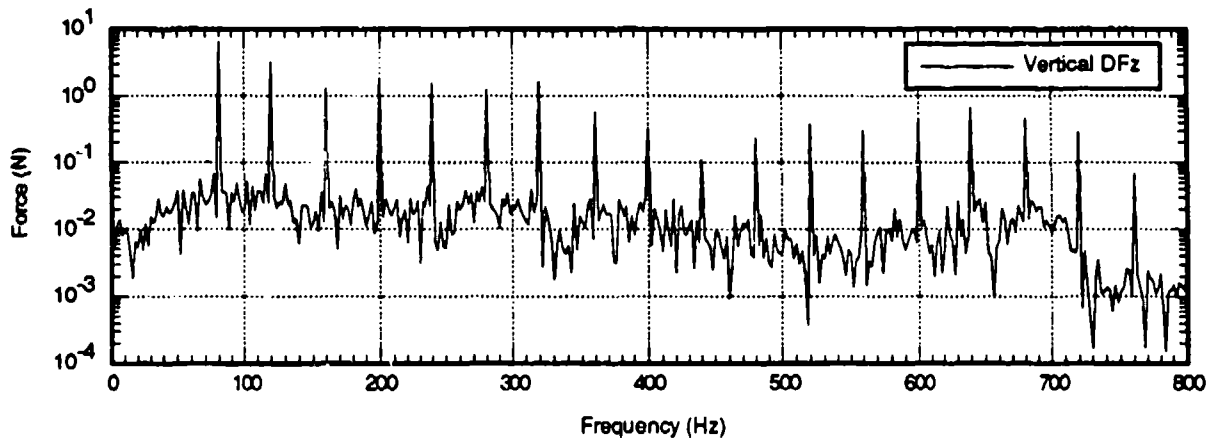
FIG. 4. Baseline compressor assembly vibration forces measured in the vertical orientation.



a) Displacer/Counterbalance Assy Fx

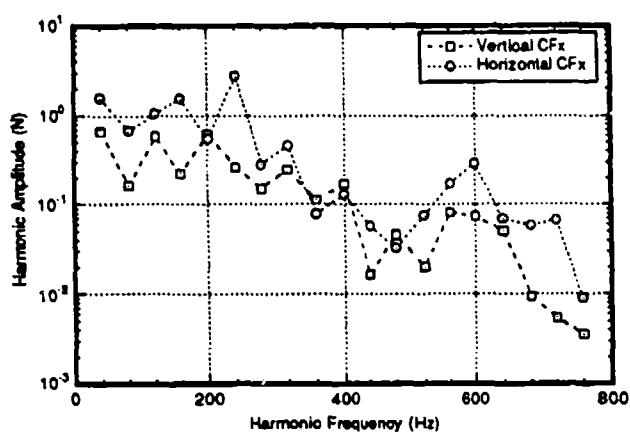


b) Displacer/Counterbalance Assy Fy

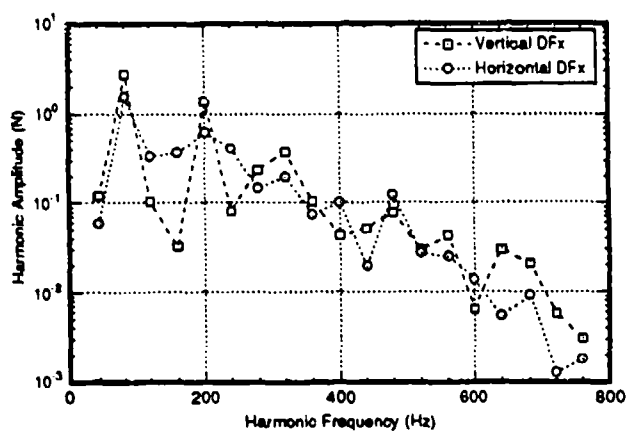


c) Displacer/Counterbalance Assy Fz

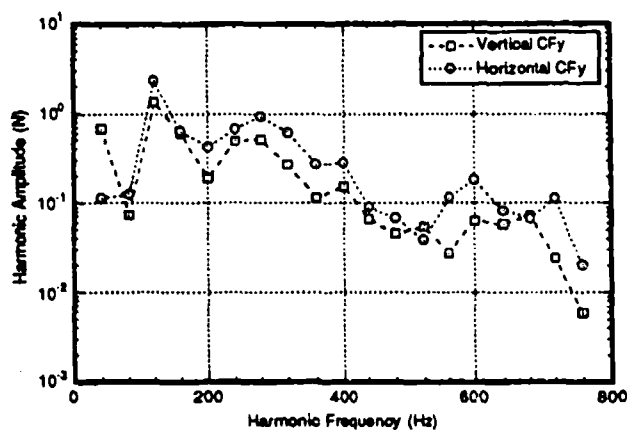
FIG. 5. Baseline displacer/counterbalance assembly vibration forces measured in the vertical orientation.



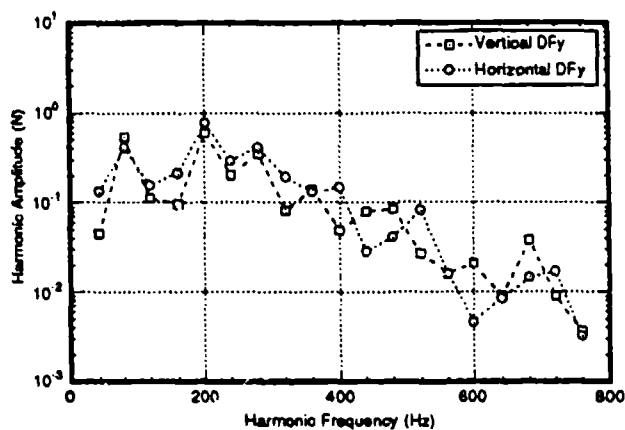
a) Compressor Assy Fx



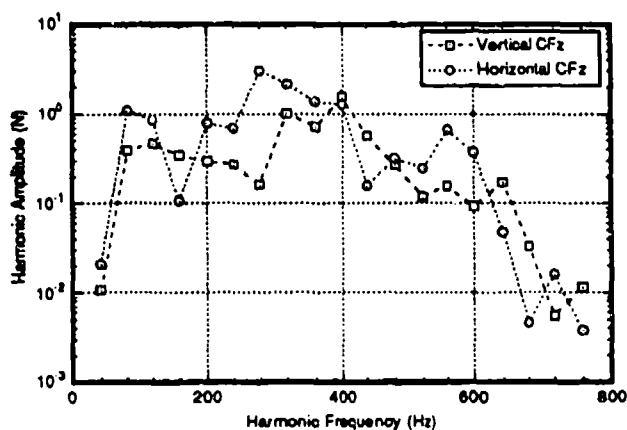
b) Displacer/C'balance Assy Fx



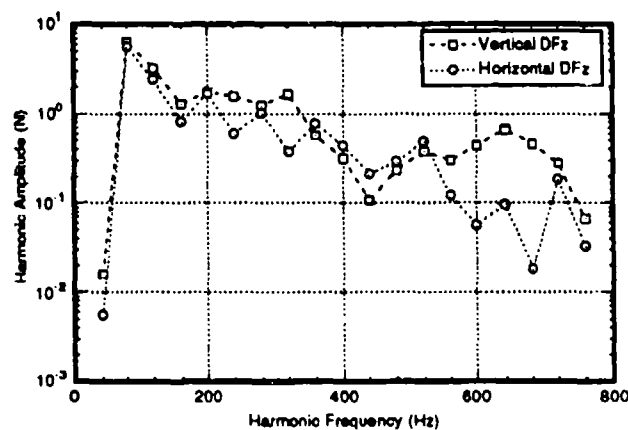
c) Compressor Assy Fy



d) Displacer/C'balance Assy Fy



e) Compressor Assy Fz



f) Displacer/C'balance Assy Fz

FIG. 6. Baseline vibration forces at the harmonics of the operating frequency for vertical and horizontal orientations.

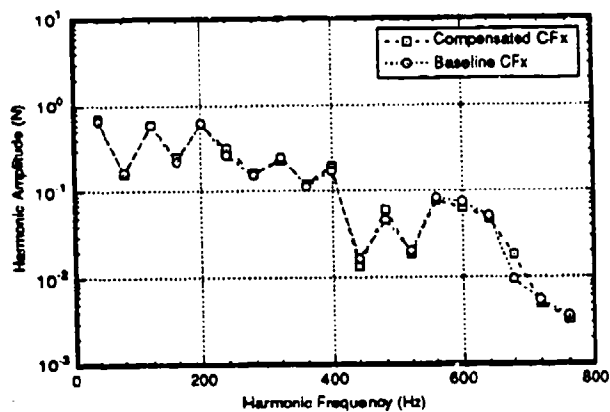
VIBRATION CONTROL TESTS

In addition to the vibration characterization tests, GSFC also used this cooler and dynamometer in the early development of a narrow-band axial-vibration control system for linear-motor cryocoolers. This simple non-realtime technique takes advantage of the dominance and stability of the harmonic content of cryocooler axial vibration forces by attempting to control only the harmonics in non-realtime rather than controlling the broadband vibration in realtime.

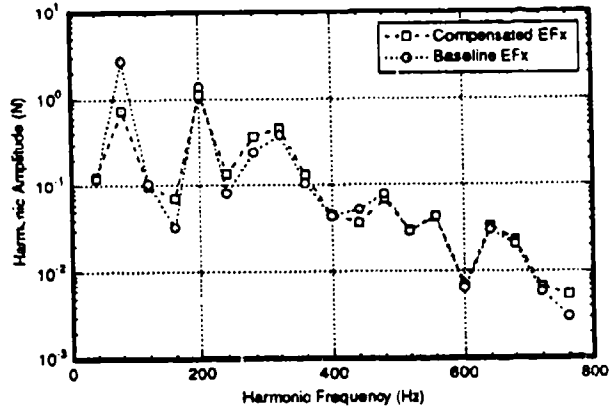
For each assembly this technique involves measuring the magnitude and phase sensitivity of each axial-force harmonic to the corresponding motor-drive-signal harmonic. Then a simple search algorithm uses these sensitivities to adjust the drive signal to minimize the axial force at each harmonic.

This technique was automated using National Instruments LabView on an Apple Macintosh II personal computer. A more complete description of the technique, its implementation, and the results of this work are described by Boyle, et al ².

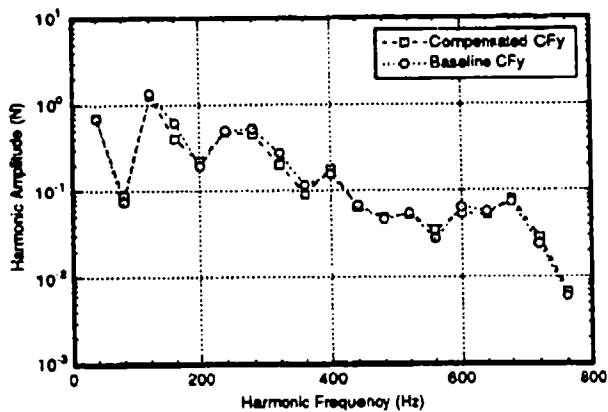
Due to time constraints, this technique was used to cancel only the first six axial force harmonics for this cryocooler. Typical results of these tests for the vertical orientation are shown in Fig. 7. Similar results were achieved for the horizontal orientation. Later work with other cryocoolers has shown that the technique can successfully reduce the magnitudes of harmonics at frequencies up to 800 Hz.



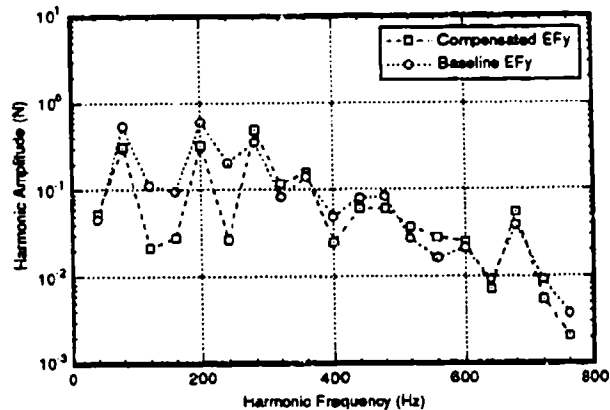
a) Compressor Assy Fx



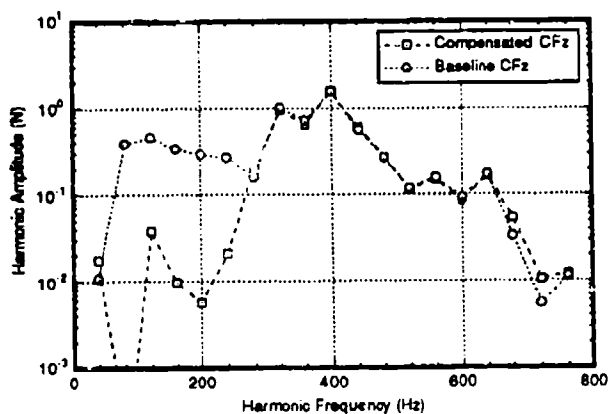
b) Displacer/C'balance Assy Fx



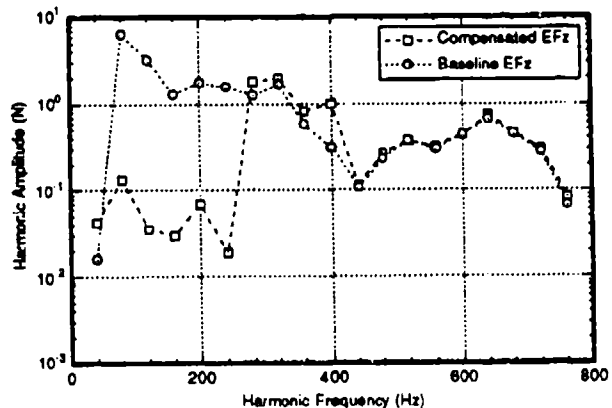
c) Compressor Assy Fy



d) Displacer/C'balance Assy Fy



e) Compressor Assy Fz



f) Displacer/C'balance Assy Fz

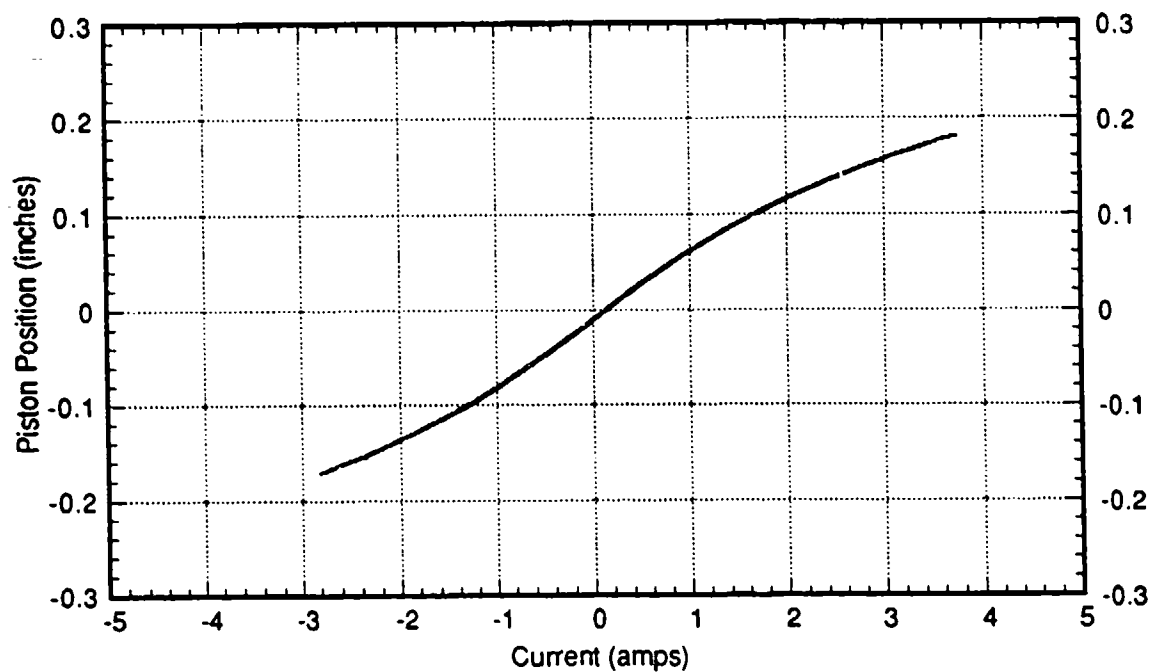
FIG. 7. Residual vibration forces at the harmonics of the operating frequency with and without harmonic cancellation for the first six harmonics of Fz.

RELIABILITY TESTS

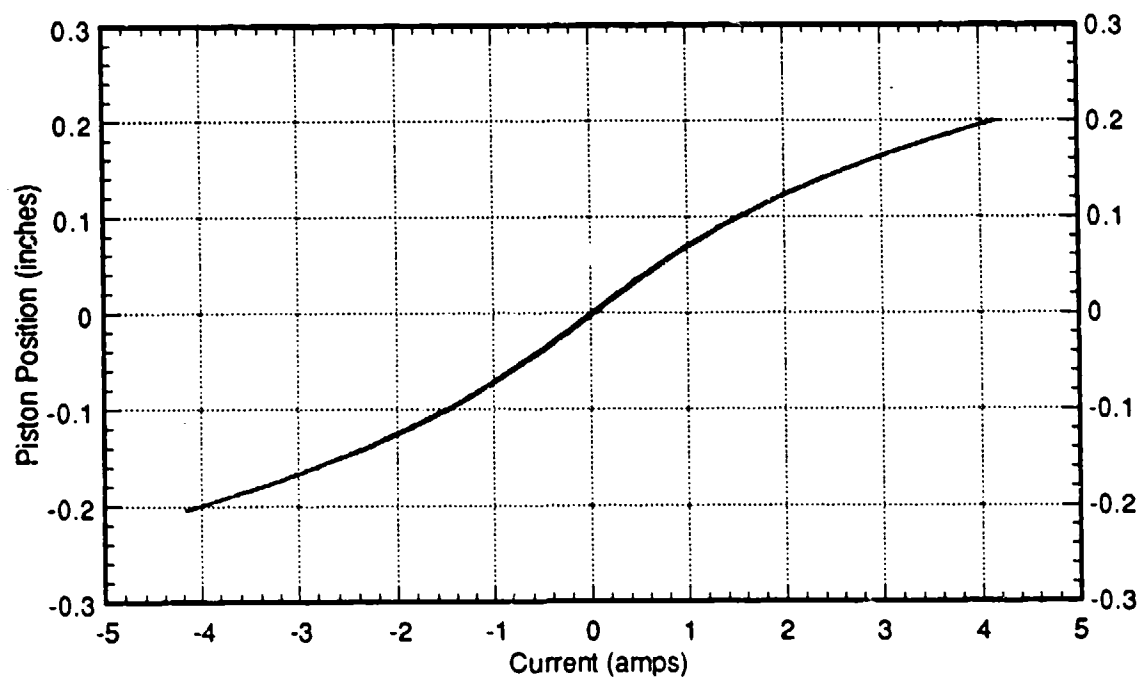
The goal of the GSFC reliability tests was to detect failures or degradation of the cooler, or conditions which would lead to such degradation. Contact between the compressor piston and the wall of the piston cylinder during operation is considered one such indicator of potential degradation. In an attempt to detect piston/cylinder contact, GSFC drove the cooler to a low cold tip temperature, and then shifted the compressor drive signal to an extremely low frequency while monitoring the motor current and piston position. Contact with the cylinder wall would be indicated by discontinuities in the piston-position vs. motor-current signal. These tests were performed only on the compressors in both the horizontal and vertical orientations.

Typical plots of compressor piston-position vs. motor-current for one cycle at 0.02 Hz are shown in Figure 8. These plots show no discontinuities which would indicate piston contact with the cylinder walls. In fact, no such discontinuities were detected during any such tests. A small amount of hysteresis is present but is not believed to be attributable to piston contact. Note that differences between the two plots can be attributed to offsets in the position sensor signal conditioning electronics and differences in the thrust/current relationships for the two motors.

These tests were conducted at 0.02 Hz due to limitations in the GSFC data acquisition system. Future tests should be conducted at lower frequencies.



a) Compressor 1, Cold Tip Temperature = 73 K



b) Compressor 2, Cold Tip Temperature = 72 K

FIG. 8. Piston Position vs. Current at 0.02 Hz.

SUMMARY

Stirling Technology Company has built a cryocooler whose cooling capacity exceeds 0.8 watts of cooling load at 80 K. This is particularly noteworthy in that it is a fully balanced free-displacer design which was developed within the funding constraints of a Phase II SBIR contract (< \$500K). Although operation of the free-displacer design required careful compressor stroke control during cooldown to avoid over-stroking the displacer, this does not appear to be a significant additional constraint for flight control electronics.

GSFC testing has indicated that the balanced cryocooler design allows the axial fundamental component of vibration in the compressor and displacer/counterbalance assemblies to be cancelled by adjusting the amplitude and phase of the secondary compressor and counterbalance drive signals respectively. In addition, the axial forces at many of the harmonics of the operating frequency can be reduced through a simple technique of characterization and non-realtime compensation of each harmonic. Lateral vibration forces may be reduced by more precise alignment of the opposing units.

GSFC's limited testing did not disclose any operating characteristics which would indicate potential failures due to contact of moving parts.

Although, considerable additional work would be needed to turn this cooler into a flight-worthy design, GSFC considers the STC 80 K TDM cryocooler to be a successful demonstration of promising long-life and low-vibration cryocooler design features.

REFERENCES

- 1 Stirling Technology Company, "Stirling Cryocooler with Extremely Low Vibration," STC Report No. 9134, 3/16/92.
- 2 R. Boyle, et al, "Non-Realtime, feedforward vibration control system development & test results", presented at the 7th International Cryocooler Conference, Santa Fe, NM (1992).

SPACECRAFT COOLER CHARACTERIZATION

D. L. Johnson, G. R. Mon, and R. G. Ross, Jr.

Jet Propulsion Laboratory
California Institute of Technology
Pasadena, California 91109

ABSTRACT

To meet the important need within the space community for reliable and accurate data on cryocooler performance, the Jet Propulsion Laboratory (JPL), under SDIO/Air Force sponsorship, is conducting an extensive space cryocooler characterization program involving long-life cryocoolers submitted by world-wide manufacturers. The objective of the test program is to gather thorough thermal, vibration, electromagnetic interference (EMI), and reliability performance data on space cryocoolers under development by, or of interest to the SDIO community. At this time cryocoolers have been tested, or are scheduled to be tested from Hughes, Creare, TRW, Lockheed-Lucas, British Aerospace, Stirling Technology, and Sunpower; in addition, several other manufacturers are in active discussions relative to testing their coolers. Although thermodynamic cooling performance is the prominent performance attribute being measured in the test program, compatibility with sensitive cryogenic-detector systems and operational life/reliability are also critically important. To support these data needs, JPL is conducting additional tests on cold finger off-state parasitics, location and amount of rejected heat, generated vibration, and EMI. An overview of JPL's AF/SDIO cooler test program is presented together with a description of the facilities and methods used for cooler testing.

INTRODUCTION

The current thrust towards developing miniature cryocoolers for multi-year space missions has peaked the awareness and interest of the space-instrument community and led to a broad commitment to the use of mechanical cryocoolers in upcoming space-flight instruments. Numerous cryocooler designs are under development, including Stirling, pulse tube, turbo-Brayton, and sorption. Within each cryocooler type, different design options are being considered; for Stirling-cycle cryocoolers, for example, design options include split versus integral and single-compressor/single-expander versus dual-compressor/single-expander with active vibration counterbalancing. These varied cryocooler design configurations can lead to widely differing performance characteristics.

To assist the space-instrument user community in understanding the mechanical and thermodynamic differences in the various cryocoolers, and in successfully applying these cryocoolers to best meet their thermal performance and integration requirements, the Jet Propulsion Laboratory (JPL) has undertaken a comprehensive cooler characterization

program. The objective of the program is to fully characterize the important existing and emerging space cryocoolers with respect to the complete spectrum of operational, systems-integration, and reliability parameters. This includes thermodynamic cooling capacity, cold finger off-state parasitics, location and amount of rejected heat, operational life and reliability, and compatibility with sensitive cryogenic detector systems -- particularly with respect to cooler-generated vibration and electromagnetic interference (EMI).

The JPL characterization program is designed to provide a comprehensive database obtained using a common set of instrumentation, test procedures, and test facilities. This helps provide standardization of test-result formats and parameter ranges to aid in comparing and interpreting cryocooler performance. The program is therefore expected to be as valuable to cryocooler developers attempting to understand the strengths and limitations of their cryocooler designs, as it is to the cooler user community.

TEST PROGRAM OVERVIEW

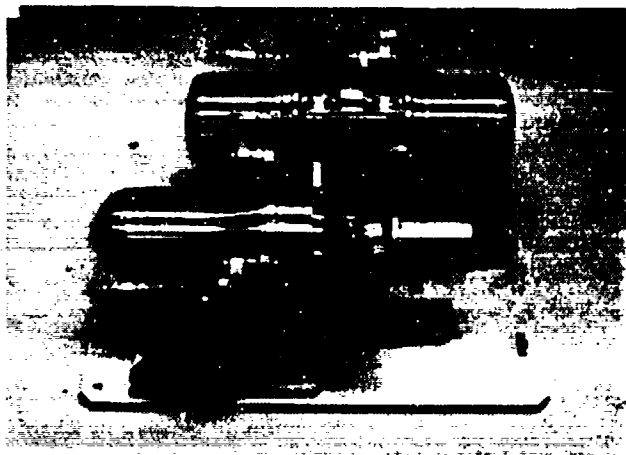
JPL has been developing diverse and sophisticated cryocooler test facilities since 1989, and began characterizing long-life space cryocoolers under JPL/NASA sponsorship in 1990 with emphasis on the British Aerospace (BAe) 80K Stirling-cycle cooler [1]. In 1991, the characterization program was expanded under the sponsorship of the Air Force Phillips Laboratory/Strategic Defense Initiative Organization (AFPL/SDIO) to fully characterize mechanical cryocoolers in the 10-K to 160-K range that have been developed under SDIO-funded efforts, or that are of interest to the Air Force/SDIO for space application. Current coolers under test, or about to be tested, include the Hughes and Creare 65 K SSC Stirling coolers -- both under development through AFPL/SDIO funding -- and coolers from BAe, Lockheed-Lucas, Stirling Technology Co., TRW, and Sunpower Corp. These coolers are shown in Fig. 1 and are described in Table I. Testing of additional cryocoolers from other manufacturers is also of great interest to the program.

TEST METHODS AND FACILITIES

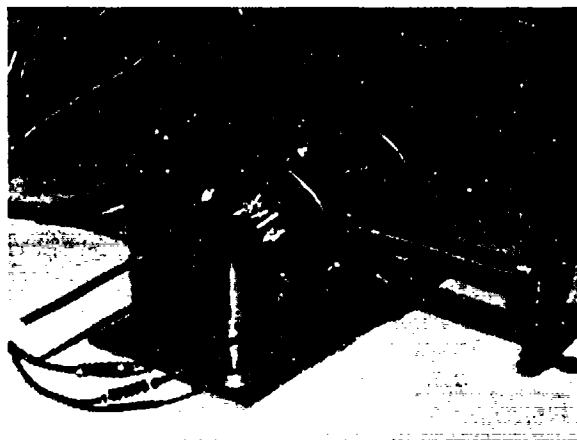
A critical step in achieving an accurate characterization of the performance of space cryocoolers is developing and calibrating the specialized test facilities and performance measurement techniques that are required. Test facilities developed and used at JPL include a unique calorimetric thermal-vacuum chamber, a facility to measure the parasitic heat conduction along the expander cold finger, a 6-degrees-of-freedom force dynamometer to measure cooler vibration, and the JPL Electromagnetic Compatibility (EMC) laboratory, where JPL flight instruments are characterized prior to spacecraft integration. The test methodology and facilities used in each of the performance areas are described below.

Thermal Performance

The thermal performance of a cryocooler remains the primary criteria for the selection of a particular cooler for a flight instrument. This includes overall cooling capacity, and cooler



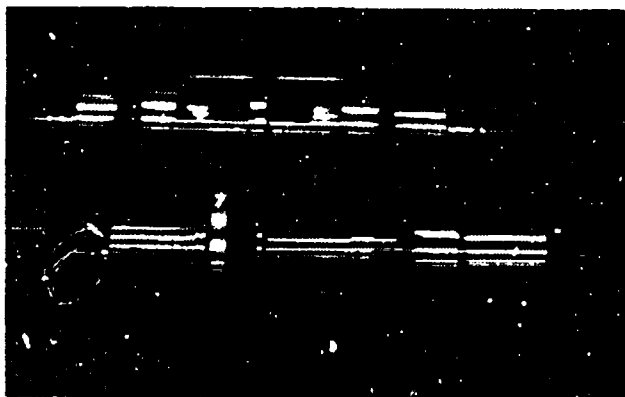
HUGHES



CREARE



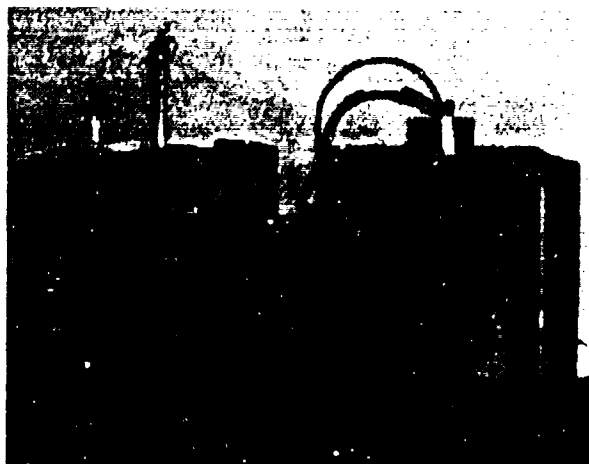
TRW



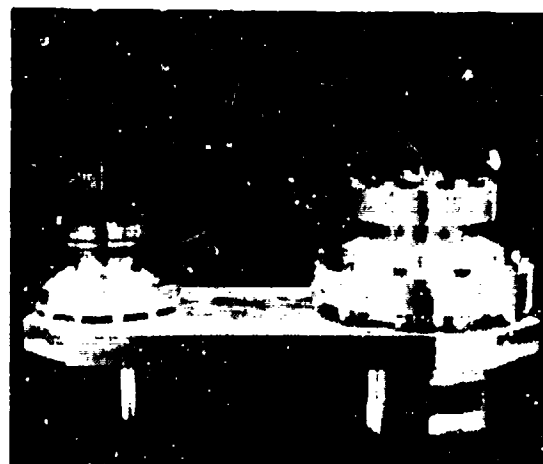
STIRLING TECHNOLOGY



SUNPOWER



BRITISH AEROSPACE



LOCKHEED/LUCAS

Fig. 1. Stirling-cycle cryocoolers currently scheduled for testing as part of the JPL/AFPL cooler characterization program.

TABLE 1. Cryocoolers scheduled for characterization testing

Company	Nominal Performance	Measured Performance		Type	Key Features
Creare	2W at 65K	.75W at 65K ^a	not measured	integral Stirling	B-B comps, diaphragms
Hughes	2W at 65K	2W at 65K ^a	34W/W ^a	split Stirling	B-B comps, exp. mass bal., HEX on Xsfer tube
TRW	.25W at 65K	.25W at 65K ^b	56W/W ^b	integral Stirling	mass bal. motor for cooler
BAe	.75W at 55K	1W at 65K ^a .8W at 65K ^b	52W/W ^a 60W/W ^b	split Stirling	single comp/exp
Lockheed-Lucas	.75W at 55K	1W at 65K ^a	37W/W ^a	split Stirling	single comp/exp
Stirling Technology Company	2.8W at 80K	3.8W at 80K ^b	25W/W ^b	split Stirling	B-B comps, free displacer, exp. mass bal. motor
Sunpower Corp	4W at 120K	4W at 120K ^a	15W/W ^a	integral Stirling	single comp/exp, free displacer, cooler mass bal.

^a Measured at Manufacturer^b Measured at JPL

thermal efficiency; the latter determines the overall input power required for the cooler. Because cooler thermal performance is dependent upon a number of operating parameters, it is important to thoroughly quantify these dependencies. Example parameters include cold-end load and temperature, piston stroke, drive frequency, and heatsink temperature.

The cooler thermal performance portion of the JPL cooler characterization program utilizes a unique calorimetric thermal-vacuum test chamber that accurately simulates the heat-transfer interfaces of space and provides a highly stable thermal test environment [2]; the high level of environmental stability achieved allows accurate repeatable measurements to illuminate subtle performance sensitivities that are difficult to quantify in typical ambient-room test environments. Two separate cooling fluid loops provide precise individual control

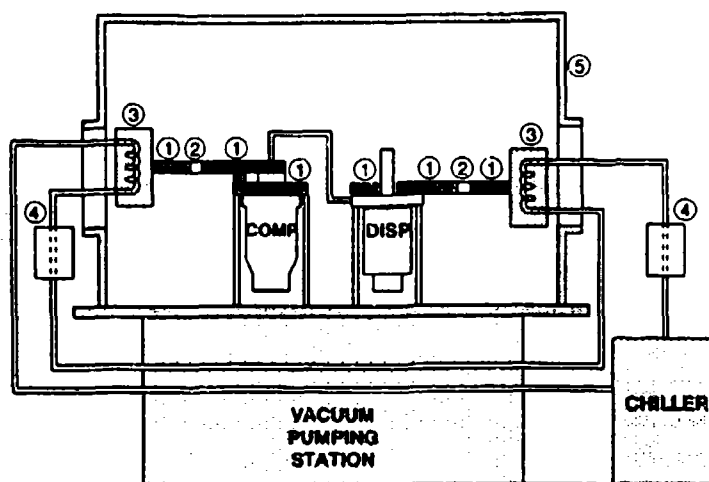


Fig. 2. Schematic of JPL thermal-vacuum calorimetric test chamber used for thermal performance characterization: 1) copper heatsinks, 2) thermal shunt for heat rejection measurements, 3) fluid-loop heat exchangers, 4) fluid-loop heaters, 5) vacuum bell jar enclosure

of the compressor and displacer heatsink temperatures (Fig. 2). This allows cooler thermal performance to be mapped for heatsink temperatures ranging over the flight operating temperature range (typically 0 to 40°C), and for a wide variety of operational variables including compressor-displacer stroke, drive frequency, and compressor-displacer phase. Temperature stabilities of 0.1°C are achieved over a temperature range of approximately -50°C to 60°C.

The thermal performance of test coolers is documented in terms of both cooling power and specific power (watts of electrical drive power for one watt of cooling power) for a broad range of coldtip temperatures, typically from 150 K down to the lowest no-load temperature (around 45 K). An example multi-variable plot developed for comparing the complex thermal-performance dependencies is shown in Fig. 3; the data, from a prior JPL characterization program [2], describe the thermal performance of the BAe 80K. cooler.

Because the quantity and location of heat rejected by the cryocooler is also of great importance to the spacecraft thermal design, each heatsink of the thermal test chamber is equipped with calorimetric instrumentation that is used to quantify the heat rejection from the individual cooler components. Quantifying the distribution of heat rejection between the compressor and displacer is very important for most cryogenic instruments because the compressor and displacer generally have separate heat conduction paths. The displacer heat rejection can be particularly critical for designs where the displacer is supported off of a cryogenically cooled optical bench; in such designs the displacer heat must either be absorbed by the optical bench cooler, or separately conducted back to the overall instrument heatsink -- a significant fraction of the electrical power input to the compressor is passed to the displacer via the transfer tube and is rejected there.

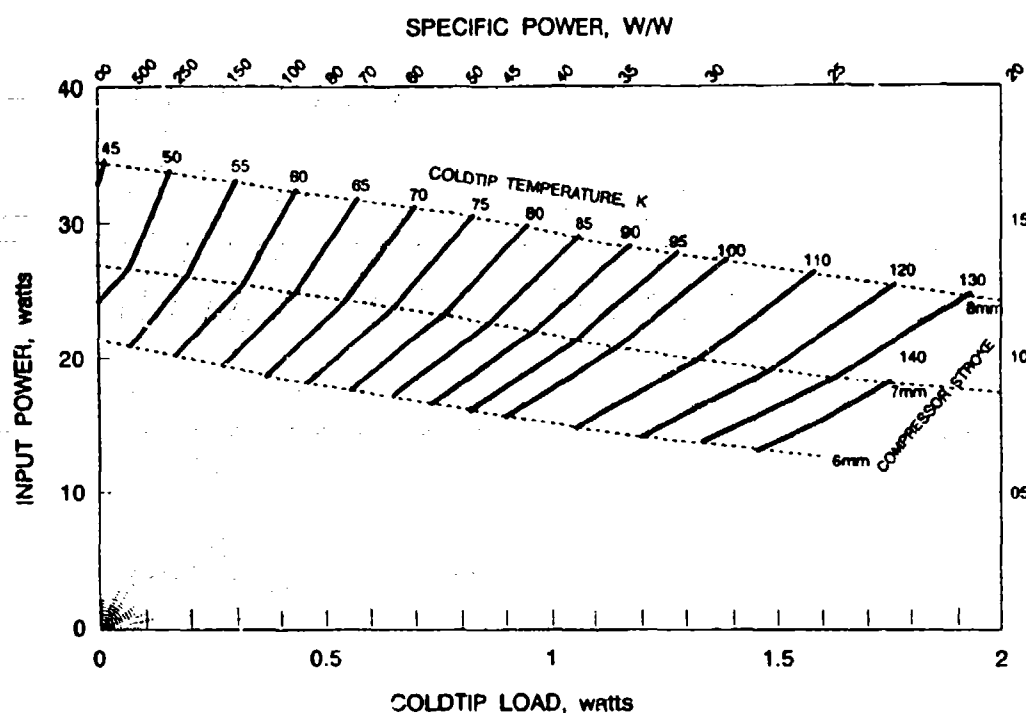


Fig. 3. Multivariable plot of the thermal performance of the BAe 80K space cooler.

The ability of the cooler to tolerate a broader heat sink temperature range (-20°C to 60°C) while not operating is also tested. In special low-frequency stiction tests, the cooler is driven at the milli-Hertz level so that the gas has sufficient time to bleed past the piston seals. The piston drive force (current to the cooler drive coil) is then monitored as a function of piston position to look for discontinuities that might indicate rubbing contact is being made. Differential material expansions or contractions that result in rubbing between moving masses and the cooler body are likely to lead to life-limiting failures.

Finally, cooler coldtip temperature stability is also measured to provide a baseline for determining temperature variations likely to be seen by the focal plane. IR focal plane array performance is highly temperature dependent, and requires very stable refrigeration. For example, the focal plane array on the NASA Eos/AIRS instrument requires short-term temperature stabilities on the order of 0.5 mK/sec .

Cold Finger Off-state Conduction Losses

For flight instruments relying on redundant coolers to provide added experiment reliability, it is important to know the thermal penalty suffered to maintain thermal connection between the cryogenic load and the non-operating (standby) cooler(s). Because the level of parasitic heat load is often a substantial fraction of the overall available cooling power from the operating cooler(s), accurate data of the heat load is essential for system design.



Fig. 4. JPL test setup for measuring coldfinger off-state conductance.

To measure the heat conductance through the coldfinger of a non-operating cooler, JPL has developed a special static conductance measurement apparatus that simulates the flight configuration of redundant coolers [3]. In this measurement technique, shown in Fig. 4, the cold finger of the test cooler is placed in a vacuum housing and attached to the coldfinger of a separate 10-K Gifford-McMahon (G-M) refrigerator that is used to cool the cold-tip of the non-operating test cooler down to typical flight operating temperatures. Note that the cold finger of the test cooler is carefully wrapped with multi-layer insulation (MLI) to prevent radiation parasitics from biasing the off-state conductance measurements. The heat flow passing through the test coldfinger to the G-M coldfinger is measured using an absolute heat flow transducer; this provides a direct measurement of the cold finger's cryogenic conductance under true steady-state conditions.

Based on the wide variability in construction of the coolers noted in Table I, the off-state parasitic conductance is expected to range from as low as 100 to 200 mW to as high as a watt or more. The parasitic load of the historical BAe 80K cooler is on the order of 330 mW at 55 K and decreases with increasing cold-tip temperature [3].

Cooler-Generated Vibration

In addition to a cooler's thermal performance, cooler-generated vibration is a particularly important parameter for precision imaging instruments. In characterizing cooler-generated vibration it is useful to speak in terms of the peak vibratory force imparted by the cooler into its supports when rigidly mounted. This force is the reaction force to moving masses within the cooler that undergo peak accelerations during various phases of the cooler's

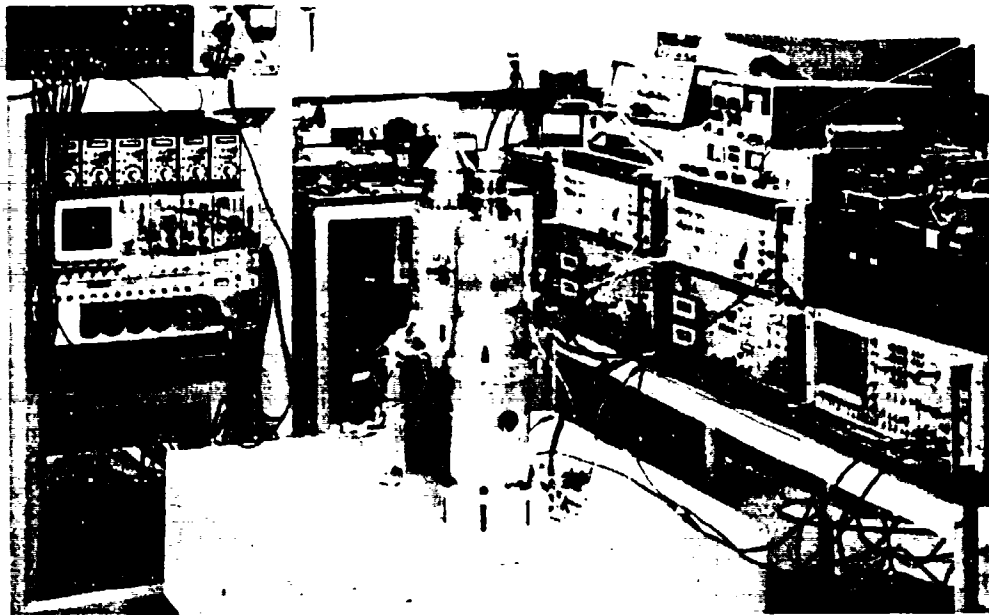


Fig. 5. JPL 6-DOF force dynamometer facility with BAe coolers undergoing vibration characterization.

operational cycle. The accelerations can be from controlled motion such as the reciprocating motion of a Stirling compressor piston or displacer, or natural vibratory resonances of the cooler's elastic structural elements.

Problems occur when the vibrating interface forces excite elastic deflections and resonances within the instrument structure and components that either adversely affect optical alignment, or generate spurious electrical signals. The latter are generated when electrical current-carrying or capacitively-coupled components undergo relative motions. To minimize excessive instrument vibratory response, a value on the order of 0.2 N (0.05 lbs) has gained acceptance as a reasonable design goal for cryocooler generated vibration.

To quantify and understand the force levels generated by present cooler designs, JPL has developed the unique 6-degree-of-freedom force dynamometer shown in Fig. 5 [4]. This dynamometer has a frequency range from 10 to 500 Hz and a force sensitivity from 0.005 N (0.001 lb) to 445 N (100 lbs) full scale. During operation the forces and moments generated about each of the cooler's axes are available simultaneously for real-time quantitative analysis.

To achieve acceptably low vibration levels, most emerging cryocoolers incorporate some sort of vibration suppression system based on momentum cancellation using back-to-back compressors and expanders, or electrically driven active counter-balancers. The lowest vibration levels are achieved when the momentum cancellation is managed using active feedback control based on nulling measured residual vibration force levels. Figure 6

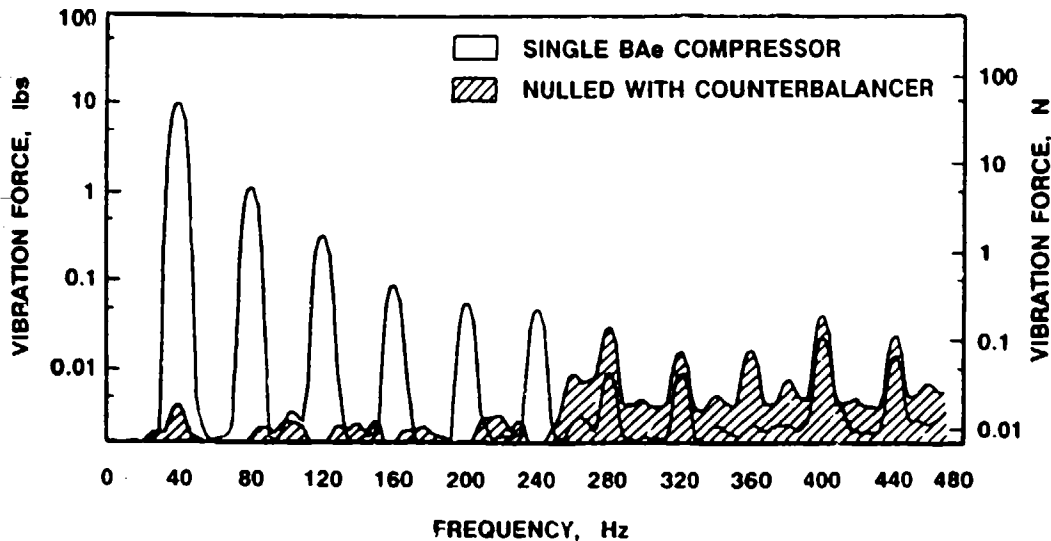


Fig. 6. Reduction of vibration harmonics of BAe 80K cooler with active counterbalancer and SatCon narrowband controller.

illustrates the typical vibratory response of a BAe 80K Oxford cooler with and without the application of a narrow-band active vibration suppression system developed by SatCon, Inc. [5,6]. All of the test coolers noted in Table I are designed for vibration suppression using momentum cancellation and are amenable to the use of advanced feedback control techniques; at least three are expected to have active vibration control upon their delivery to JPL for testing. Data such as that in Fig. 6 will be acquired on each of the test coolers and their vibration suppression electronics -- if provided.

Generated Electromagnetic Interference (EMI)

The use of mechanical cryocoolers in precision imaging instruments will require the placement of the cooler in close proximity of the sensitive detector arrays. The effect that the radiated electromagnetic fields generated by the cooler and its drive electronics will have on the detector electronics signals is not known. It is important that these generated electromagnetic fields be quantified and understood to help the flight instrument designer provide proper cooler placement and appropriate shielding within the instrument.

To characterize each test cooler's radiated EMI performance, a number of carefully controlled measurements are performed in accordance with MIL-STD 461. These test include:

- DC magnetic field profile
- AC magnetic field emissions
 - 10 Hz to 100 kHz @ 1m (MIL-STD 461:RE 04)
 - 10 Hz to 100 kHz @ 7cm (MIL-STD 461:RE 01)
- AC electric field emissions
 - 10 kHz to 40 MHz @ 1m (MIL-STD 461:RE 02)

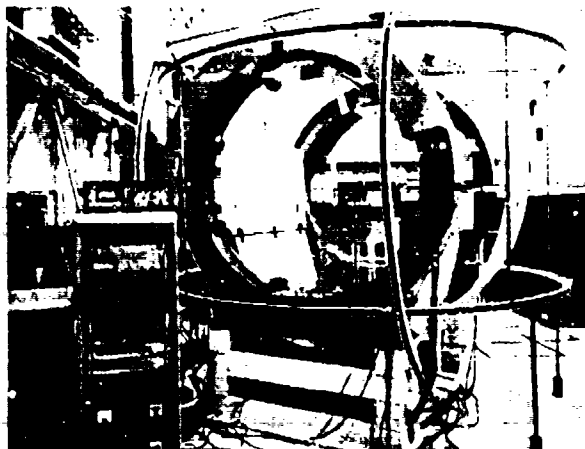


Fig. 7. JPL DC magnetic field measurement facility.

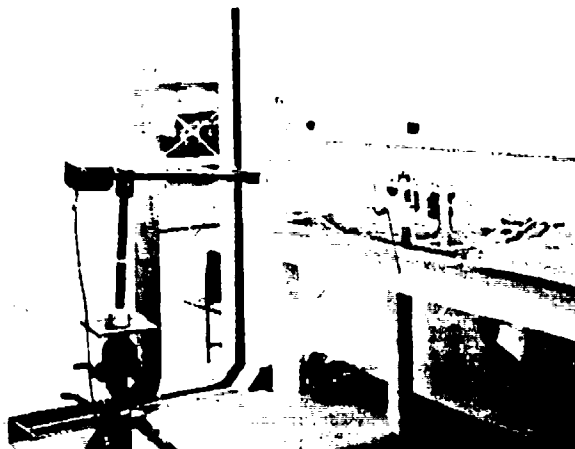


Fig. 8. JPL RF-shielded room for radiated emissions measurements.

The electromagnetic field measurements of the coolers are carried out in the JPL Electromagnetic Compatibility Test laboratory [7], which is used for testing all JPL flight instruments. DC magnetic field measurements are made in a DC magnetic field measurement facility that utilizes three large sets of Helmholtz coils to suppress background magnetic fields to the 1 nanoTesla (nT) level over a volume of 1 m³ (Fig. 7). The radiated electric and magnetic field emissions measurements are performed in a steel RF-shielded room with the facility electronics and cooler support electronics located in an adjacent room (Fig. 8). EMI characterization data on each test cooler is compared to standard requirements for acceptable levels in MIL-STD 461.

Radiated EMI and conducted current or voltage ripple fed back onto the spacecraft power bus from the cooler drive electronics also present a potential problem for other sensitive instrumentation on the spacecraft. Spacecraft designers are weighing the need to provide a separate "dirty" power bus to handle the cooler power requirements. Susceptibility and conducted emissions measurements will be included in the characterization testing when flight electronics are delivered with the cooler.

SUMMARY

The recent development of a number of long-life miniature cryocoolers has led to an explosion of interest in multi-year-life space cryogenic instruments. To assist the space-instrument user community in understanding and applying these important new cryocoolers, the Jet Propulsion Laboratory (JPL) has undertaken a cooler characterization program under the sponsorship of SDIO/AF Phillips Laboratory. Over the coming months extensive data will be available on a broad variety of space cryocoolers. The data will cover thermal performance, off-state cryogenic conductance, and generated vibration and EMI.

ACKNOWLEDGEMENT

The work described in this paper was carried out by the Jet Propulsion Laboratory, California Institute of Technology, and was sponsored by the Strategic Defense Initiative Organization through an agreement between the Air Force Phillips Laboratory and the National Aeronautics and Space Administration.

REFERENCES

1. Ross, R.G., Jr., Johnson, D.L. and Sugimura, R.S., "Characterization of Miniature Stirling-cycle Cryocoolers for Space Application," Proceedings of the 6th International Cryocooler Conference, Plymouth, MA, DTRC-91/002, David Taylor Research Center (1991), p. 27-38.
2. Kotsubo, V.Y., Johnson, D.L., and Ross, R.G., Jr., "Calorimetric Thermal-Vacuum Performance Characterization of the BAe 80 K Space Cryocooler", SAE Paper No. 929037, Proceedings of the 27th Intersociety Energy Conversion Engineering Conference, San Diego, California, August 3-7, 1992, P-259, Vol. 5, pp. 5.101-5.107.
3. Kotsubo, V., Johnson, D.L. and Ross, R.G., Jr., "Cold-tip Off-state Conduction Loss of Miniature Stirling Cycle Cryocoolers," Adv. Cryo. Engin., Vol. 37B (1991), p. 1037-1043.
4. Ross, R.G., Jr., Johnson, D.L. and Kotsubo, V., "Vibration Characterization and Control of Miniature Stirling-cycle Cryocoolers for Space Application," Adv. Cryo. Engin., Vol. 37B (1991), p. 1019-1027.
5. Johnson, B.G., et al., "Demonstration of Active Vibration Control on a Stirling-cycle Cryocooler Testbed", Proceedings of the American Control Conference, Chicago IL, June 24-26, 1992.
6. Johnson, B.G., et al., "Demonstration of Active Vibration Reduction on a Stirling-cycle Cryocooler Testbed", Proceedings of the 7th International Cryocooler Conference, Santa Fe, NM, November 17-19, 1992.
7. Johnson, D.L. and Ross, R.G., Jr., "Electromagnetic Compatibility Characterization of a BAe Stirling-cycle Cryocooler for Space Applications," Adv. Cryo. Engin., Vol. 37B (1991), p. 1045-1053.

PERFORMANCE OF A LONG LIFE REVERSE BRAYTON CRYOCOOLER

WALTER SWIFT, PRINCIPAL ENGINEER
CREARE INCORPORATED
HANOVER, NH 03755

HERBERT SIXSMITH, SENIOR ENGINEER
CREARE INCORPORATED
HANOVER, NH 03755

ABSTRACT

This paper describes a Single Stage Reverse Brayton (SSRB) cryocooler designed for long life applications in space. The cooler uses two high speed turbomachines with gas bearings to provide vibration free, reliable operation. An all metal compact heat exchanger with high performance contributes substantially to overall cycle efficiency. The system is capable of long life cooling at temperatures between 35 K and 100 K for cooling loads up to 10 W. Cycle efficiency approaches 10 per cent of Carnot.

Initial testing of a brassboard system demonstrated that temperatures below 40 K could be achieved in a single stage system without auxiliary cooling. Test results have been used to verify thermodynamic models of the components and to provide a basis for optimizing the system design. Initial test results for the brassboard system using two separate turbines are presented. System performance and physical characteristics for an optimized design are discussed.

INTRODUCTION

This paper presents initial test results on a closed loop reverse Brayton cryocooler and

predictions for the next generation device. The system is being developed for use in space, where long life, reliability, benign vibration, high performance and low mass are important operating requirements. The system is also designed for relatively low cooling loads. The technology developments that have supported this effort have focused on meeting all of these requirements. The approach has been to develop methods for fabricating small devices with a high degree of precision and combining features of the design in a way that reduces complexity where possible. The system configuration is the reverse Brayton cycle, where a continuous flow of gas is circulated by a compressor through a heat exchanger and a turbine. The two machines in the cycle each have one moving element, a high speed shaft supported on gas bearings. The challenge has been to reduce the size of these turbomachines while maintaining adequate efficiency in each to meet acceptable cycle performance levels.

The initial work on this system was reported in 1987 [1]. Since that time, the conceptual designs have become hardware, and the design point has changed somewhat (from 5 W at 70 K to 5 W at 65 K, and from a rejection temperature of 260 K to 280 K), but the objective has remained the same - to adapt turbomachine based systems to lower and lower cooling capacities.

During the past five years, we have developed and tested individual components for this cycle. A centrifugal compressor with pressurized bearings and a drilled hole impeller has evolved to its current state, using self acting gas bearings and an impeller with aerodynamically contoured blades. A unique, high efficiency inverter, particularly tailored to the characteristics of the compressor motor has been developed. Several turboexpanders have been designed and tested, the smallest of which has a rotor diameter of 2.36 mm. A very high performance, all - metal counterflow heat exchanger has been fabricated. Its performance has been confirmed in recent tests. This paper presents the results of the performance tests of this system at cryogenic temperatures. The results are encouraging, and provide confidence in what more can be accomplished.

SYSTEM DESCRIPTION

A schematic diagram of the cryocooler is shown in Figure 1. The system is designed to

operate from a supply of unregulated DC electric power. This power is first conditioned in a DC-DC regulator and then converted to three phase, ac power to drive the compressor. The compressor circulates a steady flow of gas through the cryocooler to supply refrigeration at the load. Compressor speed is set by the inverter frequency. A controller or control signal may be used to vary the compressor speed and thus change the pressure ratio for the system. Refrigeration is provided by the turboexpander at the cold end of the cycle. The turbine incorporates a brake circuit that is used to control turbine speed. The machines in the system are designed to operate without feedback control. This reduces the complexity of the electronics needed to operate the cooler. Temperature at the cold load can be adjusted by means of a trim heater if appropriate.

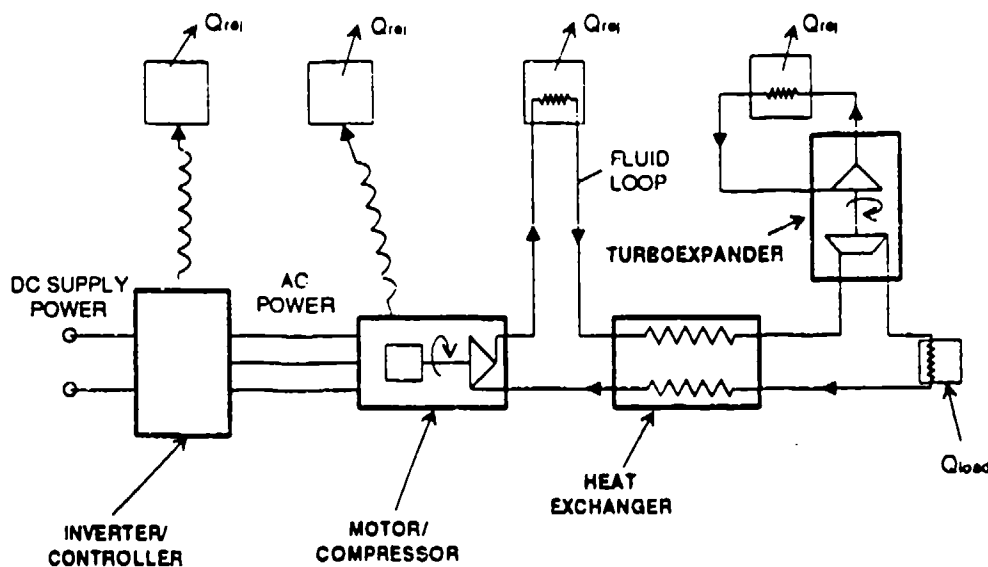


Figure 1. System Schematic

The reverse Brayton cycle is illustrated in the temperature - entropy plot shown in Figure 2. Starting at the inlet to the compressor (1), the pressure and temperature of the fluid is raised in a small centrifugal compressor that is powered by a high speed, three phase induction motor. The heat of compression (2) - (3) is removed from the gas through a heat exchanger connected to a heat rejection device (i.e., a radiator or cooling loop). The gas then enters the warm end of the counterflow heat exchanger where it is cooled by the low pressure return stream. The fluid exits from the heat exchanger (4) and enters the turbine where it expands to lower pressure and temperature (5), providing useful refrigeration. The low pressure gas returns to

the compressor inlet and cools the high pressure stream as it passes through the heat exchanger.

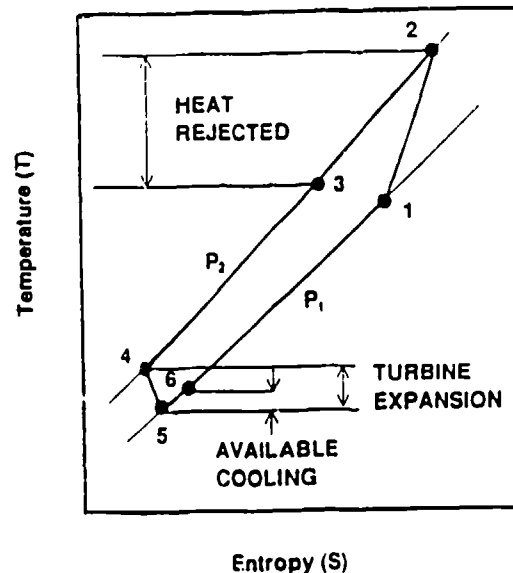


Figure 2. Cycle State Points

The cryocooler is made up of several discrete components, which provides for flexibility and some advantages in terms of integrating the system with the heat rejection system and the cooling load. First, the flow of gas is continuous, in a closed loop. The tubing at the warm end of the cycle (between the heat exchanger and the compressor) can be configured to incorporate a heat exchanger to interface directly on a radiator surface. Since the compressor circulates gas continually, the need for a separate cooling loop can be eliminated. The motor and inverter can be cooled by the cycle gas or by conduction to an appropriate heat sink. Similarly, at the cold end, heat from the load can be absorbed through a small plate by the flow of gas from the turboexpander. The warm end heat rejection interface and the cold load interface can be located at some distance from the cryocooler. The current design allows for a separation of up to one meter between the cryocooler and the load, and one meter between the cryocooler and the heat rejection loop.

Important performance parameters for the cycle and for the components are listed in Table 1. These characteristics are based on component designs that include modifications to the brassboard hardware that has been tested. The system is designed to provide 5 W of cooling at 65 K.

Table 1. SYSTEM CHARACTERISTICS

Fluid	Neon
Electric Input Power	< 200 W
Rejection Temperature	280 K
Load Temperature	65 K
Cooling Load	5 W
Cycle Pressure	1.1 atm
Pressure Ratio	1.6
Flow Rate	1.05 g/s
System Mass	14 kg
Life	> 5 yr

COMPONENTS

Inverter. The inverter uses a unique rotating field concept to convert 28 vDC input to three phase ac with a design point frequency of about 8 kHz. Primary and secondary windings of transformers are used with a digital timing circuit to produce wave forms that are nearly sinusoidal in shape. The inverter package is approximately 12 cm long by 17 cm in diameter and weighs 3.7 kg.

Motor/Compressor. The motor/compressor incorporates a centrifugal compressor driven by a solid shaft, three phase induction motor. It weighs 2.5 kg. A sectional view of the assembly is shown in Figure 3. The motor incorporates a two pole, twenty four tooth stator with 27 gage copper wire for the stator windings. An important feature of the compressor is the 1.52 cm diameter shrouded impeller. Because of the difficulties in fabricating the impeller by brazing or welding, it was machined from a solid disk of titanium alloy using spark erosion methods. The impeller incorporates eighteen blades with about 30 degrees of backsweep at the exit. The flow passages are about 0.5 mm high at the impeller exit.

The shaft is supported on self acting gas bearings. The gas bearing system employs two tilt-pad journal bearings and spiral groove thrust faces on either side of the impeller shroud.

These bearings are completely self acting and have proven to have adequate capacity for all expected operating modes to speeds of about 8,000 revs/second. In separate tests, two tilt - pad bearings of comparable design have been operating for nearly nine years in an endurance rig at 11,000 revs/second without detectable changes.

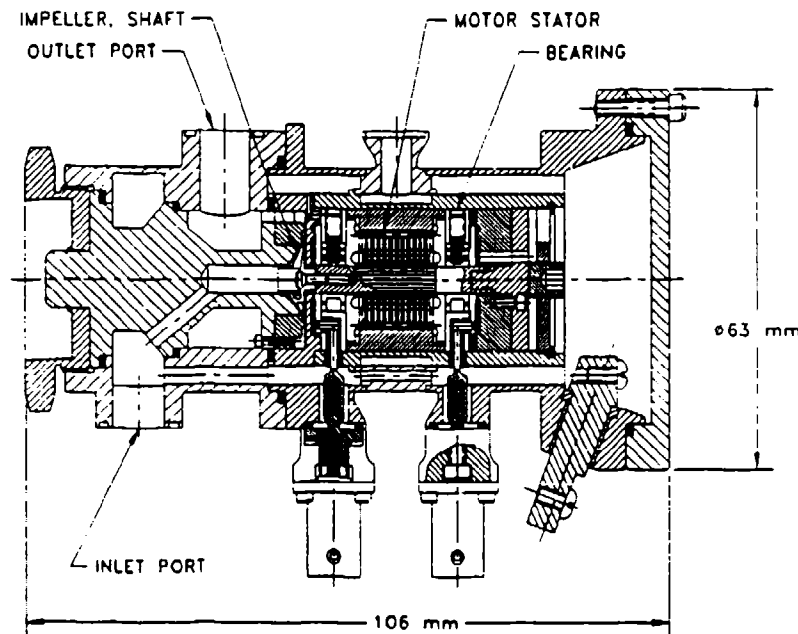


Figure 3. Compressor Assembly

Heat Exchanger. The heat exchanger is an all metal assembly consisting of counterflowing annular passages. High pressure gas enters at one end and flows through slots that are machined in 300 copper disks axially positioned within a stainless steel tube. Heat is transferred transversely through the disks to rings in an outer tube. The rings are axially positioned in line with corresponding disks. Colder gas at lower pressure flows through slots in the rings in the outer tube absorbing the heat from the high pressure stream. The design of the heat exchanger has been optimized to reduce overall losses in performance. An important feature in accomplishing the combination of high thermal effectiveness and low pressure loss in the assembly has been the ability to machine small, precise slots in large quantities with high accuracy. Figure 4 is a photo of one disk/ring pair showing four annular series of slots. Each slot is approximately 0.1 mm wide by 3 mm long. The thickness of the copper material is 0.4 mm. The heat exchanger assembly is 530 mm long by 90 mm diameter and weighs 5.8 kg.



Figure 4. Heat Exchanger Ring/Disk Pair. Scale Is In Inches.

Turboexpander. The turboexpander is principally constructed from titanium alloy. It is approximately 3 cm diameter by 10 cm long and weighs less than 1 kg. A small, high speed turbine rotor is machined using spark erosion methods into the end of a solid shaft. A brake rotor of similar geometry is machined near the other end of the shaft. Radial support for the shaft is provided by self acting tilt pad gas bearings that are similar in design to those used in the compressor. Axial load is taken by a thrust bearing at the end of the shaft. The thrust bearing is activated by a small portion of the flow circulating through the brake system.

The brake wheel circulates a small quantity of gas through a remote heat exchanger. The work of expansion is thus rejected as heat at some convenient warm gas temperature. An important consideration in the design of the turboexpander is the parasitic heat leak to the cold end through the turboexpander housing. Conduction is controlled by a combination of materials selection and geometry. Convection is controlled by balancing the pressure between the brake circuit and the nozzles. Normally, the brake rejects heat to the same heat rejection interface as the rest of the cycle. However, since the brake load is fairly low compared with

other heat rejection loads (roughly 5 % of the warm end thermal loads), other, lower temperature options may be used with very high cycle benefits. As an example, if the brake can reject heat to a single 10 watt radiator at 220 K rather than the thermal bus at 300 K, cycle input power to the cycle can be reduced by about 15 %. Since the brake is a circulator, conduction straps are unnecessary.

TESTING

During the last year, several components were assembled into a closed loop system and tested. These components are identified as brassboard because they were not optimized for system performance at the 5 W, 65 K design point. The tests were designed to provide operating experience at the system level and to provide data that could be used to check component models so that the designs could be optimized. Instrumentation during the tests was fairly extensive. Pressures and temperatures at inlet and exit ports for each of the components were recorded so that the performance of the individual components could be measured. Controls were also present so that flow, pressure, load and load temperature could be varied. Compressor speed and turbine speed could be independently varied. Flow rate to the cold end of the cycle through the heat exchanger could also be controlled, independently of pressure ratio by bypassing some of the flow from the compressor through a separate warm loop. Figure 5 shows the configuration of the counterflow heat exchanger, turboexpander and related equipment within the vacuum vessel. The compressor and inverter were located on a bench about two meters from the vacuum vessel.

Two turboexpanders were tested. The first turbine was designed for the 5 W nominal load. The turbine rotor diameter was 3.18 mm. Its nominal output capacity is 9 W at 65 K. The turbine rotor in the second turboexpander was 2.36 mm. This machine has a nominal capacity of about 4 W. The two machines were tested to provide data on the performance of the cold end components (heat exchanger and turboexpander) at a nominal 5 W load and 1 W load. The compressor and heat exchanger for both test series were unchanged.

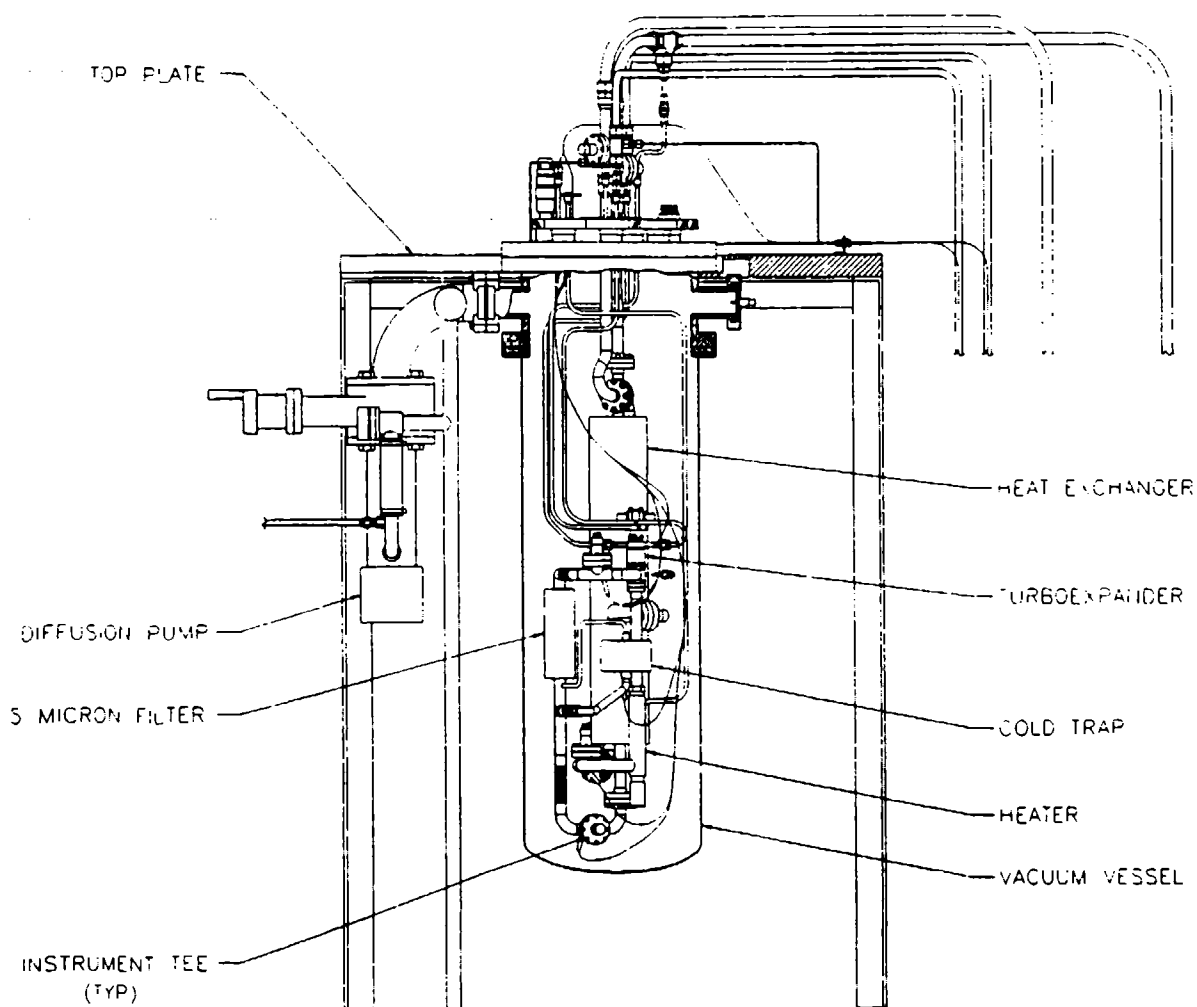


Figure 5. Cold End Assembly For Testing

Figures 6 and 7 show selected results from the cooldown and performance testing of the system. Both figures show temperature at the exit of the load, cycle input power and for some time periods, the cold load in watts. Figure 6 gives results with the 3.18 mm turbine. The compressor was operated at nearly constant speed and input power for the first 42 hours. The system cooled down from room temperature to approximately 37 K measured at the exit from the turbine within 24 hours. After the system was relatively stable at the low temperature, the load, turbine speed and compressor speed were systematically varied to obtain turbine performance data over a range of conditions and temperatures. These tests continued for another 17 hours. At the completion of the performance test matrix, the system was shut down by switching off the power to the compressor.

Figure 7 shows similar test data recorded during the cooldown and performance testing of the 2.36 mm diameter turbine. Because the turbine capacity is less than half that of the larger machine, the cooldown was assisted by an external bypass of flow through a precooling heat exchanger. The precooler used liquid nitrogen, then liquid helium to cool a portion of the neon flow that bypassed the heat exchanger and was introduced just upstream of the turbine. When the system temperature at the cold end approached 30 K, the helium precooler was isolated from the system, and the cryocooler provided the rest of the cooldown without assistance. The lowest "no - load" temperature achieved was about 27 K at the turbine exit. Tests at several loads and temperatures were then performed for a period of about 7 hours to obtain performance data for the small turboexpander.

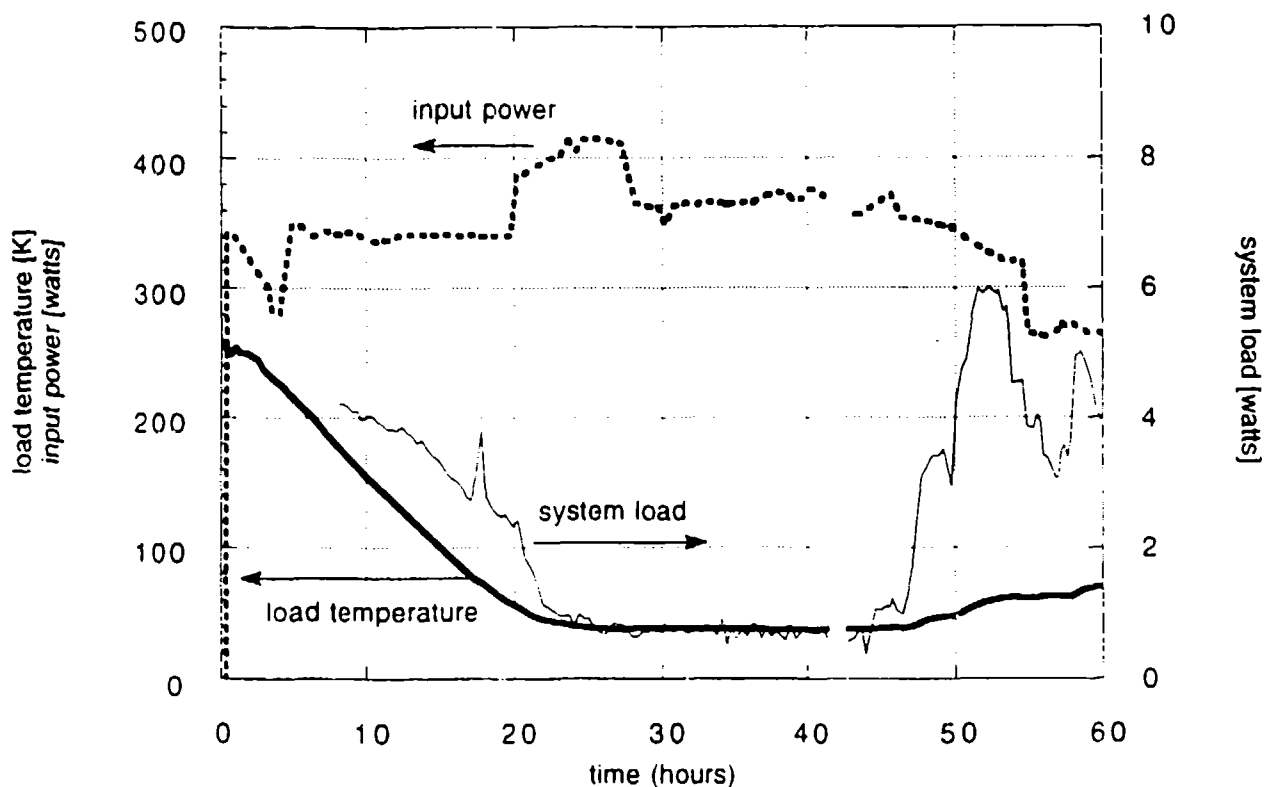


Figure 6. Cooldown With 3.18 mm Turbine

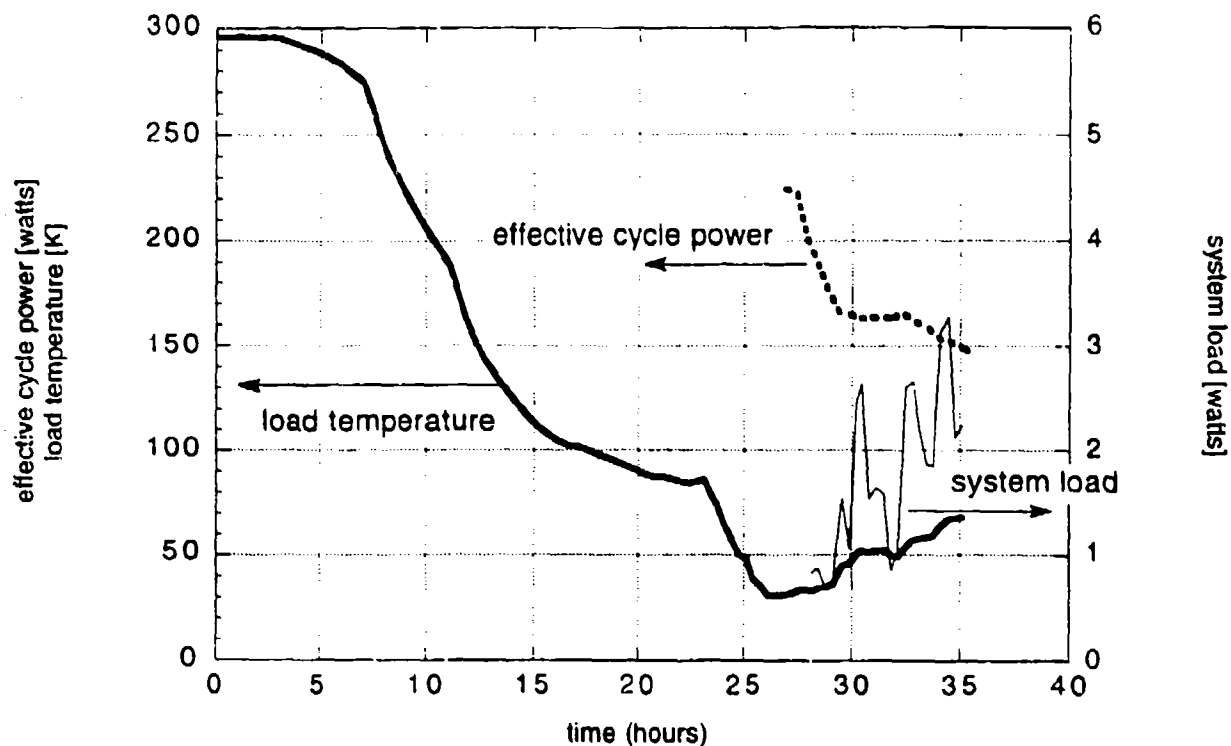


Figure 7. Cooldown With 2.36 mm Turbine

RESULTS

During testing, the system demonstrated that it could achieve temperatures well below the 65 K design point. For tests with the large turbine, the lowest temperature attained was 37 K. At this condition, the load at the cold end was about 0.5 watts. For the test with the smaller turbine, the lowest temperature achieved was 27 K. However, this temperature was attained with the liquid helium precooler assisting the cooldown. In a second series of tests, the helium precooler was isolated from the system at a temperature of 50 K. The cooler continued to refrigerate, until a no load temperature of 34 K was reached.

Input power levels to the system were higher than design targets. However, the detailed measurements for each of the components showed that the performance goals can be achieved for the 5 W, 65 K design point with relatively straightforward modifications. Furthermore, a sufficient amount of data was collected to give confidence that the system can operate at lower temperatures and lower capacity with reasonable input power requirements.

During the tests, the heat exchanger exceeded performance requirements over a broad range of conditions. At design temperatures and flows, the measured thermal effectiveness was 0.993 compared to a design goal of 0.990. This was accomplished with pressure losses in the heat exchanger that were less than predicted. The turboexpander met design expectations. However, the efficiency of this component can and will be increased by reducing conductive heat leak to the cold end by a simple modification to the design. The compressor met aerodynamic performance expectations. However, bearing drag in the motor exceeded the design expectations resulting in a lower overall efficiency for the input power train (compressor, motor, inverter) than the design target. The improvement in turbine efficiency will compensate for this.

PROJECTIONS OF PERFORMANCE

Component test results were used to identify design changes to the brassboard components in order to meet system input power goals at the design load and temperature. These results have also been used to update the system model for projecting the performance of a single stage system scaled to lower cooling capacities. The results of these scaling studies are shown in Figure 8. The curves in the figure show the relationship between predicted cooling capacity and load temperature for three systems, designed for three input power levels.

The predictions given in the figure reflect only modifications to the hardware designs, not changes to the system operation or integration. (I.e., the potential reductions in cycle power associated with reduced brake temperature are not reflected in these curves.) For the 200 W system, the only significant change to the design is a reduction of conduction between the turbine warm and cold ends. For the 150 W system and the 100 watt system, the motor/compressor size would be reduced and the shaft speed would be correspondingly increased. This is required because the reduced capacity for these two systems would be obtained basically by reducing flow rate. For the 100 W cycle, the 3.18 mm diameter turbine would be replaced by the 2.36 mm diameter machine. Additional reductions in cycle power

could be accomplished by reducing the heat rejection temperature of the turboexpander brake, thereby reducing heat leak in this component.

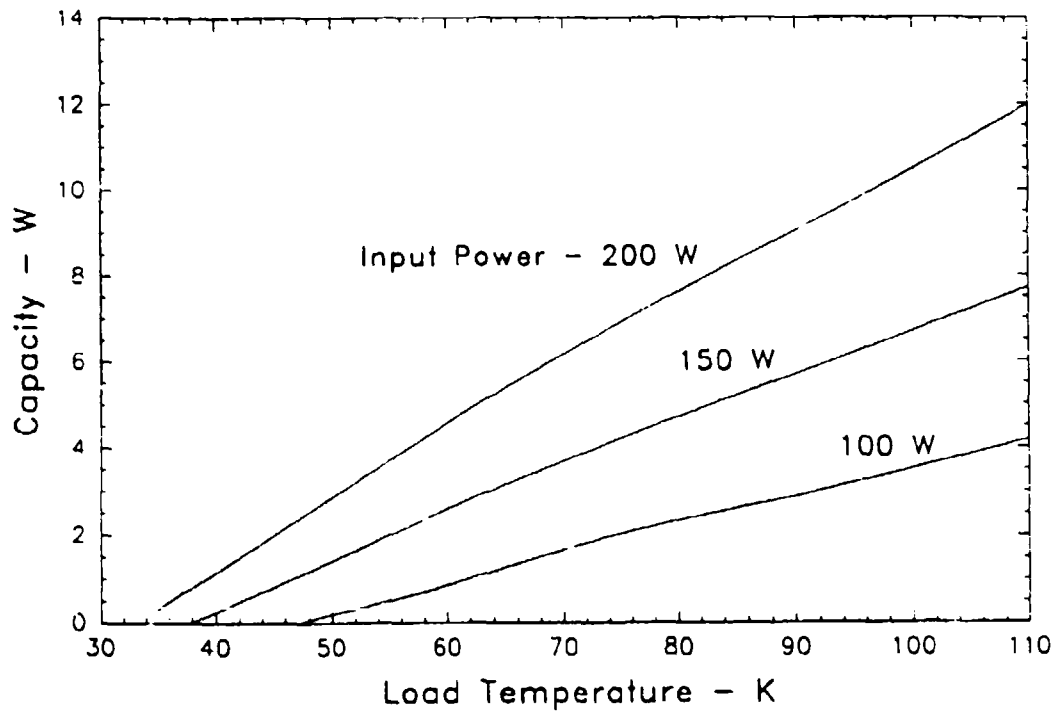


Figure 8. Predicted Cooling Curves For Three Single Stage Reverse Brayton Systems

CONCLUSIONS

The development work performed to date on this system has demonstrated that good thermodynamic performance can be achieved in a reverse Brayton system using turbomachines. We have demonstrated that with a high performance heat exchanger, temperatures as low as 35 K can be achieved in a single stage. The tests have also provided clear guidance for design modifications to the components that will further reduce the input power levels to the desired goals.

ACKNOWLEDGEMENTS

The work described in this paper has received support by SDIO, Phillips Laboratory and NASA/GSFC.

REFERENCES

1. Sixsmith, H., Valenzuela, J.A., Swift, W.L.; *Small Turbo-Brayton Cryocoolers*; Advances In Cryogenic Engineering, Vol. 33; Ed. R.W. Fast; Plenum Press: New York, 1988.

SDI CRYOCOOLER PRODUCIBILITY PROGRAM

**JEFF BRUNING, CONSULTANT
NICHOLS RESEARCH CORPORATION
P.O. BOX 108
LEASBURG, MO 65535**

INTRODUCTION

Funding constraints, escalating manufacturing costs, and a serious decline in industrial productivity have greatly increased the cost for fielding aerospace systems. Changing economic realities are forcing us to change the way we do business in the major defense system acquisition process. Within the Department of Defense, our "performance at any cost" attitude is no longer acceptable. We now must consider and evaluate the cost of systems (and their technology components) equally with performance and capability.

Under SDIO sponsorship, the Air Force Phillips Laboratory has undertaken a new cryocooler producibility initiative to address the issues mentioned above. Their goal is to reduce cooler production costs while improving both quality and reliability. This paper will briefly describe the new PL producibility initiative with emphasis on recent findings and future thrusts.

BACKGROUND

Most cryocooler developers fail to consider the manufacturing costs and expected production runs until it's too late to make any meaningful design changes that address these issues. Thus, the contractors usually miss their best opportunity to include low cost, high throughput manufacturing attributes in their cooler designs. Cryocoolers are also manpower-intensive machines that don't lend themselves well to automated production techniques. This is especially true for assembly procedures where 100% parts inspection, clean room environments, specialized equipment and parts handling fixtures, and stringent contamination

control requirements significantly increase the "touch time" needed on each cooler. It's difficult to leverage proven techniques such as *concurrent engineering* and *design for automation* when there's a fundamental gap in process technologies to replace the manpower-intensive manufacturing/assembly procedures inherently associated with cryocoolers. When we finally do achieve high throughput manufacturing economies at the component level, significant gains in overall production line flow remain "choked" at the point where assembly line operations begin.

Our experience shows us that developers who design viable coolers aren't necessarily the best available contractors to manufacture them. However, it's difficult to transfer cryocooler product information. Identifying a manufacturing "center of excellence" to produce the coolers doesn't guarantee that the enterprise can readily accommodate the existing design package. Product information transfer between cooler developer and eventual manufacturer is hampered because each uses different types of computers, CAD/CAM programs, product databases, and communications methods. Thus, the package reflects different data formats, data and file structures, and data content.

The government must invest in high capital cost equipment to achieve manufacturing economies for coolers. However, various cooler developers have refrigerator designs that meet different sets of government requirements. It's unrealistic to expect that the government will establish multiple manufacturing centers due to the enormous costs involved. Any cooler manufacturing center must ensure that their production lines are inherently flexible to accommodate a wide variety of parts, materials, in-line testing, and assembly procedures associated with diverse cooler designs.

The Strategic Defense Initiative Office (SDIO) supports our recent thrust in addressing cryocooler producibility. By "producibility", we mean the relative ease and low cost of producing high quality cryocoolers at the capacity needed by system users. SDIO's Passive Sensors Office was instrumental in helping to define the program when a fully capable Phase I deployment scenario was still envisioned for strategic defense. At that time the Brilliant Pebbles (BP) system drove the need to address producibility because of its constellation size and the cost-driven nature of its development. However, SDIO budget constraints forced deferment of its planned producibility effort until FY92.

An austere project began in January 1992 through the Air Force Phillips Laboratory (PL) to simultaneously address the problems of cryocooler critical dimension parts variations; coordinating with diverse producibility thrusts within SDIO (specifically, the Producible Technology Working Group and the new Spacecraft Fabrication and Test MODIL); and exploring the feasibility of a large-scale producibility effort through an in-depth cost benefit analysis. The cost benefit analysis serves as an interactive planning tool to help government program managers make informed decisions regarding cryocooler producibility investments. The focus of this paper is on describing the results of the cost benefit analysis results since they help bound the scope of the more detailed producibility program that SDIO may eventually pursue.

CRYOCOOLER PRODUCIBILITY REQUIREMENTS

There are a wide variety of systems within the SDI architecture that have identified the need for cryocoolers in order to operate. These include the Brilliant Eyes surveillance satellite, BP, various ground based interceptor concepts, future systems such as advanced Directed Energy Weapons and Kinetic Energy Weapons, and possibly some aspects of the Command/Control Element. Other requirements exist at the subsystem-level, such as cooling for both high and low temperature superconducting devices, long-term on-orbit cryogen storage, and chilled electronics. In addition to SDI needs, other Department of Defense and NASA system developments (e.g., the Earth Observation Satellite) also have cryocooler requirements.

The primary criterion that the cryocooler producibility effort must glean from system-level requirements is the overall production capacity needed. Because most of the cryocooler development conducted under government sponsorship is largely coordinated, the same contractors will be producing coolers for various government agencies to address their respective requirements. Most system development timelines overlap. Therefore, cooler builders will most likely be manufacturing several makes of coolers simultaneously on the same production line. Thus, it is reasonable to expect that the *cumulative government cooler manufacturing requirements establish a single overall production capacity goal*. This production capacity is the focus of the SDI producibility initiative since overall government production needs are, from strictly a cost standpoint, inseparable.

The Brilliant Eyes (BE) surveillance system now replaces BP as the requirements driver for the producibility project within SDIO. This is due entirely to the new nature of the SDI architectural construct. BE's manufacturing requirements also lead the cumulative government needs for cooler production. By focussing on BE's needs, we hope to concurrently address the concerns of other system development programs. However, in addressing BE's needs, we must be careful to remain cognizant of how other systems' cooler production requirements may differ from BE's and remain flexible in our approach so these differences can be accommodated.

In order to ascertain a system's production needs, various considerations must be taken into account that may not be readily apparent. For example, at first glance one would expect the cooler production lot for a system (Q) equals the number of systems (n_{sys}) multiplied by the number of coolers (x) needed per system:

$$Q = xn_{sys}$$

However, actual cryocooler production requirements from system Demonstration / Validation through Full Scale Development may exceed this by a substantial amount. Several factors may contribute to a higher total production requirement.

First, additional coolers are needed in order to fully characterize the operation of the production model cooler prior to its commitment to full production. Characterization tests include full functional testing, operational testing in simulated space environments within mission parameters, off-design point performance mapping, electromagnetic compatibility testing, and flight qualification testing. This requires from 2-6 separate coolers. Due to the nature of these investigations and their affects on hardware, the coolers will not be available for integration with the spacecraft after running the full gamut of characterization tests.

Second, long-life cryocoolers, especially those earmarked for space applications, have a woefully inadequate database of sustained long-duration "unattended" performance information approaching that needed for SDI systems. Most of these spacecraft need a 5-10 year continuous operational life with .95 reliability/.95 confidence. Exit criteria for proceeding into Defense System Acquisition Milestone II (Full-Scale Development, or FSD) most probably will include substantiation of life and reliability estimates for the cryocoolers baselined for FSD and Production.

Proving life and reliability estimates (at correspondingly high confidence levels) will require multiple unit endurance testing. Estimates have put the number of endurance test units at ten or more.

Finally, most systems under development that are in their Demonstration / Validation phase plan to flight test one or more of their baselined coolers having direct legacy to the eventual flight coolers slated for production. This adds to the total production requirements imposed on the manufacturing facilities of the cooler vendors and their subcontractors.

It's apparent that the total number of coolers needed for a system can exceed the "integration units" by up to 30%. For a system such as BE, this could equate to over 50 cryocoolers. Since most systems are progressed under a very stringent and compressed development schedule, this production lot size stresses the capabilities of most potential cooler vendors vying for production contracts. Adding to this is multiple systems within the government needing the same cooler from the same vendor. Unless sufficient steps are taken early to advance not only the cooler design, but also the production processes needed to produce the coolers, vendor production capacity limits could potentially delay system deployment.

PRODUCIBILITY PROGRAM OVERVIEW

Although the exact scope of the cryocooler producibility program is not finalized, the possibilities for this effort range from a parts improvement program to a full scale Manufacturing Operations Development and Integration Laboratory (MODIL) thrust. The following project objectives and approach describe how a comprehensive producibility program could be pursued for coolers.

OBJECTIVES: The main overall project goal is to reduce per unit production costs to below \$50K per cooler, cut manufacturing leadtime to less than six months, improve quality, and reduce unit-to-unit performance variations due to manufacturing processes. This is done by first achieving the following objectives:

1. Formulate common design philosophies independent of cooler make/model that facilitate system-driven low cost, high throughput production requirements. All present and future cooler developers must adhere to these philosophies from the on-set of design activities.

2. Develop cryocooler Product Data Interchange (PDI) standards and require all contractors to use them for government related cooler development and production.
3. Establish a single flexible manufacturing facility needed to produce the whole range of long-life space coolers of interest to the government.
4. Be able to meet SDI system defined production rate requirements.

APPROACH: In accordance with established concurrent engineering practice, we should examine, dissect, and assess the Standard Spacecraft Cryocooler (SSC), the Protoflight Spacecraft Cryocooler (PSC), and other viable cooler designs to determine the manufacturing and assembly functions needed to produce long-life space coolers. Afterwards, recommend redesign considerations to improve cooler producibility. Implementation of these "redesign for producibility" recommendations by cooler vendors must include strict adherence to newly established PDI standards. The initial focus will be on applying state-of-the-art manufacturing techniques to achieve the maximum possible production capacity. Assess the maximum achievable capacity and its ability to meet SDI near and far-term needs, as well as other concurrent government production requirements (e.g., NASA EOS). If production capacity is inadequate, then identify "choke point" processes in part machining, in-process testing/QC, and assembly functions that affect both capacity and costs. The next step is to pursue various concurrent MANTECH projects that initially focus on improving overall production line efficiency, automating the "hard-to-do" critical dimension parts machining processes, and enabling complete component machining and inspection automation. Concurrently with the MANTECH initiatives, we must reassess the cryocoolers and identify redesign opportunities that allow some degree of automated assembly and test. If those opportunities prove feasible, then begin new MANTECH efforts to partially automate the assembly functions. The ultimate challenge is establishing a highly automated flexible cryocooler production cell (including an automated Flexible Inspection System) capable of accommodating a variety of cryocooler designs. The cell flow line must be properly balanced to meet system-specified production rates and allow adequate buffer for accepting the parallel production flow of the flight control electronics. The production cell must be on-line and certified prior to the deadline for SDI systems' Production Readiness Reviews.

SECONDARY ACTIVITIES: The major drivers for this project are achieving the cost objective of <\$50K per cooler while achieving potentially high

throughput production rates for a variety of cryocooler designs. Secondary considerations that form the critical path to achieving these goals include the following activities:

1. Investigate wear mechanisms that impact cooler performance and reliability.
2. Perform a tactical cooler assessment to determine what lessons-learned are available from their production and manufacturing histories. Test methodologies and failure modes and effects analyses should also be assessed.
3. Determine what levels of contamination introduced by traditional manufacturing processes are tolerable by the various long-life coolers.
4. Develop a correlation matrix between operation lifetime and testing performed during manufacturing and production phases. If correlation exists, then identify opportunities where in-process testing could alleviate performance and reliability concerns. These methods should also be explored to limit unit-to-unit variations in cooler operation at the end of the production cycle.
5. Determine the effects of design tolerancing methodologies on cooler performance and identify design characteristics that allow thermal gradients to adversely affect critical dimensions. Also identify the possibilities for long-term dimensional instability.
6. Examine the possible correlation between manufacturing and assembly techniques to cooler life. Special emphasis must be given to identifying particular processes and handling techniques that contribute to dimensional instability and early cooler failure.

The Aerospace Corporation (El Segundo, CA) is assisting PL in applying Taguchi methods for reducing parts variations experienced with recently developed coolers. Lawrence Livermore National Laboratory (LLNL, Livermore, CA) is currently assisting The Aerospace Corporation with analyzing the results of recent cooler vendor site visits, participating in design surveys, and disseminating the results of related workshops (e.g., the Spacecraft Fabrication and Test MODIL Industry Briefings). These activities are still underway and the results will be reported as they become available. A top-level cryocooler producibility cost benefit analysis has been performed for PL through Nichols Research Corporation in order to assess the feasibility of pursuing all or portions of the comprehensive producibility effort described above. The remainder of this paper will describe the results of this cost benefit analysis.

COST BENEFIT ANALYSIS (CBA)

Payoffs for investing in enhanced production methods for cryocoolers must be readily apparent. The major goal of the CBA element of the overall cryocooler producibility program is to *quantitatively* determine what the payoffs are. There are various "yardsticks" useful in evaluating whether investments are worthwhile. In our CBA, these include payback period (PP), present worth (PW), uniform annual cost (UAC), and rate-of-return (ROR) or return-on-investment (ROI) methods of investment comparisons. The major premise in our CBA was that the government should, in the final analysis, evaluate investments in cryocooler producibility against the same criteria that industry evaluates any other investment they undertake: Is there a net positive benefit to the government for investing in producibility? If so, will the investment pay for itself in terms of future savings to the taxpayer?

Our CBA, while using the four comparison methods listed above, focused on the *Payback Period (PP)* method as a quick-look at investment potential. If the investment showed promise, more in-depth analysis followed, including *break-even analysis* (to determine the production rate/production cost break even point), a cooler "*per unit*" cost *determination* for various production rates possible by different manufacturing methods, and a *ROI analysis* to show when an investment can be expected to payoff and what the magnitude of the payoff will most likely be.

ASSUMPTIONS: In performing the various analyses mentioned above, it was necessary to make certain assumptions regarding key system and cost parameters. In doing so, a wide enough trade space was analyzed to cover all potential scenarios likely to be experienced by actual SDI systems. These assumptions are listed below:

1. Current cooler costs are based on those previously experienced by government contracting agencies. These costs represent expected per unit costs if no investment is made in producibility and cost reduction initiatives.
2. Cooler production cycles are expected to range between 18 months to five years.
3. Production lots range from 40 to 200 coolers.
4. Government investment in cooler producibility ranges between \$1M-\$10 M for advanced manufacturing and assembly processes, MANTECH

programs, redesign activities, and establishing a flexible manufacturing cell and its facilities.

5. Cell yearly operating costs range between \$0.5-\$1M.
6. Associated cost savings (on a per unit basis) range between 20%-90% of current cooler costs.
6. Value of money discounted at 4%.
7. Existing manufacturing case:
 - a. Labor rate (20 station production line/15 people) = \$150/hr.
 - b. Machine costs=\$3M.
 - c. Service Life=7 years.
 - d. Salvage value=\$0.
 - e. Maintenance=\$60,000/year.
 - f. Labor overhead rate=90%.
 - g. Machine overhead rate=20%
 - h. Maximum production rate possible (100% utilization)=48 coolers per year.
 - i. Value added per cooler (markup)=20% x Per unit cost.
 - j. Cooler raw material cost=\$10,000.
 - k. Manufacturing lead time=12 months.
 - l. Average time spent per processing step=8 hours.
 - m. Storage rate=13%.
 - n. Cooler production non-operating costs=\$20/part.
 - o. Number of parts/cooler=180.
8. Enhanced production case:
 - a. Labor rate (3 station production line/10 people)=\$62.50/hr.
 - b. Machine costs=\$10M.
 - c. Service Life=5 years.
 - d. Salvage value=\$1M.
 - e. Maintenance=\$100,000/year.
 - f. Labor overhead rate=40%.
 - g. Machine overhead rate=20%
 - h. Maximum production rate possible (100% utilization)=105 coolers per year.
 - i. Value added per cooler (markup)=20% x Per unit cost.
 - j. Cooler raw material cost=\$10,000.
 - k. Manufacturing lead time=6 months.
 - l. Average time spent per processing step=8 hours.
 - m. Storage rate=7%.
 - n. Cooler production non-operating costs=\$4/part.
 - o. Number of parts/cooler=130.

For the existing manufacturing case, the assumptions represent parameters historically observed, recently estimated, or within industry

norms. For the enhanced producibility case, the assumptions are best estimates, or reflect achievement of the producibility program objectives. In both cases, a conservative approach was used for the purpose of the CBA.

Payback Period Method: The PP method is a "rule of thumb" approach to identify the payoff potential of the investment. Its a fairly simple method to analyze potential yearly cost savings (S) and ascertain how quickly the investment will pay for itself (payback period, n). We assumed the net savings per year to be constant for the entire production period. The governing equation for this analytical method is:

$$n=IC/NACF$$

The term IC is the initial investment cost. In our case, this is total cost of the producibility program:

$$IC=(R\&D \text{ costs})+(Machinery/Hardware/Facility \text{ Development and Build costs})$$

The term NACF is the equivalent of our expected total yearly savings from lower cooler production and per unit costs. The relationship of savings per cooler (S_{pc}), production lot size (Q), production cycle (t), and production facility operating costs (C_{op}) is:

$$NACF=S=S_{pc}(Q/t)-C_{op}$$

Production scenarios were evaluated based on both the total government cumulative cooler requirements and the SDI-only case. The results show that even for sizeable investments to enhance production, the payback period is fairly quick (between 5-18 months).

RETURN ON INVESTMENT (ROI): This method is used to further analyze those investment/production scenarios identified as promising by the method described above. The ROI method also takes into account the time cost of money in order to show the rate at which an investment pays off. For a given annual amount saved (S), we can compute the Final Cumulative Savings (F):

$$F=S((1+i)^n - 1)/i$$

where i =discount rate=4%. The results of some of our test run calculations are shown in figure 1. Good correlation was observed between using the PP and ROI methods.

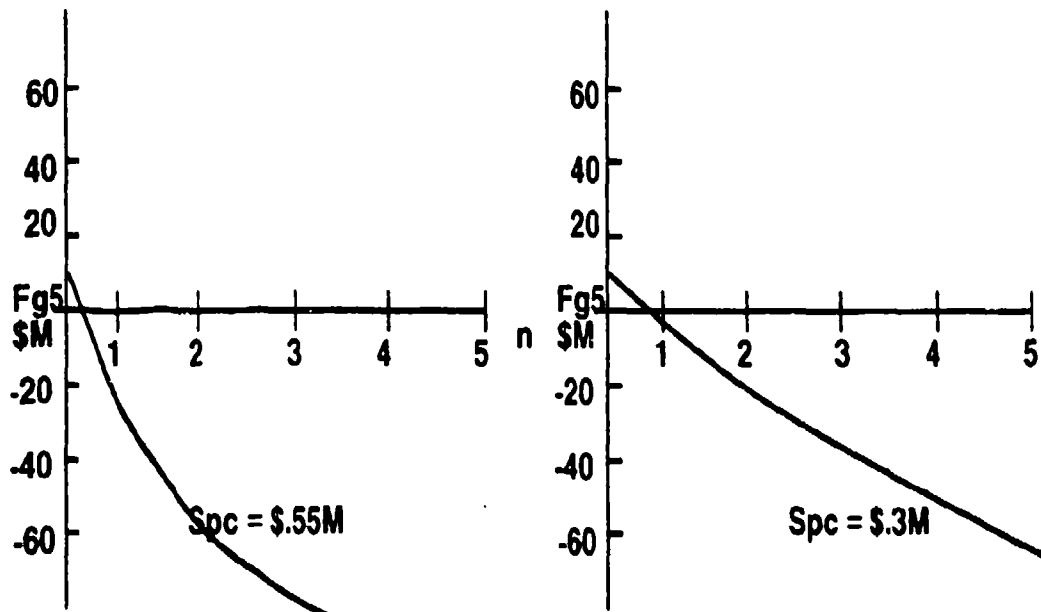


Figure 1. ROI representative results.

BREAK EVEN ANALYSIS: This method is the best way to use the results previously discussed to perform "what if" exercises to assess the affects of changes in production costs, savings, and annual cooler production rates. Two different variations of the Break Even Analysis exist-the Cost Break Even Analysis and the Profit Break Even Analysis.

The Profit Break Even Analysis is used to analyze how well a given production line can show profitability by determining what production rate must be exceeded in order for revenues (savings) to exceed production costs. Figure 2 shows an example of this analysis and its results.

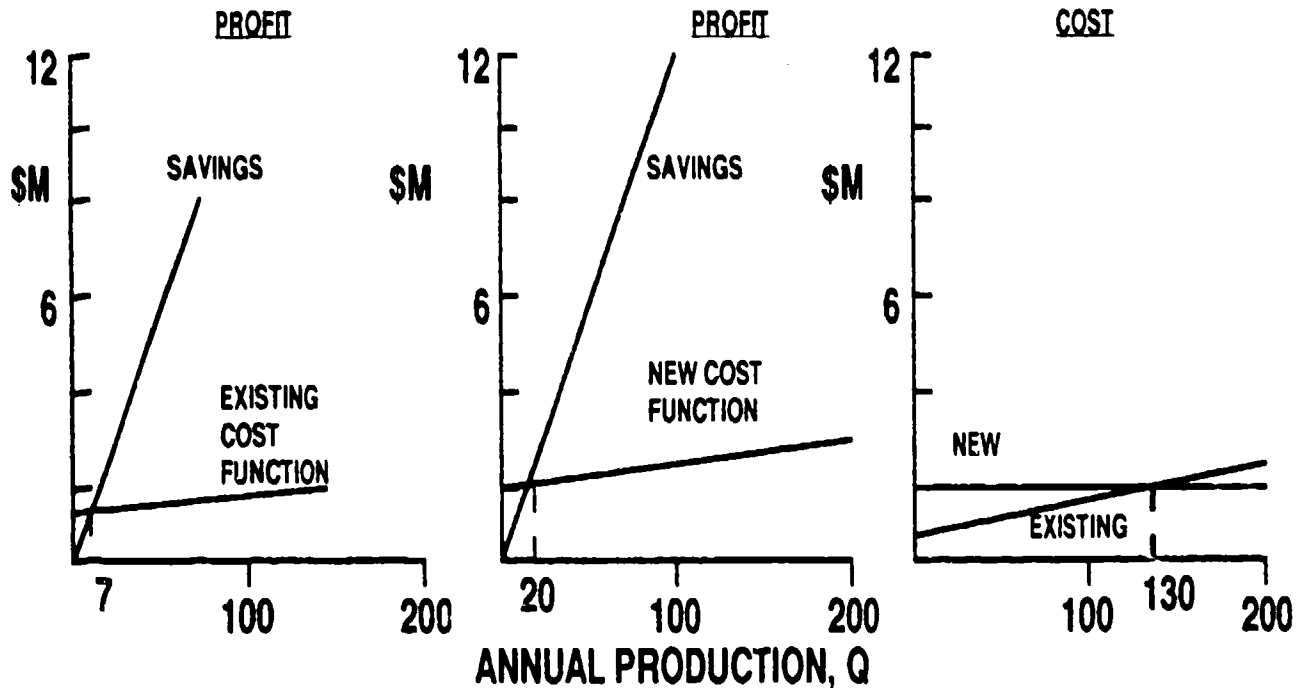


Figure 2. Break even analysis.

The Cost Break Even Analysis is used to compare different production lines (e.g., automated versus manual, etc.) to determine which has the best cost advantage for a given annual production rate. It also shows what production level must be exceeded in order to justify expenditures in advanced production methods rather than use existing manufacturing capabilities. Figure 2 also shows an example of Cost Break Even Analysis comparison curves.

Per Unit Cost of Production Analysis: This final analytical method uses the algorithms formulated in the break even analyses to determine what the per unit costs are for coolers based on various annual production rates. It also helps compare different production line types in order to show what production rate must be exceeded in order to gain per unit cost advantages for advanced production processes. An example of the type of results possible using this method is shown in Figure 3.

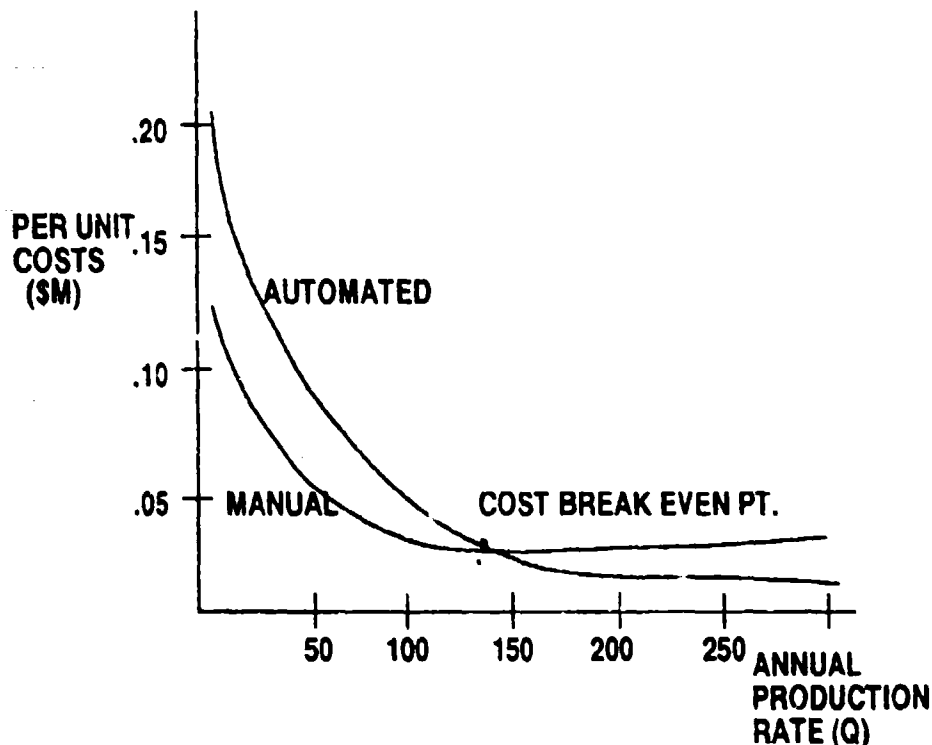


Figure 3: Cryocooler per unit cost comparisons for different production methods.

OTHER CONSIDERATIONS: There are other factors that can have far reaching affects on the production costs of cryocoolers. These include manufacturing lead time (MLT) reductions, reduced work in process (WIP), affects of hold time (non operating costs), rework/scrap, and in-process inspections to improve quality. These various considerations vary significantly between existing manufacturing methods and those possible if enhanced production methods are devised. These considerations are not as readily predictable as others we've considered, but must be observed and evaluated on an up-and-running production line. They are, in effect, measures of the efficiency of the production lines. In the case of existing manual methods, they serve as indicators of where improvements are needed. For the case of a new enhanced production capability, these parameters, once observed, show how well the new line meets expectations. They become new "yardsticks" by which we can verify

compliance with analytical predictions formulated using the various comparison methods previously discussed.

CONCLUSIONS

The cost benefit analysis performed as part of the cryocooler producibility effort revealed that substantial investments in production enhancement can realize a quick return on investment. This CBA also helped identify important cost drivers useful in focusing the thrust of the producibility program. These cost drivers are weighted differently depending on the assumptions or quantified parameters used in the analysis. These parameters are highly system specific. They'll also vary considerably among the different cryocooler development / production contractors. Thus, the CBA actually resulted in the formulation of a standardized evaluation methodology useful in performing "what if" cost comparisons between existing and new production methods. This methodology not only shows when producibility investments would pay off, but also flags conditions where we should not pursue new production capabilities (for example, if production lots are not large enough, production cycles exceed maximum capacity, etc.). Therefore, the CBA gives us an interactive tool to give government managers the ability to make informed decisions on producibility investments.

REFERENCES

1. J.Bruning, Enhanced Manufacturing of Cryogenic Coolers, PL Technical Program Plan, Phillips Laboratory, Kirtland AFB, NM, December 1991.
2. Proceedings, Space Systems Productivity and Manufacturing Conference IV, The Aerospace Corporation (publisher), Air Force Space Division (sponsor), Los Angeles, CA, August 11-12, 1987.
3. D.W. Pearce, Cost Benefit Analysis, 2nd Edition, St. Martin's Press, New York, NY, 1983.
4. G. Clews, R. Leonard, Technology and Production, Phillip Allen Publishers Ltd., Deddington, Oxford, England, 1985.

5. M. Groover, Automation, Production Systems, and Computer-Integrated Manufacturing, Prentice-Hall Inc., Englewood, CA, 1987.

MINIATURE PULSE TUBE COOLER

C.K. CHAN, C.B. JACO, J. RAAB, E. TWARD, M. WATERMAN

TRW INC.
ONE SPACE PARK, R1/1126
REDONDO BEACH, CA 90278

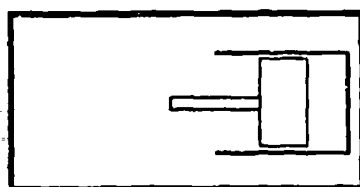
INTRODUCTION

Cryogenic coolers for use in space on small satellites require low power and minimum weight. The need for exceptional reliability in a space cooler is made even more critical on small satellites since cooler redundancy is often not an option due to weight constraints. In this paper we report on a reliable, small, efficient low power, vibrationally balanced pulse tube cooler designed specifically for use on small satellites. It has achieved an efficiency comparable to Stirling coolers.

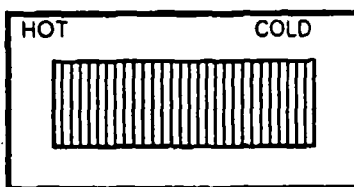
TRW has designed, fabricated, and tested an engineering model of a vibrationally balanced, miniature pulse tube cooler intended for a long-life space application. The integral cooler engineering model incorporates a nonwearing flexure bearing compressor vibrationally balanced by a motor-controlled balancer. In initial tests, the maximum cooling power measured at 80 K is 530 mW for an input power to the compressor of 17.8 watts. Initial self-induced vibration measurements indicate that the cooler can be balanced sufficiently to reduce vibration forces below 0.02 newtons from 0 to 500 Hz.

PULSE TUBE COOLER

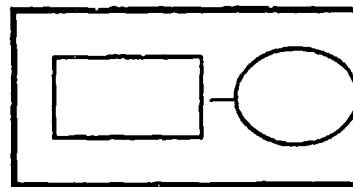
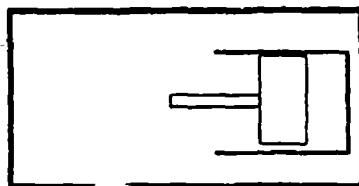
Pulse Tube and Stirling cryocoolers are thermodynamically very similar in principle,¹ as illustrated in Figure 1. In both coolers, similar compressors operate as pressure wave generators producing oscillating pressures and phase-shifted mass flows in similar regenerators. The working fluid and operating conditions (pressures, volumes, frequencies, temperatures, and loads) are very similar. As shown in Figure 1, the coolers differ in the mechanism used to control the phase difference between the oscillating pressure and the oscillating mass flow in the cooler cold head. In both

PULSE TUBE CRYOCOOLER

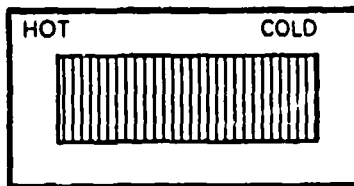
COMPRESSOR



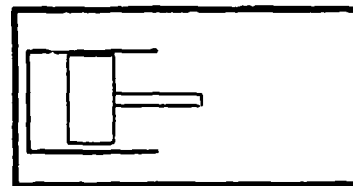
REGENERATOR

PULSE TUBE
ORIFICE AND RESERVOIR**STIRLING CRYOCOOLER**

PRESSOR



REGENERATOR



DISPLACER

Figure 1. Pulse Tube Cooler and Stirling Cooler

coolers, heat is pumped by the oscillating working fluid (typically pressurized helium gas) from the load at the cold block to ambient temperature via a regenerator which acts as a thermal sponge. The regenerator, typically a stack of screen disks, is the same for both types of cooler, differing only in the size required for a particular cooler implementation. In the Stirling cooler, the magnitude and phase of the mass flow in the cold end is controlled by the stroke and relative phase of the motion of a moving piston, the displacer. In a common implementation, the displacer and the regenerator are integrated into a single moving part which must support a large temperature gradient across its length and, in addition, operate with a small clearance seal to prevent gas from bypassing the regenerator. Pressure/volume (PV) work from the cold end is exhausted by causing the motion of the displacer. In the pulse tube cooler, the fixed geometry of a pretuned orifice connected to a gas reservoir controls the magnitude and phase of the mass flow relative to the phase of the almost sinusoidal pressure variation completely passively. The pulse tube, an empty piece of pipe, performs the required thermodynamic function of providing a mechanism through which PV work can be exhausted as well as allowing a thermal gradient to be supported between the cold head and the orifice heat exchanger.

The pulse tube cooler cold head contains no cold moving parts, no critical small dimensions, and no potential wear-out mechanisms. This feature affords the pulse tube cooler a considerable system advantage over the Stirling cooler in reliability, lifetime, and vibration at the cold head. As shown

in Figure 2, a single-stage orifice-type pulse tube cooler pumps heat from a cooling load to a heat sink, such as the ambient environment. The pulse tube cooler includes, in series, a pressure wave generator (or compressor), an aftercooler, a regenerator, a cold-end heat exchanger, a pulse tube, a hot-end heat exchanger, an orifice, and a surge tank or ballast volume². Use of a second bypass orifice enhances the efficiency³. The pulse tube cooler is filled with a pressurized gas, such as helium or hydrogen. In operation, the compressor generates an oscillating pressure wave and an out-of-phase oscillating mass flow. The alternating pressure and mass flow produced by the compressor is the PV work which causes the regenerator to pump heat from the cooling load at temperature, T_{LOAD} , through the cold-end heat exchanger to the aftercooler, at temperature, T_A , where the heat is rejected to the heat sink. In this implementation the same aftercooler is used to precool the compressed gas, whose temperature was raised to T_{CO} in the compression chamber. Meanwhile, the PV work travels down the pulse tube, where it is rejected as heat to the heat sink by the hot-end heat exchanger.

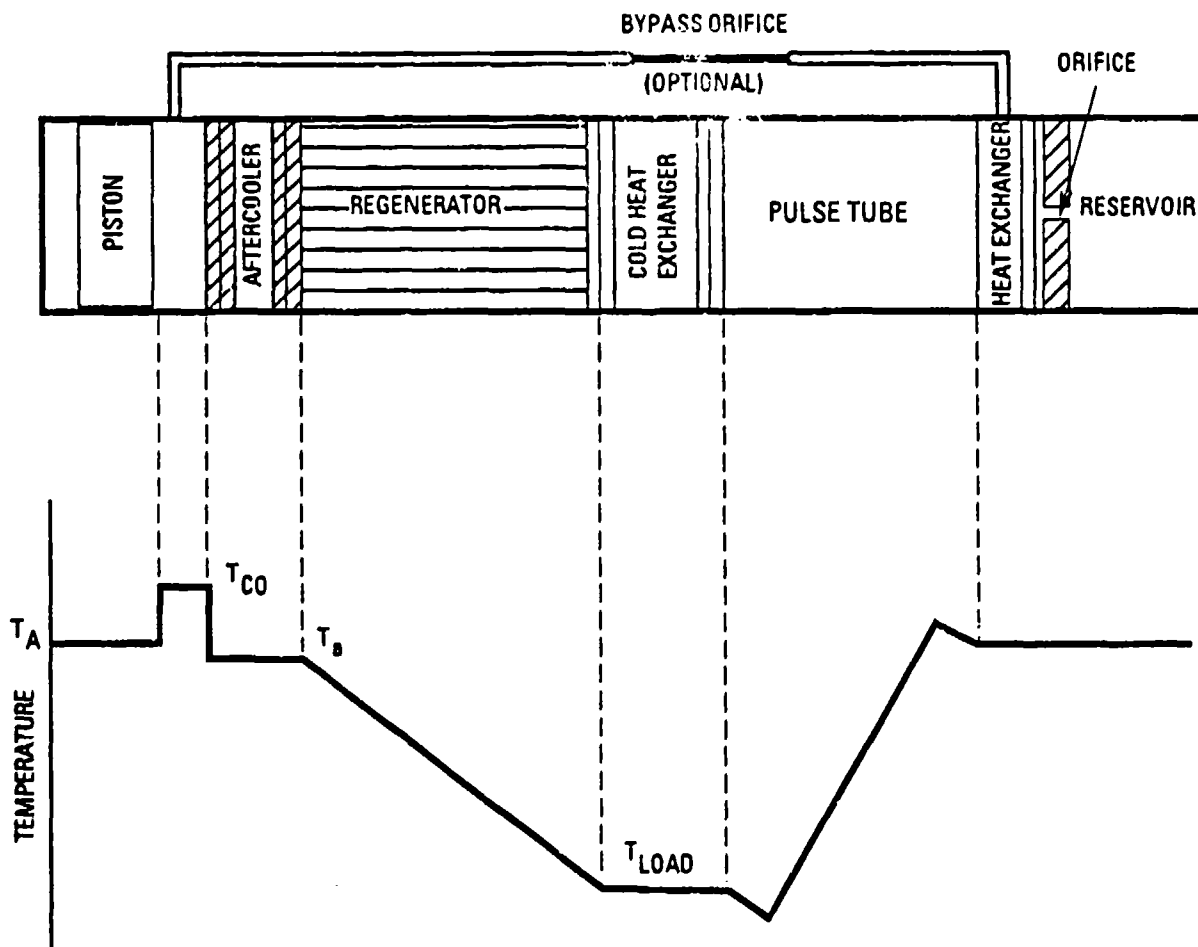


Figure 2. Single Stage Orifice Pulse Tube Cooler

COOLER DESIGN

Efficient cold-head design is the key to low input power, low system weight, reduced cooler size, and minimized vibration in the regenerative cooler. These advantages result because all the above parameters scale off the thermodynamic efficiency of the cold head in these cryocoolers. The regenerator makes the most impact on the cold head efficiency. The amount of loss in the regenerator is affected by the effectiveness of the heat transfer process, the pressure drop, and the heat conducted through the regenerator matrix. The regenerator geometries and the matrix have significant effects on the mass flow distribution and hence the heat transfer process and the pressure drop. The pulse tube is fabricated of a thin-walled low-thermal-conductivity material, such as stainless steel or titanium, with screen heat exchangers thermally connected to copper blocks to form the cold- and hot-end heat exchangers. The principal property of the chosen screens is good heat transfer to gas. The phase angle between the oscillating pressure and mass flows varies at different components and can be tuned to maximize the cooling power via orifice size and surge tank volume.

A photograph of the cooler is shown in Figure 3 and the cooler cross section in Figure 4. The compressor is driven by a linear motor with a moving coil. The moving coil is supported by flexure springs that provide drive current and maintain alignment for the attached piston, which oscillates and compresses gas into the pulse tube. A narrow clearance between the cylinder and piston seals the compression space. The clearance seal dimension is critical to cooler thermodynamic performance and input power. Figure 5 shows the sensitivity of seal power loss versus seal clearance. The compressor operates at frequencies of 40 to 60 Hz, a range chosen as a compromise between a realizable, efficient pressure-wave-generating, resonant long-life compressor and regenerator loss, which increases dramatically with frequency. It is desirable to operate the compressor at mechanical resonance. For maximum efficiency, the mechanical resonance should coincide with the maximum net cooling. The mechanical resonance is determined by the piston-coil assembly mass and the sum of the stiffnesses of the gas and mechanical spring. Mechanical spring stiffness is determined after the springs have been designed to provide infinite fatigue life. The position of the compressor piston is measured using a linear variable differential transformer (LVDT) whose output controls the compressor stroke.

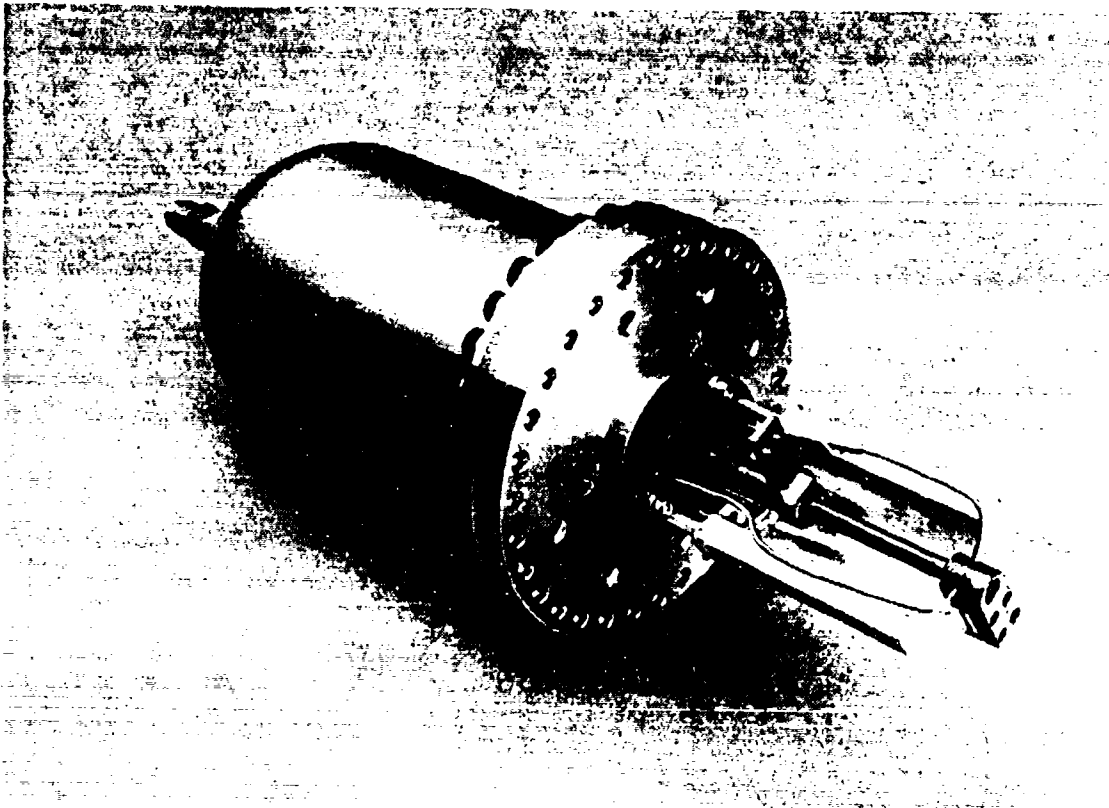


Figure 3. Miniature Pulse Tube Cooler

A permanent magnet provides the magnetic field of the motor. High-energy product magnets and high saturation iron are used to minimize the volume and weight of the circuit. The motor is linearized to the extent that it does not significantly affect the weight and/or efficiency of the compressor.

The balancer operates 180° out of phase with the compressor and is used to cancel the force imbalance at the fundamental frequency created by the compressor motion. The force imbalance at harmonics of the fundamental frequency, which arises due to drive motor and spring nonlinearities, is cancelled by essentially linearizing the compressor by shaping the electronic drive signal. A small linear motor also drives the balance mass, which is supported by flexure springs that provide the stiffness necessary to achieve resonance at the fundamental drive frequency. The balancer position is measured by an LVDT whose output is used to control its stroke.

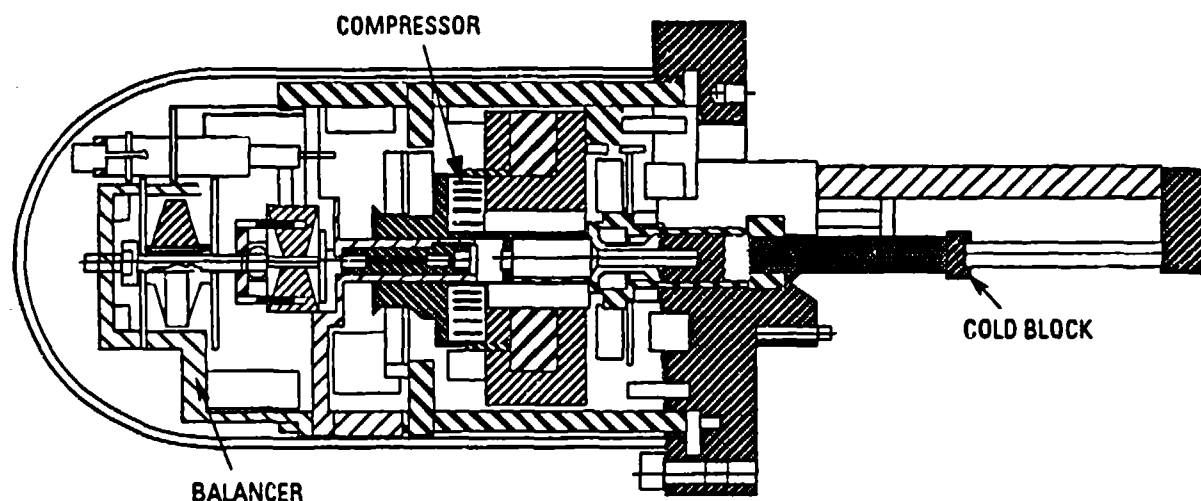


Figure 4. Cooler Cross Section

The structure connecting the compressor and balancer provides not only interfaces necessary to maintain clearances in critical areas and precision alignments so that balancing is achieved, but also the strength and stiffness required to survive launch environments without permanently deforming or damaging any internal components. The pressure vessel which contains the high-pressure helium working fluid acts as the ambient thermal interface and the mechanical interface to the spacecraft. The baseplate is designed to minimize distortions to the clearance seal area due to thermal stress and mechanically applied forces from mounting and metal O-ring seals.

The pulse tube cold head is composed of the following components: mounting flange, regenerator, cold block, pulse tube, warm-end heat exchanger body, and surge tank. The materials used include titanium alloy, copper, aluminum alloy, and stainless steel. Vacuum brazing, welding, and soldering are used to join the various components. The mounting flange, bolted to the cryocooler compressor baseplate with a metal seal, provides the primary thermal path for the rejected heat from the cold-end assembly into the baseplate and the structural support for the surge tank. The cooler performance and design capabilities are given in Figure 6.

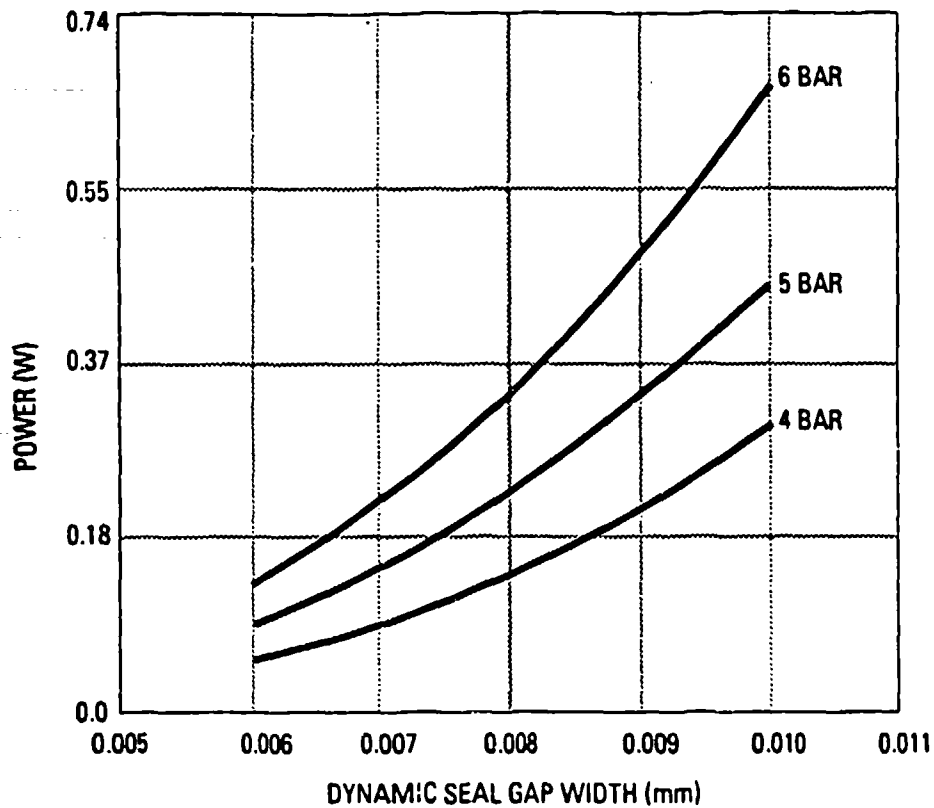


Figure 5. Power Loss from Dynamic Seals

CAPABILITY	
TOTAL POWER	23.3 watts
COOLER POWER	17.6 watts
COOLER FOOTPRINT	32.3 cm ²
ELECTRONICS POWER	5.7
ELECTRONICS FOOTPRINT	147 cm ²
VOLTAGE	22-36 Vdc
COMMAND INTERFACE	Serial
TOTAL WEIGHT	2150 gr
COOLER WEIGHT	1700 gr
ELECTRONICS WEIGHT	450 gr
COOLING POWER	0.28 watt
COLD HEAD TEMP (T _c)	<73 K
REJECT TEMPERATURE	<290 K

R1M 92.0275.04

Figure 6. Cooler Capability

The breadboard cooler electronics are shown in Figure 7. The electronics, which are autonomous, provide complete cooler control, including vibration reduction and protection against overstroke.

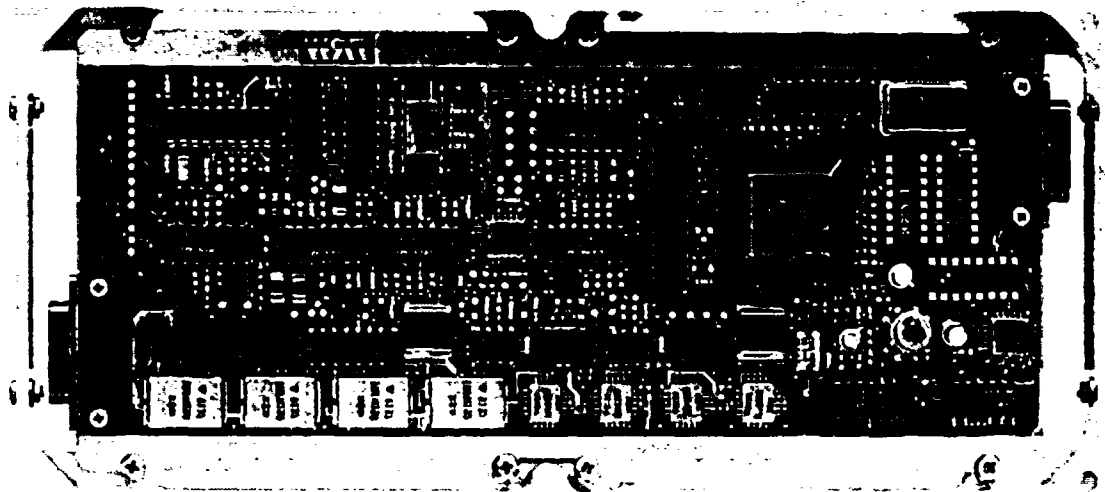


Figure 7. Cooler Miniaturized Electronics

TESTS

Initial thermodynamic performance testing of the cooler was performed by maintaining a fixed stroke on the compressor. A typical cool-down curve is shown in Figure 8 and performance data in Figure 9. The net cooling load shown was applied to the cold block with a resistive heater and measured with a silicon diode thermometer. Cooler performance as a function of input power interpolated from the constant stroke data of Figure 9 is shown in Figure 10.

Cooler vibration was measured by mounting the pulse tube cooler on a test fixture attached to a Kistler table dynamometer, which was in turn attached to a 70-ton seismic mass. The

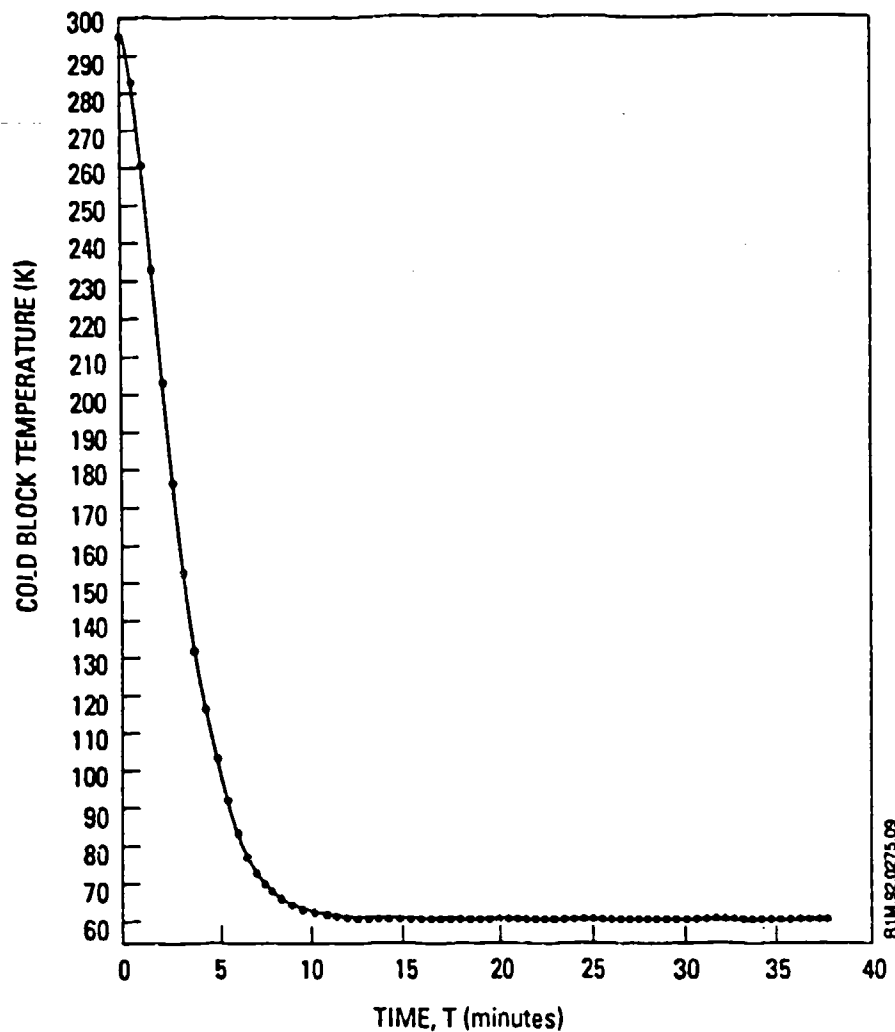


Figure 8. Pulse Tube Cooler Cool-down Curve

uncompensated force spectrum, when the moving piston was not balanced by the balancer or by drive waveform, is shown in Figure 11a. Figure 11b gives the vibration of the cooler after it is balanced.

CONCLUSION

We have designed, fabricated and tested a reliable, small, efficient, low-power, vibrationally balanced pulse tube cooler designed specifically for small satellites. Our pulse tube cooler has a cooling power of 530 mW at 80 K for an input power of 17.8 watts to the compressor. Its specific power of 33.6 W/W at 80 K into the compressor is better (lower) than that of presently available Stirling coolers. Its small size, light weight, and the fact that it is integrally balanced makes it especially attractive from a system viewpoint for small satellite applications.

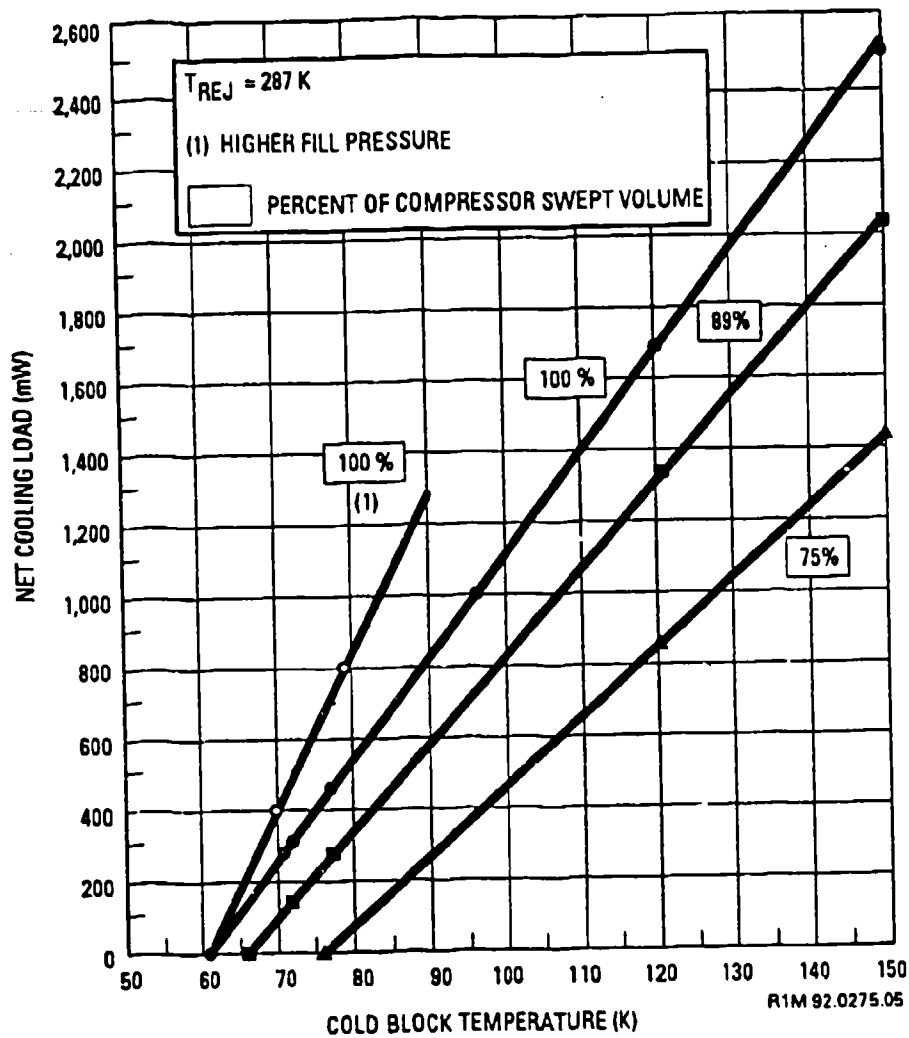


Figure 9. Heat Load Curve for Constant Compressor Stroke

References

- 1) C.K. Chan and E. Tward, "AC Thermodynamics of Regenerative Cryocoolers," to be submitted to Cryogenics.
- 2) R. Radebaugh, "A Review of Pulse Tube Refrigeration," *Advances in Cryogenic Engineering*, Vol. 35, pgs. 1191-1205 (1989).
- 3) S. Zhu, P. Wu, and Z. Chen, "Double Inlet Pulse Tube Refrigerators: An Important Improvement," *Cryogenics*, Vol. 30, pgs. 514-520 (1990).

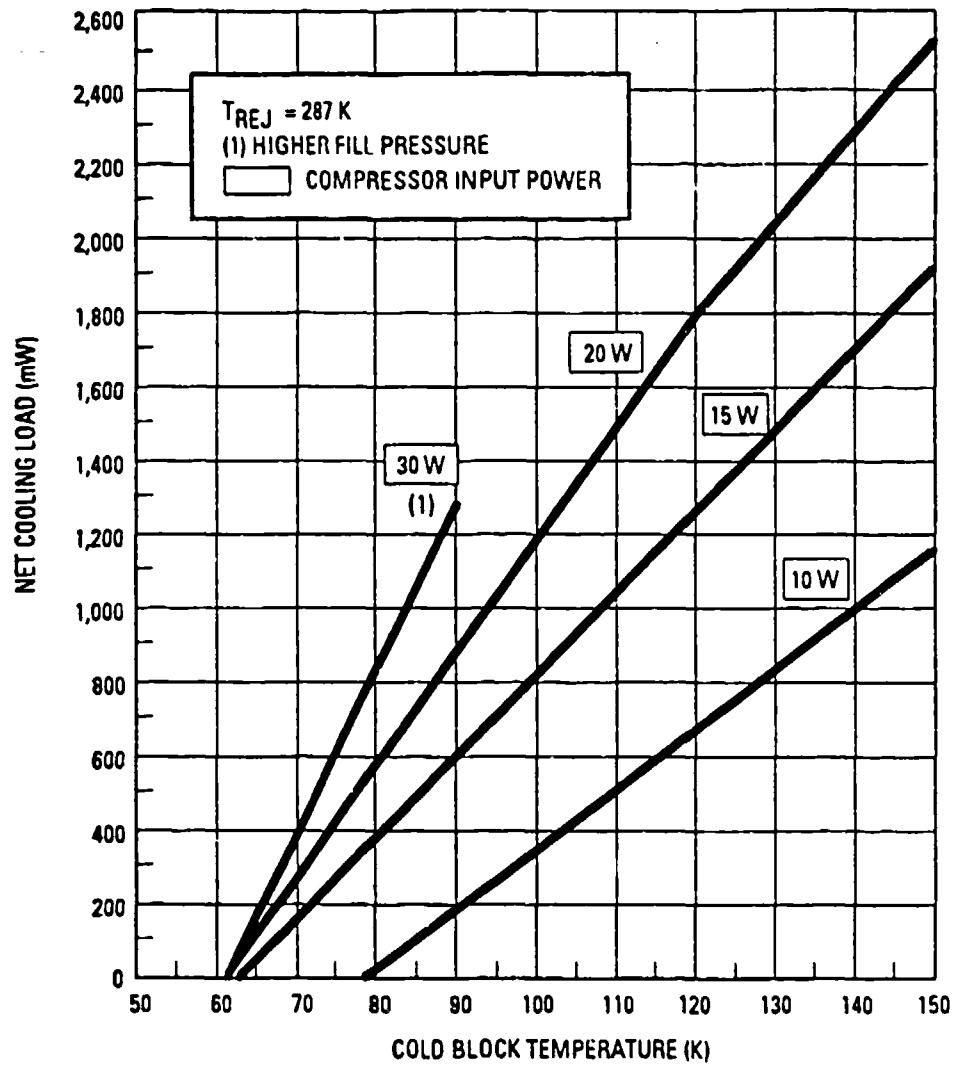


Figure 10. Cooler Performance

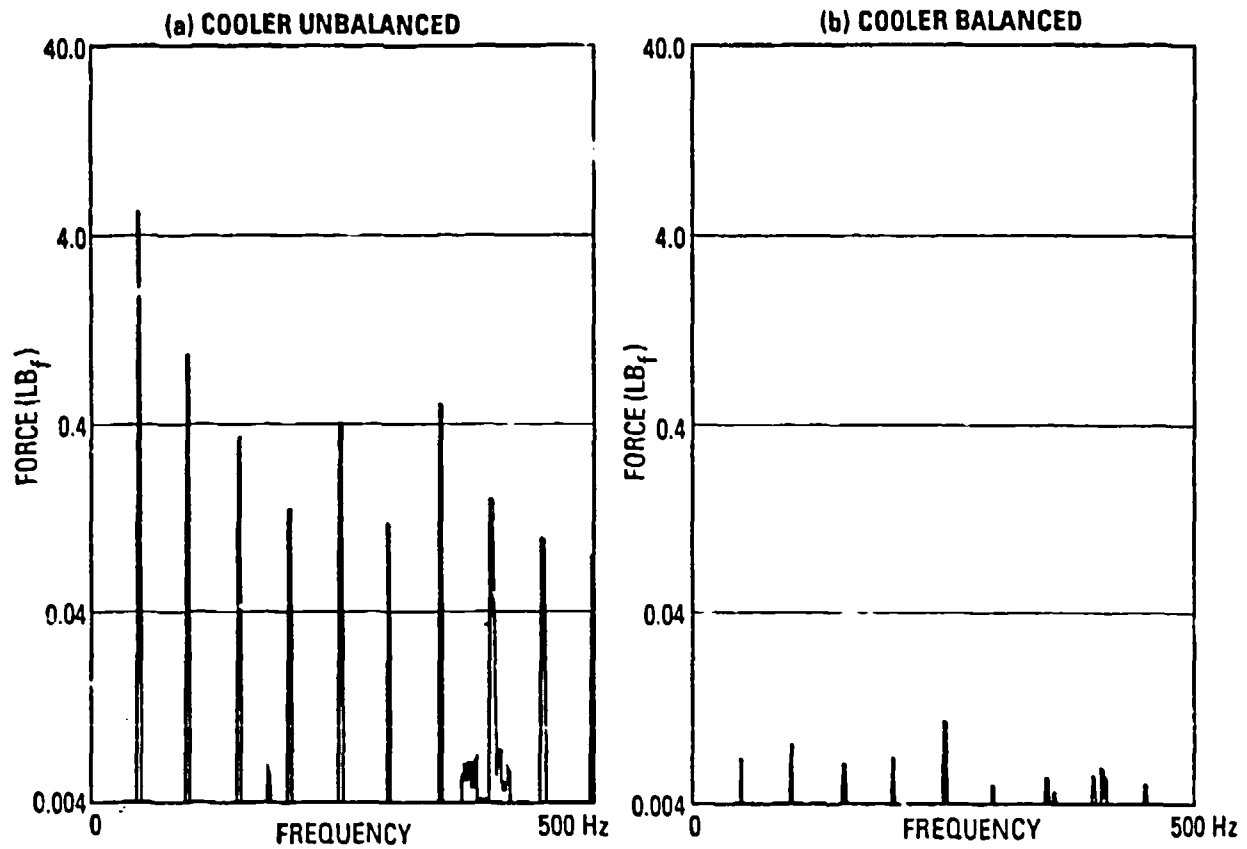


Figure 11. Cooler Vibration Control

FLOW PATTERNS INTRINSIC TO THE PULSE TUBE REFRIGERATOR

J. M. Lee and P. Kittel
NASA Ames Research Center
Moffett Field, CA 94035

K. D. Timmerhaus
University of Colorado, Boulder
Department of Chemical Engineering
Boulder, CO 80303

R. Radebaugh
National Institute of Standards and Technology
Boulder, CO 80303

ABSTRACT

Visual experiments were performed of slowly oscillating flows within an enclosed transparent tube†. A visual smoke-wire technique was used to observe flow patterns. Three isothermal oscillating flows were observed: i) incompressible flow, ii) compressible flow with a basic pulse tube configuration and, iii) compressible flow with an orifice pulse tube configuration. The incompressible flow was well described by an analytical solution for oscillating Poiseuille flow driven by a (temporally) sinusoidal pressure gradient. For our experiments, this corresponds to a piston oscillating at one end of the tube while the other end is open to atmosphere. For both the basic and orifice pulse tube compressible flow configurations, two length-scales of convective mixing were observed: one on the order of the *radius* of the tube and one on the order of the *length* of the tube. The observed flow patterns give a qualitative picture for identifying loss mechanisms.

INTRODUCTION

We have undertaken a study to examine the energy transport mechanism within the Pulse Tube Refrigerator (PTR). The goal is to develop a thorough and detailed understanding of the enthalpy transport mechanism within the *open tube* of the PTR. The compressible Navier-Stokes equations of motion are addressed for a slowly oscillating viscous fluid, and the

† The flow experiments were performed at the National Institute of Standards and Technology and at the University of Colorado, Boulder, CO.

solutions are compared to direct visual flow observations. This is the next step beyond the one-dimensional, inviscid models previously considered^{1,2}.

This paper highlights the initial stages of our flow observations. We present flow patterns for oscillating gas flow within a tube for basic and orifice pulse tube configurations and for incompressible flow. A boundary layer approximation of the incompressible Navier-Stokes equations for internal pipe flow of variable pipe radius is developed. This model is used to explain the observed flow patterns from both a mathematical and physical viewpoint. We then discuss how these flow patterns may affect the enthalpy flow.

ENTHALPY FLOW MODEL

The enthalpy flow model is derived from the unsteady, one-dimensional differential equations for mass and energy conservation. We assume an ideal gas undergoing an isentropic transport process (non-dissipative, non-conducting process). The system we are considering is strictly the "open tube" which does not include the heat exchangers at the tube ends. The equations for mass conservation, energy conservation and for an ideal gas are given by

$$\frac{1}{\rho} \frac{D\rho}{Dt} + \nabla \cdot \mathbf{u} = 0 \quad \frac{1}{T} \frac{DT}{Dt} = \frac{1}{\rho C_p T} \frac{Dp}{Dt} \quad \frac{1}{\rho} \frac{D\rho}{Dt} = \frac{1}{p} \frac{Dp}{Dt} - \frac{1}{T} \frac{DT}{Dt} \quad (1a, b, c)$$

where \mathbf{u} , ρ , T , p and t are the velocity vector, density, temperature, pressure and time, respectively. The operator, D/Dt , is the substantial (convective) derivative

$$\frac{D}{Dt} = \frac{\partial}{\partial t} + (\mathbf{u} \cdot \nabla).$$

Eliminating T between Eqs. (1b) and (1c), substitution into Eq. (1a) and using the ideal gas law, $p = \rho RT$, gives

$$\rho C_p T \nabla \cdot \mathbf{u} = \left(1 - \frac{C_p}{R}\right) \frac{Dp}{Dt} \quad (2)$$

For negligible spatial dependence of pressure, $\nabla(\rho T) = 0$ and Eq. (2) becomes

$$\nabla \cdot (\bar{h}(t)\mathbf{u}) = \frac{1}{1-\gamma} \frac{dp}{dt} \quad (3)$$

where $\gamma = C_p/C_v$ is the heat capacity ratio, $\bar{h}\mathbf{u}$ is the enthalpy flux and \bar{h} is the enthalpy density and is a function of time only, $\bar{h} = \bar{h}(t) = \rho C_p T$. The divergence of the enthalpy flux is an exact differential for this spatially one-dimensional system. Integrating over z gives

$$\bar{h}u = \frac{1}{1-\gamma} \dot{p}z + \frac{1}{A} \dot{m} C_p T \Big|_{z=z_{ref}} \quad (4)$$

where $\dot{p} = dp/dt$, A is the local cross sectional area normal to the local mass flow vector, and where the last term of Eq. (4) is the (time-dependent) integration constant determined from the enthalpy flux boundary condition at $z = z_{ref}$. Equation (4) shows that the local *instantaneous* enthalpy flux is linear in space and can be evaluated when \dot{m} and T at $z = z_{ref}$ and $\dot{p}(t)$ are known.

The time-averaged enthalpy flux, $\langle \bar{h}u \rangle$, is dependent on the time derivative of pressure,

$$\langle \bar{h}u \rangle = \frac{1}{\tau} \left[\left(\frac{1}{1-\gamma} \right) z \oint \dot{p} dt + \frac{C_p}{A} \oint \dot{m} T dt \Big|_{z=z_{ref}} \right]. \quad (5)$$

If the pressure dependent term integrates to zero over a period (i.e., periodic steady-state, $\dot{p}(t+n\tau) = \dot{p}(t)$), then the time-averaged enthalpy flow is spatially constant, in accordance with the enthalpy flow model. If the pressure term does not average to zero (pressure is not periodic steady-state), then the average enthalpy flow is linear in space. The pressure term represents changes in the enthalpy content of the system due to cool down or warm-up.

The ideal enthalpy flow model does not consider viscous and inertial momentum effects that can give rise to two-dimensional flow patterns and secondary flow phenomena. Consideration of the momentum equations will allow for linear and nonlinear viscous flow and multi-dimensional flow patterns, and will add insight into the physical mechanisms that drive such flows.

EXPERIMENT

Experimental Arrangement

A smoke-wire visual system was constructed to observe flow patterns. The system is shown in Fig. 1 with a schematic that identifies key components. A clear plexiglass tube, 41 cm long and 1.9 cm i.d. (volume 116 cm³) was attached to a dc-powered reciprocating air compressor operating with a 22 cm³ displacement volume. The tube volume was sized relative to the compressor displacement so that entrance/exit effects at the tube ends would not influence the center section of the tube where visual observations were made. The top of the tube was blocked with a clear plexiglass plug through which an illuminator light was directed down the axial coordinate of the tube. A valve was connected to a port at the top end of the tube, in series with a reservoir volume of 1 liter. A "smoke-wire" was threaded across the tube diameter at its midpoint and sealed at the tube walls. The smoke-wire was 0.076 mm diameter stainless steel and was sized to insure laminar flow. The leads of the smoke-wire extended through the tube walls and were connected to a pulsed current source. The backside of the tube was blackened for better smoke visibility. All tests were conducted with air at a mean pressure of 1 atm.

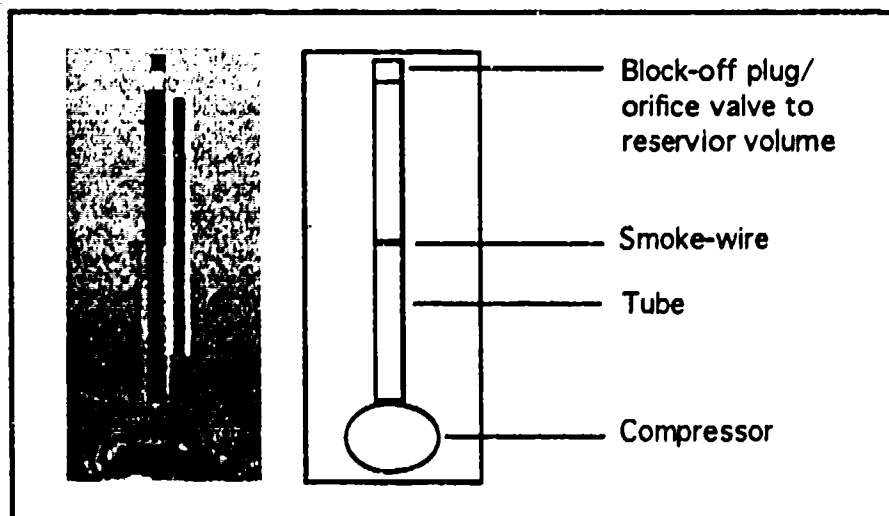


Figure 1. Smoke-wire flow visualization system.

Preceding each experimental run the smoke-wire was coated with a light petroleum-based oil. The compressor was operated at a selected frequency until periodic steady-state was achieved. When observations were desired, a single pulse of current was transmitted to the smoke-wire

(150 mA over 20 msec). The resulting Joule heating quickly vaporized the oil off the wire as a "smoke-line". The smoke-line, composed of a fine oil mist (the oil did not oxidize), reflected the light from the illuminator for observation purposes, thus allowing a clear view of the gas movement over time.

The smoke-line was somewhat smeared due to the time-interval required for the oil to vaporize (see Fig. 2). The smearing was about 20% of the forced oscillation displacement length. Each smoke-line was observed until the smoke had dissipated, usually between 10 and 100 cycles, depending on the rate of dissipation. The movement of the smoke was recorded with a video tape recorder.

Buoyancy driven flow of the smoke in the air was negligible. The rate at which the smoke attained thermal equilibrium with the surrounding air was on the time scale of the forced oscillations. The characteristic time scale for buoyancy driven flow of the smoke in stagnant air within the tube was two-orders of magnitude larger than the forced oscillation time scales. Therefore, beyond the first oscillation after triggering the smoke pulse, buoyancy driven flow was negligible relative to the observation time scale of 1/30 sec. (video frame rate of 30 frames/sec.).

Oscillating flow was observed for three different flow configurations: incompressible flow (ICF), basic pulse tube (BPT), and orifice pulse tube (OPT). The ICF configuration was obtained by removing the plug from the top of the tube so that the tube was open to the atmosphere. For the BPT configuration, the plug was replaced and the valve was closed. For the OPT configuration, the valve between the reservoir volume and the pulse tube was adjusted until the minimum in the compressor speed was obtained. This corresponded to the maximum load on the compressor. Tuning the system in this manner provided assurance that the velocity phase-shift between the two ends of the tube approached 90°.

Flow Observations

All oscillating flows were conducted at frequencies between 2 and 12 Hz. In terms of non-dimensional transport parameters, the system operated over a range of dynamic Reynolds numbers, $Re = (U_c r_0 / \nu)$, from 100 to 600 and Valensi numbers, $Va = (r_0^2 / \nu \tau)$, from 12 to 75, as defined for such oscillating flow systems (discussed below). The parameters τ , r_0 , ν and U_c are the oscillation period, the tube radius, the kinematic viscosity and the characteristic velocity amplitude, respectively. For our system, $U_c = 0.2 L / \tau$ where L is the tube length.

Incompressible Flow

A typical incompressible flow sequence for one oscillation cycle is highlighted in Fig. 2. The observed ICF flows were laminar and stable with the smoke-line remaining clear, well beyond a hundred cycles. No azimuthal velocity components were observed - the smoke-line oscillated in the plane defined by the smoke-wire and the oscillating air. The rate of smoke dissipation varied little over the range of Re and Va investigated. The observed flow was in good qualitative agreement with the theory of incompressible oscillating pipe flow (discussed below). Figure 2 shows a position phase shift between the gas near the wall and at the centerline. This is because the velocity near the wall leads the velocity at the centerline. This is typical of viscous systems in which vorticity generated at the tube wall diffuses to the tube center on a length scale of $(\nu/\omega)^{1/2}$.

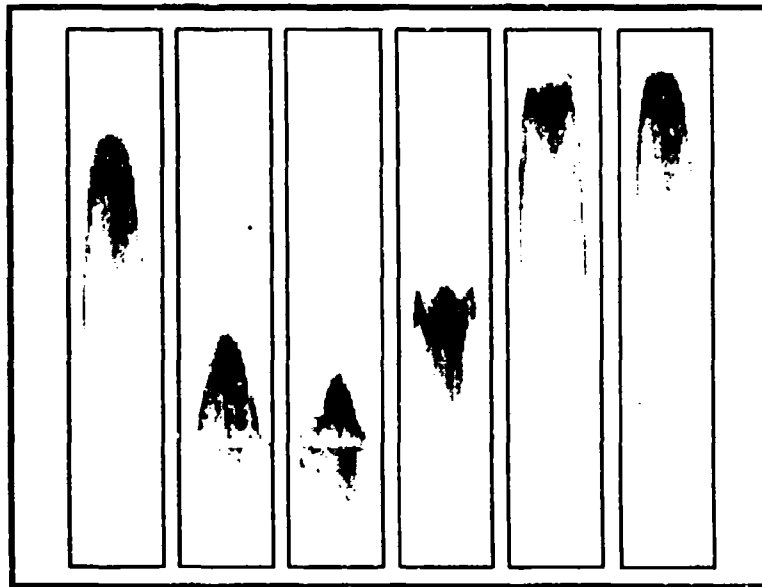


Figure 2. Sequence of frames over a single oscillation period for incompressible flow. Field of view is 40% of tube length, at the tube mid-section. The smoke-line remained distinct well over a hundred cycles. Operating parameters are 2 Hz, $Re = 100$, $Va = 12$.

BPT and OPT configurations

The observed flows for both the BPT and OPT configurations were similar and thus are discussed together. In addition to the forced-flow caused by the compressor piston motion seen during the ICF runs, two additional convective flows were observed.

Small Scale Mixing

Both the BPT and OPT configurations displayed similar mixing flow patterns on a length scale of the tube radius and on a time scale of the forced oscillation. Figure 3 shows this mixing over two consecutive cycles. The observed flow was not strictly two-dimensional axisymmetric; azimuthal velocity components were also present. The smoke-line would quickly dissipate after a small number of cycles (less than 10), and was soon observed to be uniform (in three-dimensions) in the vicinity of the smoke-wire.

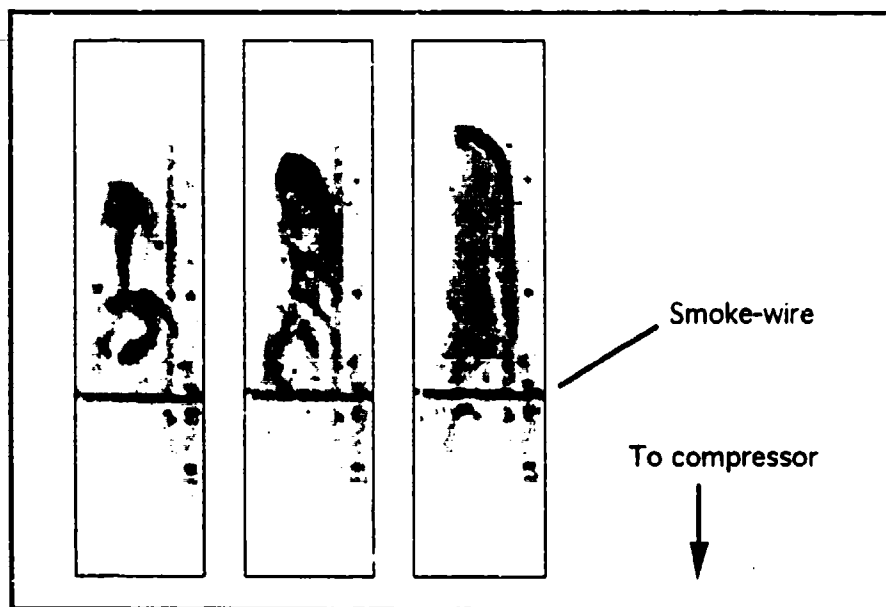


Figure 3. Mixing on a length scale of the tube radius as seen in the BPT. The time between each frame is one period. Similar dissipation at comparable rates was also observed for the OPT configuration. Operating parameters are 3 Hz, $Re = 150$, $Va = 19$.

Large Scale Streaming

Secondary flow was observed as steady streaming for both the BPT and OPT configurations. Figure 4 shows this flow component over a time interval of about 100 cycles at 3 Hz. The field of view shown in Fig. 4 is on the upper 25% of the tube with the orifice at the top and the compressor at the bottom. The length scale of this steady streaming was on the order of the tube length, with a time scale two-orders of magnitude greater than the oscillation period. This streaming component was observed to flow up along the tube walls in the viscous boundary layer towards the orifice end. Near the orifice end, the smoke reversed its flow and returned down the tube center towards the compressor.

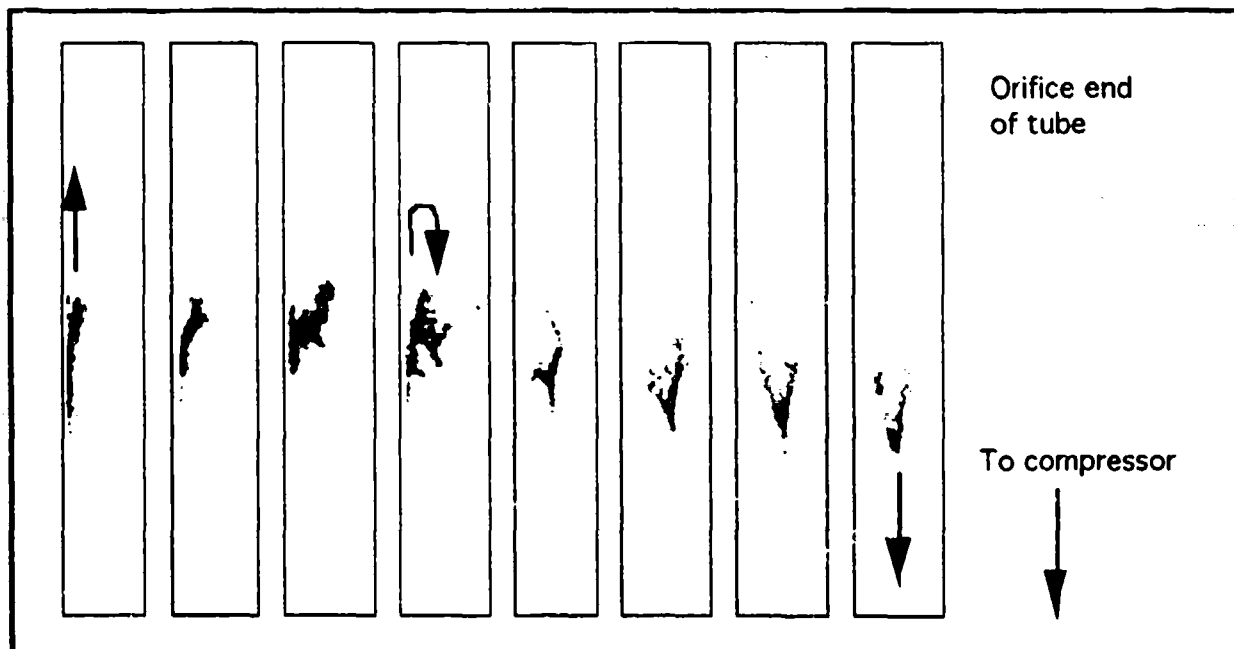


Figure 4. Steady secondary streaming flow observed in the upper 25% of the tube with the OPT configuration. The smoke flows up along the boundary layer and then returns down the tube centerline. This was also observed for the BPT configuration. System operating at, 3 Hz, $Re = 150$, $Va = 19$.

THEORETICAL INTERPRETATION

The complete solution to the compressible Navier-Stokes equations for this oscillating flow necessitates a numerical analysis that is beyond the scope of this paper. We can, however, develop an approximate solution by considering incompressible oscillating flow in a diverging tube where the tube radius is a function of z , $r_0 = r_0(z)$. The incompressible problem for a slowly diverging tube approximates the solution to the compressible problem in the limit of very small pressure ratios. The velocity boundary conditions at the two ends of a diverging tube are representative of the boundary conditions in velocity found in a BPT. The velocity near the large radius end of the diverging tube approximates the conditions on velocity near the closed end of the BPT. Correspondingly, the velocity near the small radius end of the diverging tube approximates conditions near the open end of the BPT. The diverging tube also approximates the OPT configuration if cycle-averaged boundary conditions are considered.

For $\partial p / \partial r \sim O(r_0^2 / L^2) \ll 1$, where L is the tube length, a boundary layer approximation for the momentum equation is applicable,

$$\frac{\partial u}{\partial t} - \frac{\nu}{r} \frac{\partial}{\partial r} \left(r \frac{\partial u}{\partial r} \right) = \frac{\partial U}{\partial t} + U \frac{\partial U}{\partial z} - v \frac{\partial u}{\partial r} - u \frac{\partial u}{\partial z} \quad (6)$$

$$\frac{1}{r} \frac{\partial}{\partial r} (vr) + \frac{\partial}{\partial z} u = 0 \quad (7)$$

where ν is the kinematic viscosity, u is the z -component of velocity, v is the r -component of velocity and U is the inviscid core velocity. For conditions in which the quadratic nonlinear terms are $O(U_0 / \tau L) \ll 1$ (small compared to the linear terms), a series expansion in τ can be assumed in which the first order terms satisfy the linear part of Eq. (6) and the second order terms satisfy the non-linear part,

$$U = U_0 + U_1 + O(\tau^2)$$

$$u = u_0 + u_1 + O(\tau^2)$$

$$v = v_0 + v_1 + O(\tau^2).$$

This problem has been considered by Schlichting³ for a planar geometry. Here we consider the axisymmetric cylindrical problem.

First Order Solution

Solution of the linear part of Eq. (6) for parallel incompressible oscillating flow was first given analytically by Sexl⁴, in which a sinusoidal (in time) linear pressure gradient - of the form $U_0(t) = K \cos \omega t$, where K is a constant - is imposed on the linear differential equation for u_0 .

We extend this problem for variations in z and use complex notation such that

$U_0(z, t) = U_c(z) e^{i\omega t}$ where only the real part has physical significance. The linear problem becomes

$$\frac{\partial u_0}{\partial t} - \frac{\nu}{r} \frac{\partial}{\partial r} \left(r \frac{\partial u_0}{\partial r} \right) = i\omega U_c e^{i\omega t} \quad (8)$$

where $\omega = 2\pi/\tau$ is the angular frequency. The boundary conditions are $u_0 = 0$ at $r = r_0(z)$ and $\partial u_0 / \partial r = 0$ at $r = 0$. The periodic steady-state solution is thus

$$u_0 = U_c(z) e^{i\omega t} \left[1 - \frac{J_0(\eta r)}{J_0(\eta r_0(z))} \right] \quad (9)$$

where $\eta = \sqrt{-i\omega/\nu}$, $i = \sqrt{-1}$, and J_0 is the zeroth order Bessel function. The Valensi number, Va , is defined as $Va = r_0^2/\nu\tau$ and represents the (squared) ratio between the tube radius and viscous diffusion length. An oscillating Reynolds number, Re , is defined as $Re = U_c r_0/\nu$ and represents the ratio between the oscillation amplitude and diffusion lengths. Both Re and Va are dimensionless parameters that characterize the flow.

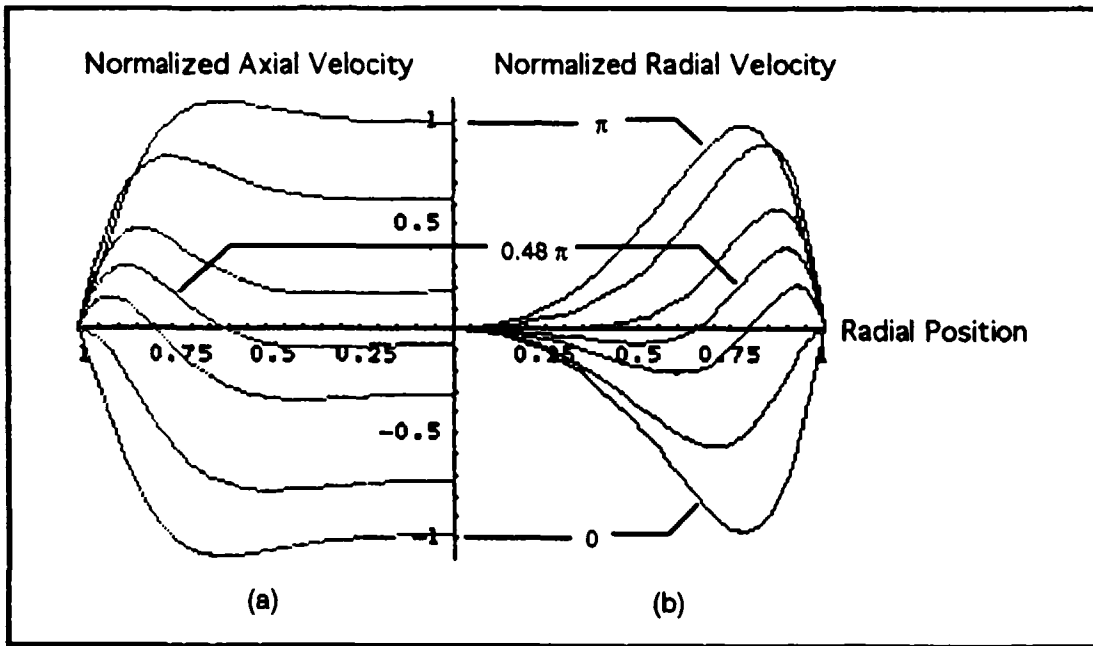


Figure 5. Normalized axial and radial velocity timelines for a diverging tube over half an oscillation cycle; incompressible flow, axisymmetric, cylindrical geometry, $Re = 100$, $Va = 12$. Time progresses upward.

The first order solution for u_0 is shown in Fig. (5a) for half a cycle with $Re = 100$ and $Va = 12$. This corresponds to the experimentally observed incompressible flow shown in Fig. (2). At these Reynolds numbers, the velocity at the centerline lags both the pressure gradient and the fluid velocity near the tube wall in the viscous boundary layer. For moderate to high Re (>10), the time-average of the squared velocity near the tube wall is greater than at the centerline.

For a flow in which U_c is not a function of z , $v = v_0 = 0$. For $U_c = U_c(z)$, v_0 is found from the mass conservation relation, Eq. (7), subject to the boundary condition $v_0 = 0$ at $r = r_0(z)$,

$$v_0 = U_c e^{i\omega t} \left(\frac{r_0}{r} \right) \left\{ \frac{r_0}{U_c} \frac{dU_c}{dz} \left[\frac{1}{2} \left(\frac{r^2}{r_0^2} - 1 \right) + \frac{1}{\eta r_0} \left(\frac{J_1(\eta r_0)}{J_0(\eta r_0)} - \frac{r}{r_0} \frac{J_1(\eta r)}{J_0(\eta r_0)} \right) \right] + \frac{dr_0}{dz} \left[\frac{r}{r_0} \frac{J_1(\eta r) J_1(\eta r_0)}{J_0^2(\eta r_0)} - \frac{J_1^2(\eta r_0)}{J_0^2(\eta r_0)} \right] \right\}. \quad (10)$$

$U_c(z)$ is obtained by applying the condition $dv_0/dr = 0$ (or $v_0 = 0$) at $r = 0$, that is, the first term in the curly brackets must go to zero as $r \rightarrow 0$ for non-singularity of v_0 . The resulting solutions for v_0 and U_c are

$$v_0 = U_c \frac{dr_0}{dz} e^{i\omega t} \left(\frac{J_1(\eta r_0)}{J_0(\eta r_0)} \right)^2 \left\{ \frac{J_1(\eta r)}{J_1(\eta r_0)} - \left(\frac{J_1(\eta r) - \eta r J_0(\eta r_0)/2}{J_1(\eta r_0) - \eta r_0 J_0(\eta r_0)/2} \right) \right\} \quad (11)$$

$$U_c(z) = \exp \left(\int_{z_{ref}}^z F(\zeta) d\zeta \right)$$

$$F(\zeta) = \frac{1}{r_0} \frac{dr_0}{dz} \left(\frac{J_1(\eta r_0)}{J_0(\eta r_0)} \right)^2 \left\{ \frac{1}{\eta r_0} \left(\frac{J_1(\eta r_0)}{J_0(\eta r_0)} - \frac{1}{2} \right) \right\}^{-1}$$

$$r_0 = r_0(\zeta)$$

Figure (5b) shows the radial velocity components corresponding to the axial velocity components. The radial components are in-phase with the axial velocity components for this incompressible system. For the compressible system of an ideal adiabatic pulse tube, we can expect that u_0 and v_0 will also be in-phase since the relaxation times for density are negligible compared to the period of the forced oscillation.

Second Order Correction

If we consider the second order correction, neglecting terms of $O(\tau^2)$ and higher, Eq. (6) becomes

$$\frac{\partial}{\partial t}(u_1 - U_1) - \frac{\nu}{r} \frac{\partial}{\partial r} \left(r \frac{\partial u_1}{\partial r} \right) = U_0 \frac{\partial U_0}{\partial z} - v_0 \frac{\partial u_0}{\partial r} - u_0 \frac{\partial u_0}{\partial z} \quad (12)$$

The terms on the right-hand-side of Eq. (12) are all known from the previous first order solution. The partial differential equation for the second order correction, u_1 , is thus linear but inhomogeneous. After substituting the real parts of Eqs. (9), (11) and $U_0(z, t)$, into Eq. (12) we find the right-hand-side to be composed of $\cos^2 \omega t$. The right-hand-side can thus be written in the general form $(1 + \cos 2\omega t) G(r, z)$; a double frequency term plus a time-independent term. It is this time-independent term that gives rise to a steady-streaming component. Since Eq. (12) is linear, u_1 can be split into a time-dependent term plus a spatial term. Taking the average of Eq. (12) over a cycle, we can then solve for the steady-streaming velocity, $\bar{u}_1 = \bar{u}_1(r, z)$. The resulting cycle-averaged equation for \bar{u}_1 is

$$\frac{\nu}{r} \frac{\partial}{\partial r} \left(r \frac{\partial \bar{u}_1}{\partial r} \right) = \overline{v_0 \frac{\partial u_0}{\partial r}} + \overline{u_0 \frac{\partial u_0}{\partial z}} - \overline{U_0 \frac{\partial U_0}{\partial z}} = G(r, z). \quad (13)$$

The convective inertial components of momentum, which are quadratic, are non-vanishing when cycle-averaged. These inertial momentum terms, known as Reynolds stresses, allow steady-streaming flow to exist, at least mathematically. Physically, the driving force for steady streaming is due to axial shear stress gradients within the boundary layer. Momentum conservation thus requires a convective mass flow in response to these shear stress gradients. What we experimentally observe is the generation of flow within the boundary layer near the tube walls. By mass conservation then, the flow reverses itself near the orifice and returns down the tube center.

DISCUSSION

Losses Associated with Radial Mixing.

The losses associated with radial mixing are ones in which heat transfer with the tube walls are enhanced by convection. Reducing the effects of radial mixing requires confining mixing to regions near the tube walls while maximizing the "inviscid" flow at the tube center, i.e., $Re \gg 1$ and $Va \gg 1$ with large diameter tubes of short length being more desirable than small diameter tubes of long length for pulse tubes of the same volume.

Losses Associated with Enthalpy Streaming

The enthalpy flow associated with the secondary streaming component can be a major loss mechanism. It represents convected enthalpy *counter* to the desired enthalpy flow for refrigeration. The streaming enthalpy flux in the boundary layer is roughly the product of the streaming mass flux integrated over the boundary layer flow area (thickness $(\nu\tau)^{1/2}$) and the enthalpy difference between the hot and cold ends.

For a first order approximation, \bar{u}_l is estimated by noting from Eq. (13) that $G(r,z)$ is on the order of $U_c(\Delta U_c/L)$ where ΔU_c is the difference in the velocity amplitudes between the ends of a tube of length L . The boundary layer thickness r_δ is on the order of the viscous diffusion length, $(r_\delta^2/\nu\tau) \sim O(1)$, thus $\bar{u}_l \sim O(U_c \Delta U_c \tau/L)$. The enthalpy flux associated with the steady streaming within the boundary layer for an ideal gas is then

$$\langle \bar{h} u_l \rangle \sim U_c \frac{\Delta U_c \tau}{L} p_m \frac{C_p}{R} \frac{\Delta T}{T_m} \quad (14)$$

where $\bar{h} \sim O(\rho_m C_p T_m = p_m C_p/R)$, T_m and p_m are the mean temperature and pressure, ΔT is the temperature difference between the warm and cold ends, and C_p is the heat capacity. The enthalpy flow due to streaming, $\langle \dot{H} \rangle_{st}$ for $r_\delta \ll r_0$ is thus

$$\langle \dot{H} \rangle_{st} \sim U_c \frac{\Delta U_c \tau}{L} p_m \frac{C_p}{R} \frac{\Delta T}{T_m} (2\pi r_0 \sqrt{\nu\tau}). \quad (15)$$

The ideal enthalpy flow at periodic steady-state, $\langle \dot{H} \rangle_{id}$, is the second term in Eq. (5). It is on the order of

$$\langle \dot{H} \rangle_{id} \sim \frac{C_p}{R} \frac{\Delta p U_c}{\tau} (\pi r_0^2) \quad (16)$$

where Δp is the dynamic pressure difference. The ratio between the streaming enthalpy and the ideal enthalpy flow (ratio between Eqs. (15) and (16)) is

$$\frac{\langle \dot{H} \rangle_{st}}{\langle \dot{H} \rangle_{id}} \sim \left(\frac{P_r + 1}{P_r - 1} \right) \left(\frac{\Delta U_c}{L/\tau} \right) \left(\frac{\Delta T}{T_m} \right) \left(\frac{\sqrt{\nu\tau}}{r_0} \right). \quad (17)$$

where P_r is defined as the pressure ratio between the maximum and minimum pressures. Equation (17) shows the important dimensionless parameters for pressure, displacement length, temperature and thickness (area normal to the flow). To first order, the streaming enthalpy is inversely related to the tube radius. This means that the enthalpy streaming losses will be much more pronounced in a small scale OPT as opposed to a large scale OPT. The streaming enthalpy ratio is also dependent on $\Delta U_c/U_c$, since $U_c\tau/L \sim 0.3$ for an OPT and $U_c\tau/L \sim P_r^{-1/\gamma}$ for a BPT. By decreasing $\Delta U_c/U_c$, the enthalpy streaming losses can be reduced.

Equations (9), (11) and the solution to Eq. (12) combine to form the laminar flow solution to the boundary layer approximation. Experimental observations suggest, however, that the flow patterns are much more complicated, as indicated by the high rate of smoke dissipation in Fig. 3. The simple two-dimensional flow may be hydrodynamically unstable, resulting in the observed azimuthal velocity components. A stability analysis of this laminar flow solution may prove fruitful in ascertaining the conditions for instability.

Reducing Steady-Streaming

Since the velocity amplitude, U_c , at the tube ends of an OPT are generally not equal, we can presume a steady streaming component to be present. Reducing $\Delta U_c/U_c$ will have the effect of reducing the streaming enthalpy flow. This can be accomplished by controlling the mass flow at the warm end of the pulse tube. This may be one reason why improved performances (relative to the OPT) are measured in the Double Inlet Orifice Pulse Tube⁵ (DOPT) and the Moving Plug Pulse Tube^{6,7} (MPT). Besides reducing the regenerator mass flow (allowing for more effective regenerators) and increasing the phase shift between \dot{m} and T , both the DOPT and MPT provide conditions in which $\Delta U_c/U_c$ is decreased, thus reducing the losses associated with enthalpy streaming. This effect may be more important for smaller scale PTRs (small tube radius) rather than for larger PTRs.

Another means by which the velocity amplitude between the two ends of a pulse tube can be reduced is by using a tapered pulse tube (TPT) configuration. The TPT would use monotonic spatial variations in the pulse tube radius to reduce velocity amplitude differences while still retaining the simplicity of an OPT.

REFERENCES

1. R., Radebaugh, J. Zimmerman, D. R. Smith and B. Louie, "A Comparison of Three Types of Pulse Tube Refrigerator: New Methods of Reaching 60K," *Adv. Cryo. Eng.*, 31, (1986) 779-789.
2. C. Wang, P. Wu, and Z. Chen, "Numerical Modeling of an Orifice Pulse Tube Refrigerator," *Cryogenics*, 32, (1992) 785-790
3. H. Schlichting, "Berechnung ebner Periodischer Grenzschichtströmungen," *Phys. A.*, 33 (1932) 327-335.
4. Th. Sexl, "Über den von E. G. Richardson entdeckten Annulareffekt," *Z. Phys.* 61 (1930), 349.
5. S. W. Zhu, P. Y. Wu and Z. Q. Chen, "Double Inlet Pulse Tube Refrigerators: An Important Improvement", *Cryogenics* (1990) 30 514-520.
6. Y. Matsubara and A. Miyake, "Alternate Methods of the Orifice Pulse Tube Refrigerator," *Proc. International Cryocooler Conference, Naval Postgraduate School, Monterey, CA* (1988) 127-135.
7. M. Kasuya, J. Yuyama, Q. Geng and E. Goto, "Optimum Phase Angle between Pressure and Gas Displacement Oscillations in a Pulse-Tube Refrigerator," *Cryogenics* (1992) 32 303-308.

EXPERIMENTAL PERFORMANCE OF MODIFIED PULSE TUBE REFRIGERATOR BELOW 80K DOWN 23K

YOSHIHIRO ISHIZAKI and ERIKA ISHIZAKI
E C T I
241 YAMANOUCHI, KAMAKURA 247, JAPAN

ABSTRACT

We wish to report experimental results on a modified pulse tube refrigerator which consists of a room temperature valveless expander that operates with a phase difference relative to the valveless compressor. With this system, refrigeration capacity of 45W was obtained at 80K with COP of 0.035. A COP of about 0.04 may be achieved with refinement of the compression system. A minimum temperature of 23.5K has been achieved with this system, which to our knowledge is the lowest temperature achieved with a single stage pulse tube.

INTRODUCTION

The pulse tube refrigerator was invented by W. Gifford and R. Longworth in 1963[1]. In the early period of development, the minimum temperature achieved was relatively high. However, a significant decrease in temperature has been achieved through more recent intensive developments by E. I. Mukulin, R. Radebaugh and Zhou et al[2-6] and others. A temperature of 28K has already been achieved by a single stage orifice type refrigerator [7] and recent reports indicate steady lowering of minimum temperature. We have also achieved 22K and 23.5K with the system explained in the following[8-9].

The most important characteristic of the pulse tube refrigerator compared with other types of regenerative refrigerators is that it does not require a displacer on which the reliability of the machine is critically related. This feature allows more degree of freedom in attachment of the cold head and also significantly reduces mechanical and magnetic noise at the cold end. Moreover, the elimination of the displacer, which usually uses plastic material, reduces generation of dust and impurity gases significantly. These features indicate that the pulse tube refrigerator promises significant improvement in reliability and cost. However, the pulse tube refrigerator at present has a somewhat lower COP and specific refrigeration power (W/m^3) than that of the Stirling refrigerator.

The main object of this study seeks a solution to this problem. To this end, a room temperature valveless expander has been introduced. With this system, a minimum temperature of 23.5K and a relatively high COP of 0.035 at 80K has been obtained.

The structure of the cryostat part which consists of the cold head with cone and flow paths, regenerator and pulse tube has been simplified. The results attained with this system, hold promise to further improvement of the modified pulse tube refrigerator where the COP and specific refrigeration power near that of the split-Stirling refrigerator.

EXPERIMENTAL APPARATUS

The fundamental structure of the experimental apparatus is shown in Fig. 1. Instead of an

office at the warm end of the pulse tube, as used in the more conventional pulse tube refrigerator, the present machine uses a moving piston at the warm end of the pulse tube to provide the proper phase between pressure and mass flow.

Our experience in development of Stirling cycle machines tells us that COP_{max} depends on a multitude of factors [11-13]. In particular, we expect the following nine factors, namely; volume ratio $\beta = V_c/V_e$ (compression volume / expansion volume), volume of compression space, crank angle α between compression piston and expander, regenerator efficiency, working gas pressure, operating speed, dead volume, behavior of working gas in pulse tube (likes, gas velocity, uniformity of gas flow, friction factor of pulse tube wall, heat transmission between pulse tube wall, and etc.) and heat leakage to be critical in determining COP_{max} for a given required refrigeration temperature.

Among these factors, we first focussed our attention on the volume ratio and constructed compression pistons and room temperature expansion pistons by which the volume ratio β could be varied between 0.44 to 15.2 as shown in Table 1.

A vessel with an inner diameter of 38mm containing type A): bronze 150mesh 665sheets + stainless steel 200mesh 557sheets + Pb 0.3mm ϕ spheres 259g 45cc, type B): bronze 150mesh 1,025sheets + stainless steel 150mesh 580sheets as regenerator materials were used for the regenerators. And type C is just like type B except for it is a coaxial configuration. If rare earth material is used for the regenerator, the minimum temperature would easily be less than 20K, but the disadvantages are the high cost of such material and the uncertain long-term chemical and physical stability of these materials.

Helium with a mean pressure of 15 and 17.5atg was used mostly as the working gas.

The crank angle α was set to be $\alpha=0$ when the compression and expander piston was at the upper limit. Usually the angle of the expander is more advanced than the compression piston as in the Stirling cycle. The crank angle could be regulated at an arbitrary value by an AC-servo-motor. Operating speed was set at 2.0, 3.0, 3.83, 5.75 and 7.0Hz. The dead volume was regulated by varying the inner diameter and length of a flexible tube connecting the compression space and the radiator, and the room temperature expander and the pulse tube, respectively. The maximum power of main motor used was 5.5 kW and the AC-servo-motor was 1.5 kW. A maximum power of 100W could be applied to the electric heater on the cold head. A platinum thermometer (Lakeshore) and thermocouples were used as temperature sensors, and the dynamic pressure was measured by a strain gauge (Honeywell).

RESULTS and DISCUSSION

The results for the minimum temperature obtained shown in Fig. 2 shows that the temperature decreases as the volume ratio β increases. A minimum temperature of about 26K was obtained at $\beta=8.09$. It can be seen that for β larger than 8, temperatures below 40K may be readily obtained with the modified pulse tube refrigerator for α between 7.5° and 50° . The minimum temperature of course depends strongly on the operating speed and the dead volumes of the regenerator and the flexible tube and also on thermal conduction of heat from room temperature along the pulse tube. In particular, effects due to the diameter and length of the flexible tube are large. In this study, the diameter and length of the flexible tube from the compression space to the radiator, and also from the expander were made 8mm diameter and 500mm, respectively. Experiments with larger volume ratios have also been made.

Fig. 3 shows the variation of the minimum temperature with crank angle and operating speed (Hz) for $\beta=9.87$. The lowest temperature of 23.5K was obtained using regenerator type A), operating speed 3.0Hz and crank angle $\alpha=30^\circ$. It is seen that α tends to decrease as the minimum temperature decreases and that there is an optimum value for the volume ratio, operating speed and α for a given refrigeration temperature.

Fig. 4 shows the relation between the crank angle and COP at 80K. Maximum COP is attained at $\alpha=22.5^\circ$ with an input power of 1,290W and refrigeration capacity of 45W.

The coefficient of performance is therefore $45/1,290 = 0.035$.

The electromagnetic and mechanical losses at no load and 3.83Hz amounted to 680W for the 5.5kW motor and the piston drive mechanism used in the present study. We estimate that these losses may be held down to below 400W by constructing a fixed expander crank angle piston drive mechanism, designed to match the size of the refrigerator for industrial application. Although the percentage of electromagnetic losses increase for smaller power motors, we estimate that the COP would then be about 0.04.

Fig. 5 shows the PV diagram of the compression volume and expansion volume at 80K under the same condition as Fig 4. The results show a strong similarity to the PV diagram of a Stirling cycle.

Fig. 6 shows the results of measurements of the temperature distribution of the outer walls of the pulse tube and regenerator at various crank angles α . Regenerator A) with a length of 200mm and a pulse tube 250mm long was used with $f=3.83\text{Hz}$ and volume ratio 7.55. For this volume ratio and the cold end at 34.7K, the temperature rises to a peak value of 581K at 144mm, decreases to 480K at 190mm and then rapidly decreases to 330K at 280mm, the location of the entrance to the expander. We believe that this rapid decrease is caused by effects due to the expander.

Fig. 7 shows a picture of the compressor pistons and expander pistons and cylinders with different diameters used to change the volume ratios over a wide range (Table 1).

CRYOSTAT DESIGN

Fig. 8 shows the structure of the cryostat part which consists of the cold head with cone and flow paths, regenerator and pulse tube [10]. In order to make the system as compact as possible, the regenerator was placed outside and concentric to the pulse tube. To cool the gas from the compression space and the pulse tube, a radiator was placed at the hot end of the pulse tube where the temperature rises above room temperature. The cold head has a cone and flow paths designed to accelerate and decelerate the reciprocating flow of the gas between the pulse tube and the regenerator effectively, and also to improve the heat transfer by making the heat transfer area large. A hole with a diameter of 30mm corresponding to the outer diameter of the pulse tube is opened through the center of bronze 150mesh 1,025 sheets and stainless steel 150mesh 580 sheets regenerator material (type C). Thermal interference between the regenerator and the pulse tube may be made small by employing a double wall structure. The structure, however, becomes complex and in the present case, the pulse tube with an inner diameter of 16mm and length 250mm was teflon coated to provide thermal insulation from the regenerator material.

Fig. 9 shows the cool-down time under conditions identical to the case shown in Fig. 8. Using regenerator type C) with $P_m=17.5\text{atg}$, $f=5.75\text{Hz}$ and volume ratio 7.55, 80K was reached in about 6.5 minutes. The minimum temperature reached for this case was about 48K.

Fig. 10 shows experimental results of the relation between α , operating speed and refrigeration capacity at 80K for a refrigerator operated with volume ratio 7.55, $f=7.0$, 5.75 and 3.83Hz, and $V_0=298.4\text{cc}$. It was found that the value of α which gives maximum refrigeration capacity changes when the operating speed of the refrigerator is altered.

Fig. 11 shows the outside structure of the cryostat part. Vacuum flange diameter is 120mm, length between cold head and vacuum flange is about 200mm.

Fig. 12 shows a picture of the parts of a mini-modified pulse tube refrigerator presently under construction where the structure shown in Fig. 8 and Fig. 1 has been made more compact.

Experiments have been performed on a pulse tube refrigerator developed to improve the COP and specific refrigeration power. A minimum temperature of 23.5K was achieved by introducing a room temperature valveless expander and compressor in the system. The COP at 80K was 0.035. Our results indicate the possibility of generating low temperatures by a more simplified structure of the cryostat part, namely the cold head with cone and flow paths, regenerator and pulse tube assembly.

We expect that the COP, and the specific refrigeration power of our modified pulse tube refrigerator, in which the volume of the expander operating at room temperature may be varied according to the required refrigeration temperature, will come close to that of a split-Stirling refrigerator in the near future.

It is noted that as the primary object of our present study was in accumulating sufficient experimental data for future studies, pistons and other parts employed were the ones made in our previous study of Stirling cycle machines. Theoretical analysis of the refrigeration cycle has not yet been made.

ACKNOWLEDGMENTS

We wish to acknowledge and heartily thank Mr. T. Matsui and Mr. T. Inoue (AISIN), Mr. Y. Hayashi (IRIE KOUKEN), Prof. Y. Matsubara (Nihon Univ.), Dr. R. Radebaugh (NIST), Mr. T. Negishi (STC) and Dr. T. Ohtsuka (ULVAC Japan Ltd.) for their kind cooperation over an extended period in various stages of this study.

REFERENCES

- [1] W.E. Gifford and R.C. Longworth, Pulse tube refrigeration, ASME paper No. 63-WA 290 presented at Winter Annual Meeting of the American Society of Mechanical Engineers, Philadelphia, Penn. (Nov. 17-22, 1963).
- [2] E.I. Mikulin, A.A. Tarasov and M.P. Shkrebyonock, Low temperature expansion pulse tubes, Adv. Cryog. Eng., Vol. 29, Plenum Press, New York (1984) p. 629.
- [3] R. Radebaugh, J. Zimmerman, D.R. Smith and B. Louie, A COMPARISON OF THREE TYPES OF PULSE TUBE REFRIGERATORS: NEW METHODS FOR REACHING 60K, *ibid.* Vol. 31 (1985) p. 779.
- [4] P.J. Storch and R. Radebaugh, DEVELOPMENT AND EXPERIMENTAL TEST OF AN ANALYTICAL MODEL OF THE ORIFICE PULSE TUBE REFRIGERATOR, *ibid.*, Vol. 33, (1987) p. 851.
- [5] R. Radebaugh and S. Herrmann: 4th Intl. Cryocooler Conf. (1987) Proc. 119.
- [6] S. Zhou, P. Wu and Z. Chen: Proceedings ICEC 13, Beijing (1990) p. 257.
- [7] A. Ravex, P. Rolland and J. Liang, EXPERIMENTAL STUDY AND MODELISATION OF PULSE TUBE REFRIGERATOR, ICEC 14, June, Kiev (1992).
- [8] Y. Ishizaki and T. Matsui, 46th Meeting on Cryogenics & Superconductivity, Program, p. 125, The Cryogenic Society of Japan, Kobe (Nov. 25-27, 1991).
- [9] Y. Ishizaki and T. Matsui, 47th *ibid.*, Program, p. 283, Nagoya (May 27-29, 1992).
- [10] Y. Ishizaki, T. Matsui and Y. Hayashi, 48th *ibid.*, Program, p. 175, Iwate (Oct. 30-Nov. 1, 1992).
- [11] Y. Ishizaki, Stirling Engine Technology in Japan, 14th Intersociety Energy Conversion Eng. Conf., Boston (1979).
- [12] Y. Ishizaki, 50 kW Stirling Engine, 17th *ibid.*, Los Angeles (1982).
- [13] T. Fujita, T. Ohtsuka and Y. Ishizaki, Japanese Activities in Refrigeration Technology, 2nd Biennial Conf. on Refrigeration for Cryogenic Sensors and Electronic System, Greenbelt, Maryland (Dec. 7-8, 1982).

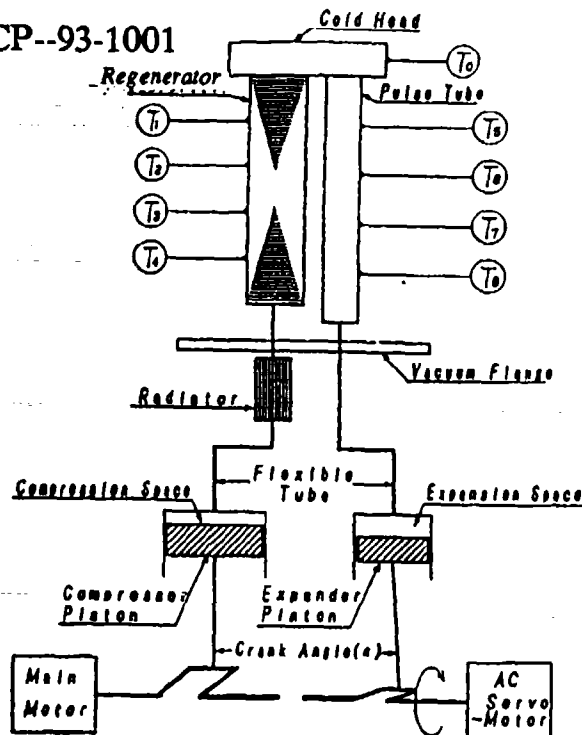


Fig. 1 A schematic of the experimental apparatus for the Modified Pulse Tube Refrigerator.

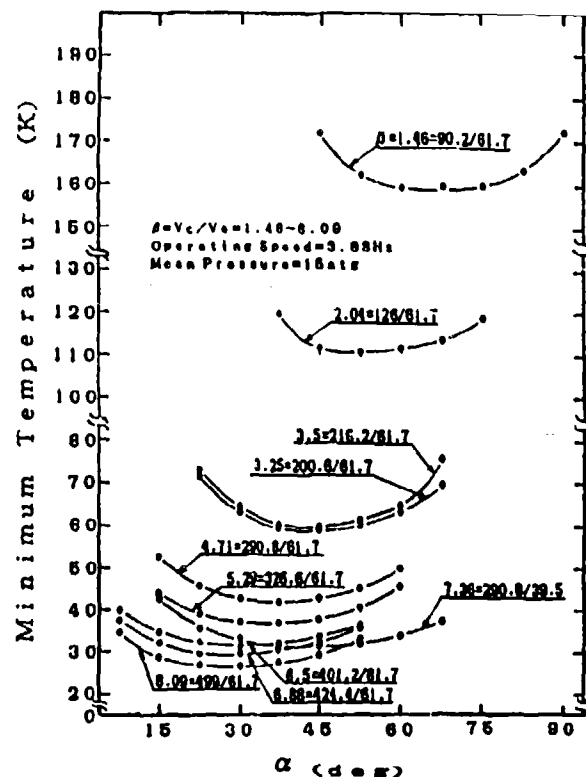


Fig. 2 Minimum Temperature vs. Volume Ratio and Crank Angle.

Table 1. Volume Ratio (β) and Regenerator Materials

Volume Ratio = β = Compression Volume / Expansion Volume

Expansion Volume (cc)	Compression Volume (cc)											
	Vol 1)	2)	3)	4)	5)	6)	7)	8)	9)	10)	11)	12)
	688.6	489.0	424.4	401.2	388.4	378.6	370.4	364.2	359.6	355.6	352.0	348.2
Vol 1)	284.6											
Vol 2)	288.6											
Vol 3)	81.7											
Vol 4)	81.6											

Regenerator Materials

Tree A): Bronze 100 mmh 600 sheets + 300 200 mmh 287 sheets + Pt 0.3 mmφ Sphered 200 g 45 mm.
Tree B): Bronze 100 mmh 1,025 sheets + 200 100 mmh 600 sheets.
Regenerator Vessel: Stainless Steel, 30 mmφ 10.1 mm thickness, 200 mm length, respectively.
Tree C): 30 mmφ, Bronze 100 mmh 1,025 sheets + 200 100 mmh 600 sheets (Structure of Fig. 6).

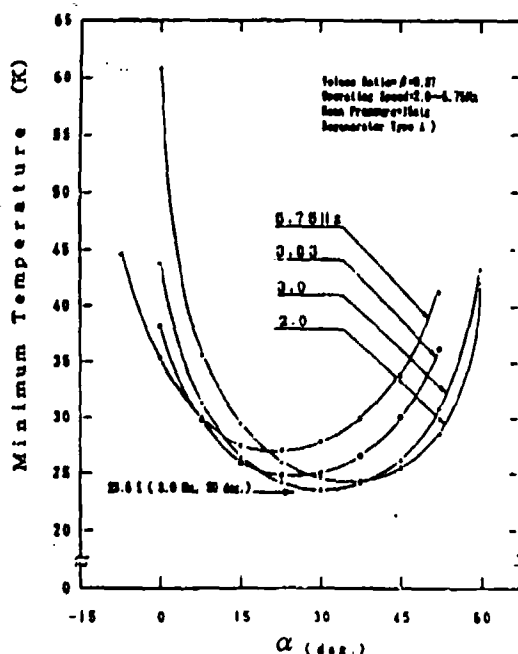


Fig. 3 Minimum Temperature vs. Operating Speed and Crank Angle

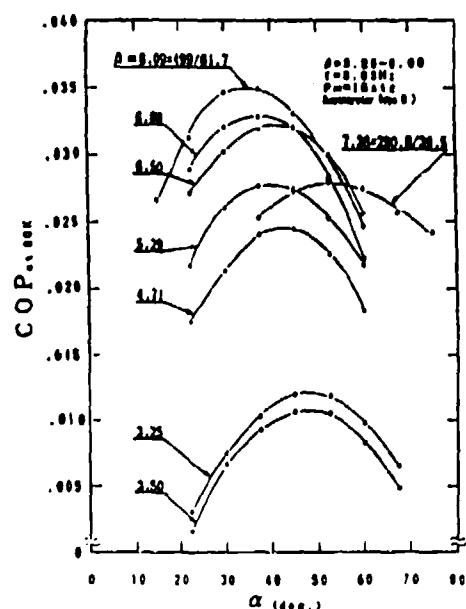


Fig. 4 Relation between the Volume Ratio, Crank Angle and COP at 80 K.

PL-CP-98-1001

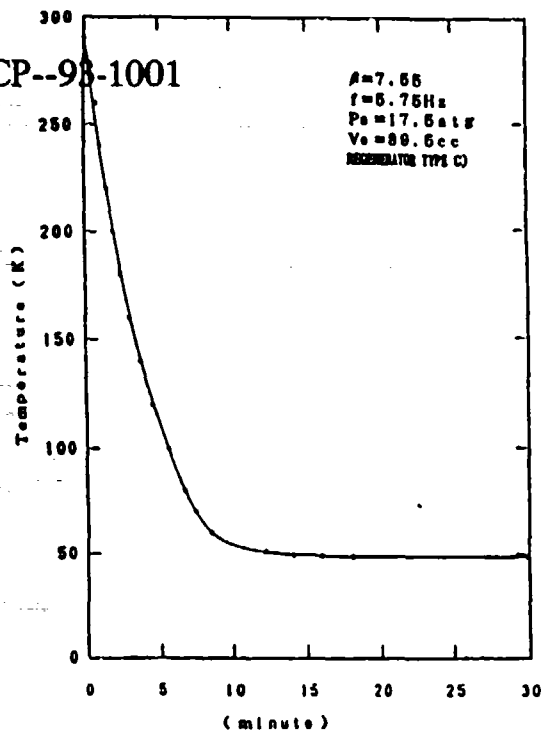


Figure 9. Cooling Speed.

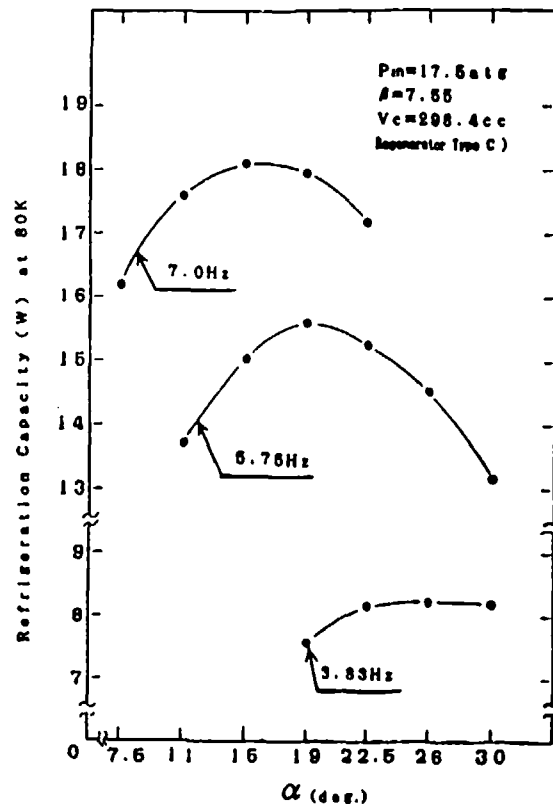


Fig.10 Refrigeration Capacity at 80K vs. Crank Angle and Operating Speed.

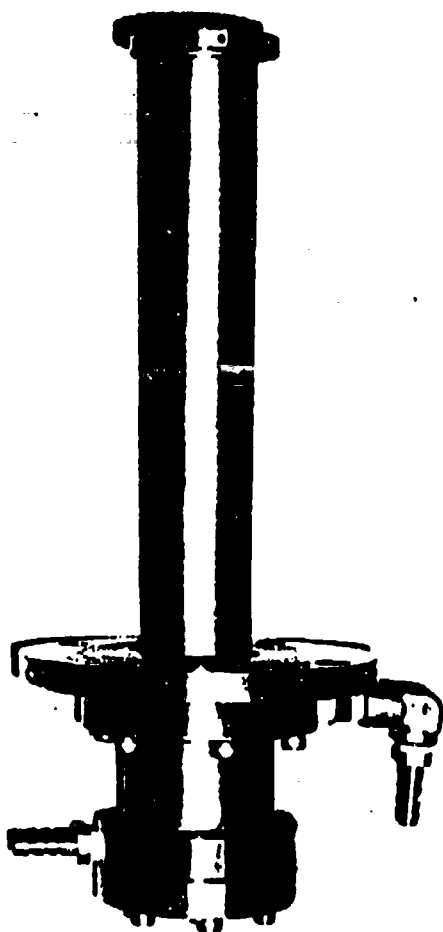


Fig. 11 The Outside Structure of Cryostat Part.

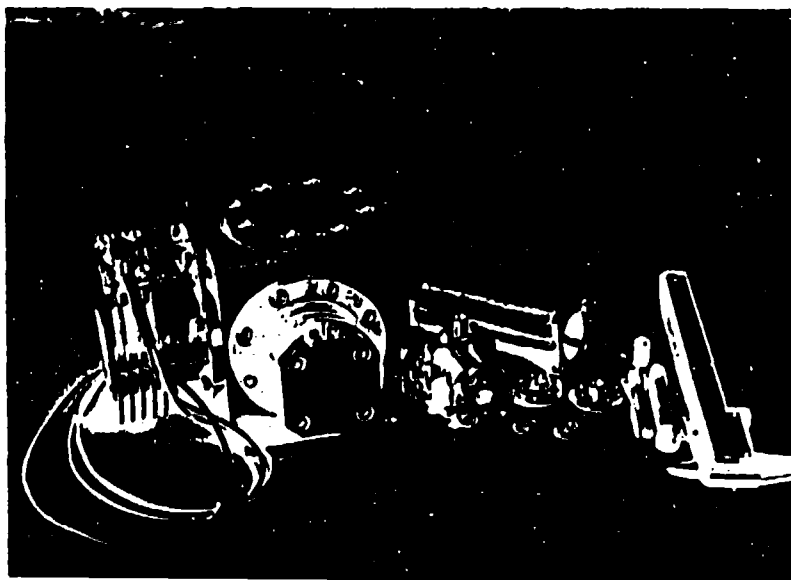


Fig. 12 A Picture of The Parts of Mini-Modified Pulse Tube Refrigerator.

PULSE TUBE REFRIGERATOR RESEARCH

Y. Zhou and Y. J. Han
Cryogenic Laboratory
Academia Sinica
P. O. Box 2711
Beijing 100080
China

1. INTRODUCTION

Pulse tube refrigerator has shown its great potential applications on many cryogenic circumstances because of the attractions of constructional simplicity and mechanical reliability. It has no moving part and no source of vibration at the cold end, and therefore long service life.

Co-axial pulse tube refrigerator is more attractive due to its compactness. The technological process is more simple and the distance between the pressure generator and the pulse tube is adjustable.

With the increasing tendency of getting lower and lower temperature in either single-stage or multi-stage refrigerators, pulse tube refrigerators are winning a great advantage. Cryogenic laboratory of Academia Sinica has achieved successes both in technological process of various types of pulse tube refrigerators and in application exploiting.

2. EXPERIMENTAL RESEARCH

A pulse tube with axial curvature was investigated in our lab at the beginning in order to improve the flexibility for pulse tube within a compact space. A coiled pulse tube has been compared experimentally and theoretically with the corresponding straight one under the same conditions. The

performance of the coiled pulse tube is degraded by its flow resistance due to the curved structure. The experiment shows that the curving ratio R/r should be 8 or higher to get a satisfactory performance, where the R is the curvature radius and the r is the pipe radius. It is possible to construct a practical compact cryocooler with the coiled pulse tube in a limited space.

Two-stage pulse tube refrigerator was then carried out in our lab. The two stages are consisted of their respective orifice pulse tubes. Each stage uses a compressor as the pressure wave generator. The first stage provides precooling for the second one, and a lowest temperature of 31k can be obtained. It is also found that the temperature ratio ($T_{\text{hot}}/T_{\text{cold}}$) in the second stage is in a linear relationship with the pressure ratio ($P_{\text{max}}/P_{\text{min}}$).

In 1989, more encouraging work was done on a single stage orifice pulse tube refrigerator which reaches the temperature of 49k, the lowest in the world then, with a specific power input of 120W/W for 12W net refrigeration capacity. The influence of the ratio of the regenerator volume to the pulse tube volume on the minimum temperature was investigated. It is found that there is an optimum ratio for best performance and an optimum average pressure for the system. The minimum temperature is lower at higher average pressure. The performance of regenerator is also related to how the matrix materials are packed.

The experimental apparatus of 49k was then improved to a two stage orifice pulse tube refrigerator with only one compressor. A lowest temperature of 36k was obtained.

In 1989, with cooperating with Xi'an Jiaotong University, another important refrigerator was made. It is known as the single stage double-inlet pulse tube refrigerator, in which a second valve is added between the valveless compressor

outlet and the pulse tube hot end. Therefore, a side stream of mass flow will occur, which causes to change the phase shifts. The new type of the refrigerator which reached a temperature of 42k was constructed in our lab with a matching setting of the two orifices. Meanwhile, a conventional orifice pulse tube can only reach the temperature of 55k when compared with the above refrigerator. It is obvious that a double-inlet pulse tube machine can decrease a minimum temperature and increase refrigeration capacity.

For recent years, more attention has been paid to single stage co-axial pulse tube refrigerators. The refrigerator is small, light and compact. It is consisted of two co-axial cylinders. The annulus part is regarded as the regenerator and the inner tube is regarded as the pulse tube, as shown in Fig.1. With

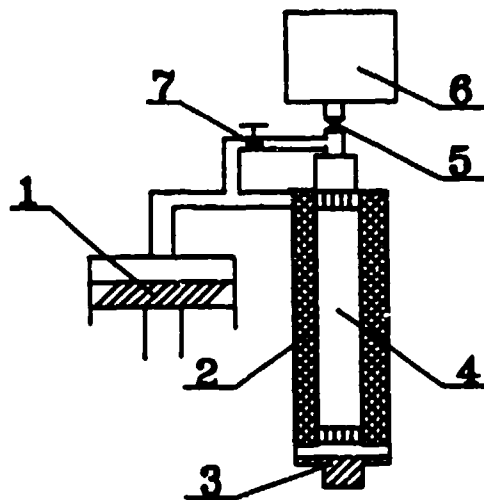


Fig.1 The constructure of the co-axial pulse tube refrigerator
 1.Compressor 2.Regenerator 3.Cold end 4.Pulse tube
 5.Orifice 6.Reservoir volume 7.Double-inlet valve

a co-axial single-stage pulse tube, we have got a temperature of 62k with 2.5w net refrigeration capacity at 77k. It is noted that the tube connecting the compressor and the regenerator should be as short as possible to minimize the loss of dead volume. The performance of co-axial pulse tube

is not as good as that of U-shape one. This is perhaps due to the following two reasons: one is the heat transfer between the regenerator and the pulse tube, the other is the abrupt flow resistance in the corner between the regenerator and the pulse tube. The co-axial pulse tube refrigerator is specially practical for applications in space and military.

In 1990, a temperature of 20k was achieved by a single-stage co-axial pulse tube with liquid nitrogen precooling.

Recently we have successfully developed a single-stage co-axial pulse tube refrigerator with multi-bypass. Now we are applying for the Chinese patent.

Fig.2 shows the flow chart of this system. Besides the double inlet valve 1, another valve 2 is added between the middle of the pulse tube and the regenerator. The experimental result of the cold end temperature vs the opening of valve 2 is shown in Fig.3. The regenerator has been improved and a minimum temperature of 33k has been achieved. It is evident that the performance of a multi-bypass refrigerator is much better than that of a double-inlet one.

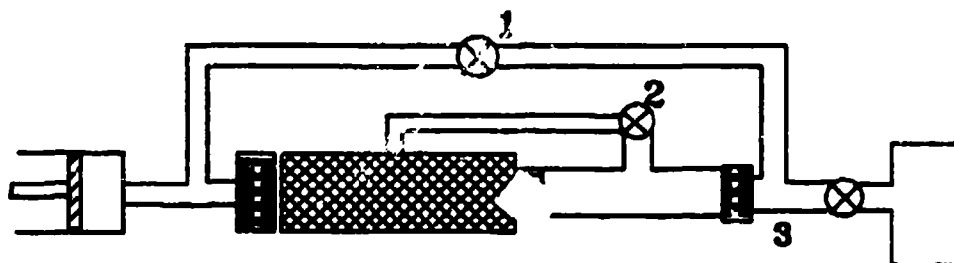


Fig.2 Flow chart of the multi-bypass pulse tube refrigerator
1.Double-inlet valve 2.Multi-bypass valve 3. Orifice

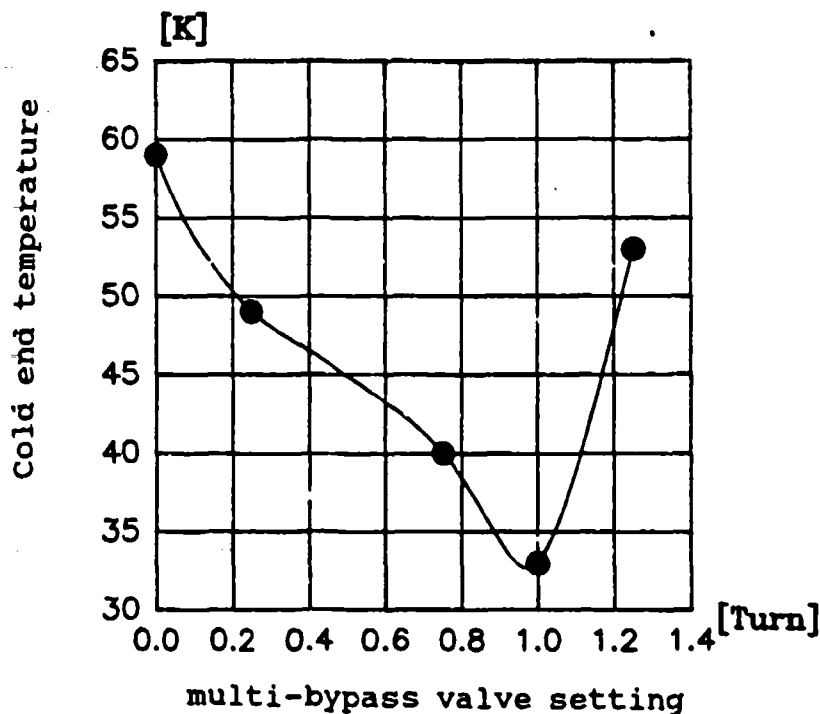


Fig.3 Cold end temperature vs multi-bypass valve setting with orifice and double-inlet valve being in optimum position

3. MECHANISM RESEARCH

Experimental analysis with phase shifts for pulse tube refrigerators has been described to explain the mechanism. For a period of time, it is believed that the pulse tube refrigerator is a variation of the Stirling-cycle one where the moving displacer is substituted by the orifice in the pulse tube machine. In a Stirling cryocooler, the displacer leads the motion of the piston by about 90° angle. As a result, an orifice at the hot end of the pulse tube should play an important part in marking a proper phase relationship between the mass flow rate and the pressure wave in order to get a best performance. However, this is a controversial point in a double-inlet pulse tube refrigerator achieved in our experiments. When the double-inlet valve is closed and the orifice at the warm end is at an optimum setting, the angle phase between the mass flow rate and the pressure wave

is not closed to zero but 48° and therefore the performance of the refrigerator is not in a best state. If the double-inlet valve is opened afterwards with an optimum setting, as shown in Fig.4, we have a angle phase relationship of about zero between the mass flow rate and the pressure wave. The refrigerator then leads to a lowest temperature with a favorable performance. An assumption is made that the mass flow both from the orifice and from other bypasses have their own influence on the refrigerator running.

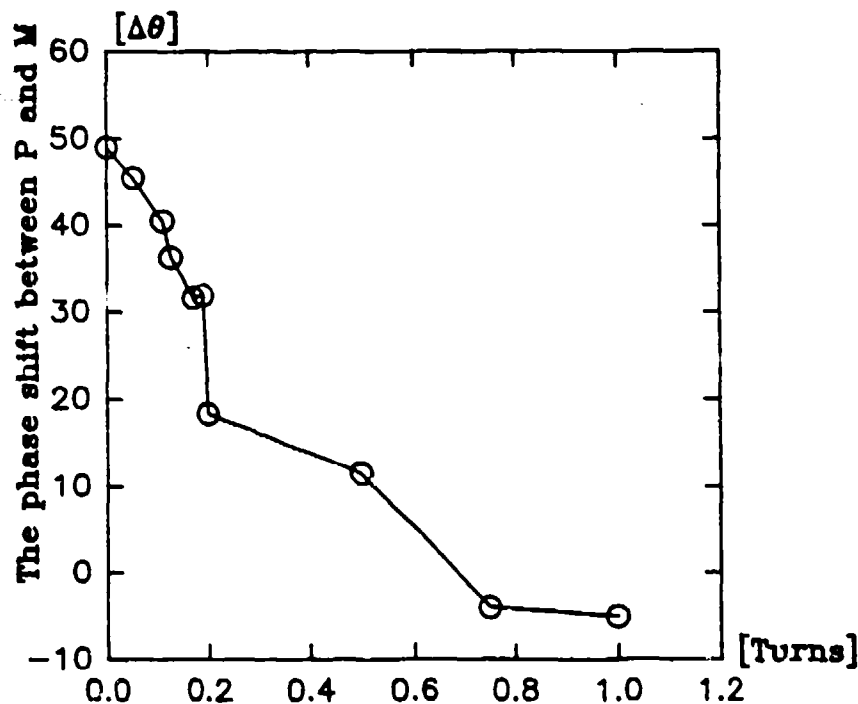


Fig.4 Variation of the phase shift with the turning of double-inlet valve

Thermoacoustic theory is currently developed to account for the operation principle in our experiments. From the theory, a cryocooler with small disturbance can be regarded as a linear thermoacoustic device. The oscillation of gaseous medium is longitudinally transmitted in the way of acoustic wave. The regenerator works on travelling wave while the pulse tube on standing wave. Thermoacoustic effects for a cryocooler can be classified into two kinds: one is with isothermal wall, as in heat exchangers which exchange the heat with its environment; the other is with adiabatic one,

as in regenerators and pulse tubes in which the acoustic energy is consumed to pump heat. The refrigerator performance can be determined by two sets of equations, the pressure-velocity wave equation and the energy-temperature equation. One result of numerical calculation for the performance comparison of three types of pulse tube refrigerators is shown in Fig.5. With the same temperature, the refrigeration power of the multi-bypass refrigerator is higher than that of the double-inlet one and the performance of the orifice refrigerator is the lowest. It is well in agreement with the experimental results.

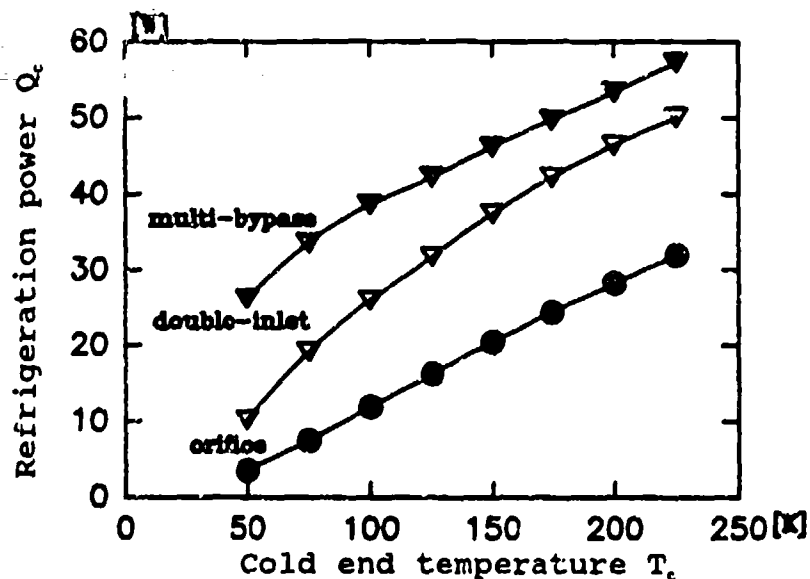


Fig.5 Performance comparison of there types of pulse tube refrigerators

4. APPLICATIONS

Interests in the applications of pulse tube refrigerators have grown rapidly in recent years. Single stage co-axial orifice pulse tube refrigerators with a double-inlet have been studied for the laboratory uses in the fields of infrared detector, high-temperature superconductor testing, cryogenic surgical knife and low-temperature physics.

A cooling device is necessary for an advanced low noise infrared detector. Generally, the cooling device should be light and 0.3-2w refrigeration capacity is needed. Several

kinds of refrigerators have been used for the purpose. However, they are not very satisfactory. In our lab, two types of single stage co-axial orifice pulse tube refrigerators with double-inlet have been produced for the cooling purpose in 1991. These two co-axial refrigerators are very compact. Both weight are less than 0.3kg. The temperature of 62k and 47k can be reached respectively, with a refrigeration capacity being over 1w at 77k, which meets the cooling needs for infrared detectors. When compared with the Stirling refrigerator, the pulse tube refrigerator can be fitted in any directions in reliable operation.

Photo 1 shows a cryogenic surgical knife with a small single stage co-axial pulse tube refrigerator operated by a valveless compressor. It can be used in surgical operations and skin beauties. The cold tip is unfixable. A temperature indicator is connected to the cold tip and the lowest temperature of the cold tip of 173k can be reached without any insulator within five minutes. This refrigeration method is superior to other ones for the medical use.

Pulse tube refrigerators have also been studied as the cold source of low-temperature refrigerator mainly used in cold treatment and testing for materials and cryogenic storage for hospitals, biological departments and other research institutes.

Usually, freon cascade refrigeration systems are utilized in low-temperature refrigerators. When the required temperature is below -80°C , the whole system is very complex, brings about a low efficiency and places a limit to the minimum temperature. Moreover, freon pollution is challenging the world. Now people are searching for a new approach for the substitution.

However, if the temperature is below -80°C , pulse tube refrigerators are competitive in taking the place of freon

cascade refrigerators because of the high efficiency and reliability. Feasible experiments have been done on a pulse tube refrigerator. It is easy to get a temperature below 193k. New refrigerators for hospital and biological uses in the temperature range from 293k to 193k are being constructed.

Photo 2 shows another application of a single stage pulse tube refrigerator with double-inlet. It is designed in order to determine the suitability for cold testing of electric properties in high temperature superconductor device. A temperature range from 273k to 65k is available. It works on helium under a noise less than 60dB. After 40 minutes, the refrigerator reaches a minimum temperature of 70K with a refrigeration capacity of 0.3w at 77k. A motor power of 150w is needed. As mentioned previously, no moving part at the cold end of pulse tube is of great importance in cryocooler applications. Therefore the designed co-axial pulse tube refrigerator has the advantages for lower cost, higher reliability and less vibration. When the refrigerator is used, samples of superconductor materials can be replaced simply and conveniently.

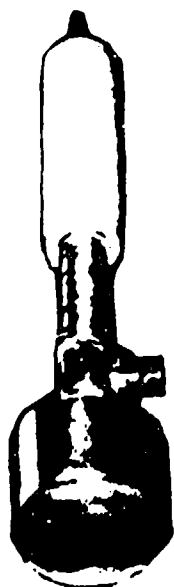


Photo 1.
Cryogenic surgical knife

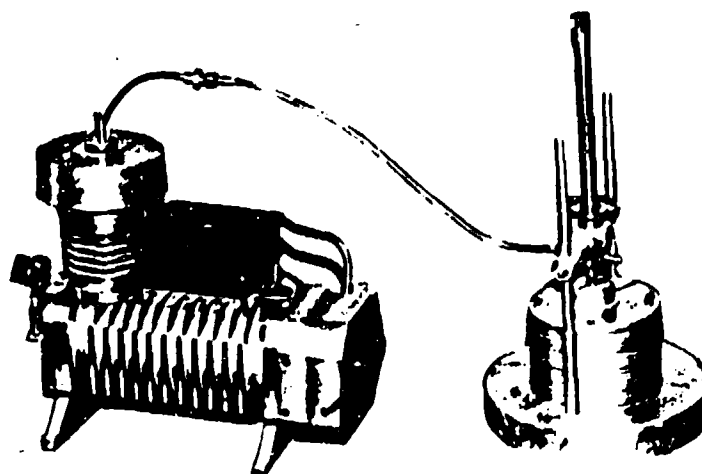


Photo 2.
Pulse tube refrigerator used
in superconductor testing

5. CONCLUSION

Applications in various fields with single-stage co-axial pulse tube refrigerators have been shown primarily in the past few years. New embodiments of pulse tube refrigerators have been developing in our lab. Although experiments and theoretical analysis for these refrigerators have been done, there are still much room to exploit in technology and refrigeration mechanism in the future.

6. REFERENCES

- [1] Y. Zhou, Wenxiu Zhu and J. T. Liang, Two-Stage Pulse Tube Refrigerator, Proceedings of the international cryocooler conference, U.S.A., 1988
- [2] J. T. Liang, Y. Zhou and Wenxiu Zhu, Development of Single-stage Pulse Tube Refrigerator capable of reaching 49k, Cryogenics, 1990
- [3] J. J. Wang, Wenxiu Zhu, Pingsheng Zhang and Y. Zhou, A Compact Co-axial Pulse Tube Refrigerator for Practical Application, Proceedings of the 13th international Cryogenic Engineering Conference, China, 1990
- [4] Ray Radbaugh, A Review of Pulse Tube Refrigeration, Advances in Cryogenic Engineering, Vol.35, 1990
- [5] J. H. Xiao, Thermoacoustic Theory for Cyclic Flow Regenerators, Part 1, Fundamentals, Cryogenics, Vol.32, 1992

DEVELOPMENT OF PULSE TUBE REFRIGERATOR
WITH LINEAR-MOTOR DRIVE COMPRESSOR

Toru Kuriyama, Hideo Hatakeyama,
Yasumi Ohtani, and Hideki Nakagome
Energy and Mechanical Research Laboratories
Toshiba Research and Development Center
Ukushima, Kawasaki, Japan

Yoichi Matsubara
Atomic Energy Research Institute
Nihon University
Funabashi, Chiba, Japan

Haruyuki Okuda and Hiroshi Murakami
The Institute of Space and Astronautical Science
Sagamihara, Kanagawa, Japan

ABSTRACT

This paper describes the experimental results of an orifice type pulse tube refrigerator. The purpose of this study was to demonstrate a high refrigeration efficiency at 80 K with the higher operation frequency than the usual pulse tube refrigerator for compacting size. The highest COP (coefficient of performance) value of 0.032 at 80 K was achieved with the 9.6 W refrigeration capacity and the 300 W electrical input power in the 17 Hz operation frequency. The lowest temperature of 36.5 K and the largest refrigeration capacity of 13.6 W were also obtained.

The main technical points were to adopt a double inlet line for the pulse tube, to optimize the regenerator for the higher frequency operation comparing to the usual pulse tube refrigerator (more than 10 Hz), and to use a high efficient linear-motor drive compressor.

INTRODUCTION

The pulse tube refrigerator is attractive as a high reliability and low vibration refrigerator, because there is no moving part at the cold section. In 1963, Gifford and Longworth⁽¹⁾ first invented the basic pulse tube refrigerator, and achieved a temperature of 124 K by a single stage⁽²⁾. In 1984, Mikulin et al.⁽³⁾ developed the orifice pulse tube refrigerator and the lowest temperature of the pulse tube refrigerator has been improved. Radebaugh et al.⁽⁴⁾ achieved the lowest temperature of 60 K by the orifice pulse tube refrigerator. Zhu et al.⁽⁵⁾ developed a double inlet type pulse tube refrigerator, in which the compressor and the hot end of the pulse tube were connected by a double inlet line. They achieved the lowest temperature of 42 K⁽⁶⁾. Thus, pulse tube refrigerators have been improved remarkably during these several years.

The authors have developed a high efficient pulse tube refrigerator, and the COP value of 0.032 at 80 K has been achieved by a single-stage double inlet type pulse tube refrigerator with a linear-motor drive compressor.

SYSTEM DESIGN

Pulse Tube and Regenerator

Figure 1 shows a schematic diagram for the pulse tube refrigerator, and Figure 2 shows the photograph. The size of the refrigerator was approximately 330 mm in maximum diameter and 700 mm in length. The total weight was about 50 kg excluding a power supply.

The pulse tube was made of a 0.3 mm thick stainless steel tube, and the hot end of the pulse tube was cooled by water. An orifice valve was attached to the hot end of the pulse tube and controlled the helium gas flow rate to a reservoir, whose volume was approximately 1600 cm³. A double inlet valve was also attached to the hot end of the pulse tube.

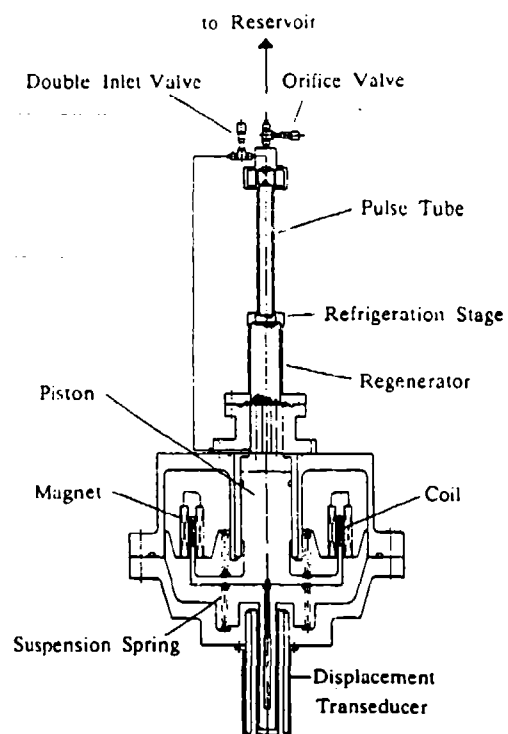


Fig. 1 Schematic diagram of pulse tube refrigerator

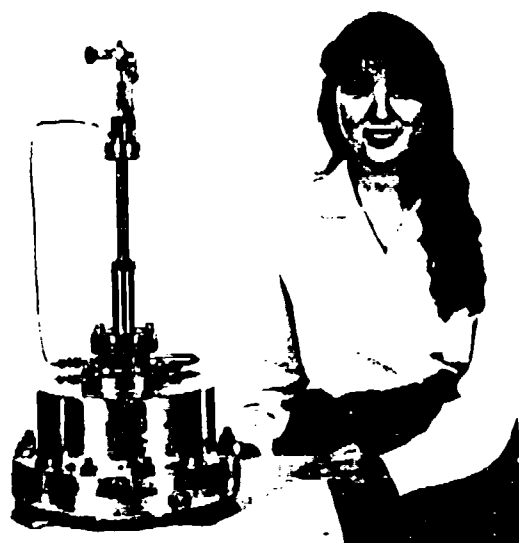


Fig. 2 Photograph of pulse tube refrigerator

A hybrid structure of stainless steel and phosphor bronze was adopted for the regenerator materials. Stainless steel meshes (#300) were filled in one-half volume of the higher temperature part, and phosphor bronze meshes (#325) were filled in the lower temperature part. These meshes were stacked in a 0.5 mm titanium tube, which reduced the heat loss by the thermal conduction.

Linear-motor Drive Compressor

A linear-motor drive compressor is commonly used for a miniature Stirling refrigerator⁽⁷⁾. The compressor for this system mainly consisted of a piston with a moving coil, a rare earth permanent magnet, two suspension coil springs, and a displacement transducer. The piston diameter was 60 mm and a rubbing seal was installed to minimize the helium leakage. The compressor cylinder was made of ceramic (silicon nitride, Si_3N_4) and its surface was finely polished to reduce the seal abrasion. No lubricative oil was used in the compressor.

The compressor piston was supported by two coil springs. When the piston is moving, the spring force from the compressed or expanded helium gas is added to the mechanical spring force. If coil springs have a side force to the piston, the frictional loss at the rubbing seal increases. On the other hand, the gas spring force gives no side force to the piston in principle. Then, the mechanical spring constant was designed small enough compared to that of the gas spring constant. The mechanical spring constant was about 4.9×10^3 N/m, meanwhile the calculated gas spring constant was about 4.6×10^4 N/m when the mean pressure was 1.2 MPa. The gas spring constant was designed about ten times as large as that for the mechanical spring.

For compacting size, the authors intended to operate this system at relatively higher frequency of around 18 Hz compared to other pulse tube refrigerators. For example, Radebaugh et al.⁽⁴⁾ operated at 9 Hz to achieve 60 K and Zhu et al.⁽⁸⁾ operated at 7 Hz to achieve 42 K. For the linear-motor drive compressor, the highest compressor efficiency is obtained at the resonance frequency⁽⁸⁾. Then, a piston diameter and a

piston weight were designed so that the resonance frequency was near 18 Hz. The resonance frequency was roughly calculated from the spring constant (sum of the gas spring and the mechanical springs) and the piston weight. The calculated results of the resonance frequency for this system was 17.3 Hz when the mean pressure was 1.2 MPa.

Instrumentations

The pressure at the compression space was measured by a pressure transducer. The electrical input power to the compressor was calculated by integrating the instantaneous voltage and current values. An electrical heater and a carbon glass resistance (CGR) thermometer were mounted at the refrigeration stage to measure the refrigeration capacity. The COP value was estimated from the refrigeration capacity and the input power.

EXPERIMENTAL RESULTS

First, the relation between the compressor swept volume (V_c) and the refrigeration capacity or the COP value at 80 K were investigated (Fig. 3). In this experiment, the operation frequency was fixed at 17 Hz, which was near to the calculated resonance frequency for the compressor, and the mean pressure was 1.2 MPa. The compressor swept volume was varied from 50.4 cm³ to 74.2 cm³ (V_{cmax}). The refrigeration capacity increased with increasing V_c and a maximum refrigeration capacity of 13.6 W at 80 K was obtained for V_{cmax} . The COP value, however, had the highest value and the highest COP value of 0.032, where the refrigeration capacity was 9.6 W and the input power was 300 W, was obtained at $V_o = 62.8$ cm³ (V_{copt}).

Secondly, the dependency of COP at 80 K on the operating frequency has been investigated. The experimental results are shown in Fig. 4, where the compressor swept volume was kept constant value (V_{copt}), which resulted in the highest value of COP at 80 K shown in Fig. 3. The optimum frequency, where the COP value was the highest, was 17 Hz and

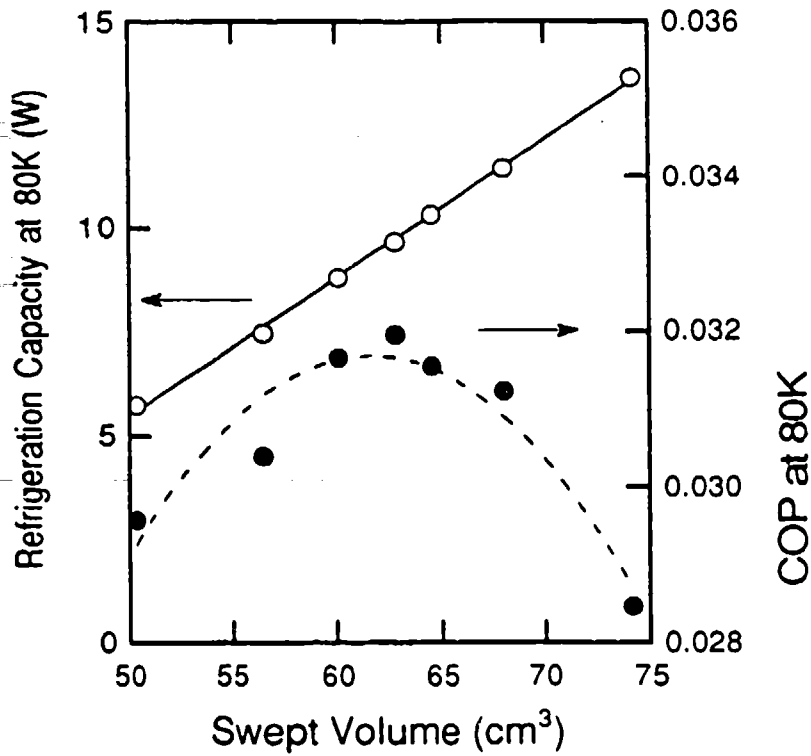


Fig. 3 Relation between compressor swept volume and refrigeration capacity or COP value at 80 K
Operation frequency = 17 Hz, Mean pressure = 1.2 MPa

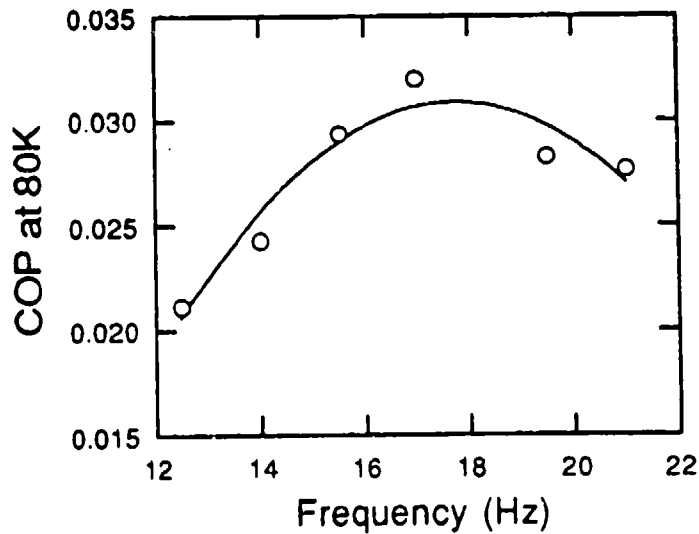


Fig. 4 Relation between operating frequency and COP value at 80 K
Operation frequency = 17 Hz, Mean pressure = 1.2 MPa

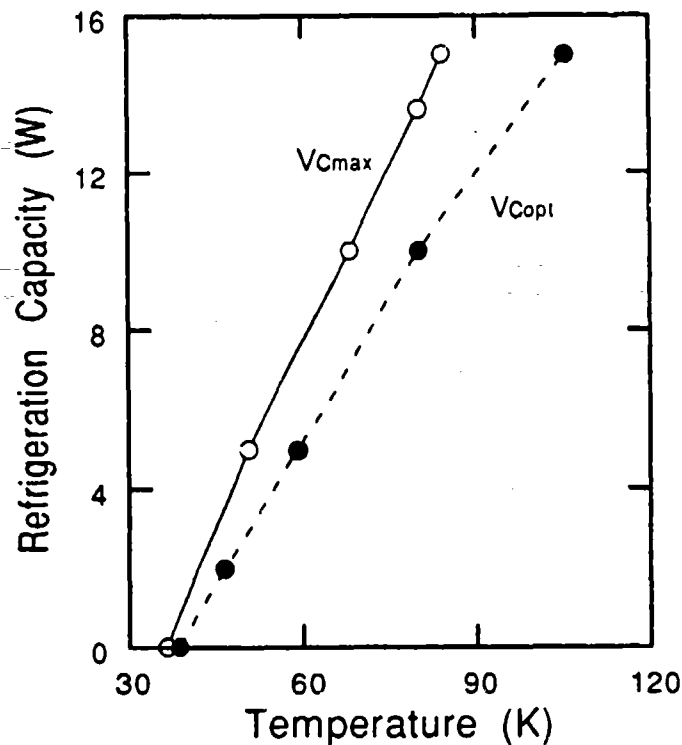


Fig. 5 Relation between refrigeration temperature and refrigeration capacity
 Operation frequency = 17 Hz
 Mean pressure = 1.2 MPa

well agreed with the calculated resonance frequency mentioned in the previous section.

Figure 5 shows the relation between the refrigeration temperature and refrigeration capacities which were obtained for the swept volumes of V_{Cmax} and V_{Copt} . The refrigeration capacity for V_{Cmax} was larger than V_{Copt} for every temperature level, and the lowest temperature of 36.5 K was achieved for V_{Cmax} .

Figure 6 shows the COP values calculated from the refrigeration capacity data shown in Fig. 5. In spite of the highest COP value at 80 K for V_{Copt} , the COP value for V_{Cmax} was higher than that for V_{Copt} below about 60 K.

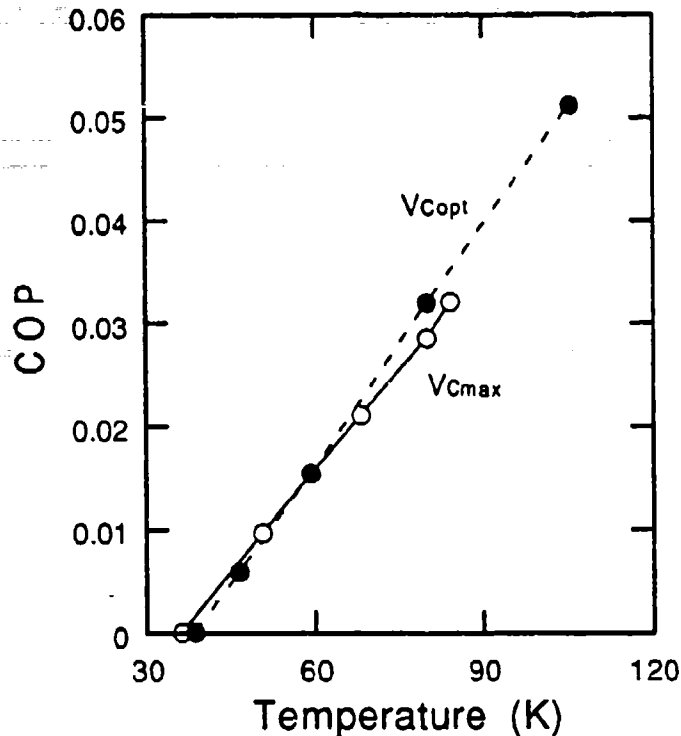


Fig. 6 Relation between refrigeration temperature and COP value at 80 K

Operation frequency = 17 Hz

Mean pressure = 1.2 MPa

CONCLUSIONS

The high efficient pulse tube refrigerator with a linear-motor drive compressor was designed and constructed. The following conclusions were drawn from the experimental results.

- (1) The optimum operation frequency, where the COP value at 80 K was the highest, was about 17 Hz and well agreed with the calculated resonance frequency.

- (2) The highest COP value of 0.032 at 80 K, where the refrigeration capacity was 9.6 W and the input power was 300 W, was obtained for 62.8 cm³ of the compressor swept volume.
- (3) The lowest temperature of 36.5 K was achieved and the largest refrigeration capacity of 13.6 W at 80 K was obtained for 74.2 cm³ of the compressor swept volume.

REFERENCES

- (1) W.E. Gifford and R.C. Longworth, "Pulse-tube refrigeration", ASME paper No.63-WA-290 presented at Winter Annual Meeting of the American Society of Mechanical Engineers, Philadelphia, Pennsylvania (Nov. 1963) pp. 17-22.
- (2) W.E. Gifford and R.C. Longworth, "Pulse tube refrigeration progress", Advances in Cryogenic Engineering, Vol. 10B (1965) p. 69.
- (3) E.I. Mikulin, A.A. Tarasov, and M.P. Shkrebyonock, "Low-temperature expansion pulse tubes", Advances in Cryogenic Engineering, Vol.29 (1984) pp. 629-637.
- (4) R. Radebaugh, J. Zimmerman, D.R. Smith, and B. Louie, "A Comparison of Three Types of Pulse Tube Refrigerators: New Methods for Reaching 60 K", Advances in Cryogenic Engineering, Vol.31 (1986) pp. 779-789.
- (5) Z. Shaowei, W. Peiyi, and C. Zhongqi, "Double inlet pulse tube refrigerator: an important improvement", Cryogenics, Vol.30 (1990) pp. 514-520.
- (6) S. Zhu, P. Wu, and Z. Chen, "A single stage double inlet pulse tube refrigerator capable of reaching 42 K", Cryogenics, Vol.30 September Supplement, (1990) pp. 257-261.
- (7) G. Davey and A.H. Orlowska, "Miniature Stirling cycle cooler", Cryogenics, Vol.27 (1987) pp. 148-152.
- (8) T.W. Bradshaw, J. Delderfield, S.T. Werrett, and G. Davey, "Performance of the Oxford Miniature Stirling Cycle Refrigerator", Advances in Cryogenic Engineering, Vol.31 (1986) pp. 801-809.

AN EXPERIMENTAL AND ANALYTICAL INVESTIGATION
OF 4 K PULSE TUBE REFRIGERATOR

Y. Matsubara and J. L. Gao*
Atomic Energy Research Institute
Nihon University
Chiba 274, Japan

K. Tanida and Y. Hiresaki
Cryogenic Division
Suzuki Shokan Co., Ltd.
Saitama 350, Japan

M. Kaneko
JECC Corporation
Saitama 350, Japan

ABSTRACT

In the viewpoint of equivalent P-V diagram at the cold end of pulse tube, the performance of the pulse tube refrigerator could be greatly improved by use of simple phase shift valve without reservoir at the hot end of pulse tube (similar to that in G-M cycle). The single stage four-valve pulse tube refrigerator has been developed in which the minimum temperature below 30 K and the cooling power 10 Watts at 55 K were achieved. Another experiment has been done on the single stage pulse tube refrigerator coupled with a G-M cryocooler. The minimum temperature at the cold end of pulse tube obtained by this unit was 3.5 K when the hot end of pulse tube was located at room temperature and the hot end of final stage regenerator was precooled at 15 K. The optimum operating condition of the two experimental units was both at mean pressure around 1.0 to 1.5 MPa and with frequency about 1 to 2 Hz. This makes it possible to reach 4 K with two or three-stage pulse tube refrigerator only using one compressor with single regenerator set. Heat flow and losses analysis, as well as arrangement of the multi-stage pulse tube refrigerator are briefly discussed.

INTRODUCTION

The performance of the pulse tube refrigerator is greatly improved after the orifice was introduced to the closed end of the pulse tube[1][2]. In the viewpoint of the equivalent P-V diagram at the cold end of the pulse tube, it is indicated that there are some limitations of minimum attainable temperature due to the limited phase shift effect in the simple orifice pulse tube refrigerator[3]. By using of second inlet tube[4], second valve[3] and second piston[5] at the hot end of the pulse tube, the recent progress on the single stage pulse tube refrigerator has given much lower attainable temperature and much higher performance.

* an invited researcher from Zhejiang University in China

In the pulse tube refrigerator no moving parts at low temperature makes it easy to add any number of stages. In the case of the orifice pulse tube refrigerator, the enthalpy flow through the pulse tube from the cold end to the hot end, which gives the cooling power at the cold end, is transformed to heat at the hot end. In the multiple stage pulse tube refrigerator, the refrigeration performance and the minimum attainable temperature will depend on which temperature region could be selected to locate the phase shifter for the lower stage pulse tube and how to remove that heat at the hot end of the lower stage pulse tube to increase the regenerator performance and to decrease the pulse tube losses.

Under consideration of the gas piston inside of the pulse tube, if the movement of this piston not only could prevent the mass flow from the hot end to with the mass flow at the cold end but also had good adiabatic performance, in the multiple stage pulse tube refrigerator the phase shifter of the lower stage pulse tube could be located at the higher temperature than that at the upper stage cold end, even located at room temperature. In such a case the heat at the hot end of the second stage pulse tube would be rejected at room temperature without using the upper stage cooling power.

The purpose of this study is to compare with several kinds of construction for the hot end of the pulse tube in which the cold end of the pulse tube was operated at liquid helium temperature and to find out how to arrange the multiple stages for 4K pulse tube refrigerator to minimize the pulse tube loss and to increase the regenerator performance. The concept of the equivalent P-V diagram at the cold end of the pulse tube has been described incorporated with the experimental results of the single stage pulse tube refrigerator.

PERFORMANCE OF SINGLE STAGE PULSE TUBE REFRIGERATOR

The pulse tube refrigerator could be considered as a variation of Stirling cryocooler in which the cold mechanical piston is replaced by gas oscillation column (gas piston) within the pulse tube. In the stirling cycle the cooling effect at expansion space is obtained by the phase lag of the solid expansion piston movement. In the case of harmonic motion of two pistons' mechanic movement, the maximum P-V area in the expansion space can be obtained from the volumetric flow rate in phase with the pressure. In a pulse tube refrigerator, however, there is the intrinsic difference between gas oscillation in the pulse tube and mechanic movement of main piston. The cooling capacity per unit mass flow rate in the simple orifice pulse tube refrigerator could not be obtained as same as that in Stirling cryocooler because only using a simple orifice and a reservoir at the hot end of the pulse tube should lead to larger mass flow rate with phase angle behind pressure at the cold end of the pulse tube and lower performance of the regenerator. The recent development of the pulse tube refrigerator by using of second phase shifter, such as a moving plug (second piston), second inlet tube, and second valve at the hot end of the pulse tube made further improvement in the performance. After given by Storch and Radebaugh[6], the enthalpy flow analysis is used to explain the simple orifice pulse tube refrigeration. Based on the first law of the

thermodynamics, the energy balance at the cold end of the pulse tube is given by

$$\dot{Q}_c = \langle \dot{H} \rangle - \langle \dot{H}_r \rangle - \dot{Q}_{loss} \quad (1)$$

here \dot{Q}_c is the cooling capacity at the cold end of the pulse tube, $\langle \dot{H} \rangle$ is the average enthalpy flow through the pulse tube from the cold end to the hot end, $\langle \dot{H}_r \rangle$ is the average enthalpy from the regenerator to the cold end, \dot{Q}_{loss} is the pulse tube losses which should be included the total heat flow from the hot end to the cold end in the pulse tube.

The cooling capacity \dot{Q}_c can be increased by minimizing both the regenerator loss $\langle \dot{H}_r \rangle$ and the pulse tube losses \dot{Q}_{loss} . In order to easily describe how the second phase shifter can be increased the performance of the pulse tube refrigerator, the equivalent PV diagram at the cold end of the pulse tube will be discussed in the following, as well as the testing results of the single stage four-valve pulse tube refrigerator.

Equivalent PV Diagram at The Cold End of The Pulse Tube

The pulse tube refrigerator with different hot end boundary conditions is shown in Figure 1 to be analyzed for the equivalent P-V diagram at the cold end of the pulse tube. To find how the pressure in the pulse tube varies during the periodic oscillation, the fact is used that in a closed-cycle cooler the total mass of gas taking part in the process is constant. After obtained the pressure and mass flow rate in each controlling volume by the Runge-Kutta method, the equivalent volume flow at the cold end of the pulse tube, by using gas state equation, will be expressed in Eq.(2) which is defined by the mass flow rate passing through the cold end of the regenerator.

$$P \frac{dV_{pe}}{dt} + \frac{dP}{dt} V_{pe} = RT_{pe} \dot{m}_{pe} \quad (2)$$

where P is the pressure in the pulse tube, V_{pe} is the equivalent volume flow at the cold end of the pulse tube, R is the gas constant, T_{pe} is the temperature at the cold of the pulse tube, and \dot{m}_{pe} is the mass flow rate at the cold end of the pulse tube. The equivalent P-V diagram at the cold end of the pulse tube is obtained under the equivalent volume definition of Eq.(2). The equivalent expansion work produced when a gas at the cold end of the pulse tube is expanded cyclicly is (per cycle):

$$W_c = \oint P dV_{pe} \quad (3)$$

This quantity can be represented by the area within the closed curve describing the cycle in the equivalent P-V diagram.

One of the most important improvement on the pulse tube refrigerator after the orifice has been made by the second inlet tube shown in Figure 1(1) and (2). The following discussion on the equivalent P-V diagram at the cold end of the pulse tube will be focused on the second inlet tube mode. As our consideration, the phase shift effect in the second inlet pulse tube refrigerator is achieved by matching of three flow resistances from the regenerator, second inlet tube and orifice. The mass flow rate through the regenerator, orifice

and second inlet tube is assumed to express as follows respectively

$$\dot{m}_1 = \alpha_1 (P_c^2 - P_p^2) \quad (4)$$

$$\dot{m}_2 = \alpha_2 (P_b^2 - P_o^2) \quad (5)$$

$$\dot{m}_3 = \alpha_3 (P_c^2 - P_p^2) \quad (6)$$

here \dot{m}_1 , \dot{m}_2 and \dot{m}_3 is the mass flow rate through the regenerator, the orifice and the second inlet tube respectively, α_1 , α_2 and α_3 are the friction factors of the regenerator, the orifice and the second inlet tube, P_c is the pressure in the compressor volume, P_p is the pressure inside of the pulse tube and P_o is the pressure in the reservoir. The mass flow rate at both end of the pulse tube could be written as

$$\dot{m}_{pe} = \dot{m}_1 - \frac{\frac{dP_p}{dt} V_r}{2RT_{pe}} \quad (7)$$

$$\dot{m}_{ph} = \dot{m}_2 + \dot{m}_3 \quad (8)$$

here V_r is the void volume in the regenerator, \dot{m}_1 is the mass flow rate at the hot end of the pulse tube.

Equivalent PV diagrams at the cold end of the pulse tube are shown in Figure 2, in which the system dimension was based on an actual double inlet pulse tube refrigerator[7]. In the case of simple orifice ($\alpha_2=0$), the shape of the P-V diagram indicates that it requires a significant mass flow rate through the cold end of the regenerator, because the maximum mass flow rate is roughly proportional to the equivalent volume at the point of the peak pressure. In the case of $\alpha_2=10$, the expansion work is greater than other cases, that means the high COP (shown in table 1) could be obtained with this condition. The phase shift effect by this case, however, is still very small so that the cooling capacity per unit mass flow is not so large which will also increased the regenerator loss. To keep high COP needs to make the sufficiently good regenerator. In the case of $\alpha_2=50$, the COP is very low, and the cooling capacity per unit mass flow rate is larger than other cases which is due to the great phase shift effect by the large opening of the second inlet tube. However to get large cooling capacity needs to increase the input power and total system working volume. The case of $\alpha_2=30$ gives more interesting equivalent P-V shape at the cold end of the pulse tube, in which both COP and We/mp (shown in table 1) can be obtained moderately. It indicated the same friction factor of the regenerator and second inlet tube could be one of the key parameter to design and operate a double inlet pulse tube refrigerator.

The thermodynamic comparison of four typical cases is given as Table 1. The cooling capacity will be decreased with opening the second inlet tube because the mass flow rate through the cold end of the regenerator is decreased when the second inlet tube is opened. The

cooling capacity per unit mass flow rate at the cold end of the pulse tube, however, is increased with opening the second inlet tube due to the great phase shift effect of the second inlet tube. The comprehensive performance in the second inlet pulse tube refrigerator could be much higher than that in the simple orifice when the three friction factors are optimized.

With the concept of the equivalent P-V diagram at the cold end of the pulse tube, it could be concluded that the effect of the second inlet tube, compared with the simple orifice, is not only on decreasing the mass flow rate through the regenerator to minimize the regenerator losses $\langle \dot{H}_r \rangle$ and also on obtaining greater phase shift effect which give larger cooling capacity per unit mass flow rate with smaller volume flow at the cold end of the pulse tube to minimize the heat transfer and gas mixing losses $\dot{Q}_{i,gg}$ in the pulse tube.

Test Results of The Single Stage Four-Valve Pulse Tube Refrigerator

To confirm the analytical predication that the regenerator and pulse tube losses can be decreased by using the second phase shifter, the experimental device of the single stage pulse tube refrigerator operated by a valved compressor shown in Figure 3 was fabricated and tested. The size of the pulse tube used here is 1.9 cm of the inner diameter and 23.7 cm of the length, the regenerator filled 300 mesh copper screen disks is 3.6 cm of the inner diameter and 12.3 cm of the length. This system can be worked as several modes such as simple orifice, second inlet tube and four-valve type of Figure 1(4) modified from Figure 1(3).

The calculation with the model of Figure 1(2) using the actual size and operating condition of this test pulse tube refrigerator has been done for the case of valved compressor type. The Figure 4 shows the equivalent P-V diagram at the cold end of the pulse tube with optimum operating condition of both simple orifice and second inlet tube. The indications from this equivalent P-V diagram for the valved compressor type are similar to that for valveless compressor type discussed before.

The testing results on this device is shown in Figure 5. Optimum operating frequency was about 2 Hz at mean pressure of about 1.5 MPa. The cooling capacity at 80 K of second inlet type was 12 Watts and that of four-valve type was 17.5 Watts. In the case of simple orifice type the optimal operating condition only gave 58 K of minimum temperature at the cold end of the pulse tube. However the minimum temperature of the second inlet type and the four-valve type was 32 K and 29.5 K respectively.

The most attractive advantage of the pulse tube refrigerator is the increase in simplicity. To achieve much lower temperature for some applications with the pulse tube refrigerator, multi-staging must be well constructed to keep its simplicity and acceptable performance[8][9].

**PERFORMANCE OF SINGLE STAGE PULSE TUBE REFRIGERATOR
COUPLED WITH A G-M CRYOCOOLER**

To investigate what kinds of the staging method should be the best choice for multiple stage pulse tube refrigerator, we fabricated the single stage pulse tube precooled by a two-stage G-M cryocooler as shown in Figure 6. The regenerator for the pulse tube refrigerator was constructed by three stages. Copper mesh, lead shot and Er,Ni shot were installed in each stage. The hot end of last stage regenerator was precooled by second stage of the G-M cryocooler about 15 K to 20 K. The cold end of the first stage regenerator was precooled by first stage of the G-M cryocooler about 50 K to 70 K. Figure 6 shows the schematic of the experimental device with four different type pulse tubes. The design parameters of the regenerators and the pulse tubes are shown in Table 2.

Experiment on Type A of The Pulse Tube

In the case of type A, the hot end of the pulse tube was copied by first stage of the G-M cryocooler. The reservoir of 123 cm³ is located in the vacuum chamber, therefore its temperature is almost same as the hot end temperature of the pulse tube. The stainless steel filter of 7 micron mesh was installed as the orifice at the hot end of the pulse tube. The minimum temperature obtained in this simple orifice case was about 10 K when the hot end of the pulse tube was cooled at 66 K and the hot end of last regenerator was cooled at 20 K. A stainless steel capillary tube then has been used for second inlet tube, and its flow resistance was controlled by changing the total length of this tube. With this configuration, 4.5 K of minimum temperature was achieved at the operating condition shown in Table 3 of the case A.

Experiment on Type B of The Pulse Tube

The longer pulse tube having the total length of 32 cm was used for the case of type B. The hot end of the pulse tube is fixed at room temperature. The orifice and second inlet tube were removed to outside of the vacuum chamber. To make it easy doing experiment, at this time the controllable orifice and second inlet valve were used. The minimum temperature from this type was 8.1 K and the liquid helium temperature could not be obtained by this size of the pulse tube. Here we consider the effect of the equivalent expansion volume discussed before. To increase the equivalent expansion P-V work per unit mass flow through the regenerator, additional mass flow through the second inlet tube must be required which increases the apparent regenerator performance. However, at the same time, it may give additional heat flow from the hot end to the cold end of the pulse tube due to the compression heat of much larger mass flow from the second inlet. Therefore the type C was fabricated and test to confirm this consideration and to minimize that heat flow.

Experiment on Type C of The Pulse Tube

The phase shifter at the hot end of the pulse tube shown in the type C is also moved from inside of the vacuum chamber to room temperature. The stainless steel tube filled with stainless steel shot is used here to connect the warm end of the pulse tube to the phase shifter. The warm end was connected thermally with a copper bar to

first stage of the G-M cryocooler. The minimum temperature obtained by this unit was 3.6 K when the hot end of pulse tube was cooled 73.5 K and the hot end of final stage regenerator was precooled at 15 K. The optimum operating frequency is about 1.5 Hz and the mean pressure is 1.0 MPa. It indicated to approach liquid helium temperature in the pulse tube refrigerator is also needed lower operating frequency as same as the G-M and Stirling cryocoolers[10][11].

Experiment On The Heat Flow Measurement

To measure the heat flow through the copper bridge located between the warm end of the pulse tube and the 1st stage of the G-M cryocooler in the type C, at first the experiment was done only operating the G-M cryocooler for calibration of the thermal conductivity of this copper bridge. The heater was set on one side of this thermal bath which is removed from the connection with the warm hot end of the pulse tube. After heating with different power Q the value of Q/dT at particular mean temperature T_m was given in Figure 7 and was used as the calibration for the heat flow measurements. Figure 8 shows the heat flow through that copper bar in the case of the type C. At minimum temperature of 3.8 K, it is noted that the negative heat flow of 0.7 watts through that thermal bath has been measured. This negative value means that the heat flow is from the first stage of the G-M cryocooler to the warm end of the pulse tube. The heating load was then applied to the cold end of the pulse tube. At 8 K with 500 mW of the heating load this heat flow is near zero. Below 8 K the heat flow is always negative. The results shown in Figure 8 also indicate the enthalpy flow through the pulse tube is not dissipated yet at that warm end of the pulse tube, because the heat flow through the thermal bath is always below the cooling power at the cold end of the pulse tube. We decided to remove this thermal bath and tested again as type D.

Experiment on Type D of The Pulse Tube

The cooling performance and optimum operating condition of type D are shown in Figure 9 and Table 3 of the case D. The minimum temperature was 3.5 K when the hot end of final stage regenerator was precooled at 15K. The cooling capacity of type D at 5 K was 88.5 mW. During experiment with the type D, the hot end of last regenerator in the pulse tube refrigerator was warmed up to 20K by heating on the cold end of second stage of the G-M cryocooler, the minimum temperature is 4K at this condition. Of the four types of the pulse tubes the type D gave the best performance.

MULTIPLE STAGING METHOD FOR THE PULSE TUBE

In the pulse tube refrigerator it is easy to make the multiple stage like type A to type D as shown in Figure 6. However the reasonable multi-staging method and phase shifter should be developed to minimize both regenerator loss and pulse tube loss.

One of the problem in the case of the type A is that the generated heat at the hot end of the lower stage pulse tube must be removed by the upper stage cooling power. Therefore it requires the excessive cooling power of the upper stage to maintain the precooled temperature required for the lower stage regenerator.

In the case of the type B the heat at the hot end of the lower stage pulse tube is removed at room temperature without using upper stage cooling power. During experiment on the type B the second inlet tube could not be opened largely to get much more cooling capacity per unit mass flow through the regenerator and to reach the temperature below 8K. It indicated that in the type B the pulse tube loss due to heat transfer between the gas and the inner surface of the pulse tube wall would be very larger because the gas compression in the pulse tube could build much greater temperature gradient from the cold end to some point of the pulse tube where the temperature is much higher than room temperature.

To reduce the peak temperature along the pulse tube in the type B, one of reasonable methods is to install a sort of regenerator between the warm end of the pulse tube and the second inlet tube at room temperature. This configuration is realized by type C and type D.

So far the experiment have not done on the four-valve pulse tube precooled by the G-M cryocooler, however the comparison experiment on the single stage pulse tube refrigerator discussed before indicated that the performance of the four-valve type is better than that of the second inlet type. It could give better result to apply the four-valve type to a multiple stage pulse tube refrigerator.

In such a viewpoint the multi-staging of type D with four-valve phase shifter seems to be one of the most attractive methods in a multiple stage pulse tube refrigerator if this phase shifter could be compacted.

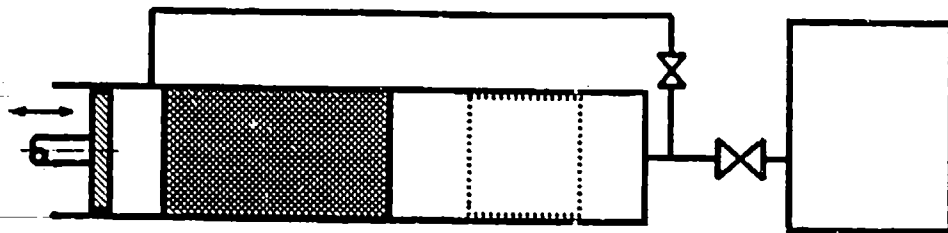
CONCLUSIONS

There remains a lot of works to optimize the multi-stage pulse tube configuration to reach 4 K, however, we found that the single pulse tube without any precooling can be operated at the liquid Helium temperature. It seems to be important to install the regenerative materials in the warm part of the pulse tube to reduce the heat flow through the pulse tube from the hot end to the cold end. Detailed numerical investigation on this effect was included in our further studies. Present study indicates there is a possibility to reach 4 K with three-stage pulse tube refrigerator and for each stage to be operated at same mean pressure and same frequency only using one compressor with single regenerator set. However in multi-stage pulse tube it requires different phase shifters for each stage to get the optimum phase between the pressure and the mass flow rate. The present experimental results also indicates that the use of the higher phase shift effect four-valve system for each stage could be allowed in the multi-stage pulse tube because each phase shifter could be located at room temperature. This construction does not required any reservoir and makes it easy to compact refrigerator system.

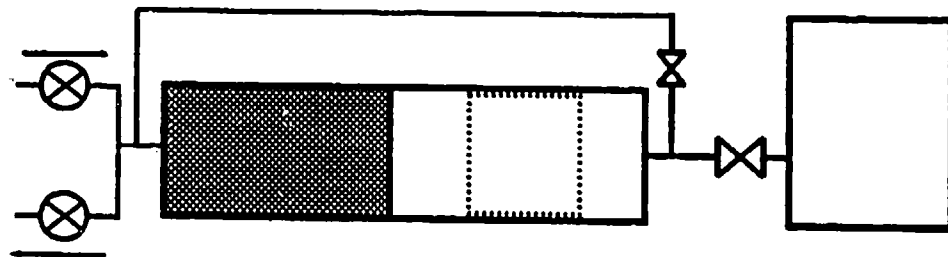
The authors thank TOSHIBA Research and Development Center for providing the Er_3Ni of the regenerator material.

REFERENCES

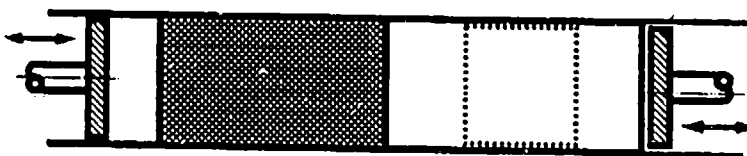
- [1] Mikulin, E.L., Tarasov, A.A., and Shkrebyonock, M.P., Low Temperature Expansion Pulse Tube, Adv. Cryog. Eng. 29, 629 (1984).
- [2] Radebaugh, R., Zimmerman, J., Smith, D.R., and Louie, B., A Comparison of Three Types of Pulse Tube Refrigerator: New Methods for Reaching 60 K, Adv. Cryog. Eng. 31, 779 (1986).
- [3] Gao, J.L. and Matsubara, Y., Equivalent P-V Diagram at The Cold End of The Pulse Tube in A Pulse Tube Refrigerator, Proc. 47th Meeting On Cryogenics And Superconductivity in Japan (in Japanese), 284 (1992)
- [4] Zhu Shaowei, Wu Peiyi and Chen Zhongqi, Double Inlet Pulse Tube Refrigerator: An Important Improvement, Cryogenics 30, 514 (1990)
- [5] Matsubara, Y. and Miyake, A., Alternative Methods of The Orifice Pulse Tube Refrigerator, Proc. Fifth Intl. Cryocooler Conf., 127 (1988)
- [6] Storch, P.J. and Radebaugh, R., Development and Experimental Test of An Analytical Model of The Orifice Pulse Tube Refrigerator, Adv. Cryog. Eng. 33, 851 (1988)
- [7] Kuriyama, T., Hatakeyama, H., Otani, Y., Nakagome, H., Matsubara, Y., Okuda, H., and Murakami, H., Development of Pulse Tube Refrigerator with Linear-Motor Drive Compressor, Proc. Seventh Intl Cryocooler Conf., to be published.
- [8] Zhou, Y., Zhu, W. and Liang, L., Two Stage Pulse Tube Refrigerator, Proc. Fifth Intl Cryocooler Conf., 137 (1988)
- [9] Tward, E., Chan, C.K. and Burt, W.W., Pulse Tube Refrigerator Performance, Adv. Cryog. Eng. 35, 851 (1990)
- [10] Kuriyama, T., Hakamada, R., Nakagome, H., Tokai, Y., Sahashi, M., Li, R., Yoshida, O., Matsumoto, K. and Hashimoto, T., High Efficient Two-Stage GM Refrigerator With Magnetic Material in The Liquid Helium Temperature Region, Adv. Cryog. Eng. 35, 1261 (1990)
- [11] Nakashima, H., Ishibashi, K. and Ishizaki, Y., Development of A 4-5 K Cooling Stirling Cycle Refrigerator, Proc. Fourth Intl Cryocooler Conf., 263 (1986)



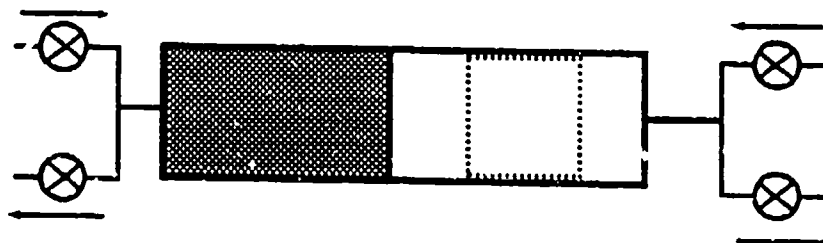
(1) Second inlet type using a valveless compressor.



(2) Second inlet type using a valved compressor.



(3) Two-piston type.



(4) Four-valve type.

Figure 1. Schematic of the modified pulse tube refrigerators.

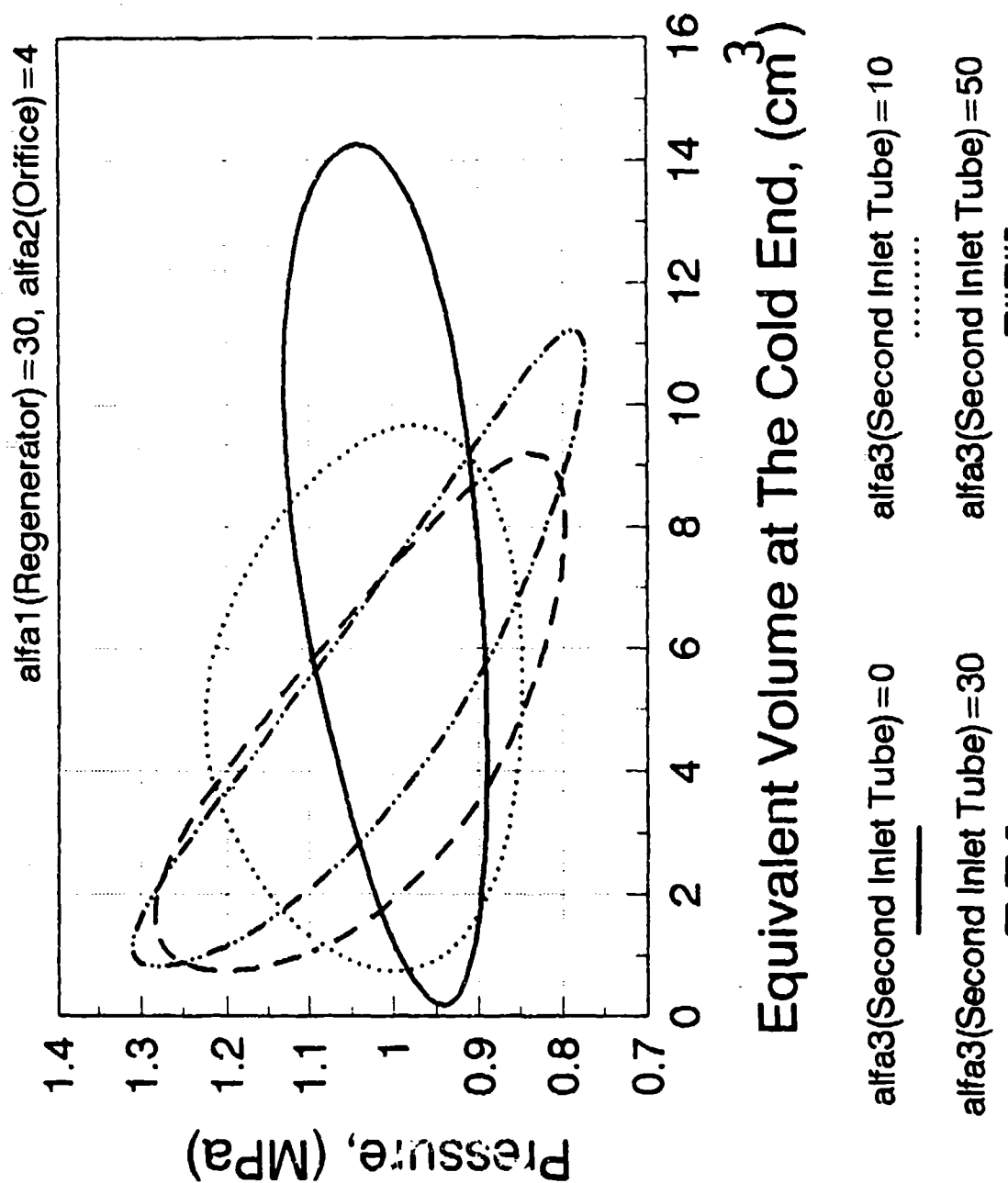


Figure 2. Equivalent P-V diagram at the cold end of the pulse tube. (for a case using a valveless compressor)

Table 1. Comparison of The Pulse Tube Refrigerator

	CASE 1	CASE 2	CASE 3	CASE 4
alf1	30	30	30	30
alf2	4	4	4	4
alf3	0	10	30	50
Pph(MPa)	1.14	1.22	1.28	1.31
Ppl(MPa)	0.90	0.85	0.81	0.77
Wc(Watt)	263.7	271.5	273.2	272.3
We(Watt)	-34.7	-37.8	-30.6	-24.5
Wi(Watt)	34.7	37.8	30.6	24.5
mp ⁽⁺⁾ (g/s)	6.12	4.30	2.70	1.96
mp ⁽⁻⁾ (g/s)	-4.44	-3.02	-1.84	-1.32
We/mp ⁽⁺⁾	-5.67	-8.78	-11.12	-12.50
C.O.P	-0.099	-0.139	-0.112	-0.090

Here Pph and Ppl are the maximum and minimum pressure in the pulse tube, Wc is the compression work of the compressor, We is the equivalent expansion work at the cold end of the pulse tube, Wi is the heat rejected at the hot end of the pulse tube, mp is the peak mass flow rate at the cold end of the pulse tube, C.O.P=We/Wc.

Input basic system parameters[7]:

Vco(compressor swept volume)=40(cm³),
 Vcd(void volume of compressor)=10(cm³),
 Vr(regenerator void volume)=40(cm³),
 Vp(pulse tube volume)=30(cm³),
 Vb(reservoir volume)=1000(cm³),
 P0(intial pressure=1.0(MPa),
 F(operating frequency)=15(Hz),
 Th(temperature at the hot end)=300(K),
 Tc(temperature at the cold end)=80(K).

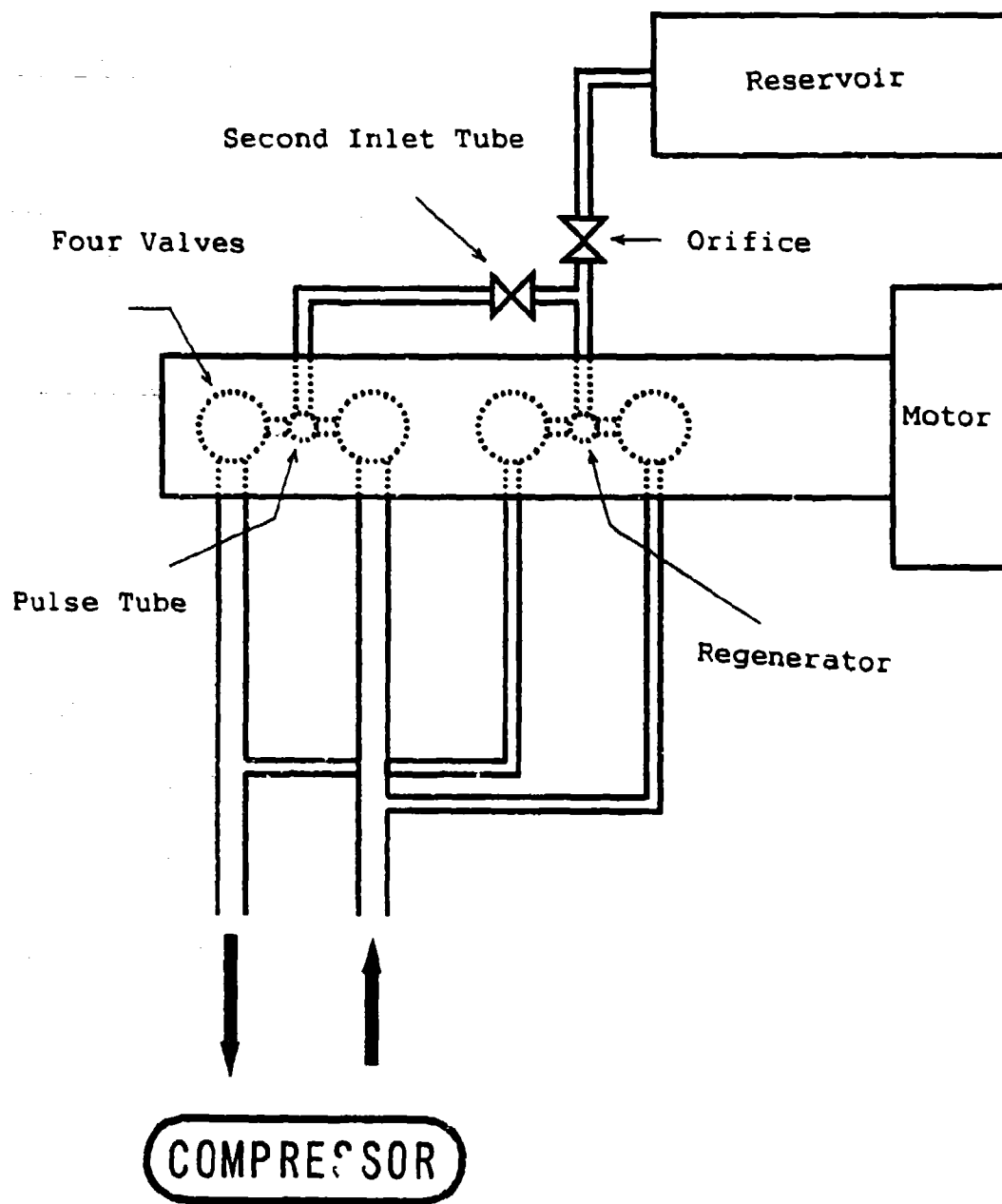


Figure 3. Schematic of test apparatus for single stage pulse tube refrigerator.

Equivalent PV Diagram

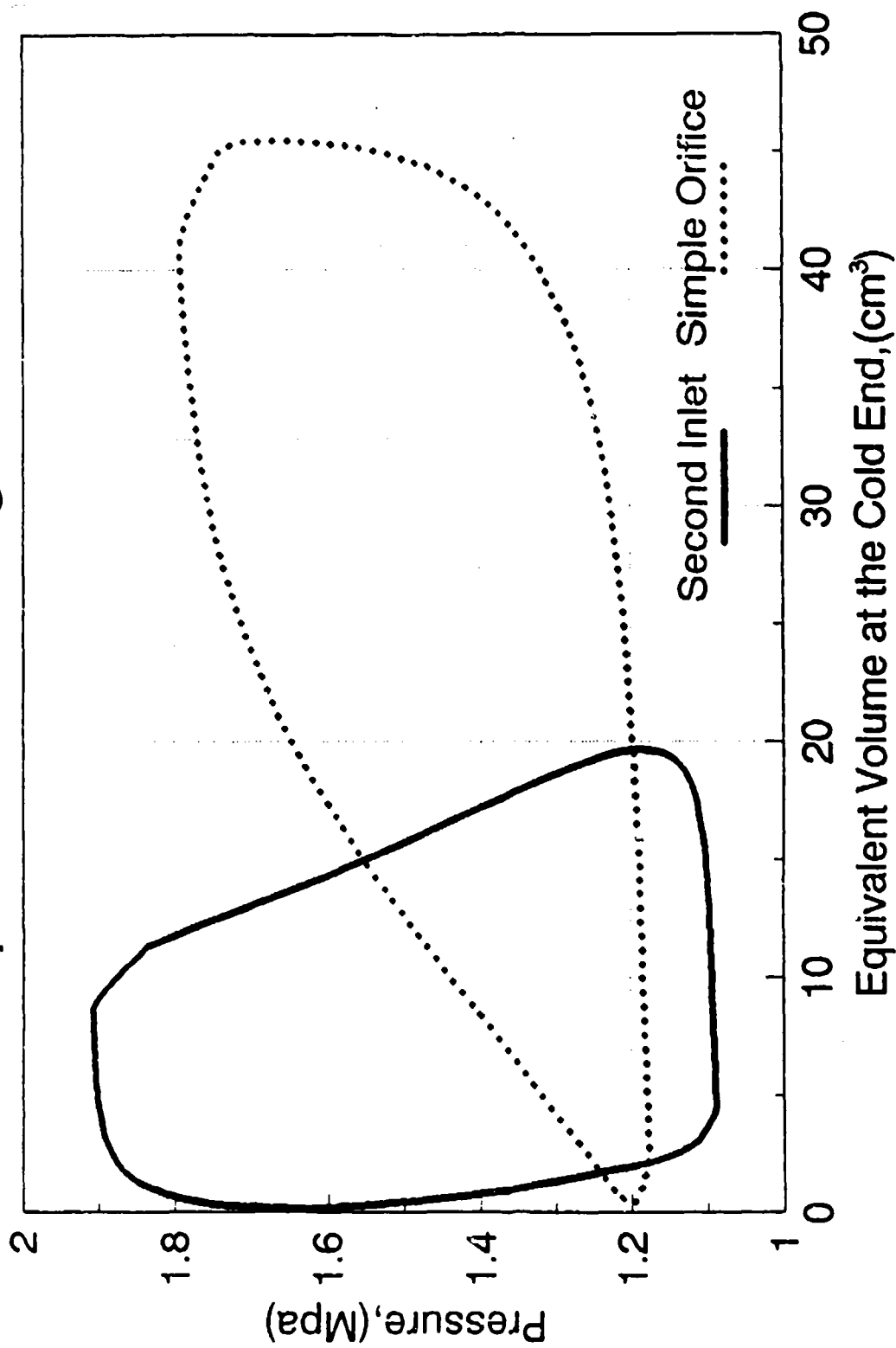


Figure 4. Equivalent P-V diagram at the cold end of the pulse tube. (for a case using a valved compressor)

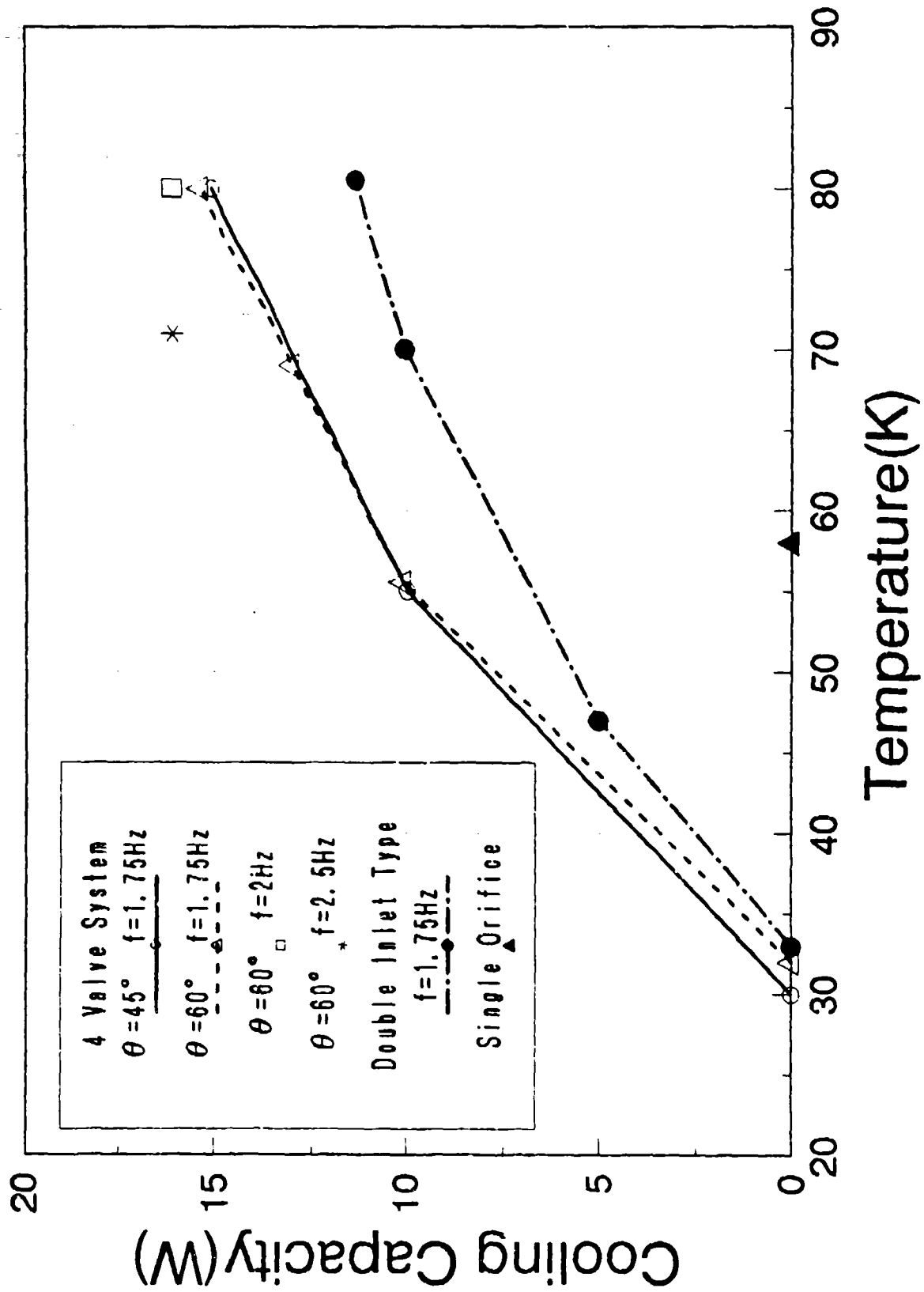


Figure 5. Cooling capacity of single stage pulse tube refrigerator.

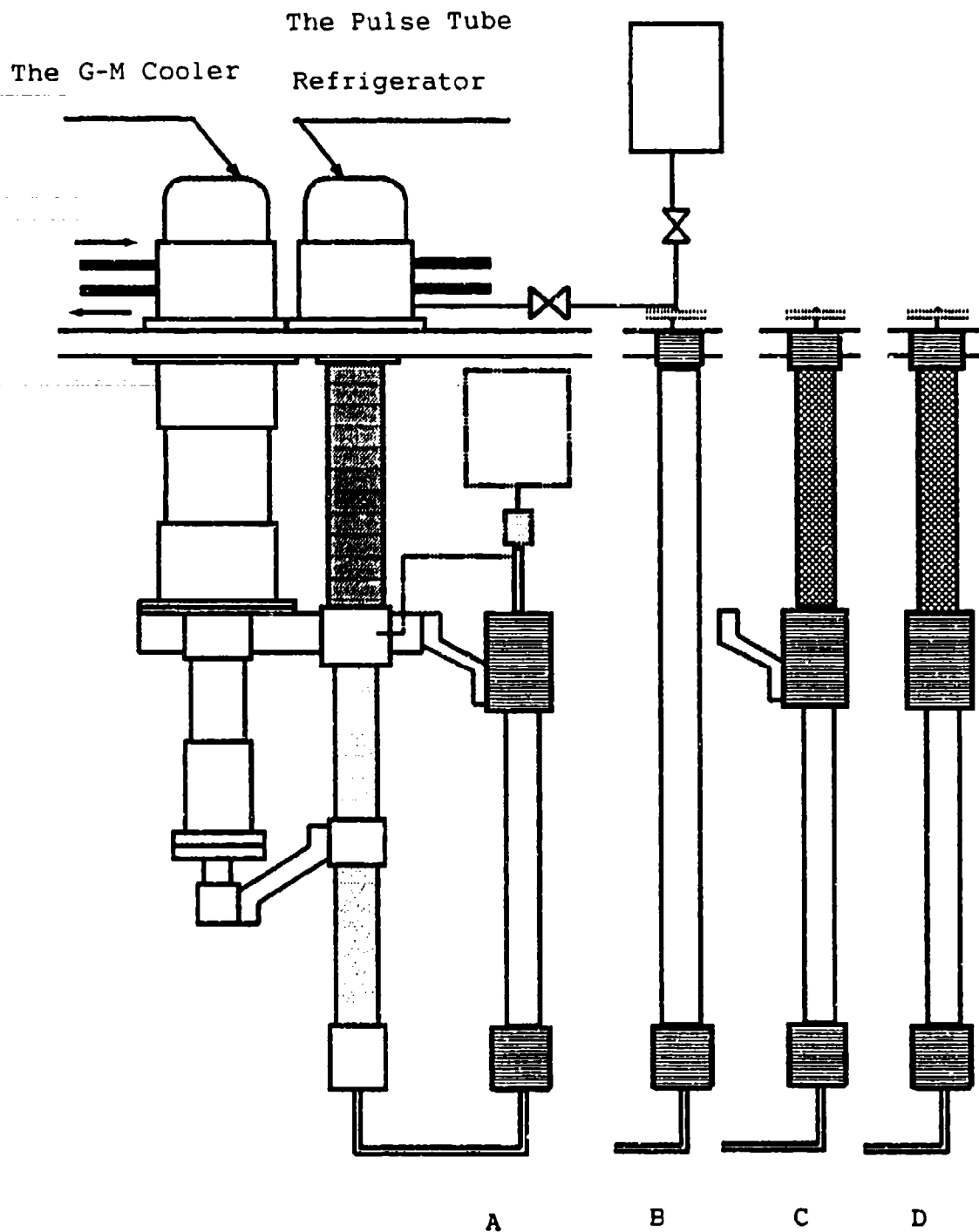


Figure 6. Schematic of test apparatus for single stage pulse tube refrigerator pre-cooled by a two-stage G-M cryocooler.

Table 2: Description of Regenerator and Pulse tube

Component	Materials	Size
1st Stage Reg.	Stainless steel tube filled with 300# bronze mesh	Φ20X0.5X85
2nd Stage Reg.	Stainless steel tube filled with Pb shot	Φ17X0.5X80
3rd Stage Reg.	Stainless steel tube filled with Er3Ni shot	Φ17X0.5X75
Pulse Tube A	Stainless steel tube	Φ9X0.5X100
Pulse Tube C & D	Pulse Tube A + Stainless steel tube filled with stainless steel shot	Φ9X0.5X100 and Φ8X0.5X210
Pulse Tube B	Stainless steel tube	Φ8X0.5X320

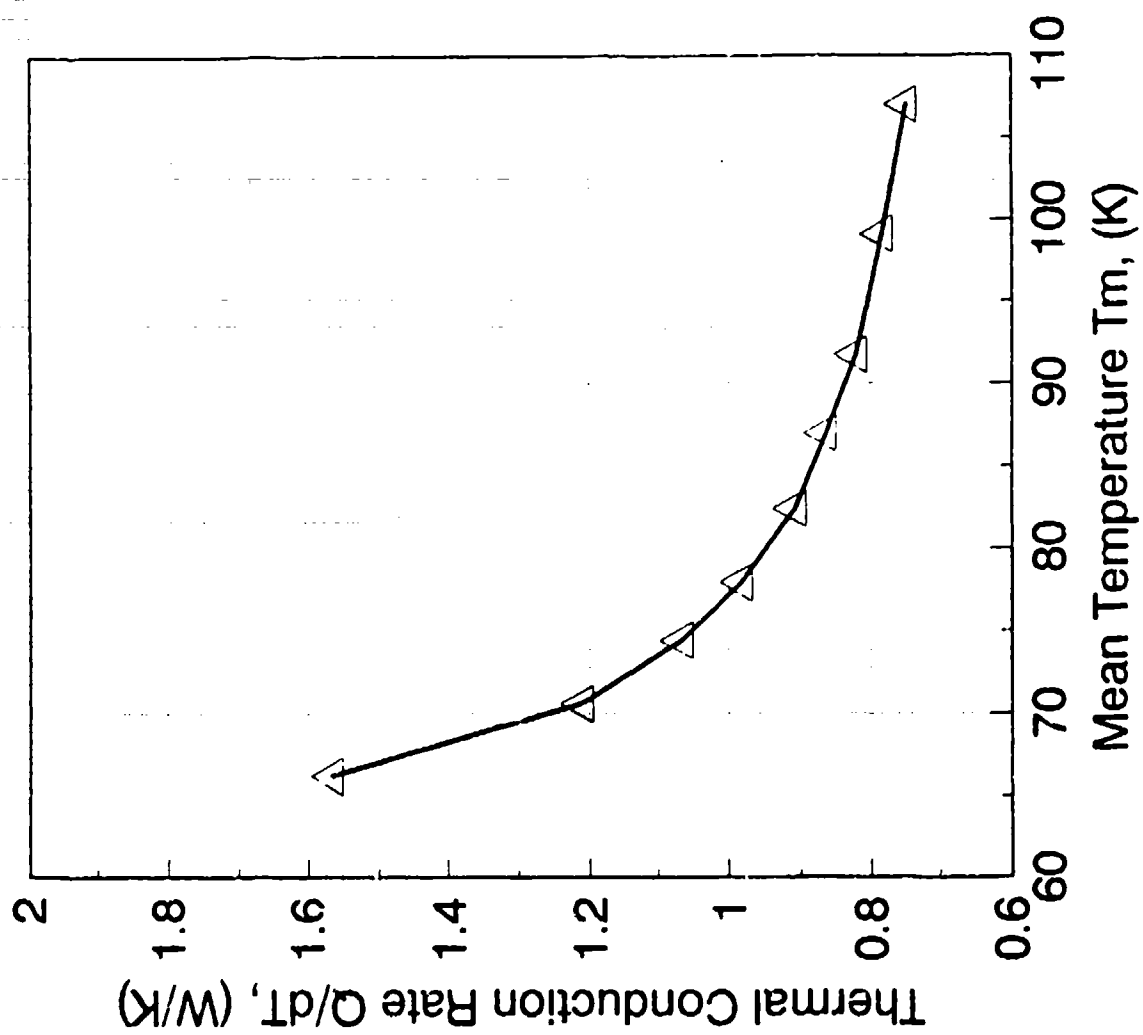


Figure 7. Thermal conductivity calibration for the thermal bath.

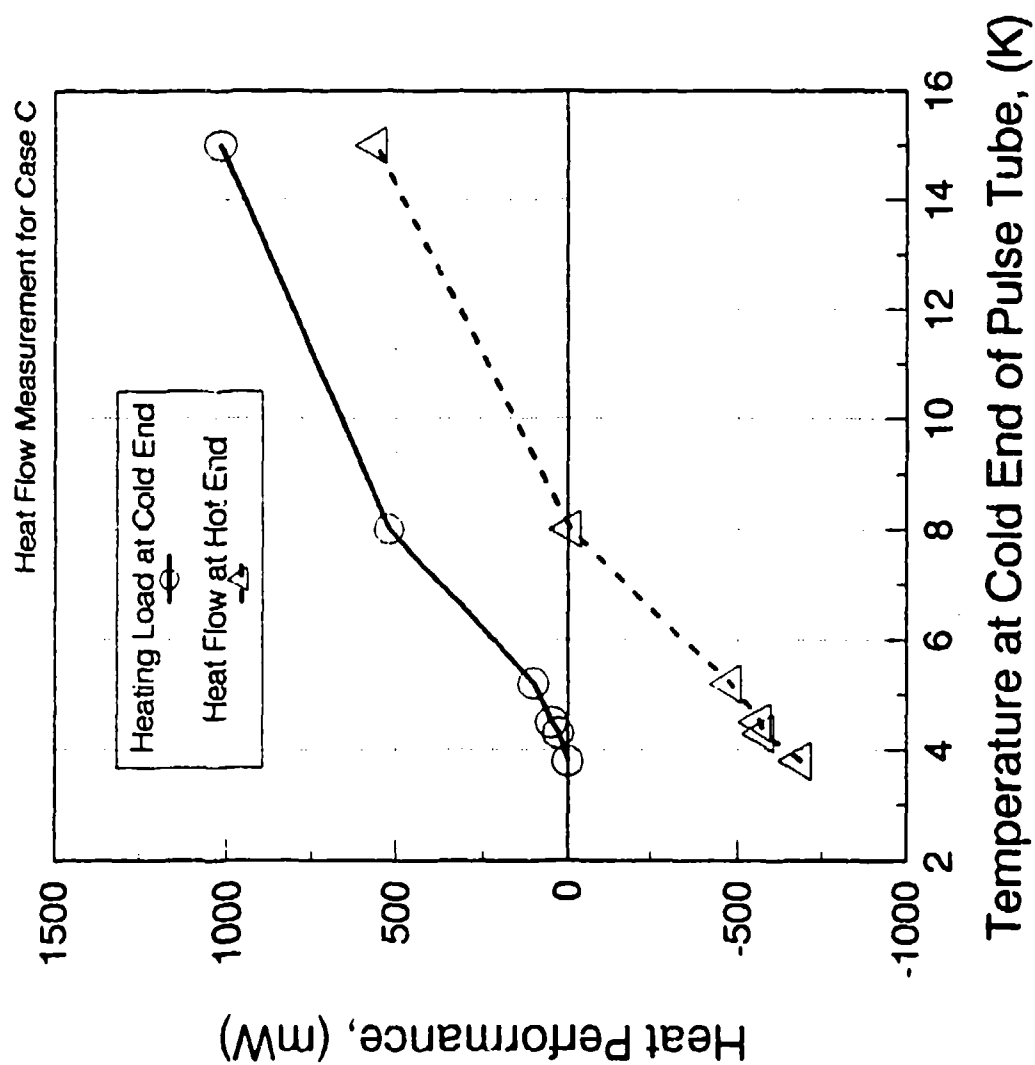


Figure 8. Variation of heat flow with temperature and heating load at the cold end of the pulse tube.

Table 3. Optimal Operating Condition

Parameters	Case A	Case B	Case C	Case D
Mean Pressure, (MPa)	0.35	0.8	1.0	1.0
Pressure Ratio	1.6	1.5	1.8	1.8
Frequency, (Hz)	2.1	3.5	1.5	1.5
Tc of PT, (K)	4.5	8.1	3.6	3.5 {4.0}
Th of PT, (K) [Tw of PT, (K)]	50	300	300 [73.5]	300 [58.8] [{63}]
Th of 3reg, (K)	12.5	14	15	15 {20}
Cooling Power at 5K, (mW)	25		60	88.5

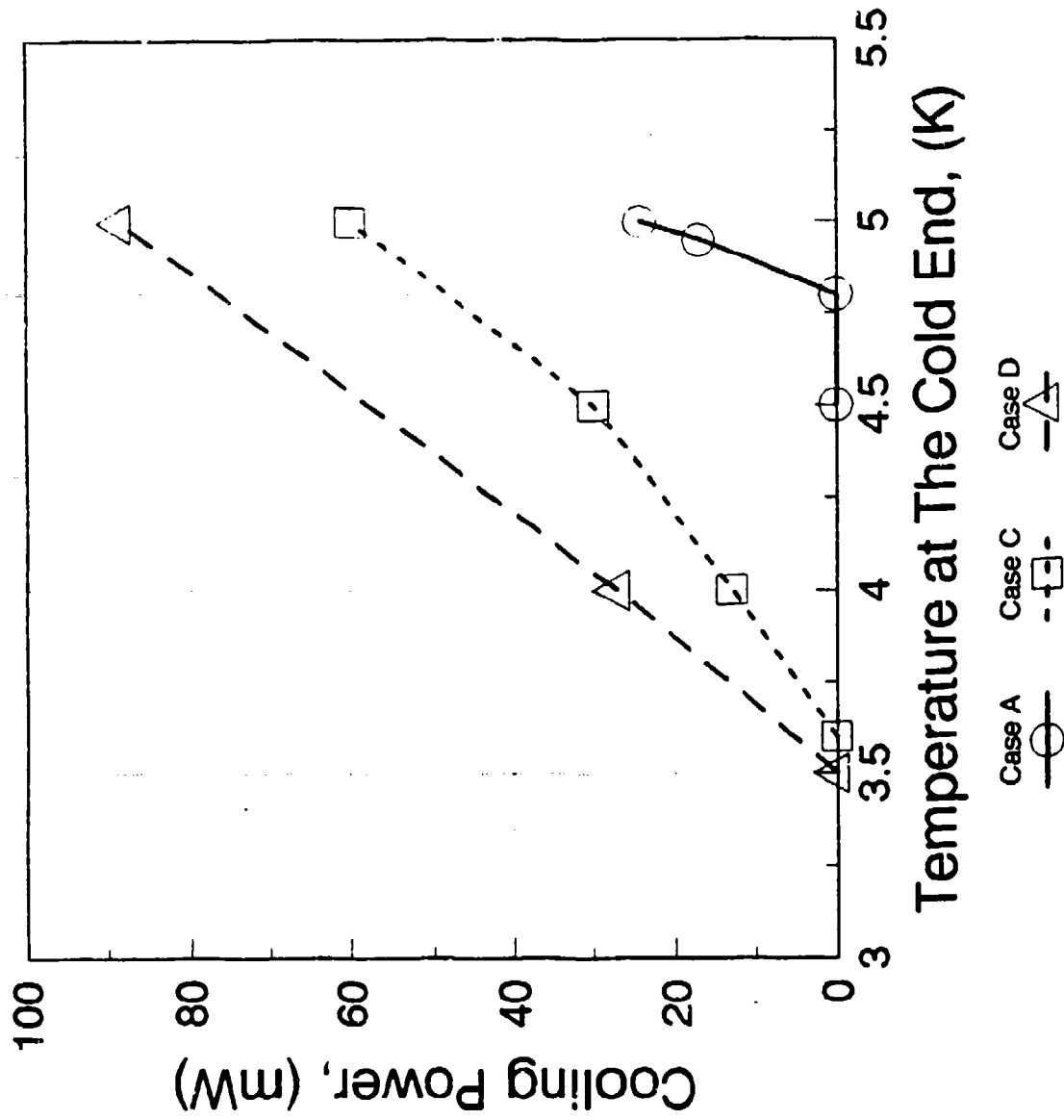


Figure 9. Cooling capacity of three types of the pulse tubes.

**A NEW CONFIGURATION FOR SMALL-CAPACITY,
LIQUID-HELIUM-TEMPERATURE CRYOCOOLERS**

J. ALAN CRUNKLETON
BOREAS, INC.
BURLINGTON, MA 01803

ABSTRACT

A recently-patented process of refrigeration is presented which is appropriate for cooling capacities up to a few watts at liquid helium temperatures. The process integrates heat exchangers and expansion engines in a configuration that is fundamentally different than Gifford-McMahon or Gifford-McMahon/Joule-Thomson cryocoolers. The technique achieves high heat-exchange effectiveness over the entire temperature range from room temperature down to liquid-helium temperatures by using counterflow heat exchange almost exclusively in the colder stage and by using a combination of both counterflow and regenerative heat exchange in the upper stages. Characterization curves are presented for a prototype producing 1.0 W at 4.5 K.

INTRODUCTION

Since the early 1980's, demand for affordable, reliable 4.5-K refrigeration has increased significantly, primarily due to the emergence of magnetic resonance imaging (MRI) for medical diagnostics. Historically, the Gifford-McMahon (GM) cycle has dominated small-scale refrigeration down to about 10 K. Extending the useful refrigeration range of this cycle to liquid-helium temperatures, however, has proved difficult and expensive. Of course, the Collins cycle has been and remains the only practical way to produce large quantities of liquid helium. Unfortunately, the number of discrete components a Collins machine requires has prevented further miniaturization of this cycle.

In 1984, a development program began at M.I.T.'s Cryogenic Engineering Laboratory to develop a small-capacity, 4.5-K refrigerator that would circumvent the shortcomings of existing thermodynamic cycles. This work was supervised by Prof. J.L. Smith, Jr. and funded by Toshiba Corporation. Rather than attempting to improve on existing GM or Gifford-McMahon/Joule-Thomson (GM/JT) designs, a different approach was taken which focused on development of a fundamentally new process of refrigeration capable of high reliability and power efficiency. Essential design criteria included:

- a simple mechanical configuration
- elimination of small clearances and/or orifices (e.g., JT valves)
- elimination of materials which can degrade over time (e.g., lead shot, rare earths).

By 1987, this project resulted in a concept for producing 4.5-K refrigeration using a high-pressure-ratio, wet-expansion engine integrated into a counterflow heat exchanger.^{1,2,3} A critical realization was that for a relatively small device, the surface area required for counterflow heat exchange is available on the walls of the expansion engine.

In 1988, Boreas, Inc. was founded to continue development and commercialize the technology. Initial funding was provided by DOE SBIR grants, followed by venture capital funding. The primary challenge was to combine the cold-stage design developed at M.I.T. with warmer-stage designs that were simple and could utilize proven, reliable technologies. The patented refrigeration method integrates a multistage expansion engine into a concentric-tube heat exchanger.⁴ In a simple mechanical configuration, the cycle employs counterflow heat exchange below about 20 K and both counterflow and regenerative heat exchange in the warmer stages.

The first three-stage prototype incorporating this new refrigeration process was tested in 1990 and produced approximately 0.25 watt at 4.5 K. Since then, the primary focus has been on improving manufacturability and reliability of the complete cryocooler system. More recent prototypes provide 1 W at 4.5 K.

PROCESS OF REFRIGERATION

A representative pressure-volume plot is shown in Figure 1. With the piston at the minimum-volume position, the intake valve opens at point 1 to pressurize the piston-to-cylinder gap and any other dead volume. Once the dead volume is charged to maximum intake pressure, the piston begins to move, thereby increasing the cold expansion volumes. Gas which fills the dead volumes and the cold expansion volumes in the two warm stages is cooled both regeneratively and by low-pressure gas flowing in the return passage. The concentric tubes which form the piston and cylinder are the regenerator. Gas which flows to the third stage is cooled primarily by exchanging heat with low-pressure gas flowing in the return passage. This, of course, is due to the low heat capacity of stainless steel relative to the cold, dense helium. At point 3, the intake valve closes and expansion begins. This essentially adiabatic process significantly lowers gas temperatures throughout the cylinder. Two-phase helium is produced in the third stage. At maximum volume, point 4, the exhaust valves open and some blowdown occurs. Both warm and cold exhaust valves open during process 4-6 but not necessarily at the same time. Cold gas exiting at the warm end cools the cylinder/piston structure in preparation for the next cycle. When the cold valve opens, a two-phase mixture is discharged into the cold surge volume. A load heat exchanger present in this surge volume transfers heat from an external load to the two-phase mixture, thereby vaporizing the liquid fraction. Both exhaust valves are closed at position 6 resulting in some thermal recompression. The cycle can be operated with various amounts of constant-pressure intake and constant-pressure exhaust, depending on the performance characteristics desired for a particular application.

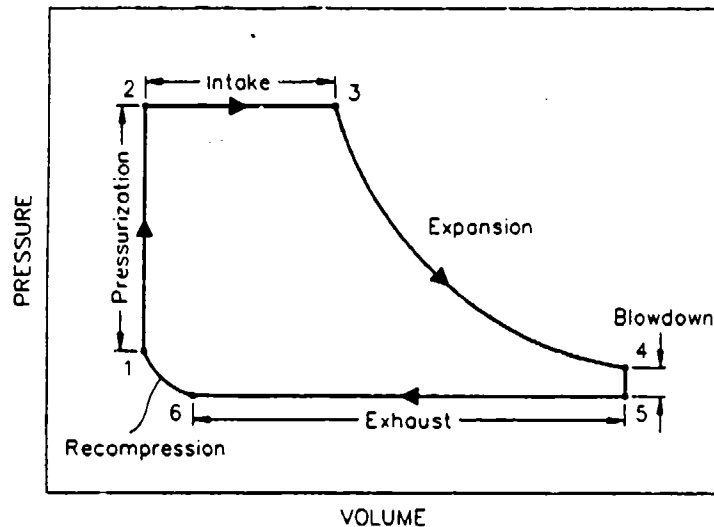


Fig. 1 - Representative Pressure-Volume Diagram

THERMODYNAMIC CONSIDERATIONS

This new high-pressure-ratio process has a fundamental advantage over the Gifford-McMahon cycle at temperatures below 8 K. The Boreas cycle is able to take advantage of the non-ideality of helium properties, specifically enthalpy, that occurs at low pressures and temperatures. A rough comparison between the cycles can be made by considering the case of isothermal expansion and a perfect precooling heat exchanger. A simple first and second law analysis for a control volume enclosing the cold stage reveals a strong dependence of available cooling power on pressure ratio and pressure level. Figure 2 is a comparison between the new Boreas process and a typical Gifford-McMahon process. In this comparison, the Boreas refrigerator is assumed to operate with 20 atm intake and 1 atm exhaust pressures, and the Gifford-McMahon refrigerator is assumed to operate at 20 atm intake and 6 atm exhaust. The y-axis is the ratio of the maximum refrigeration capacity to the indicated work from the pressure-volume diagram. The x-axis is the temperature at which the refrigeration load is applied. The plot of Figure 2 shows the clear advantage of using a high pressure ratio for refrigeration below 8 K. At 4.5 K, more than seven times the cooling capacity is available from the Boreas process in comparison with the Gifford-McMahon for identical work extraction from the cold stage.

A high pressure ratio is more easily implemented in the Boreas process because gas expanded in the cold stage, which is a significant portion of the total mass flow, returns to room temperature through a separate flow passage. Thus, the pressure ratio can be chosen for greater work extraction rather than minimal pressure drop. In a totally regenerative cycle, all mass flow enters and exits through the same flow passage. Thus, the pressure ratio is effectively limited by the cross sectional area for flow in the regenerator. This area must be large enough so that the low-pressure-flow pressure drop through the regenerator is not excessive.

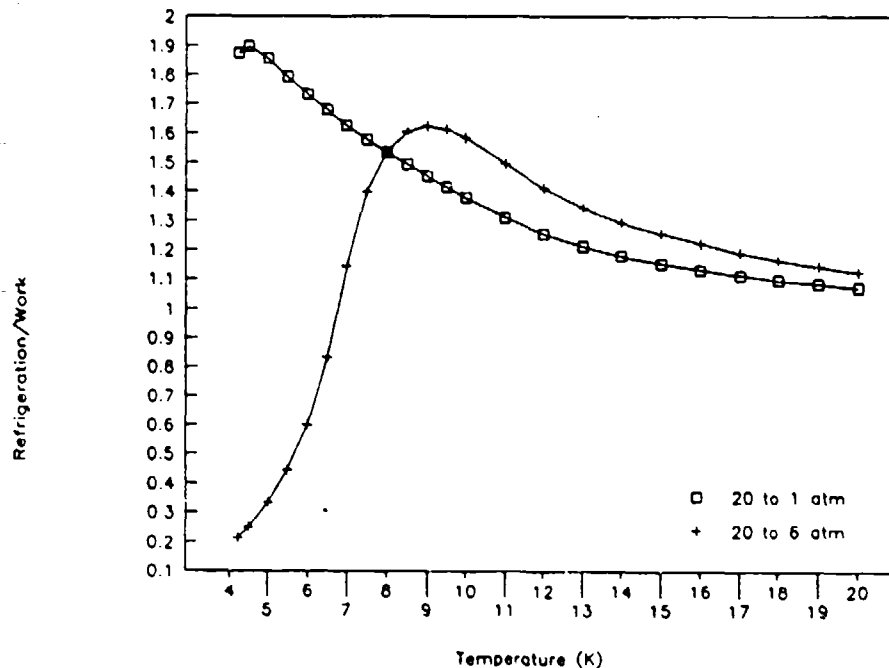


Fig. 2 - Effect of Exhaust Pressure on Ideal Performance

HARDWARE DESCRIPTION

A representative three-stage configuration is shown in Figure 3. A single reciprocating piston and cylinder comprise three expansion stages. Typical operating temperatures are 80, 20, and 4.5 K for the first, second, and third stages, respectively. Figure 4 outlines dimensions of the prototype coldhead. A separate compressor supplies gas at 20 atm and accepts return gas at approximately 1 atm. Two flexible hoses and several electrical cables connect the compressor and coldhead. A photograph of the complete system is shown in Figure 5.

Annular gap heat exchangers provide precooling for each stage. The piston-to-cylinder gap serves as the high-pressure heat exchange passage. Bushings center the piston within the cylinder. A low-pressure return passage is formed by an annular gap between the OD of the cylinder tube and the ID of an outer shell tube which is concentric with the cylinder. A spiral spacer separates the cylinder and shell tubes.

Helium enters the coldhead through an intake valve operating at room temperature. Two valves exhaust helium from the working volumes. The warm exhaust valve operates at room temperature exhausting gas from the first and second stages. The cold exhaust valve provides a flow passage to the low-pressure counterflow passage. A surge volume separates the cold valve from the low-pressure return passage. This volume is sized to provide substantially constant flow in the low-pressure return passage.

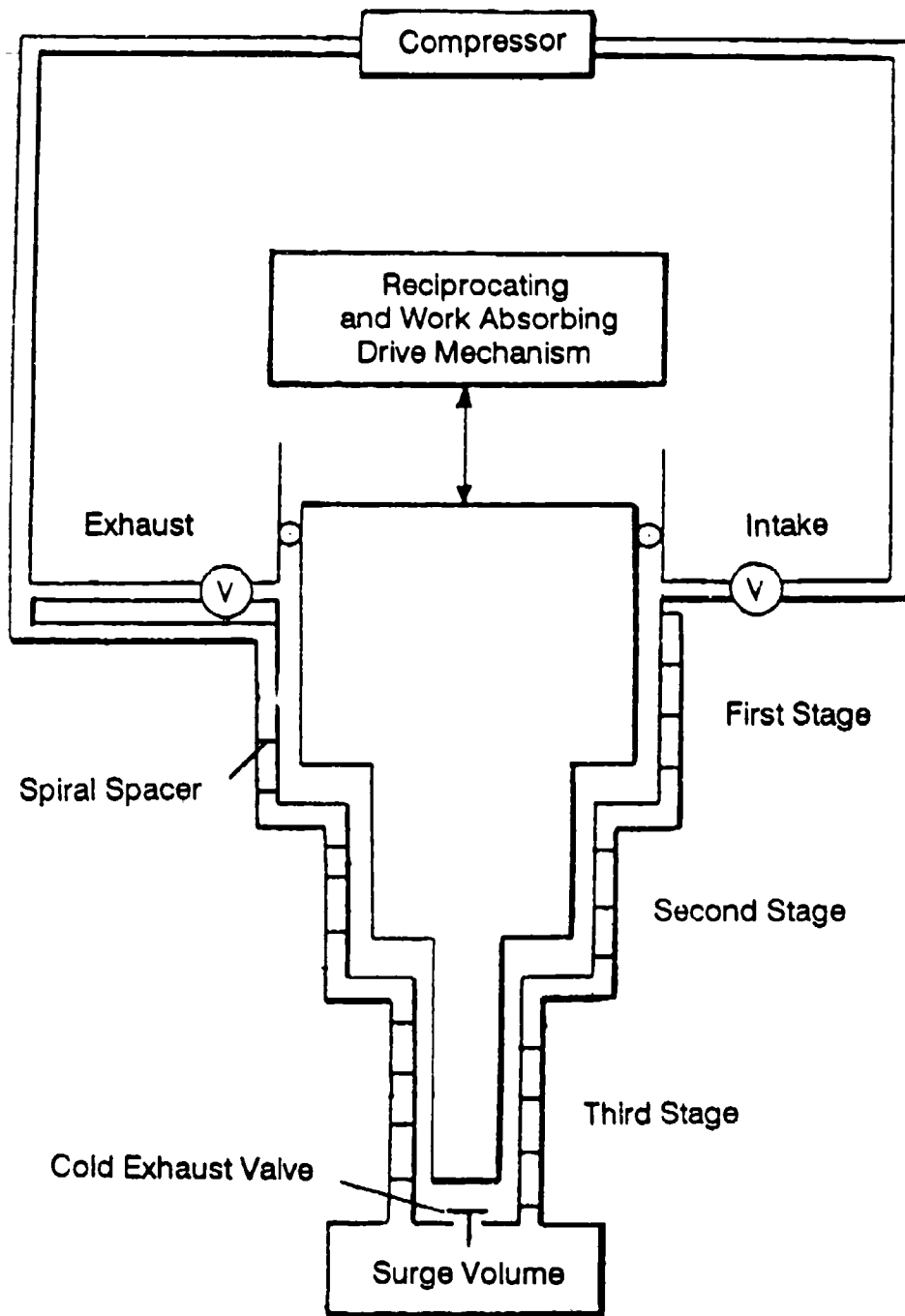
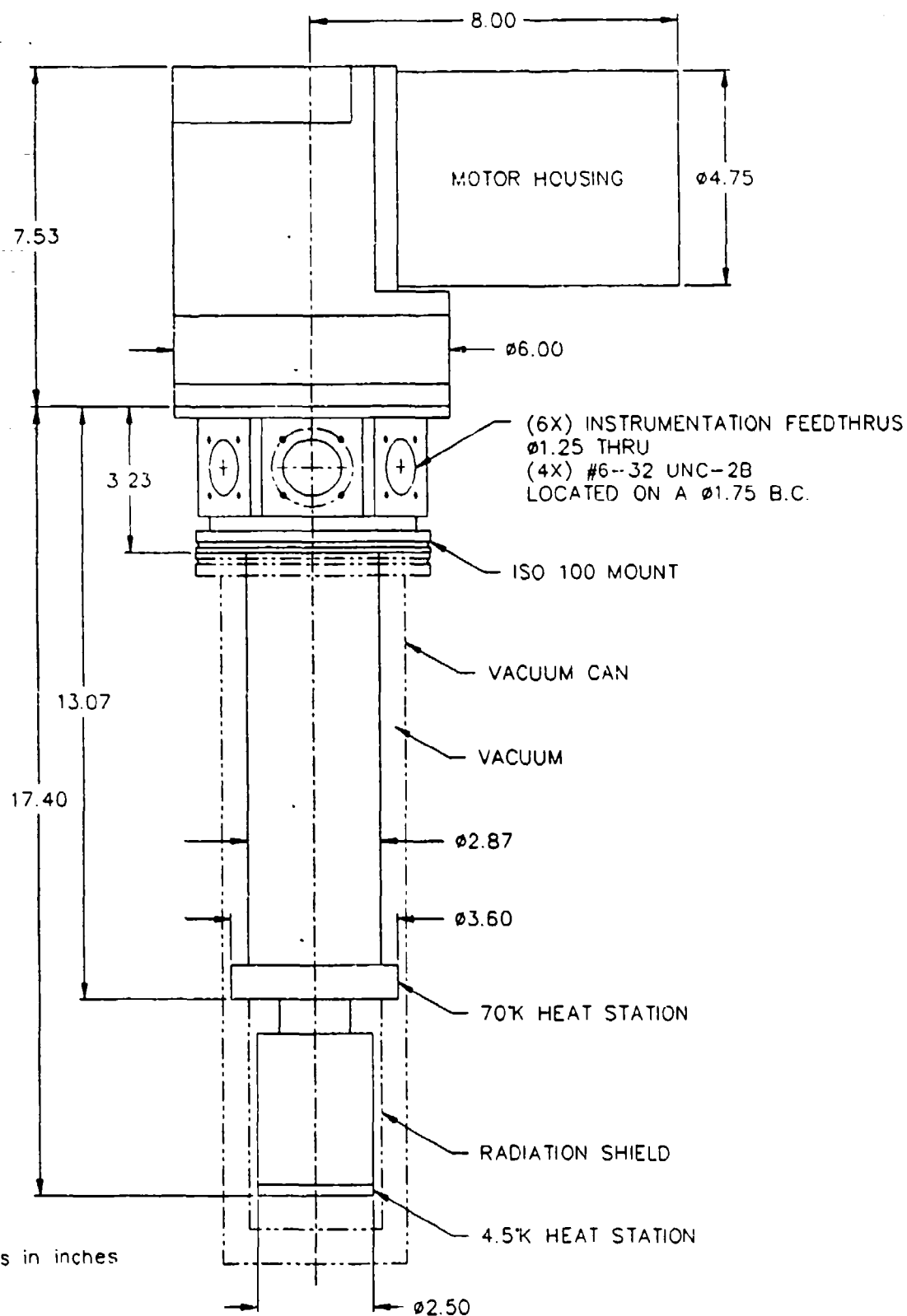


Fig. 3 - Boreas Cycle Schematic



Note: All dimensions in inches

Fig. 4 - Coldhead Dimensions

The piston, cylinder and outer shell are all made of stainless steel tubing. A vacuum inside the piston minimizes axial heat leaks. This piston configuration allows the three stages to be convoluted. In other words, because only the surfaces of the cylinder and piston are required for heat exchange, the second stage can be folded into the first stage and the third stage can be folded into the second stage, creating a compact three-stage configuration.

In the configuration of Figure 3, a reciprocating and work absorbing drive mechanism is shown which requires a high-pressure seal. A pressure-balanced displacer with either a Scotch yoke or pneumatic drive mechanism is also applicable.

The cold valve used in the prototypes is a custom electromagnetic valve carefully optimized for operation at low speeds and cryogenic temperatures.

EXPERIMENTAL RESULTS

Refrigeration capacity was measured for both the first and third stages. Electrical resistance heaters and diodes were mounted on the first and third stages. For the third stage, the temperature was used as feedback for a proportional heater controller. The heater power necessary to maintain a given temperature in the cold surge volume was integrated to give an average refrigeration capacity. The total steady-state power draw for the system during these tests was approximately 2.6 kW.

In one test, heat was applied only to the third stage. A characterization curve for the prototype being used as a single-point refrigerator is shown in Figure 6. Although not designed to provide excess refrigeration at warmer temperatures, the coldhead was also tested as a dual-point refrigerator where cooling was supplied at 4.5 K on the third stage and at a warmer temperature on the first stage. Figure 7 is a plot of the third-stage load sustained at 4.5 K when heat is applied to the first stage. Figure 8 shows the variation in first-stage temperature under varying heat loads.

FUTURE WORK

The demonstrable refrigeration capacity of these prototypes is expected to increase as further improvements are implemented. Efforts are now underway to develop a true multiple-point cryocooler capable of providing refrigeration at liquid-helium temperatures plus significant refrigeration at a warmer temperature. This cryocooler will basically consist of a scaled version of the cryocooler presented above, utilizing core technologies developed over the past several years at Boreas and requiring no breakthroughs.

The Boreas cryocooler appears to have the capability of eventually being able to meet market requirements for an inexpensive, reliable, small-scale, 4.5-K refrigerator. Potential applications include MRI and other existing and emerging superconducting magnet and electronic applications such as research magnets, small SMES, JJ circuitry, and MAGLEV.

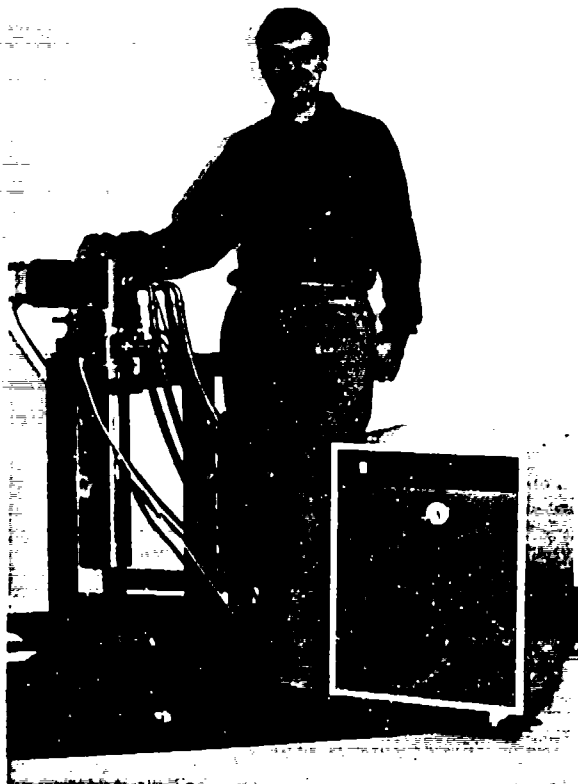


Fig. 5 - 1 Watt Prototype

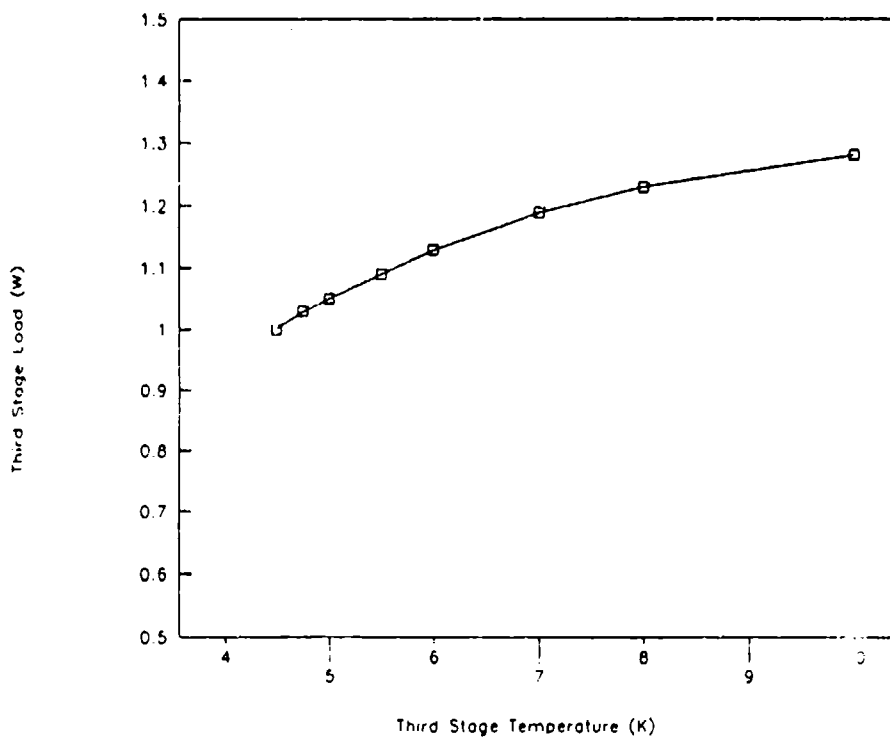


Fig. 6 - Third Stage Load Characterization

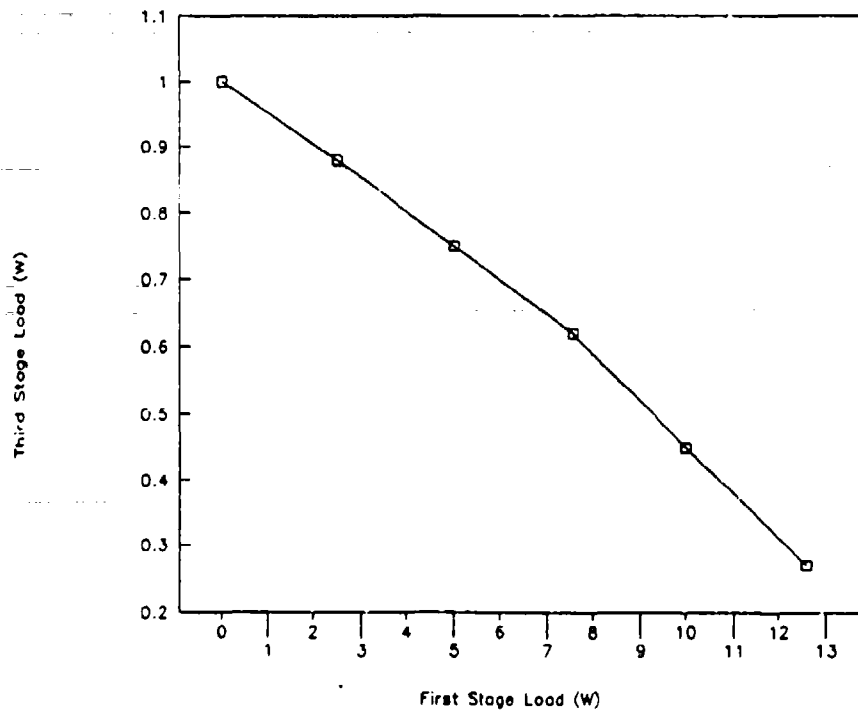


Fig. 7 - Third Stage Capacity @ 4.5 K versus First Stage Load

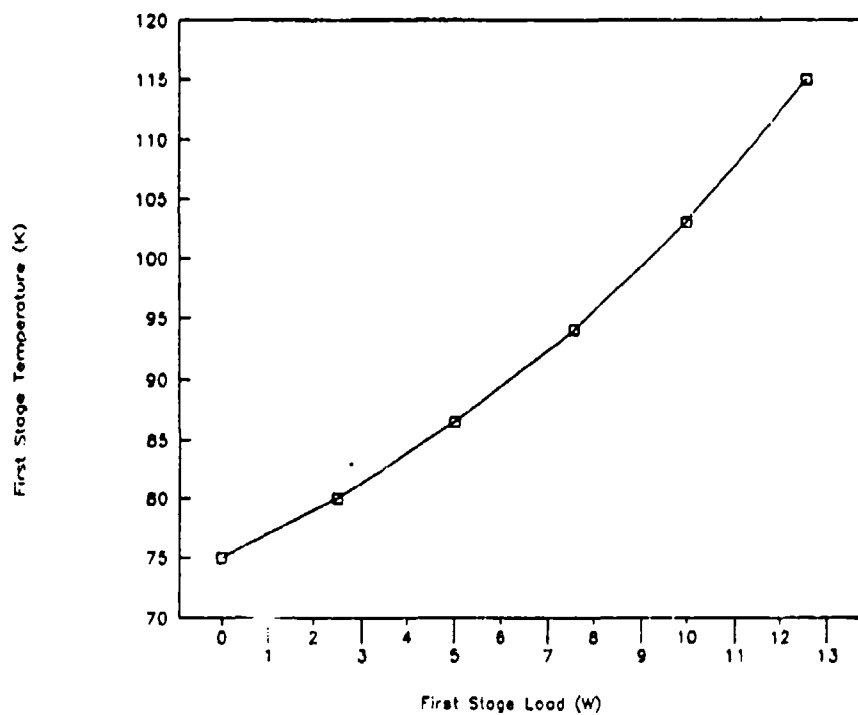


Fig. 8 - First Stage Load Characterization

REFERENCES

1. J.A. Crunkleton, "A New Configuration for a Liquid Helium Temperature Cryocooler", M.I.T., Ph.D. thesis, 1987.
2. J.A. Crunkleton, J.L. Smith, Jr., Y. Iwasa, "High Pressure Ratio Cryocooler with Integral Expander and Heat Exchanger", Advances in Cryogenic Engineering, Vol. 33, pp. 809-818, 1988.
3. J.A. Crunkleton, J.L. Smith, Jr., U.S. Patent 4,862,694, "Cryogenic Refrigeration Apparatus", issued September 3, 1989.
4. J.A. Crunkleton, U.S. Patent 5,099,650, "Cryogenic Refrigeration Apparatus", issued March 31, 1992.

ANALYSIS OF A MINIATURE TWO-STAGE CRYOCOOLER

Eric B. Ratts and Dr. Joseph L. Smith, Jr.
Cryogenic Engineering Laboratory
Massachusetts Institute of Technology
Cambridge, MA 02139

Dr. Yukikazu Iwasa
Francis Bitter National Magnet Laboratory
Massachusetts Institute of Technology
Cambridge, MA 02139

ABSTRACT

Optimizing and integrating the two stages of a 1W 14K two-stage helium gas cryocooler is examined. The stage configuration considered is a laminar regenerative heat exchanger and an expander constructed from three concentric tubes, designed by Crunkleton and Smith at this laboratory. The two annular gaps between the tubes make up the counterflow passages of the regenerative heat exchanger, and the inner-most tube makes up the piston.

Individual analytical models were developed for the two stages, the refrigeration stage and the precool stage. The second order numerical models included imperfect heat exchange losses, pressure drop losses, mixing losses, conduction losses, and shuttle losses. The refrigeration stage was optimized by maximizing the coefficient of performance. The precool stage was optimized by maximizing the inter-stage mass flow per unit of compressor work. Comparison and integration of the two results are made to develop the optimal two-stage configuration.

Several conclusions are made about integrating the refrigeration stage and precool stage. For a given refrigeration capacity of the refrigeration stage, there is one optimal configuration. In order to increase refrigeration capacity it is optimal to increase size rather than using multiple configurations in parallel, because parasitic losses scale inversely with size. The optimal refrigeration stage and optimal precool stage are not geometrically compatible. Therefore, for a given refrigeration capacity of the two-stage configuration there is a tradeoff between the stages' configurations.

Critical to the design is the heat exchanger performance as concluded from the numerical analysis. A heat exchanger is currently being built that physically realizes the model heat exchanger requirements.

INTRODUCTION

Cryocoolers in the 1W, 4K range are generally systems of modified existing equipment which provide high reliability. To have a closed cycle miniature refrigerator with high efficiency, basic development work in understanding the basic loss mechanisms is necessary [1]. A previous optimization study developed a one stage design with a compact annular regenerative/counterflow heat exchanger [2]. The advantages, compactness and manufacture ease, of this design warrants continued effort to design an efficient two-stage configuration.

Efforts at this laboratory are to understand the losses associated with the design of a two stage cryocooler using the heat exchanger design. The two stage cryocooler consists of two stages, refrigeration and precool. Each stage will utilize the annular counterflow heat exchanger concept.

This paper discusses the model development used to investigate the two-stage design and presents conclusions for a final two-stage design.

MODEL DEVELOPMENT

The final two-stage design is shown in Figure 1. In order to understand the development, the cycle process is explained. The cycle begins with the piston at top dead center and all valves closed. The first process is the intake process. The warm intake valve opens and the piston moves upward. The high pressure gas flows in the gap between the piston and inner cylinder where the gas is cooled by the existing wall temperature gradient. The gas exits the gap and fills the two working volumes. The second process is the expansion process. At some point during the stroke the intake valve closes and the gas within the working volumes are expanded. The gas in the gap volume is also expanded and a portion of the gas flows into the working volumes. In order to simplify the analysis, we assumed that the gas is completely expanded to the exhaust pressure of the surge volumes, although it is not optimal to extract the last amount of work from the gas at the expense of parasitic losses. The third process of the cycle is the exhaust process. At bottom dead center the cold exhaust valves are opened. The piston moves downward forcing the cold gas from the working volumes into the surge volumes. The cold gas within the surge volumes provides the refrigeration. The gas flows through the gap between the inner cylinder and the outer cylinder where the gas is heated by the existing wall temperature gradient. The final cycle process is the recompression process. At some point of the stroke the cold exhaust valves are closed and the gas within the working volumes and the gap volumes are recompressed to the inlet valve pressure.

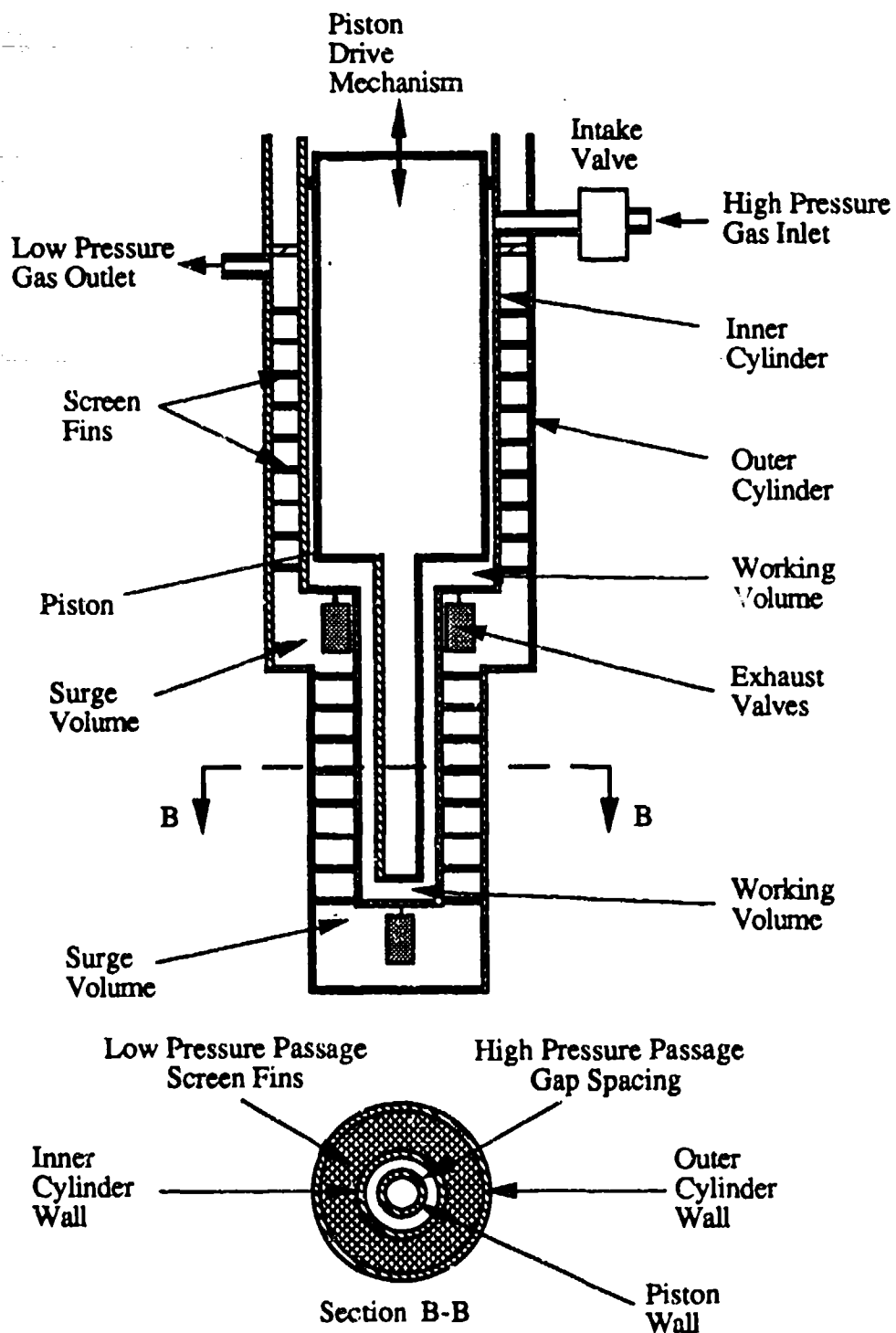


Figure 1 : Schematic of the Two-Stage Configuration. (Not to Scale.)

The gas from the working volumes is forced back into the gap to recompress this space. Again it is not optimal to fully recompress the gas. There is a tradeoff between blowin losses and parasitic losses.

The simplified thermodynamic model schematic for the concentric tube heat exchanger and expander unit is shown in Fig. 2. The system consists of a heat exchanger with a High Pressure Passage (HPP) and Low Pressure Passage (LPP), and an expansion volume. The heat exchanger is subdivided into major and minor entities. The single model represents the refrigeration stage or the precool stage. When the model is used for the refrigeration stage all of the mass that flows through the HPP is expanded in the expansion volume, i.e. $d\tilde{m}_{H,ref}$ and $d\tilde{m}_{L,ref}$ are zero.

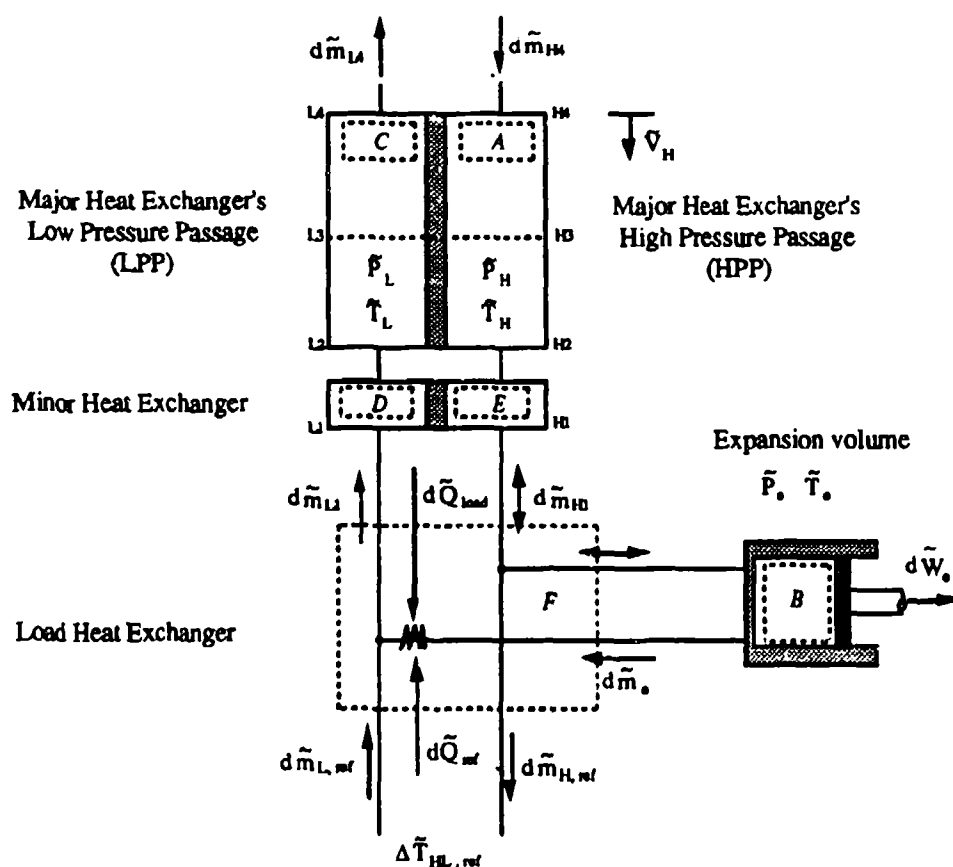


Figure 2: Schematic of Single-Stage Model

The model differential equations were derived from the schematic control volumes. Making several assumptions, the differential equations were integrated analytically with respect to the HPP volume to obtain a set of ordinary differential equations in time. These equations were then

rearranged for each part of the cycle so that the boundary conditions could be applied. The boundary conditions were the independent mass flows, independent gas pressures, and temperatures. This approach allows us to model the valves as fully open or closed.

ASSUMPTIONS

Major assumptions to develop the governing equations are:

- 1) *Working fluid is a perfect gas.*
- 2) *Properties are assumed uniform and evaluated at volume-averaged temperatures.*
- 3) *Flow in heat exchanger is fully developed and laminar.* Steady flow Nusselt number was used and is reasonable based on the analysis provided by Jeong[3].
- 4) *Wall heat capacity is much larger than the gas heat capacity.* The fluctuations in the wall temperature are assumed negligible.
- 5) *Perfect mixing occurs in the expander.*
- 6) *Expanders are adiabatic.* Expander heat transfer losses are neglected. Kornhauser and Smith have investigated this phenomenon in considerable detail [4].

MASS, ENERGY, AND MOMENTUM EQUATIONS

The equations were nondimensionalized with respect to maximum expander volume, maximum inlet pressure, and cold-end heat exchanger wall temperature. The nondimensionalized variables are defined in the nomenclature.

The HPP continuity equation was derived from the mass balance on control volume A, a differential element of gas within the heat exchanger. The equation was analytically integrated from the warm end of the HPP to the cold end as shown below.

$$d\tilde{m}_{H4} - d\tilde{m}_{H1} = d \int_0^{\tilde{V}_{H41}} \frac{\tilde{P}_H}{\tilde{T}_H} d\tilde{V}_H \quad (1)$$

where

$$\tilde{V}_{H41} \equiv \frac{V_{H41}}{V_{e, \max}} \quad (2)$$

is the nondimensional heat exchanger dead volume parameter. This ratio is associated with the loss

due to mixing of the inflow to the expander during the expansion process. The heat exchanger is very effective such that the gas-wall temperature difference is small. Therefore the change in mass in the gap is linearly dependent on the gas pressure. The pressure is assumed equal to the expander pressure and independent of position in the heat exchanger. The gas temperature is assumed constant in time and to follow the wall temperature.

The HPP energy equation was derived from the energy balance on control volume A. We neglected the shuttle heat transfer in this equation but it is addressed later. Again we assume that the gas temperature gradient follows the wall temperature gradient to simplify the energy equation. Substituting Eq. 1 into the energy equation and solving for the local gas-wall temperature difference, the differential equation is

$$\tilde{T}_H - \tilde{T}_C = \frac{-d\tilde{m}_H \left(\frac{d\tilde{T}_C}{d\tilde{V}_H} \right) + \left(\frac{\gamma_{He} - 1}{\gamma_{He}} \right) d\tilde{P}_H}{\tilde{h}_H} \quad (3)$$

where

$$\tilde{h}_H \equiv \left(\frac{Nu k_{He}}{2 g_H^2} \right) \left(\frac{R_{He} T_{Cl}}{\omega C_{P, He} P_{max}} \right) \quad (4)$$

is the nondimensional heat transfer coefficient. A similar coefficient \tilde{h}_L is necessary to define the LPP heat transfer. Eq. 3 shows that the enthalpy flux down the heat exchanger is strongly dependent on the wall temperature gradient. In order for the cycle enthalpy flux of the heat exchanger to be the same at every position the wall gradients must be different at every position. The curvature of the wall temperature along the heat exchanger should be positive (concave up). The wall temperature profile was assumed to be a second order polynomial to provide the wall temperature profile curvature.

The time dependent expander volume was the driving function for the simulation. The arbitrary volume variation had the following form.

$$\tilde{V}_e = 1 + \frac{1}{2} [\tilde{V}_{e, min} - 1] [1 + \cos \alpha] \quad (5)$$

The precool stage mass flow during the intake process is divided into two parts. A portion of the flow passes through the heat exchanger and the expansion volume and out the lower end of the system to the refrigeration stage, defined as the inter-stage mass flow. The other portion is expanded in the precool stage. The inter-stage mass flow which flows only during intake is

assumed to be proportional to the mass flow into the expansion volume during intake. A similar scheme is used during the exhaust.

The expander volume energy equation derived from the energy balance on the gas within the expander, control volume B, is

$$d\tilde{P}_e \frac{\tilde{V}_e}{\gamma_e} = \tilde{T}_{H1} d\tilde{m}_{H1} - \tilde{P}_e d\tilde{V}_e - d\tilde{m}_{L1} \tilde{T}_e \quad (6)$$

During the expansion process the gas at the expansion volume inlet is equal to the gas temperature within the heat exchanger. The inflow temperature is approximated with the cold wall temperature. The enthalpy load from the gas-wall temperature difference is accounted for as is discussed later in this paper. During the recompression process, the piston forces gas from the working volume into the heat exchanger. The gas temperature gradient and the wall temperature gradient are significantly different at the heat exchanger/expander interface. Eq. 3 does not apply at this end of the exchanger. Therefore the minor heat exchanger is a small portion of the heat exchanger that accounts for the heat exchanger/expander interface. The gas temperature changes (relative to wall temperature) associated with this end effect are neglected in the continuity equation.

The HPP momentum equation was derived from the momentum balance on control volume A. Assuming inertia effects are negligible compared to viscous effects, we obtained the differential HPP pressure drop equation. The pressure drop equation requires that the pressure be position dependent, but our major assumption is that pressure is uniform. To satisfy both requirements we divided the major HPP heat exchanger into two parts. Within each sub-volume the pressure was uniform but different for the two sub-volumes. The pressure drop equation has the following form.

$$\tilde{P}_e - \tilde{P}_{H1} = \frac{\tilde{\mu}_H}{\tilde{V}_{H42}^2} \left[\int_0^{\tilde{V}_{H41}} d\tilde{m}_H \frac{\tilde{T}_H}{\tilde{P}_H} d\tilde{V}_H + \int_{\tilde{V}_{H41}}^{\tilde{V}_{H42}} d\tilde{m}_H \frac{\tilde{T}_H}{\tilde{P}_H} d\tilde{V}_H \right] \quad (7)$$

where

$$\tilde{\mu}_H \equiv 24 \frac{Pr}{Nu} \tilde{h}_H \frac{\omega^2 L^2}{R_{H4} T_{C1}} \quad (8)$$

is the nondimensional pressure drop parameter. The pressure in the first integral is the HPP inlet pressure, and the pressure in the second integral is the expander pressure. Again the temperature

was assumed equal to the wall temperature.

Similar equations for the LPP, control volume C, were derived from Eq. 1, 3, and 7. The equations are simpler since there is no variable mass storage within the passage.

The minor heat exchanger is subject to the constraint that energy must be conserved over the cycle and the enthalpy flux must be the same as the major heat exchanger.

PARASITIC LOSSES

The imperfect heat exchange loss, conduction loss, and shuttle loss were neglected in the preceding development, but are now considered as additional heat loads on the available refrigeration.

The loss due to the imperfect heat exchange in the major heat exchanger is equal to the net cyclic HPP and LPP enthalpy flux at any location of the heat exchanger. The corresponding equation used to calculate the loss is

$$\tilde{Q}_{H1} = \oint d\tilde{m}_{H12} \tilde{T}_{H12} - \oint d\tilde{m}_{L12} \tilde{T}_{L12} \quad (9)$$

The longitudinal temperature gradient along the cylinder walls is a path for heat. The heat that enters the cold space is an additional heat load which reduces the available refrigeration. A cycle average conduction heat load was calculated from Fourier's law of conduction using a linear temperature gradient. The conduction wall cross-sectional area is a function of the pressure difference based on minimum wall thickness for thin-walled vessels. The conduction heat load equation is

$$\tilde{Q}_{cond} = 3 \tilde{k} \tilde{V}_{H1}^2 (\tilde{T}_{C1} - \tilde{T}_{C1}) \frac{\tilde{h}_H}{Nu_H} (\tilde{P}_{H,max} - \tilde{P}_{L,min}) \quad (10)$$

where

$$\tilde{k} \equiv 2 \left(\frac{k_w}{k_H} \frac{P_{max}}{\sigma_w} \right) \frac{V_{c,max}}{L^3} \quad (11)$$

is the nondimensional conduction parameter.

The oscillating expander and its longitudinal temperature gradient is also a path for heat. A cycle average shuttle heat load was based on Zimmerman and Longworth's work [6]. The

equation for the heat load is

$$\tilde{Q}_{shuttle} = \left(\frac{192 \pi^2 Pr (1 - \tilde{V}_{eo})^2}{\tilde{\mu}_H \tilde{k}^2 \tilde{L}^2 \tilde{V}_{H4I}^3} \right) (\tilde{T}_{C4} - \tilde{T}_{C1}) \quad (12)$$

where

$$\tilde{L} \equiv \frac{L}{\sqrt{R_{H_2} T_{C1}}} \frac{\sigma_{m, CP, H_2}}{k_{ss}} \quad (13)$$

is the nondimensional shuttle parameter.

COMPRESSOR MODEL

In order to determine the efficiency of the stage, the required compressor work must be calculated. The compressor work was evaluated from assuming it comprised of two adiabatic and one isothermal compression. The adiabatic compressors compress the gas until the temperature change of the gas is equal to the corresponding gas-wall temperature difference. The isothermal compressor compresses the gas equal to the reduced pressure ratio determined by the adiabatic compressors. Isentropic relations were used to evaluate the intermediate pressures for the isothermal compression. The total compressor work is the sum of these individual work terms.

NUMERICAL METHOD

The cycle of the system was divided into four processes. Boundary constraints on the mass flow and gas pressures were made during each process of the cycle. The processes and boundary conditions are:

Process 1: The expander exhaust mass flow, dm_{L1} , is zero during the intake stroke. For the refrigeration stage the HPP inlet pressure, P_{H4} , is constant. Also the inter-stage flow, $dm_{H,ref}$, is zero. For the precool stage the expander pressure, P_e , is constant.

Process 2: The heat exchanger inlet mass flow, dm_{H4} , and the expander exhaust mass flow are zero during the expansion stroke. It is important to note that the gas is expanded through the entire pressure ratio.

Process 3: The heat exchanger inlet mass flow is zero during the exhaust stroke. For the refrigeration stage the LPP outlet pressure, P_{L4} , is constant. For the precool stage the expander

pressure is constant.

Process 4: The heat exchanger inlet mass flow and the expander exhaust mass flow are zero during the recompression stroke. Again it is important to note that the gas is compressed through the entire pressure ratio.

Fixed constraints for the analysis were the heat exchanger temperature ratio of 4.64 and a pressure ratio of 10.

With boundary conditions and constraints, the system equations were integrated over the cycle. The equations were integrated with a numerical software package, SIMNON [6]. The cycle was repeated until initial and final thermodynamic properties converged satisfying cycle energy balances of the components. The efficiency of the stage, defined below, was maximized by iterating on the nondimensional parameters.

REFRIGERATION STAGE RESULTS

The refrigeration per cycle was evaluated from the energy balance on control volume F. The heat load \tilde{Q}_{Load} shown in Fig. 2 is the sum of the conduction and shuttle heat loads. The refrigeration stage efficiency was defined as

$$COP \equiv \frac{\tilde{Q}_{Load}}{\tilde{W}_{comp, total}} \quad (14)$$

For a fixed nondimensional size, the system equations were numerically integrated. The system parameters were varied to obtain the maximum COP. The maximum COP for three different sizes are shown in Fig. 3.

As the size increases, the parasitic losses decrease but at the expense of increasing the load heat exchanger loss. At some point, design of the load heat exchanger would become more important than the regenerative heat exchanger. We concluded from this figure that for a given refrigeration capacity, it is optimal to design one refrigeration unit versus multiple units in tandem. This is important in designing the two stage machine which is discussed later in the paper. Since full recompression and expansion provide small capacities, frequency is increased to improve capacity until the efficiency decrease is unacceptable.

Another interesting result is the effect of the heat exchanger design temperature on the stage's dimensional values. For a given optimal nondimensional solution there is a corresponding optimal dimensional solution based on the average temperature of the stage. If we assume that viscosity

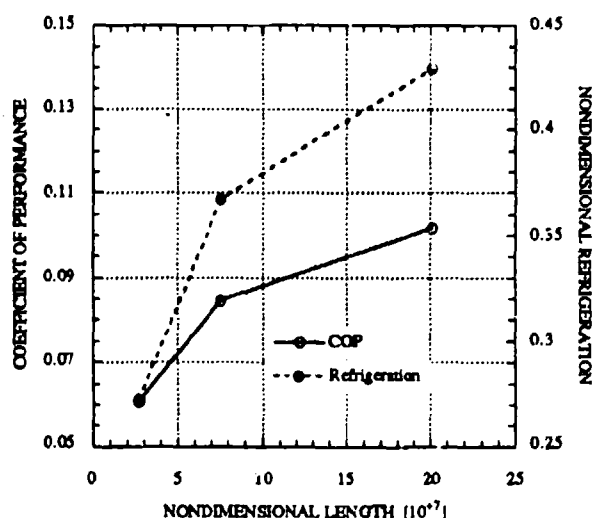


Figure 3 : Effect of Size on COP and Refrigeration.

and thermal conductivity vary with the square root of temperature and specific heat is constant, then the stage's speed and dimensions scale with temperature by the relations below.

$$\omega \sim \frac{1}{\sqrt{T}} \quad g, L \sim T \quad V_e, V_{H41} \sim T^3 \quad (15)$$

Also as size increases, the optimum frequency decreases. This suggests that it is not optimum to operate the two stages at the same speed, and it is not optimum to mechanically connect the two stages through the expander stroke. The efficiency of the overall cryocooler is affected by how efficient the precool stage delivers the mass to the refrigeration stage. The precool stage model relates compressor power to the inter-stage mass flow required by the refrigeration stage.

PRECOOL STAGE RESULTS

The capacity of the precool stage is the amount of mass that can be provided to the refrigeration stage at a given temperature and a given refrigeration-stage heat exchanger temperature difference. An energy balance on the precool load heat exchanger and additional component connections, control volume F, gives the necessary refrigeration-stage-inlet cycle enthalpy flux.

Since the refrigeration stage requires a given temperature difference, we fixed the inlet and

outlet gas temperatures connected to the refrigeration stage. We also fixed the pressure ratio at the connection. The pressure changes at the warm end of the heat exchanger varied, and were accounted for in the compressor work. The size of the device must be specified by the amount of mass allowed to flow to the refrigeration stage. A given inter-stage mass can be supplied by one or more precooling expanders operating in parallel over the same temperature span. On the other hand one precooling expander can supply the inter-stage mass flow to several refrigeration expanders operating in parallel. The parallel expander ratio is the ratio of parallel refrigeration expanders to parallel precooling expanders. The system parameters were iterated upon to maximize the refrigeration mass flow per unit of compressor work, Eq. 16.

$$\tilde{m}_{eff} \equiv \frac{\int_0^{\alpha_{stroke}} d\tilde{m}_{H_4} d\alpha}{\tilde{W}_{comp, total}} \quad (16)$$

Assuming a parallel expander ratio of one and optimizing the free parameters, the solution was obtained and is tabulated in Table 1 under the unconstrained column. It is unconstrained in the sense that the precool stage frequency, stroke, and intake stroke were not fixed. In a constrained system, the two stages are fixed by a common expander as shown in Fig. 1. The two stages are mechanically constrained by frequency, stroke, and intake stroke. Assuming the precool system is constrained by the same refrigeration stage, only one free parameter is available for optimization. The solution is in Table 1. As expected from Eq.15, the unconstrained precool stage decreased in frequency and increased in size compared to the refrigeration stage frequency and size. The constrained condition reduces the size and increases the frequency and decreases overall efficiency 20%.

The effect of the parallel expander ratio was investigated. Figure 4 shows the results of the investigation. There was no advantage to operating expanders in parallel. The proportional relationship between size and efficiency was the controlling factor. Either stage that contained parallel expanders had a reduced efficiency that reduced the overall efficiency.

CONCLUSIONS

Particular to this system we found that an ideal gas cryocooler stage, with a given pressure ratio and temperature span, can be optimized with five nondimensional parameters. A single size

Geometry	Constrained	Unconstrained
Expander Volume [cm ³]	50.0	71.2
Heat Exchanger Volume [cm ³]	12.8	22.3
Gap [m]	5.63E-05	9.35E-05
Length [m]	0.542	0.725
Diameter [m]	0.134	0.105
Frequency [rpm]	35.1	21.2
Stroke [m]	3.56E-03	8.24E-03
Energy, Mass, and Efficiency		
Compressor Power [W]	93.5	63.8
Warm End Cycle Mass Flow [g/s]	.0554	.0464
Cold End Cycle Mass Flow [g/s]	.0303	.0303
Coefficient of Performance	.0096	.0123

Table 1: Comparison of Precool Stage for the Mechanically Constrained and Unconstrained Conditions.

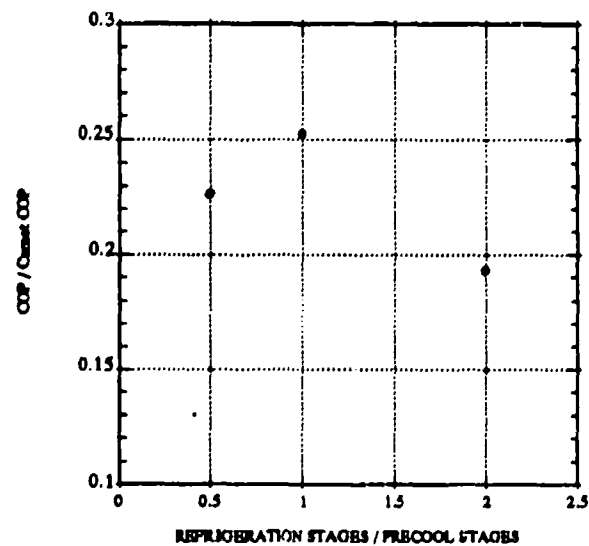


Figure 4: Effect of Frequency on Two-stage Capacity and Efficiency

variable determines the optimum. The optimum COP of the nondimensional stage increases with size. Also the dimensional variation of the optimum design was scaled with temperature.

For the model development, this analysis has the flexibility to be used to analyze other types of cryocooler configurations. The major assumptions are common to other cryocooler cycles.

FURTHER DEVELOPMENT

From the model we found that the LPP gap was not an ideal heat exchanger geometry for this system. The larger gaps provided smaller pressure losses but significantly increased the temperature difference. A helical flow passage as designed for the original heat exchanger also has this limitation. A new geometry for the LPP passage heat exchanger being investigated employs screen fins. This provides large amounts of heat exchanger area and overall heat transfer with relatively small pressure drop. Using an existing LPP gap solution for a parallel expander ratio of 1, a LPP finned heat exchanger was designed. The heat exchanger is currently being constructed and will be tested.

ACKNOWLEDGMENTS

This work was supported by Daikin Industries of Japan. This publication is based on a thesis to be submitted in February 1993 by E.B. Ratts in partial fulfillment of requirements for the degree of Doctor of Philosophy in Mechanical Engineering at the Massachusetts Institute of Technology.

REFERENCES

1. Smith, Jr., J.L., Robinson, G.Y.; Iwasa, Y., Survey of the State-of-the-Art of Miniature Cryocoolers for Superconducting Devices. Naval Research Laboratory Report 5490, December 1984.
2. J.A. Crunkleton, J.L. Smith, Jr., Y. Iwasa, "High Pressure Ratio Cryocooler with Integral Expander and Heat Exchanger." *Advances in Cryogenic Engineering*, Vol.33, pp. 809-818, 1987.
3. Jeong, Eun Soo, "Heat Transfer with Oscillating Pressure in Reciprocating Machinery," Ph.D. Thesis, Massachusetts Institute of Technology, February 1991.
4. Kornhauser, A., Gas-Wall Heat Transfer During Compression and Expansion," Sc.D. Thesis,

Massachusetts Institute of Technology, January 13, 1989.

5. Zimmerman, F.J., and Longworth, R.C., "Shuttle Heat Transfer." Advances in Cryogenic Engineering, Vol.16, p. 342, 1970.

6. Department of Automatic Control, Lund Institute of Technology, SIMNON User's Guide for MS-DOS Computers, Studentlitterature AB, Lund, 1987.

NOMENCLATURE

c_p	Specific heat at constant pressure
c_v	Specific heat at constant volume
g	Heat Exchanger's passage width
h	Heat transfer coefficient
\tilde{h}	Nondimensional heat transfer coefficient (Eq. 4)
k	Thermal conductivity
\tilde{k}	Conduction Parameter, (Eq. 11)
dm	Differential mass element
$d\tilde{m}$	Dimensionless differential mass element = $dm R_{He} T_{C1} / P_{H,max} V_{e,max}$
L	Heat Exchanger Length
\tilde{L}	Shuttle Parameter, (Eq. 13)
P	Gas Pressure
\tilde{P}	Dimensionless Pressure = $P / P_{H,max}$
Pr	Prandtl number = $\mu_{He} c_{p,He} / k_{He}$
\tilde{Q}	Dimensionless Heat Load = $Q_{cond} R_{He} / P_{H,max} V_{e,max} c_{p,He}$
R	Gas constant
T	Gas Temperature
\tilde{T}	Dimensionless Gas Temperature = T / T_{C1}
V	Volume
\tilde{V}	Dimensionless Volume = $V / V_{e,max}$
\tilde{W}_{comp}	Dimensionless Compressor Work = $W_{comp} R_{He} / P_{H,max} V_{e,max} c_{p,He}$

Greek Symbols

α	Expander angle
γ	Specific heat ratio = c_p / c_v
μ	Viscosity
$\tilde{\mu}$	Pressure drop Parameter, (Eq. 8)
ω	Expander angular frequency
π	$\pi = 3.14159$
σ	Wall yield stress

Subscripts

C	Cylinder wall
$comp$	Compressor
$C1, C2, C4$	Location on cylinder wall
e	Expander
eo	Clearance
ΔH	Enthalpy Flux
HC	Difference in HPP and cylinder wall
He	Helium gas
H	Heat exchanger high pressure passage
HL	Difference in HPP and LPP at a location
$H41$	Difference of one location and another location in HPP
$H1, H2, H4$	Location in heat exchanger HPP
$L1, L2, L4$	Location in heat exchanger LPP
max, min	Maximum and minimum values
ref	Refrigeration

POWER, EFFICIENCY, AND OPTIMUM DESIGN OF ELECTROCHEMICAL
REFRIGERATORS

R. T. Ruggeri
Flight Thermal & Contamination Technologies
Boeing Defense & Space Group
Kent, WA

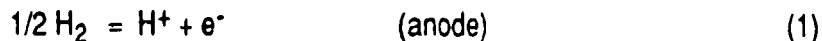
ABSTRACT

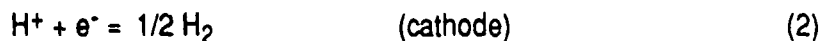
The electrochemical compressor is a variable capacity device for compressing a working fluid using only an applied electric potential. It has no moving parts, and consequently wear and wear related failures are eliminated. In the past the electrical efficiency of electrochemically compressed refrigerators was lower than the efficiency of some other systems such as those utilizing Stirling technology, but recent technological advances have made the efficiencies comparable. Nevertheless, confusion over the power consumption of an electrochemical compressor or refrigerator can result because the efficiency is not a constant. It depends on the operating conditions and mass throughput.

Power consumption and efficiency of the electrochemical compressor are reviewed and the effect of design objectives on the operating efficiency are discussed. Analytical results are presented to show how a minimum weight design is affected by power efficiency requirements.

INTRODUCTION

The electrochemical compressor utilizes the principle of ionic migration to compress the working fluid to a high pressure. Molecules of a neutral gas such as hydrogen are converted to an ionic form which migrates through a solid electrolyte membrane under the influence of an applied electric field. The membrane material is chosen to be highly permeable to ions and impermeable to neutral molecules, thereby preventing high-pressure working fluid from escaping to the low-pressure region by passing through the membrane. This process requires two electrodes, one to convert the working fluid into its ionic form, and another to convert the ions back into neutral molecules. The electrochemical reactions for the hydrogen system are shown below:





The rate at which these reactions proceed, and thereby the efficiency of the compressor depends on the applied electric potential in a predictable way.

The efficiency of the electrochemical cell is based on the isothermal compression energy of the working fluid, or alternatively, the Nernst potential of the cell. Consider an electrochemical cell consisting of a solid, hydrogen-ion-conducting electrolyte, a porous anode, and a porous cathode. The open circuit potential for the anodic half reaction can be written as follows:

$$V_{0a} = V_r + RT/F \ln(P_a). \quad (3)$$

where

- V_{0a} = the half cell voltage (V),
- V_r = the standard half cell potential (V),
- R = the ideal gas constant (J/(mole K)),
- T = the absolute temperature (K),
- F = the Faraday constant (C/eq), and
- P_a = the partial pressure of hydrogen over the anode (atm).

A similar equation can be written for the open circuit cathodic reaction:

$$V_{0c} = V_r + RT/F \ln(P_c). \quad (4)$$

where

- V_{0c} = the half cell voltage (V),
- P_c = the partial pressure of hydrogen over the cathode (atm).

In terms of these variables the open circuit cell potential (Nernst potential) is :

$$V_N = V_{0c} - V_{0a} = RT/F \ln(P_c/P_a) \quad (5)$$

The minimum power required to perform a compression from P_a to P_c can be obtained by multiplying the Nernst potential by the cell current. The current is directly proportional to the mass flow of working fluid.

$$r = M \cdot I / (nF) \quad (6)$$

where

- r = the mass flow rate of working fluid (g/s),
- M = the molecular weight of the working fluid (g/mole),
- n = the magnitude of the charge on the working fluid (eq/mole),
- and
- I = the total current flow through the electrochemical cell (C/s).

The minimum power can therefore be expressed as:

$$W = V_N \cdot I = (r/M) \cdot RT \ln(P_c/P_a) \quad (7)$$

The minimum energy per unit mass is:

$$E = W/r = RT/M \ln(P_c/P_a) \quad (8)$$

In general the measured cell voltage is greater than the Nernst potential, and the measured cell current is greater than the current calculated from eqn 6. The power efficiency of the compressor can be obtained by dividing eqn 7 by the measured cell voltage and current:

$$\epsilon_P = V_N \cdot I / (V \cdot I \epsilon_I) = V_N \epsilon_I / V \quad (9)$$

where ϵ_P = the power efficiency,
 ϵ_I = the current efficiency,
 V = the measured cell voltage (V), and
 I = the current obtained from eqn 6 (amps).

Usually the current efficiency is near unity. Therefore: the power and voltage efficiencies are nearly equal and to a good approximation,

$$\epsilon_P = \epsilon_V = V_N / V \quad (10)$$

The voltage efficiency is based on the Nernst potential, or equivalently, the isothermal energy of compression. On this basis the voltage efficiency of a typical electrochemical compressor cell can be expanded as follows:

$$\epsilon_V = \frac{\ln \left(\frac{P_c}{P_a} \right)}{\ln \left(\frac{P_c}{P_a} \right) + \frac{2}{a} \sinh^{-1} \left(\frac{i}{2i_o} \right) + \frac{n F r l i}{RT}} \quad (11)$$

where i_o = a kinetic parameter called the exchange current density (amps/cm²),
 r = the resistivity of the electrolyte material (ohm*cm),
 i = the operational current density (amps/cm²), and
 l = the thickness of the electrolyte (cm).

The first term in the denominator of eqn 11 represents the Nernst potential. As expressed, the term depends only on the compression ratio and is unaffected by either the pressure level, temperature, or current density. The second term in the denominator represents the electrode potential. The lower case a represents a constant with a magnitude on the order of 0.5. The exchange current density i_o is a kinetic parameter with the units of amps/cm². It increases exponentially with temperature, and decreases with pressure raised to

approximately the one-half power. (For precise work the power is usually determined empirically.) The third term in the denominator represents the ohmic loss in the electrolyte. This term is proportional to the bulk resistivity r of the electrolyte material, the electrolyte thickness l , and the current density i . The term is also highly temperature dependent through the material resistivity which decreases exponentially with increasing temperature.

Equation 11 suggests that the optimum design of an electrochemical compressor is favored by using the strongest (and thinnest) materials with the lowest resistivity, employing electrodes with high exchange current densities, and operating at the highest practical temperature. Equation 11 also suggests, however, that the highest efficiencies can be achieved by operating at very low current densities (I/area). However, this is frequently impractical because the mass and size of the compressor increase in proportion to the active area of the electrodes. Thus, the primary compromise with this type of system involves trading mass of the compressor for mass of the electrical power system.

ELECTROCHEMICAL CELL

Figure 1 illustrates the cell voltage and the components of cell voltage found in a typical compressor cell. The cell voltage is usually less than one volt, and it is composed of the three major components discussed above: the Nernst potential, the electrode voltage, and the resistive heating of the electrolyte. The dependence of each voltage component on

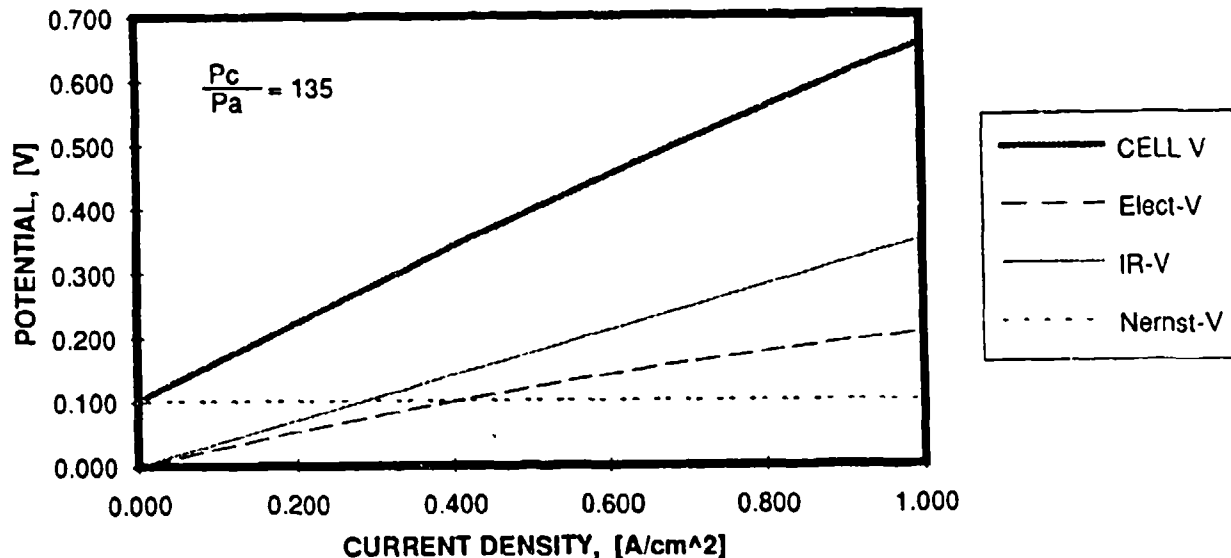


Figure 1 Electrochemical Compressor Cell Voltage Components

applied current density is illustrated in figure 1 for current densities up to 1.0 amp/cm^2 . The electrode voltage exhibits only slight curvature, and is therefore in the low field region. In this region it is very difficult to distinguish between the resistive, or ohmic potential ($IR-V$) and the electrode potential, but there is little practical advantage to be gained by determining the exact curvature in this mode of operation. The Nernst potential is a constant in this figure because the compression ratio was held constant at 135. It is clear from this figure that the highest efficiencies are obtained at the lowest current densities.

ELECTROCHEMICAL COMPRESSOR

Figure 2 illustrates how the compressor mass, power, and efficiency vary with current density. The compressor mass is roughly proportional to the active electrode area which is highest at low current density. Therefore, the mass begins at a high level and drops rapidly as the current density rises. Power consumption exhibits the opposite trend, increasing roughly in proportion to the current density, and the efficiency decreases with increasing current density as predicted by eqn 11.

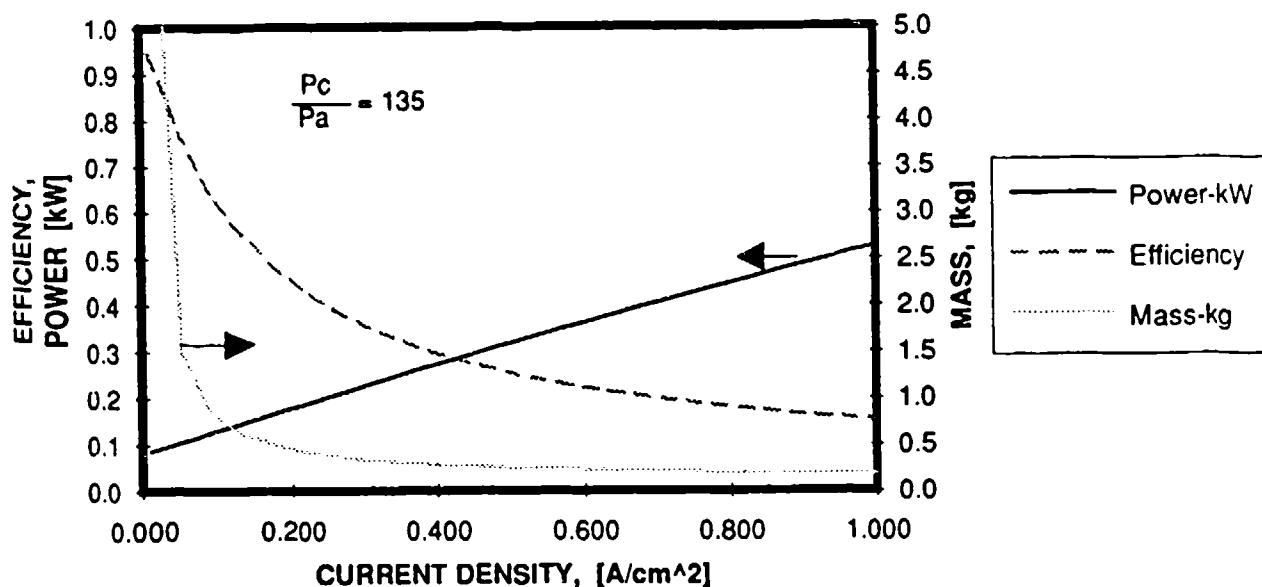


Figure 2 Electrochemical Compressor Mass, Power, & Efficiency

A compressor requires power to operate, and the mass of the power system is roughly proportional to the maximum delivered power. The data presented in figure 2 clearly shows that a composite system composed of a compressor and power supply would exhibit a

minimum mass at a current density somewhere near 0.1 amp/cm^2 . The optimum value of current density and the mass of the system both depend on the mass of the power system, but regardless of the details, the composite system would exhibit a minimum mass at some current density.

Figure 2 shows that if the system has an optimum near 0.1 amp/cm^2 , then the efficiency of the electrochemical compressor is about 60%. A small mechanical compressor operating at the same compression ratio of 135 would require approximately 4 stages and might have an efficiency of 20% or less.

ELECTROCHEMICAL REFRIGERATOR

The compressor is one component of an electrochemical refrigerator. The efficiency of the refrigerator depends on the thermal efficiency of the cooling cycle as well as the electrical efficiency of the compressor, and the mass of the refrigerator depends on the operating conditions of the refrigerator and also on the relative importance assigned to parameters such as mass and power. We have used the "system launch mass" to evaluate different refrigeration systems. This approach assumes that system mass is the figure of merit for a spacecraft cryocooler. The system launch mass includes the mass of the refrigerator, the mass of the electrical power system required to power and control the refrigerator, and the mass of the thermal control system required to radiate waste heat from the refrigerator. The mass of the power and thermal subsystems are determined by applying mass coefficients to the delivered power and area of the thermal radiators, respectively.

The mass coefficient for the power subsystem is specific for the power supply being analyzed, and values between 15 and 350 grams per watt of electrical power have been used to model different subsystems. Within this range, the particular value of the coefficient has a great effect on not only the mass of the power subsystem, but also on the optimum mass of the compressor, the thermal control subsystem, and the minimum launch mass of the cryocooler.

Since the power subsystem mass is based solely on the electrical power required by the refrigerator, the system launch mass will be affected by any operational parameter that affects the compressor's electrical efficiency or the efficiency of the thermodynamic refrigeration cycle. These parameters include the compressor temperature and outlet pressure, the cryostat's operating temperature, and the refrigeration load. Other parameters, such as the current density or the temperature at other locations within the refrigerator, also affect system efficiency.

The mass of a refrigeration system (including radiators) is shown in Figure 3. The minimum mass (optimum) condition occurs at a current density of 0.2 amp/cm^2 for a power mass coefficient of 15 g/W, and at 0.1 amp/cm^2 for a power mass coefficient of 250 g/W. Clearly, variations in the mass of the power system affect both the mass and optimum efficiency of the refrigeration system.

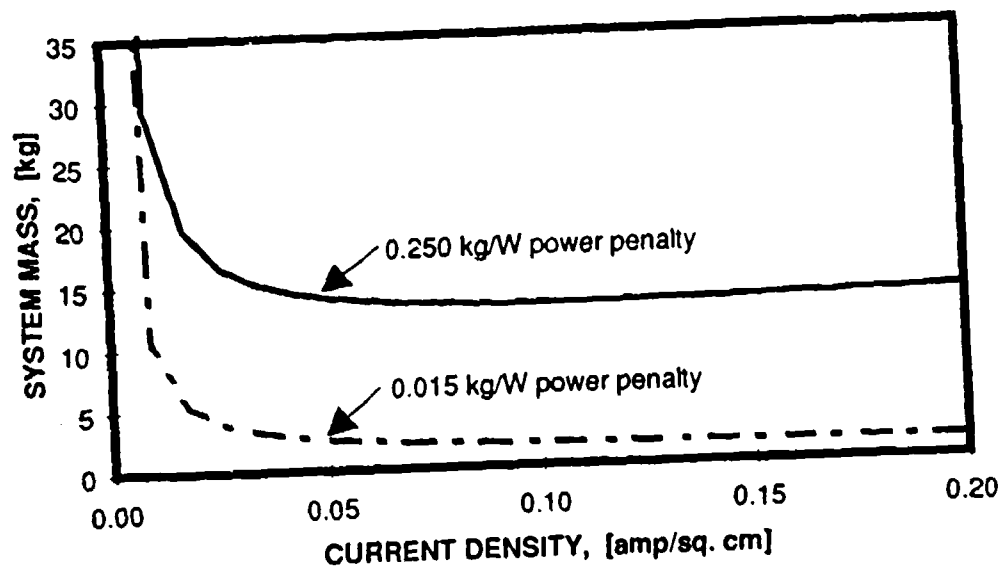


Figure 3 Refrigeration System Launch Mass vs Current Density

Table 1 illustrates another example of the effect of power subsystem mass on the efficiency of the electrochemical refrigerator. An electrochemical refrigerator is compared with a Stirling system. Each system provides 2 W of cooling at 65 K. The table shows mass and power requirements of both systems assuming two values of the mass coefficient of power (power penalty): 0.015 kg/W, and 0.250 kg/W. The overall efficiency of the electrochemical refrigerator is different in each case. The highest overall efficiency results when the mass coefficient is high.

Table 1 also shows that the overall efficiency of the electrochemical system is roughly equivalent to that of the Stirling system. The primary mass advantage for the electrochemical refrigerator results from the use of smaller thermal radiators. The electrochemical compressor rejects waste heat at a relatively high temperature, whereas waste heat is rejected by the Stirling system at less than 100 C. As a result the electrochemical system operates at an overall efficiency of 1.7% and has a mass of only 36% of the Stirling system for the case of a low power penalty. The electrochemical system operates at an overall efficiency of 2.1% and offers a 16% mass advantage when the power penalty is high.

CRYOCOOLER SYSTEM MASS COMPARISON 2 W of Refrigeration @ 65 K POWER PENALTY = 0.015 kg/W		
	BOEING CRYOCOOLER (kg)	STIRLING (kg)
REFRIGERATOR	0.7	1.5
THERMAL RADIATOR	0.5	5.0
POWER SUPPLY	1.8	1.9
TOTAL MASS	3.0	8.4
POWER REQUIREMENT	119 W	126 W

CRYOCOOLER SYSTEM MASS COMPARISON 2 W of Refrigeration @ 65 K POWER PENALTY = 0.25 kg/W		
	BOEING CRYOCOOLER (kg)	STIRLING (kg)
REFRIGERATOR	2.4	1.5
THERMAL RADIATOR	0.5	5.0
POWER SUPPLY	23.5	31.5
TOTAL MASS	26.4	38.0
POWER REQUIREMENT	94 W	126 W

Table 1 Cryocooler System Mass Comparison

The data presented above show that the electrochemical compressor is capable of operating throughout a range of electrical efficiencies depending on the current density, temperature, and compression ratio. When a power supply is included as part of the compressor system, additional constraints tend to reduce the compressor's efficiency to between 50% and 80%. When considering a spacecraft cryocooler with power supply and thermal control subsystems, the overall efficiency, composed of the efficiencies of the compressor and the thermodynamic cycle, is further reduced by constraints to limit the mass of the power system. In the cryocooler system the overall efficiency is approximately 1% to 3%, equivalent to that of other spacecraft cooling systems. It is clear that the efficiency of the electrochemical refrigerator is only one method of evaluating the system for spacecraft applications. Based on current technology, the electrochemical refrigerator provides competitive voltage and power efficiencies, and current trends indicate that improved efficiencies can still be expected.

Linearized Pulse Tube Cryocooler Theory

HAROLD MIRELS
THE AEROSPACE CORPORATION
El Segundo, CA 90245-4691

PRESENTED AT: THE 7TH INTERNATIONAL CRYOCOOLER CONFERENCE
SANTA FE, NEW MEXICO
17-19 NOVEMBER 1992

LINEARIZED PULSE TUBE CRYOCOOLER THEORY

HAROLD MIRELS
THE AEROSPACE CORPORATION
EL SEGUNDO, CA 90245-4691

ABSTRACT

Results from a linearized theory for orifice-type pulse tube cryocooler performance are summarized. Analytic expressions are presented for the dependence of effective expansion volume and refrigeration power on cryocooler geometry and temperature. Numerical results are presented for $\gamma = 7/5$, where γ is the specific heat ratio. The variation of refrigeration power with orifice area is shown to have a local maximum. When operating at, or near, the optimum orifice area, an increase in the amplitude of the first order (sinusoidal) heat transfer within the pulse tube leads to a decrease in refrigeration power. It is found, for $\gamma = 7/5$, that the optimum refrigeration power available from a basic pulse tube (zero orifice area) is about 7% of the optimum value from an orifice-type pulse tube. The corresponding result for $\gamma = 5/3$ is 10%. The refrigeration power from an orifice-type pulse tube cryocooler is shown to be less than the refrigeration power available from the corresponding Stirling cycle cryocooler.

INTRODUCTION

A schematic representation of an orifice-type pulse tube refrigerator (OPTR) is illustrated in Fig. 1. The corresponding closed-end configuration (i.e., zero orifice area) is referred to as a "basic pulse tube refrigerator (BPTR)." The first BPTR apparatus was described by Gifford and Longworth.¹⁻³ The concept of including an orifice and a reservoir was introduced by Mikulin *et al.*⁴⁻⁶ This modification led to a significant increase in refrigerator performance. Further analytic and experimental study has been presented by Radebaugh and co-workers,⁷⁻¹⁰ as well as by others.

A mathematical model for estimating OPTR performance is presented in Ref. 6. This model requires the numerical integration of a system of partial differential equations. Some numerical results were included in Ref. 6. A numerical model is also presented in Ref. 11. On the other hand, Ref. 7 provides analytic expressions for OPTR performance. However, these are in terms of a phase angle which is not derived and which is inferred from experimental data.

A linearized theory is presented in Ref. 12 which provides explicit expressions for OPTR performance without recourse to experimental data. It is assumed that the pressure, throughout the device, is uniform at each instant and that piston-induced perturbations are small. A gas spring hysteresis model, developed in Ref. 13, is used to model energy dissipation within the pulse tube.

The purpose of the present paper is to summarize the results of Ref. 12 with regard to the variation of effective expansion volume and refrigeration power with pulse tube orifice area, pulse tube volume, and heat transfer.

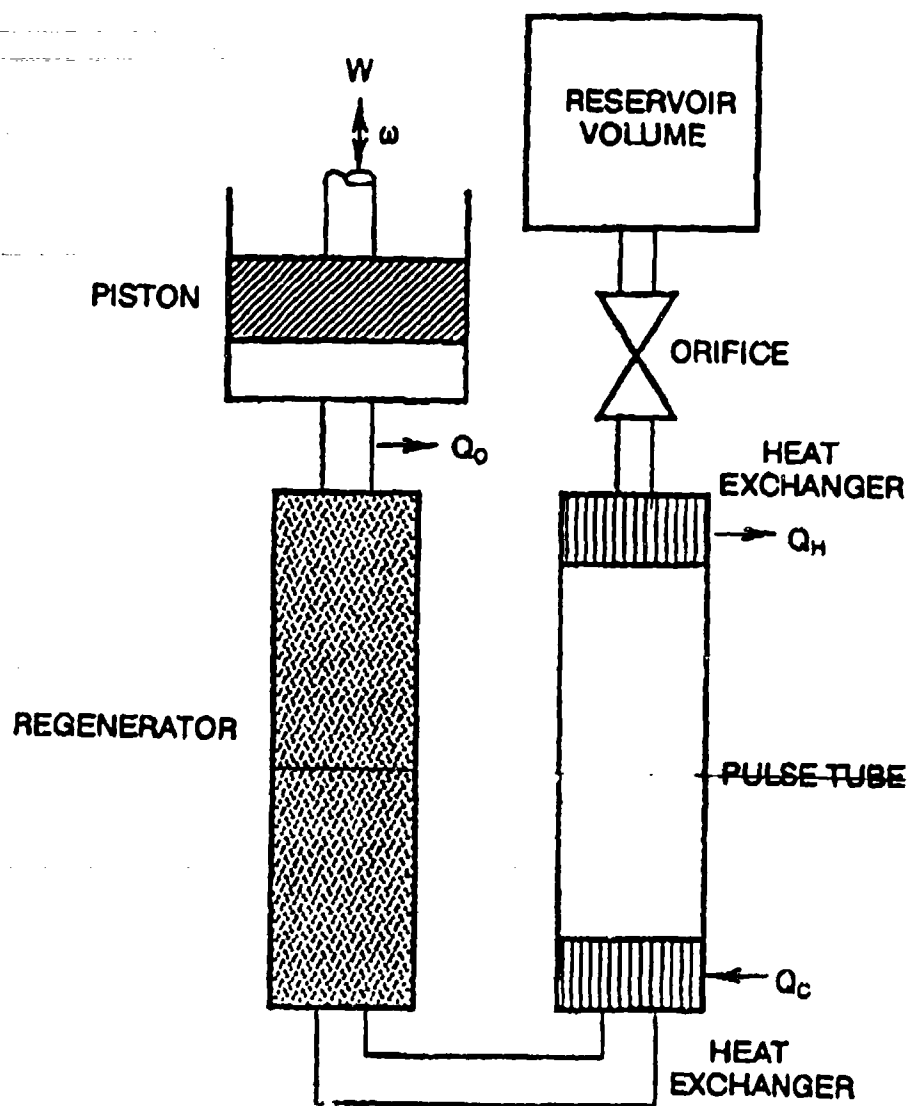


Figure 1. Schematic representation of pulse tube cryocooler.

THEORY

The orifice pulse tube cryocooler configuration considered in Ref. 12 is indicated in Fig. 2. The cryocooler is assumed to consist of a compression volume V_C (which contains a compression piston), a dead space volume V_D (which contains a regenerator), and a pulse tube volume V_F . A portion of the pulse tube volume, denoted V_E , is assumed to behave like the expansion volume in a conventional (two-piston) Stirling cycle cryocooler. The expansion volume V_E is separated from the remainder of the pulse tube by a contact surface which acts like the expansion piston in the corresponding Stirling cycle cryocooler. The magnitude of V_E is initially unknown.

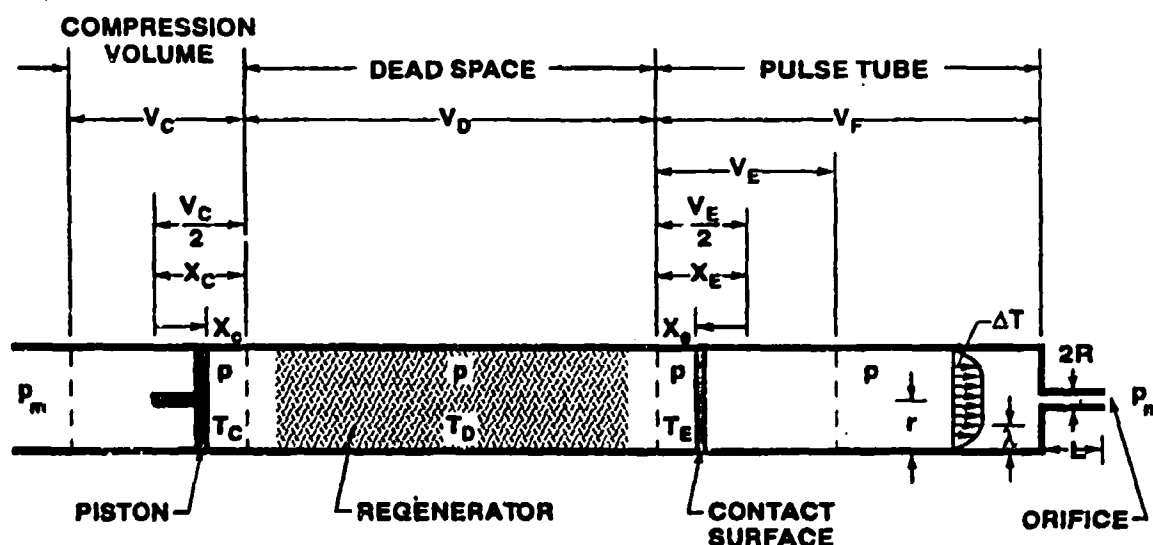


Figure 2. Pulse tube cryocooler configuration considered in Ref. 12. Not to scale.

The compression piston and the contact surface undergo sinusoidal motions which are represented by the real part of the expressions¹²

$$X_c/X_C = e^{i\omega t} \quad (1a)$$

$$X_e/X_E = e^{i(\omega t + \phi_e)} \quad (1b)$$

It is assumed that the ratio of the fluid mass in V_C to the fluid mass in V_D is small, namely

$$\frac{T_D}{T_C} \frac{V_C}{V_D} \ll 1 \quad (2)$$

As a consequence, the pressure perturbation $\Delta p/p_m \equiv (p - p_m)/p_m$ is small¹² and also varies sinusoidally. It is further assumed that Δp is uniform throughout the device (i.e., the pressure drop in the regenerator is neglected).

Flow conditions within the volumes V_C , V_D , and V_E are found using the theory of Schmidt.¹⁴ The latter assumes isothermal compression and expansion in regions V_C and V_E , respectively. The flow within the remaining portion of the pulse tube (bounded by the contact surface and the orifice) is found by using the gas spring hysteresis model of Ref. 13, which assumes

$$V_E/V_F < 1. \quad (3)$$

The magnitude of V_E and the contact surface phase ϕ_e can then be found by imposing the condition that flow velocity and pressure are continuous across the contact surface. The refrigeration power P_E equals the average power expended by the contact surface. The latter is equal to the second-order heat transfer, from gas to wall, within the pulse tube, plus the power dissipated in the orifice. The resulting expressions for V_E , ϕ_e , and refrigeration power P_E are¹²

$$\frac{T_C V_E}{T_E V_C} = \frac{H_1(\alpha^2 + \beta^2)^{1/2}}{[(1 + \alpha H_1)^2 + (\beta H_1)^2]^{1/2}} \quad (4a)$$

$$\sin \phi_e = \frac{\beta/(\alpha^2 + \beta^2)^{1/2}}{[(1 + \alpha H_1)^2 + (\beta H_1)^2]^{1/2}} \quad (4b)$$

$$\begin{aligned} P_E &= \frac{16(T_C/T_E)P_E}{\omega p_m V_C} \left[\frac{V_D}{V_C} \frac{T_C}{T_D} \right] \\ &= \frac{2\beta H_1}{(1 + \alpha H_1)^2 + (\beta H_1)^2} \end{aligned} \quad (4c)$$

where

$$H_1 = \frac{1}{\gamma} \frac{V_F}{V_D} \frac{T_D}{T_E} \quad (5a)$$

$$\alpha = 1 + Gb \quad (5b)$$

$$\beta = K + Ga \quad (5c)$$

$$G = (\gamma - 1)/2 \quad (5d)$$

$$K = \frac{\gamma \pi p_m R^4}{8\mu L \omega V_F} \quad (\text{Poiseuille}) \quad (5e)$$

$$\begin{Bmatrix} a \\ b \end{Bmatrix} = \frac{\sinh 2y + \sin 2y}{y(\cosh 2y + \cos 2y)} \quad (5f)$$

$$y = r/\lambda \quad (5g)$$

$$\lambda = \sqrt{2\bar{\alpha}/\omega} \quad (\text{Stokes}). \quad (5h)$$

For a given specific heat ratio, γ , Eqs. (4) are functions of H_1 , K , and y . The quantity H_1 equals $T_F/(\gamma T_E)$ times the ratio of the mass in volume V_F to the mass in volume V_D . Thus, H_1 is a measure of the magnitude of the pulse tube portion of the cryocooler. The combination of Eqs. (3) and (5a) provide the requirement

$$H_1 > > \frac{1}{\lambda} \frac{T_D}{V_D} \frac{V_E}{T_E}, \quad (6)$$

which is a consequence of the gas spring model of Ref. 13. The quantity K is approximately equal to the ratio of the mass displaced through the orifice divided by the mass displaced by the contact surface motion.¹² Equation (5e) assumes Poiseuille flow of a fluid with viscosity μ through an orifice of radius R and length L (Fig. 2). The quantity y equals the ratio of the pulse tube semiwidth r divided by the thermal boundary layer thickness λ associated with an unbounded ($r \rightarrow \infty$) geometry. Equation (5h) is Stokes' expression for λ . Here, $\bar{\alpha} = k/(\rho c_p)$ is thermal diffusivity. The case $y = r/\lambda > > 1$ is illustrated in Fig. 2. The parameter y characterizes the gas-to-wall heat transfer within the pulse tube portion of the cryocooler. The heat transfer is sinusoidal, to first order, and to this order there is no net transfer of heat to the wall per cycle. The limits $y \rightarrow 0, \infty$ correspond to isothermal and isentropic compressions, respectively, in the pulse tube. The amplitude of the first order heat transfer within the pulse tube is a maximum and a minimum at these limits, respectively. The second order solution to the heat transfer equations indicates a small net heat transfer, from gas to wall, per cycle. The latter is a maximum for values of y of order one.¹³

The normalized refrigeration power of a conventional Stirling cycle cryocooler is obtained from

$$(\dot{P}_E)_{SC} = 2 \left(\frac{V_E}{V_C} \frac{T_C}{T_E} \right) \sin \phi_c. \quad (7)$$

Equation (7) applies to pulse tube cryocoolers, provided suitable values of V_E and ϕ_c are used [e.g., Eq. (4)].

RESULTS

Numerical results were obtained in Ref. 12 for the variation of pulse tube cryocooler performance with K , y , and H_1 , assuming $G = 0.2$ (i.e., $\gamma = 7/5$). A portion of these results are presented in Figs. 3 to 5.

The variation of \bar{P}_E with K for $y = 1$ and $0.01 \leq H_1 \leq 10.0$ is given in Fig. 3a. These curves indicate that for a fixed pulse tube geometry (i.e., fixed H_1) and fixed y , there is an optimum value of orifice area for obtaining maximum refrigeration power. This result is in accord with experiment. Analytic expressions for the maxima are given in Ref. 12. For fixed y and H_1 , the maximum refrigeration power is defined by¹²

$$K = [(1 + \alpha H_1)/H_1] - G\alpha \quad (8a)$$

$$\bar{P}_E = 1/(1 + \alpha H_1). \quad (8b)$$

The maximum value of \bar{P}_E , and the corresponding value of K , increases as H_1 decreases. The maximum value of \bar{P}_E approaches 1 as $H_1 \rightarrow 0$. However, the present model is not applicable in this limit [see Eq. (6)], and a nonlinear theory is needed to evaluate \bar{P}_E for small H_1 . Values of $(T_C V_E)/(T_E V_C)$ and $\sin \phi_e$ are given in Figs. 3b and 3c, respectively. The quantity $(T_C V_E)/(T_E V_C)$ equals the ratio of expansion volume mass to compression volume mass.

The variation of \bar{P}_E with K , for $H_1 = 0.1$ and $0.0 \leq y \leq 100.0$, is indicated in Fig. 4a. For $H_1 = 0.1$, refrigeration power \bar{P}_E is relatively insensitive to y for $K > 0(1)$. At the maximum power point, $K \approx 10$, the refrigeration power decreases by about 3% as y decreases from 100 (near isentropic flow) to 0 (isothermal flow). Thus, the effect of the first order (sinusoidal) heat transfer in the pulse tube is to decrease refrigeration power. The decrement in refrigeration power, due to the first order heat transfer, is a function of γ and H_1 and becomes more severe as γ and H_1 increase. The latter trend can be seen by considering the limits $y = 0$ and $y = \infty$. Assume fixed H_1 , and let $\bar{P}_{E,0}$ and $\bar{P}_{E,\infty}$ denote the maximum refrigeration power for $y = 0$ and ∞ , respectively. In these limits, Eqs. (5) and (8b) indicate¹²

$$\frac{\bar{P}_{E,0}}{\bar{P}_{E,\infty}} = \frac{1 + H_1}{1 + \gamma H_1} \leq 1. \quad (9)$$

Equation (9) quantifies the observation that, when the orifice area is optimized, the effect of the first order heat transfer in the pulse tube is to decrease refrigeration power. The latter result is in accord with experimental observations.⁹ The variation of $(V_E T_C)/(V_C T_E)$ and $\sin \phi_e$ with K is given in Figs. 4b and 4c. These too are relatively insensitive to y for $H_1 = 0.1$ and $K \geq 0(1)$. For smaller values of K , energy dissipation within the orifice plays a lesser role and cryocooler performance becomes dependent on the net second-order heat transfer from gas to wall.

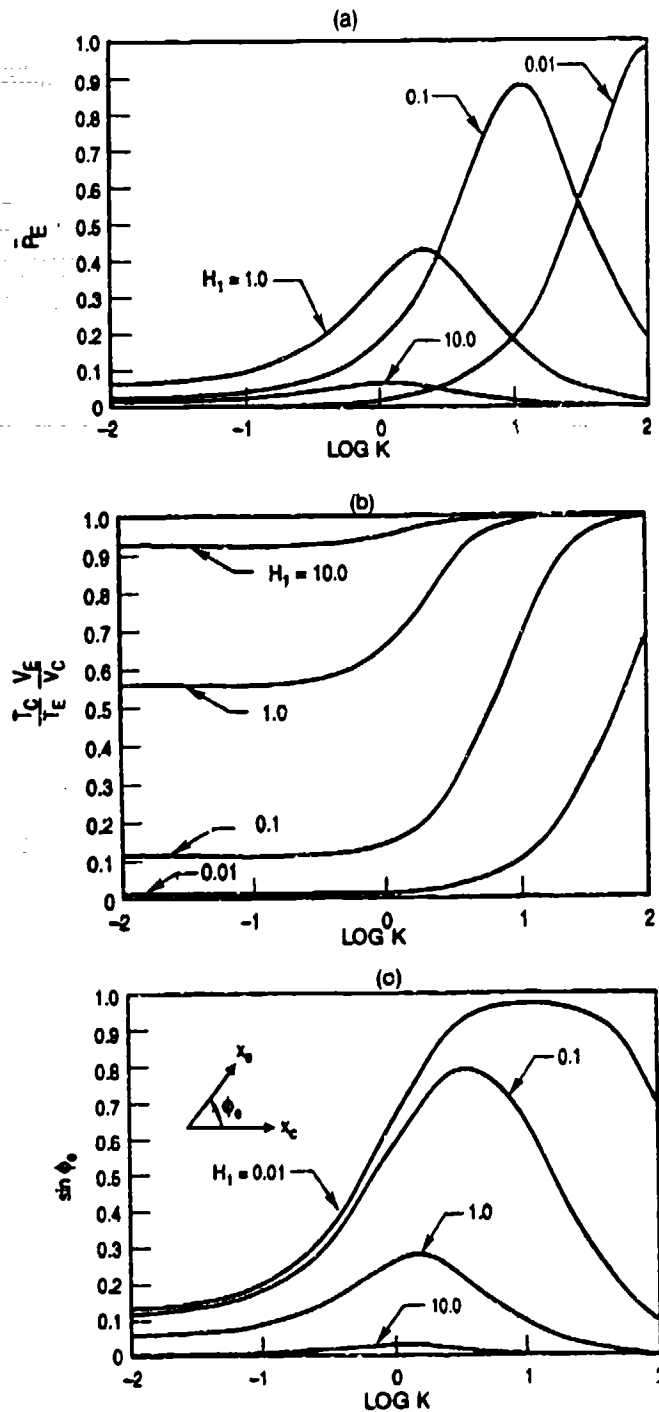


Figure 3. Variation of pulse tube performance with K for cases $G = 0.2$, $\gamma = 1.0$, and $H_1 = 0.01, 0.1, 1.0$, and 10.0 . (a) P_E ; (b) $(T_C/T_E)(V_E/V_C)$; (c) $\sin \phi_e$.

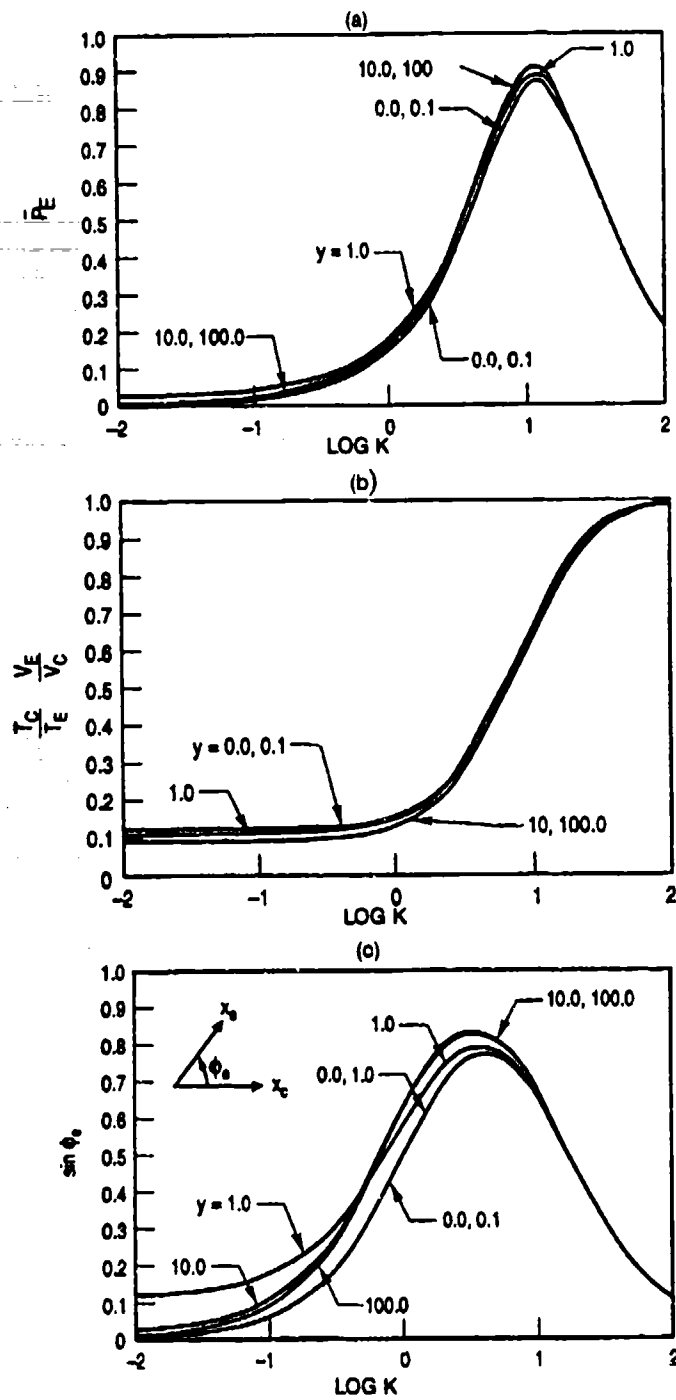


Figure 4. Variation of pulse tube performance with K for cases $G = 0.2$, $H_1 = 0.1$, and $y = 0.0, 0.1, 1.0, 10.0$, and 100.0 . (a) \bar{P}_E ; (b) $(T_C/T_E) (V_E/V_C)$; (c) $\sin \phi_e$.

Figures 5a through 5c provide results for a "basic" pulse tube (i.e., the case of no orifice, $K = 0$). The variation of \bar{P}_E with y , for $0.01 \leq H_1 \leq 10.0$, is given in Fig. 5a. The power is a maximum, $\bar{P}_E = 0.068$, for $H_1 = 0.819$ and $y = 1.210$. The optimum power \bar{P}_E decreases rapidly with departure of y from $y = 1.210$. The latter is the value of y for which the net (second-order) heat transfer from gas to wall is a maximum. Thus, for $\gamma = 7/5$, the refrigeration power available from a basic pulse tube ($\bar{P}_E \leq 0.068$) is roughly equivalent to 7% of the refrigeration power available from an orifice-type pulse tube ($\bar{P}_E \leq 1.0$). For $\gamma = 5/3$, the refrigeration power available from a basic pulse tube is¹² $\bar{P}_E \leq 0.101$. The effectiveness of the orifice, in increasing refrigeration power, is demonstrated by these results.

The refrigeration power obtained from a conventional Stirling cycle cryocooler is given by Eq. (7), where ϕ_e and $(V_{ETC})/(V_{CTE})$ are design variables. By choosing $\phi_e = \pi/2$ and $(V_{ETC})/(V_{CTE}) = N > 1$, the Stirling cycle cryocooler provides $2N$ times the refrigeration obtained from a corresponding pulse tube cryocooler. Hence, the Stirling cycle cryocooler provides greater refrigeration power than the corresponding pulse tube cryocooler.

CONCLUDING REMARKS

The linearized theory of Ref. 12, for pulse tube cryocooler performance, has been summarized. Analytic expressions are presented for normalized refrigeration power \bar{P}_E , expansion volume V_E and contact surface phase ϕ_e as functions of normalized pulse tube volume H_1 , pulse tube semiwidth y , and orifice area K . Numerical results are given in Figs. 3 through 5. The major conclusions are:

1. The variation of refrigeration power with orifice area has a local maximum, in agreement with experiment.
2. When operating near the local maximum, an *increase* in the first order (sinusoidal) heat transfer from gas to wall results in a *decrease* in refrigeration power, in agreement with experiment.⁹
3. Conclusion 2 suggests that "surface heat pumping" invoked by previous authors^{2,15} does not play an important role in orifice-type pulse tube cryocoolers. However, the effect of convection, on the heat transfer within the pulse tube, was neglected in Ref. 12. Inclusion of convective heat transfer and pressure drop, in a nonlinear model, may increase the effect of heat transfer on pulse tube performance.
4. The maximum refrigeration power available from a basic ($K = 0$) pulse tube is about 7% of the power available from an orifice pulse tube ($K \neq 0$), for $\gamma = 7/5$, and is about 10% for $\gamma = 5/3$.
5. Less refrigeration power is available from a pulse tube cryocooler than from the corresponding Stirling cycle cryocooler.

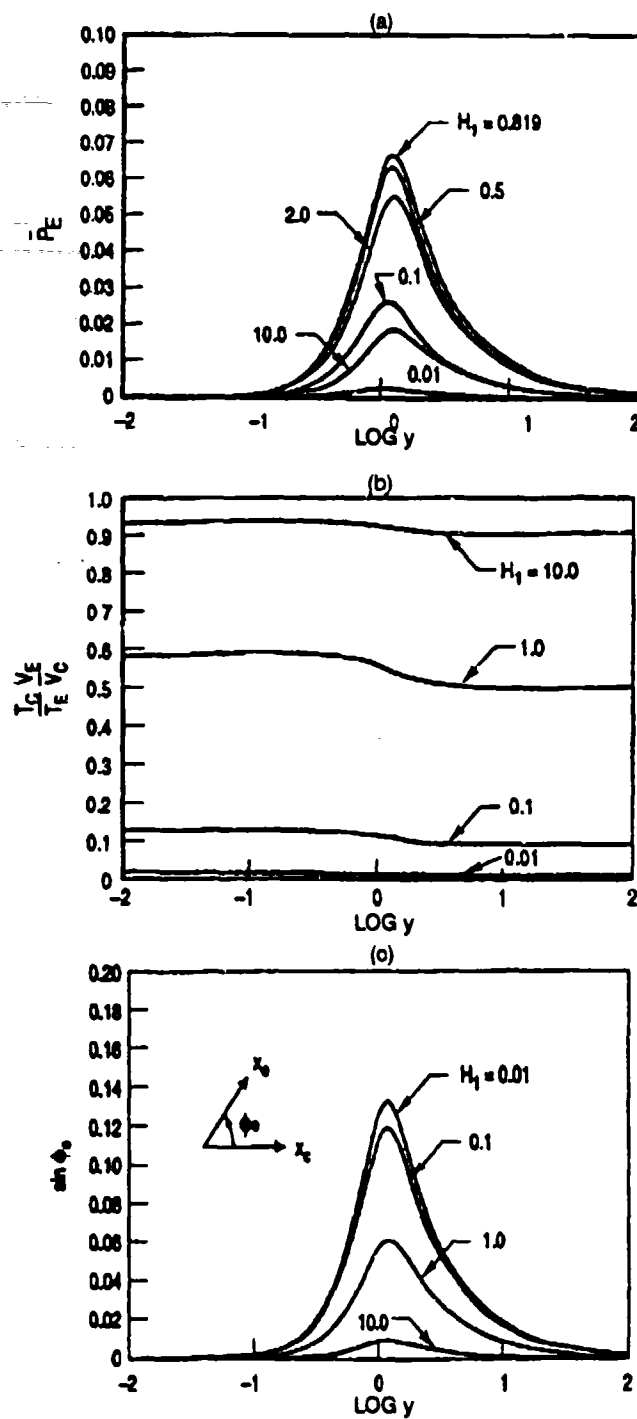


Figure 5. Variation of basic ($K = 0$) pulse tube performance with y for $G = 0.2$, and values of H_1 in the range $0.01 \leq H_1 \leq 10.0$. (a) \bar{P}_E ; (b) $(T_C/T_E) (V_E/V_C)$; (c) $\sin \phi_e$.

REFERENCES

1. Gifford, W. E., and R. C. Longworth, "Pulse-Tube Refrigeration," Transactions of the ASME, Vol. 63, 1964, p. 264.
2. Gifford, W. E., and R. C. Longworth, "Surface Heat Pumping," *Advances in Cryogenic Engineering*, Vol. 11, Plenum Press, New York, 1966, p. 171.
3. Longworth, R. C., "An Experimental Investigation of Pulse Tube Refrigeration Heat Pumping Rates," *Advances in Cryogenic Engineering*, Vol. 12, Plenum Press, New York, 1967, p. 608.
4. Mikulin, E. I., Shkrebyonock, M. P. and A. A. Tarasov, "Investigation of Cryogenic Pulse Tube," (In Russian), *Higher Educational Institutions News, Machinery Engineering*, 1:71 (1983).
5. Mikulin, E. I., M. P. Shkrebyonock, and A. A. Tarasov, "Expansion Cryogenic Pulse Tube," (in Russian), *Higher Educational Institutions News, Machinery Engineering*, 9:76 (1982).
6. Mikulin, E. I., A. A. Tarasov, and M. P. Schkrebyonock, "Low Temperature Expansion Pulse Tubes," *Advances in Cryogenic Engineering*, Vol. 29, Plenum Press, New York, 1984, p. 629.
7. Storch, P. J., R. Radebaugh, and J. E. Zimmerman, "Analytical Model for the Refrigeration Power of the Orifice Pulse Tube Refrigerator," NIST Tech. Note 1343, 1990.
8. Radebaugh, R., J. E. Zimmerman, D. R. Smith, and B. Louie, "A Comparison of Three Types of Pulse Tube Refrigerators: New Methods for Reaching 60 K," *Advances in Cryogenic Engineering*, Vol. 31, Plenum Press, New York, 1986, p. 1979.
9. Radebaugh, R., and S. Hermann, "Refrigeration Efficiency of Pulse Tube Refrigerators," *Proceedings of the 4th International Cryocooler Conference*, Boulder, Colorado, 1986.
10. Radebaugh, R., K. Chowdhury, and J. E. Zimmerman, "Optimization of a Pulse Tube Refrigerator for a Fixed Compressor Swept Volume," *Proceedings of the 5th International Cryocooler Conference*, 1988.
11. Peiyi, Wu, and Zhu Shaowei, "Mechanism and Numerical Analysis of Orifice Pulse Tube Refrigerator with Valveless Compressor,"
12. Mirels, H., "Linearized Theory for Pulse Tube Cryocooler Performance," The Aerospace Corporation, ATR 92(8489)-2, 1992.
13. Mirels, H., "Effect of Orifice Flow and Heat Transfer on Gas Spring Hysteresis," The Aerospace Corporation, ATR 92(8489)-1, 1992.
14. Walker, G., *Cryocoolers Part 1: Fundamentals*, Plenum Press, New York, 1983, pp. 1-28, 134-142.
15. Lee, J. M., and H. R. Dill, "The Influence of Gas Velocity on Surface Heat Pumping for the Orifice Pulse Tube Refrigerator," *Cryogenic Engineering Conference*, 1989.

VIBROIMPACT RESONANCE APPLICATION FOR THE DISPLACER MOTION PASSIVE
CONTROL IN THE SPLIT CRYOGENIC COOLER

Alexander Veprik and Nachman Pundak
Ricor Ltd. Cryogenic & Vacuum Systems
18960 En Harod Ihud
Israel

INTRODUCTION.

One of the main problems in the *Split Stirling* cooler design is the maintenance of an expansion volume oscillation delay of about 90° vs driving pressure.

The various types of displacers with special phase delay control means, consisting of linear mass-spring systems with dry friction, viscous flow or eddy current dampers were developed (see, for instance, [1]).

The principal disadvantages of such devices are the mechanical complication, additional power consumption, expander compartment overheating, noise and vibration levels increase.

An alternative way of phase delay control is the linear resonant mass-spring system with minimal damping usage. Such design seems to be much more natural: the inertial and elastic forces are balanced, the required driving force equals the minimal damping force and the mentioned phase delay is about 90° perfunctorily.

The practical experience indicates some disadvantages:

- high sensitivity to small system parameter variations (fill pressure, temperature, input voltage or frequency, etc.). Slight difference between the natural and excitation frequencies leads to operation out of resonance.

- displacer/regenerator assembly operation is very sensitive to the location of statical equilibrium - its improper choice may cause the vibroimpacts (which in turn may overheat the displacer cold point and increase vibroactivity) or dead volume appearance (which also decreases the operational efficiency). As a matter of fact, to select a suitable displacer/regenerator dynamical parameters it is necessary to try a large amount of versions.

The present paper depicts the preliminary results of the lightly damped resonant expander design improvement. For this matter the case of the resonance in the strongly nonlinear system will be analyzed [2].

DYNAMICAL ANALYSIS OF THE SPRINGLESS DISPLACER.

Fig.1.a.,b. depicts the simplified physical and corresponding dynamical models of the pneumatically driven springless displacer.

The piston dictated stroke $2a\sin(\omega t)$ (a - amplitude, ω - angular velocity) produces the gas volume V_1 periodical compression and decompression, which in turn causes displacer mass M_d periodical motion $X_d(t)$, inducing the gas volumes V_2, V_3 periodical compression

and decompression. Representing the gas volumes $V_{1,2,3}$ as gas springs $C_{g1,2,3}$ and dampers $b_{g1,2,3}$ one can get the dynamical model of the pneumatically driven displacer.

The absence of the mechanical spring causes displacer oscillation within two elastic bumpers (rubber ring sets, for instance) providing total clearance D . In another words, we replace the linear metal spring (as in the traditional design) with a nonlinear one (the threshold type of nonlinearity).

The motion equation of the nonlinear system from fig.1.b. is as follows

$$M_d d^2 X_d / dt^2 + C_{eq} X_d + b_{eq} dX_d / dt + Q(X_d) = F \cos \omega t \quad (1)$$

where

$C_{eq} = C_{g1} + C_{g2} + C_{g3}$ - equivalent spring stiffness,

$b_{eq} = b_{g1} + b_{g2} + b_{g3}$ - equivalent damping,

$F = a(C_{g1}^2 + b_{g1}^2 \omega^2)^{0.5}$ - driving force amplitude, (2)

$Q(X_d) = J\delta(X_d - D/2) - J\delta(X_d + D/2)$ (3)

- the force of symmetrical impact interaction (J - impact force impulse, $\delta(*)$ - Dirak function. Notation (3) means, that each time crossing the positive ($D/2$) and negative ($-D/2$) restraint levels

the displacer mass gets the impacts - short time duration (in comparison with the oscillation period) force interaction with the elastic bumpers.

Taking into account the only periodical displacer motion with two symmetrical opposite impacts over the period $\tau=2\pi/v$, the impact force notation may be rewritten as follows

$$Q(X_d) = J\ddot{x}/2(t) = Q(t) \quad (4)$$

The process $X_d(t)$ is symmetrical and periodical $\{X_d(t)=X_d(t+\tau)$ and $X_d(t)=-X_d(t+\tau/2)\}$, so it is enough to find the solution of (1) over the time interval $0 < t < \tau/2$.

The condition of impact at the $t=0$ in according with the Newton hypothesis:

$$X_d(0)=D/2 \quad R d[X_d(-0)]/dt = - d[X_d(+0)]/dt \quad (5)$$

where R - coefficient of velocity restoration, $0 < R < 1$.

- $d[X_d(-0)]/dt$ - mass velocity before the impact.

- $d[X_d(+0)]/dt$ - mass velocity after the impact.

From (5) follows

$$J = M_d(1+R) d[X_d(-0)]/dt \quad (6)$$

Solution of (1) within the time interval $0 < t < \tau/2$ may be expressed in the integral form

$\tau/2$

$$X_d(t) = Y_d(t) - \int_0^{\tau/2} H(t-s)Q(s)ds$$

$$0 < t < \tau/2$$

(7)

where

function $Y_d(t) = A \cos(\omega t + h)$ where

$$A = P[(-M_d \omega^2 - C_{eqv})^2 + \omega^2 b_{eqv}^2]^{-0.5} \quad (8)$$

$$h = \arctg[b_{eqv}/(-M_d \omega^2 - C_{eqv})] \quad (9)$$

describes impactless motion (the linear solution of (1)

in case $D \rightarrow \infty$),

$H(t)$ - periodical Green function - linear system response
on the periodical symmetrical impacts [2]:

$$H(t) = \exp(-bt)(M_d \omega_0)^{-1} [\sin \omega_0 t + \exp(-b\tau/2) \sin \omega_0 (t - \tau/2)] *$$

$$* [1 + \exp(-b\tau) + 2 \exp(-b\tau/2) \cos(\omega_0 \tau)]^{-1}, \quad 0 < t < \tau/2 \quad (10)$$

where $b = b_{eqv}/2M_d$ and $\omega_0^2 = C_{eqv}/M_d$.

Substituting (8) into (7), using the Dirak function quantities
and (4) finally we can obtain

$$X_d(t) = A \cos(\omega t + h) - JH(\tau - p), \quad 0 < t < \tau/2 \quad (11)$$

where p is the unknown phase of impact relatively to the impactless motion and impulse values are to be defined also. For this purpose the impact conditions (5) at moment $t=p$ with notation $h^* = h+p$ may be used:

$$D/2 = A \cosh^* - JH(0)$$

$$J = [-\omega A \sinh^* - JdH(-0)/dt](1+R)M_d \quad (12)$$

After a number of rearrangements

$$J_1 = \{-DH(0)/2 + [A^2 H(0)^2 - \omega^{-2} V(D^2/4 - A^2)]^{0.5}\} / [H(0)^2 + \omega^{-2} V^2]$$

$$J_2 = \{-DH(0)/2 - [A^2 H(0)^2 - \omega^{-2} V(D^2/4 - A^2)]^{0.5}\} / [H(0)^2 + \omega^{-2} V^2]$$

$$\sinh^*_{1,2} = -J_{1,2} V / \omega A, \quad \cosh^*_{1,2} = [D/2 + J_{1,2} H(0)] / A$$

$$\text{where} \quad V = dH(-0)/dt + (1+R)^{-1} M_d^{-1} \quad (13)$$

Stability analysis shows, that only oscillations with the biggest value of impact impulse (J_1) are physically stable.

The equations (8), (9) and (13) fully describes the system dynamics and may be used to interpret its useful quantities.

Fig.2.a.,b. depicts qualitatively (as an illustration only) the spring supported (natural frequency - 42 Hz) and springless displacer frequency responses: dependencies of displacer amplitude and oscillation phase shift vs the piston oscillations upon the operational frequency.

In case of linear displacer oscillations the amplitude and phase characteristics vary quickly, the offered displacer stroke and phase can be acquire in the narrow resonant frequency vicinity. That explains the limitation of linear resonance usage, for example, in the case of cold tip temperature control by frequency change.

It is quite clear, that in case of restricted displacer oscillations its peak-peak value can't become more than the clearance value - it must be precisely equal to the clearance (in our case that will be 4mm within the frequency range 20-50 Hz).

The system hard nonlinearity causes the phase-frequency characteristic distortion - the phase shift of about 90° is obtained within the wide frequency range (in our case - 30-50 Hz) - the range of the nonlinear resonance.

The numeric calculations show low sensitivity to system parameters variations which are not so small.

In other words: The dictated displacer full stroke and optimal phase delay can be reached precisely and almost automatically due to the oscillating system internal features only.

EXPERIMENTAL ANALYSIS OF A COOLER WITH ROTARY MOTOR/RECIPROCATING
COMPRESSOR AND THE SPRING-LESS DISPLACER.

The experiments were carried out with a standard 1/4W *Split Stirling* cooler (model Ricor K-526). The standard displacer with a driving piston of 2mm and regenerator having a flow rate of 72 ccm was modified in the following way. The suspension spring was removed, the displacer oscillations inside the displacer compartment were restricted by a steel washer (mounted over the plunger) and two rubber O-rings (see fig.1.a). The total displacer stroke was predefined as 4mm.

The aim of the experiment was to correlate the theoretical analysis with the experimental data and to obtain the preliminary comparison between the standard and springless displacer operation. For the purity of the experiments same displacer and compressor were used. In order to find the "optimal" springless displacer parameters additional experimental research is required.

The parameters which were measured during the experiments were: gas pressure oscillations at the compressor output, gas pressure oscillations in the displacer compartment, cold finger temperature, the displacer compartment vibration and input drive power.

The experiment scenario was as follows.

The fill gas pressure was installed as 32 atm and heat load simulation as 1/4W. The operational frequency was changed from 22Hz to 58Hz in steps of 2Hz. After each frequency change the cooler operated for about 5 minutes to reach steady-state and corresponding measurements were carried out.

Test results indicate:

Firstly, in a wide frequency range of 26-42Hz phase shift between the gas pressure oscillations at the compressor output and gas pressure oscillations in the expander "pneumatic pillow" appears to be very close to optimal 90° ($\pm 5^\circ$). In the full frequency span (22 - 58 Hz) the deviation is $\pm 10^\circ$.

Secondly, the cold finger temperature and cooler power consumption are considerably lower over a wider frequency range in comparison with the standard case (see fig.3,4).

Thirdly, the cold finger compartment vibroactivity was decreased by half in comparison with the standard case during all the operational periods (the start-up and the steady state employment) due to springs elimination and elastic stoppers installation (see fig.5).

Fourthly, in comparison with the standard case the cold finger compartment assembly was simplified.

REFERENCES.

1.N.Pundak, S.Shtrikman. Passive motion control of pneumatically driven displacers in cryogenic coolers. Proceedings of the Third Cryocooler Conference. National Bureau of Standards. Boulder, Colorado. September 17-18, 1984, p.161-163.

2.Babytsky V.I. The theory of the vibroimpact systems. Nauka, Moscow, 1978.

Springless displacer scheme

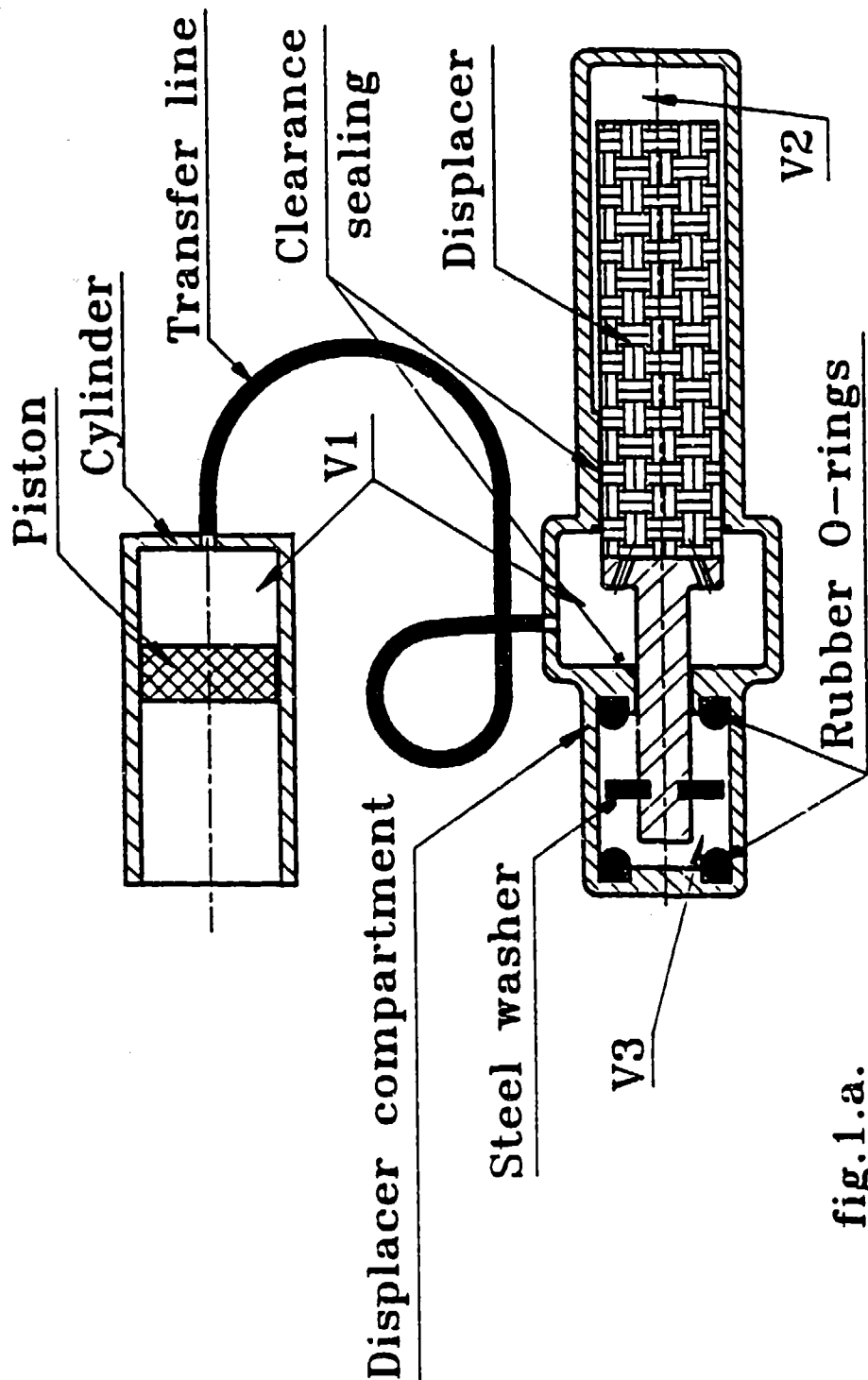


fig.1.a.

Springless displacer model

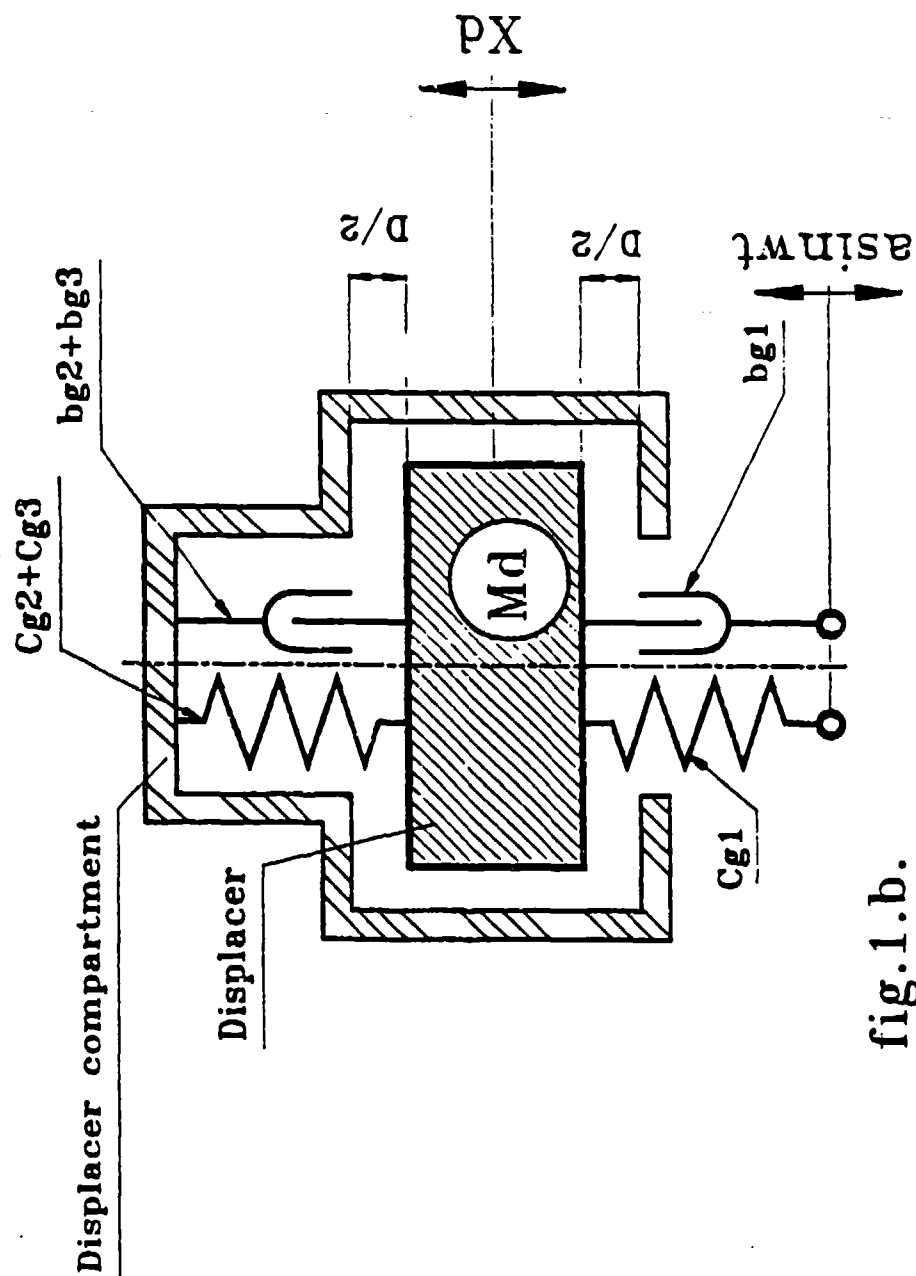


fig. 1.b.

LINEAR DISPLACER FREQUENCY RESPONSES

$B_{g1}/C_{g1} = .4 \text{ 1/s}$; $B_{eq}/C_{eq} = 4.5E-04 \text{ 1/s}$

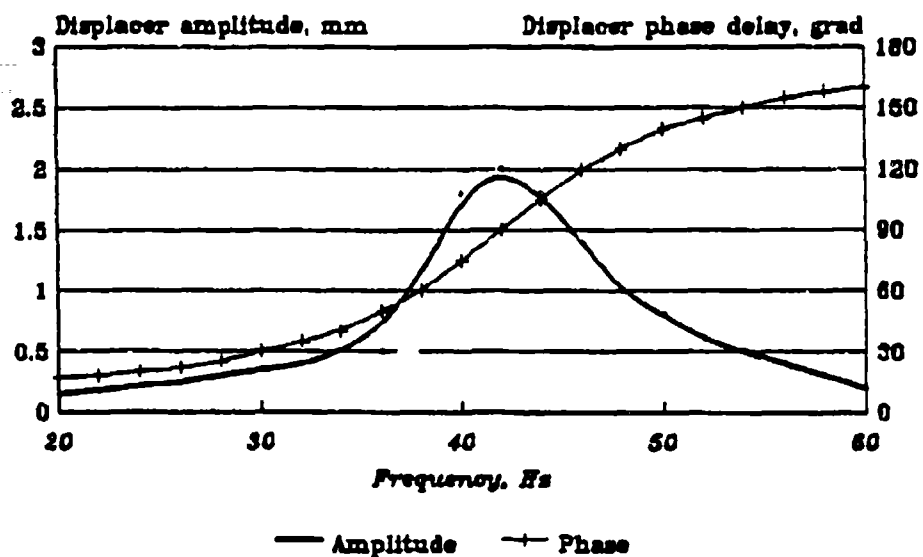


fig.2.a.

SPRINGLESS DISPLACER FREQUENCY RESPONSES

$B_{g1}/C_{g1} = .4 \text{ 1/s}$; $B_{eq}/C_{eq} = 4.5E-03 \text{ 1/s}$

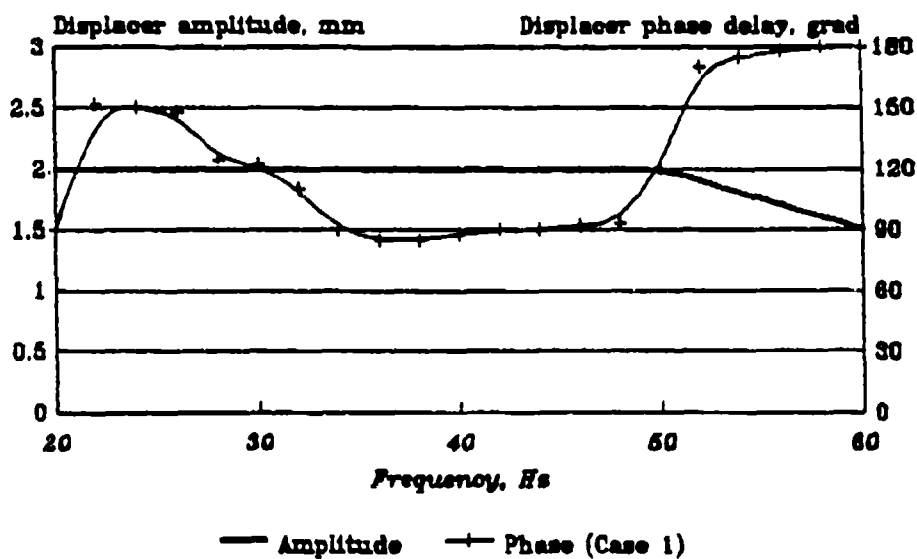


fig.2.b.

COLD FINGER TEMPERATURE vs FREQUENCY
HEAT LOAD 1/4W
FILL PRESSURE 32 atm

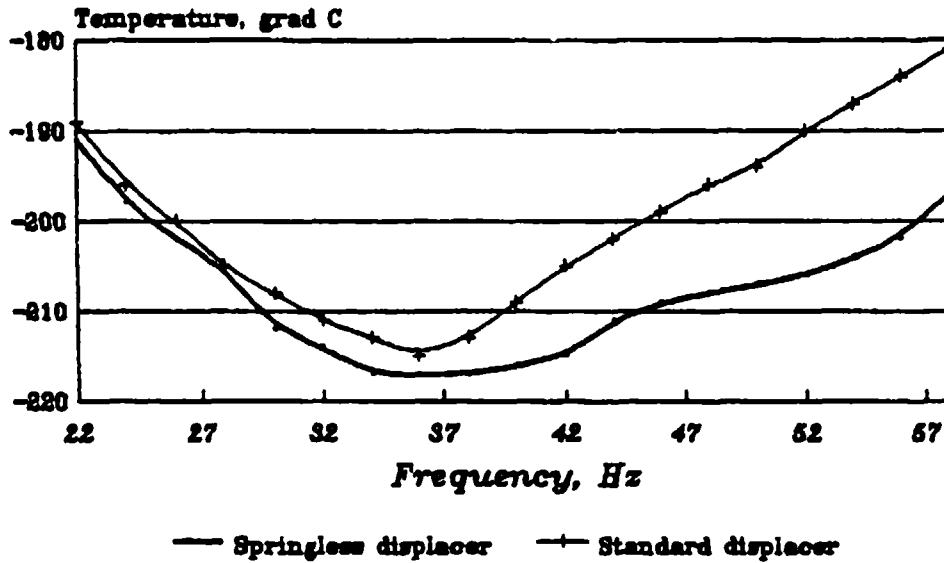


fig.3

POWER CONSUMPTION vs FREQUENCY
HEAT LOAD 1/4W
FILL PRESSURE 32 atm

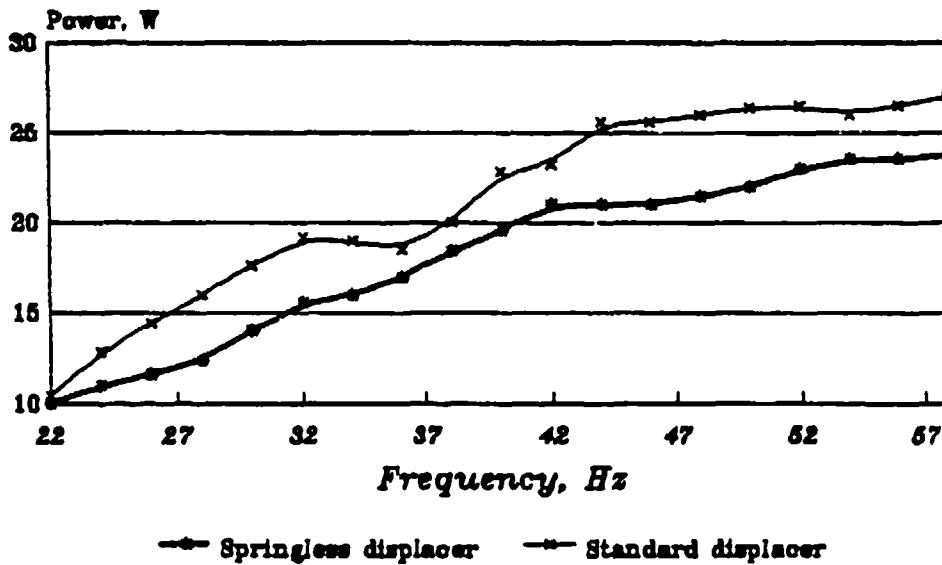


fig.4

COLD FINGER VIBROACTIVITY vs TIME

Operating frequency - 40 Hz

Filling pressure - 32 atm

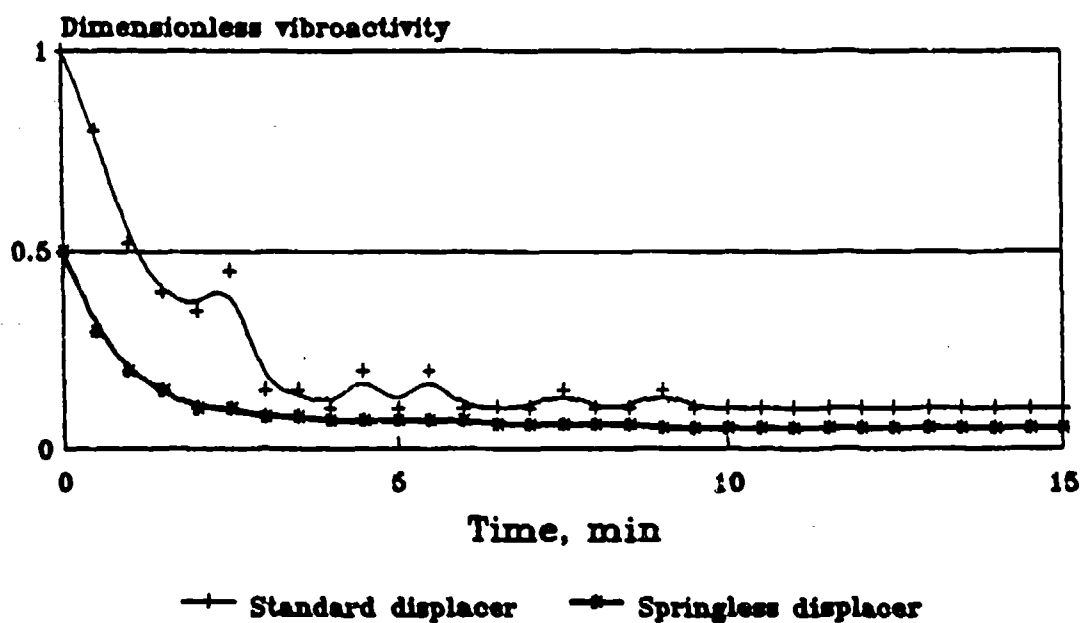


fig.5

**A HIGHLY RELIABLE, MINIATURE
STIRLING-CYCLE CRYOCOOLER**

CHI SING KEUNG AND GERARD ESPOSITO
MAGNAVOX ELECTRONIC SYSTEMS COMPANY
ELECTRO-OPTICAL SYSTEMS
46 INDUSTRIAL AVENUE
MAHWAH, NJ 07430

ABSTRACT

Magnavox EOS has designed and prototyped a miniature Stirling-cycle cryocooler, the MX8000, for military and commercial applications. The design goals of small size, low weight and low power were achieved. The MX8000 prototypes demonstrated a cooling capacity of over 500 mW at 77°K and 23°C ambient. Nominally, the MX8000 cryocooler produces 150 mW of cooling at 77°K and 23°C ambient with a DC input power of less than 8 Watts, and weighs 1 pound. The compressor utilizes a dual opposed piston configuration driven to achieve low output vibration. The expander features a very rigid cold finger thereby reducing environmentally induced deflection of the cold end. This is a highly desirable feature for integrated Dewar/cooler applications. This paper describes the design, fabrication, performance test results and the intermediate results of the 4000-hour life test.

INTRODUCTION

The MX8000 cooler is designed for both military and commercial markets, and is intended for use in a wide variety of applications including, man-portable IR systems which are powered solely by battery, and other light weight IR camera applications requiring a low-cost and long-life cryocooler. The cold finger is designed for Integrated Dewar Assembly (IDA) applications which require a high degree of stiffness. The prototype of the MX8000, shown in Figure 1, illustrates the larger compressor housing with bolted flanges, which was used only during development of the cooler. Figure 2 shows the production MX8000 outline drawing. To

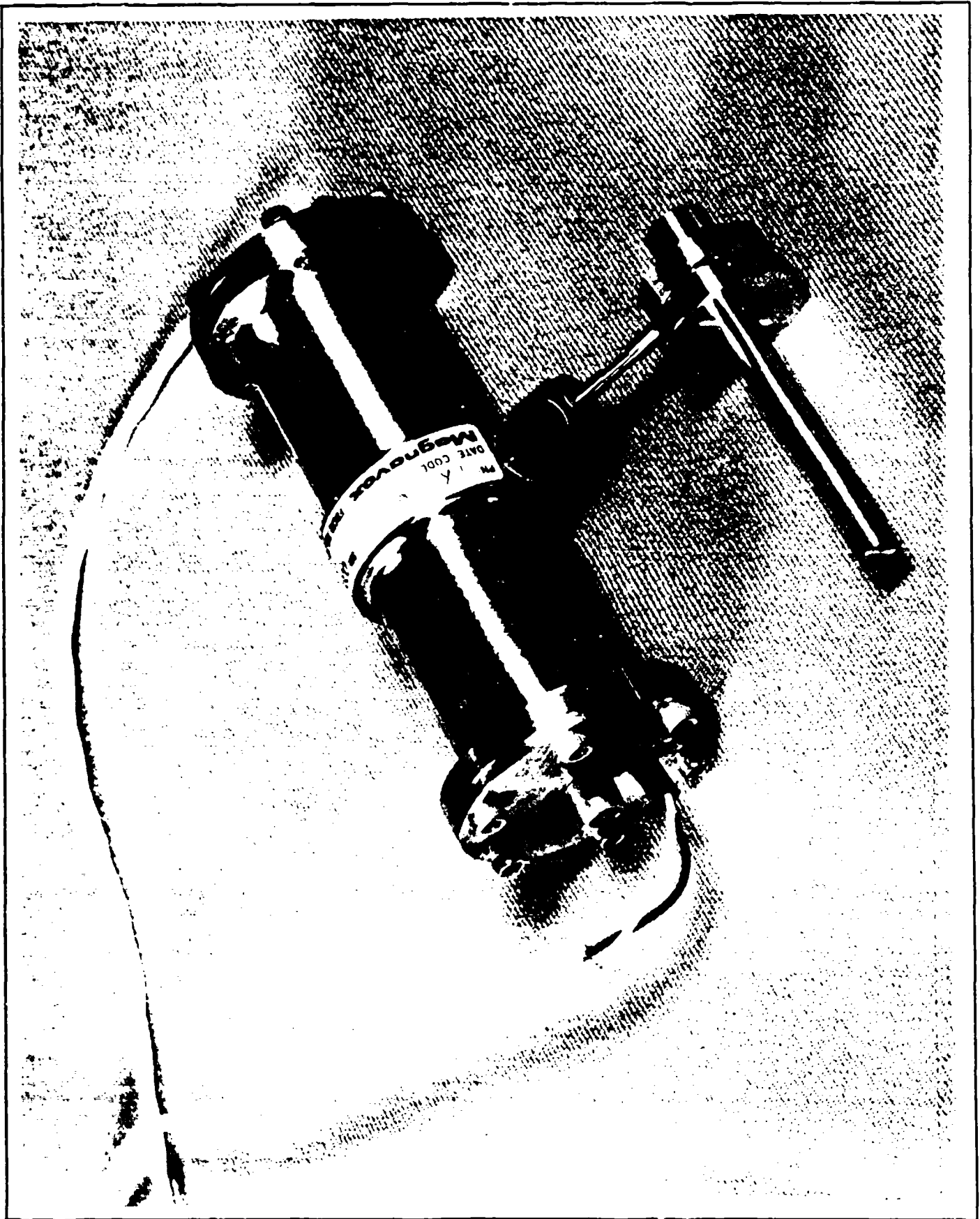
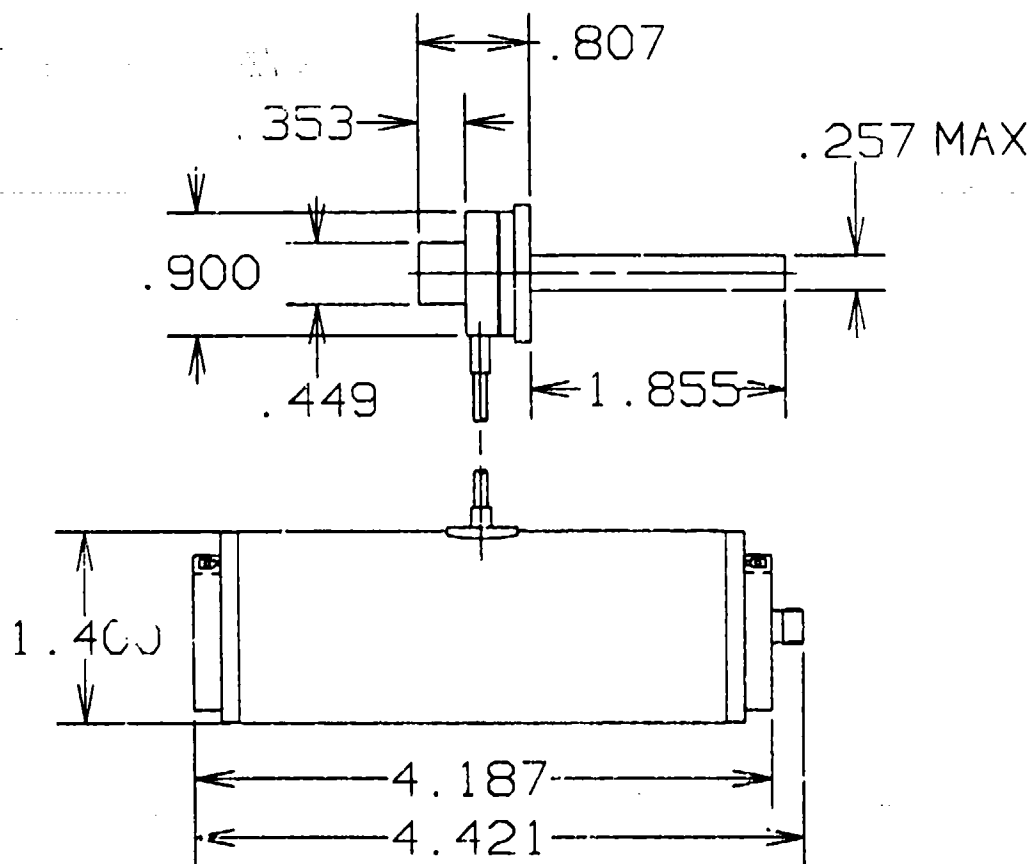


Figure 1. MX8000 Prototype



DIMENSIONS IN INCHES

Figure 2. Magnavox MX 8000

broaden the market for the MX8000, thus achieving the potential of higher production quantity and lower cost, the cooler is engineered to provide highly efficient operation within a wide range of cooling capacities from a few milliwatts to over half a Watt and a cold temperature down to below 40°K. The operable ambient temperature range of the MX8000 is from -41°C to 70°C.

The design objectives achieved by the MX8000 are summarized as follows:

- Small size (see Figure 2)
- Low weight: about 1 pound
- Low input power: 8 watts DC max input power, 150 mW cooling, at 77°K
- Structurally stiff cold finger for IDA applications
- Capable of a minimum of 250 mW, 77 °K cooling at 70°C ambient
- High reliability: Greater than 4000-hour life
- Low cost
- Minimum self-induced vibrations

KEY DESIGN APPROACHES

The MX8000 compressor design, shown in Figure 3, utilizes a dual opposed piston configuration in order to minimize output vibration. Each piston is driven by a permanent magnet, linear motor and employs dry polytetrafluoroethylene (PTFE) bearing and clearance seal technology. The expander design, shown in Figure 3, is passively driven by the compressor's pressure wave. The cooler design has incorporated several unique design features. The first is a rigid cold finger, which is designed to minimize cold end deflection, typically induced by vibration environments. By selecting a relatively large diameter to length ratio along with an appropriate wall thickness and a low conductivity alloy, the cold finger is optimized to achieve a relatively rigid design while maintaining the cooler's thermodynamic performance. This particular attribute is a requirement of integrated Dewar/cooler applications.

In general, a shorter cold finger with larger diameter will cause high conduction losses down the cold finger stem resulting in poorer cooling performance. On the other hand, a larger diameter cold finger can accommodate a larger expansion volume and more heat regeneration material, which results in a higher gross cold production and a higher efficiency regenerator with less flow losses. In designing the thermodynamics of the MX8000, all these performance trade-offs were

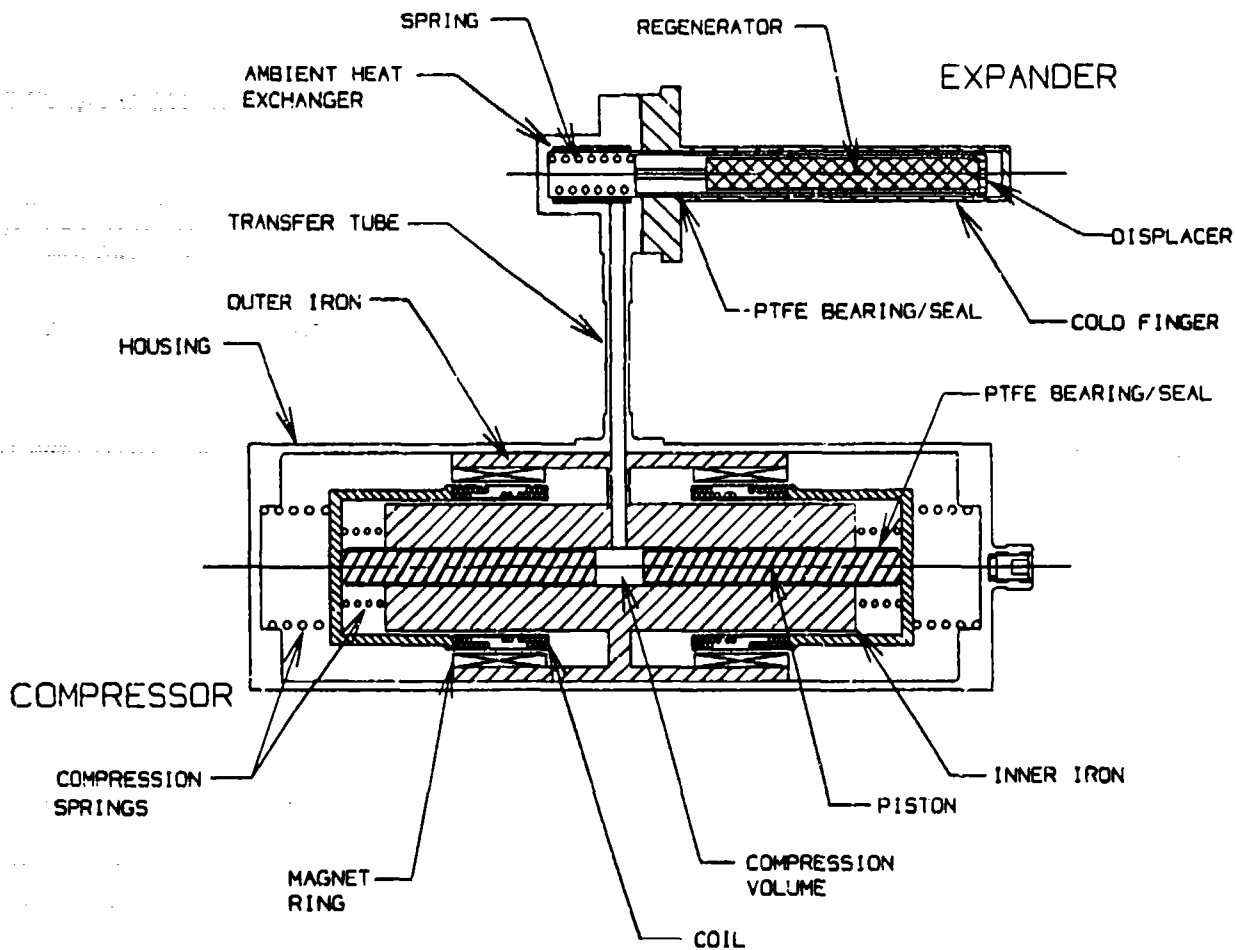


Figure 3. MX 8000 Cooler Configuration

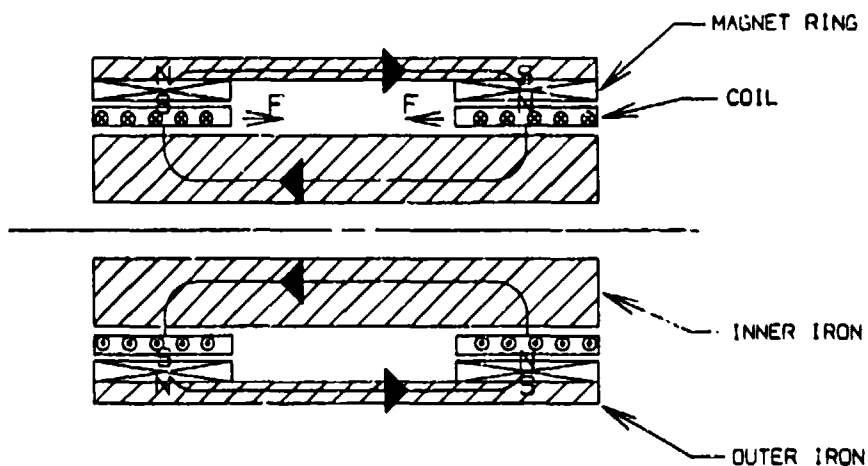


Figure 4. Electro - Magnetic Motor Circuit

carefully analyzed in great detail. The cold finger design is optimized for the best combination of rigidity and thermal performance.

Since the life of the cryocooler is mainly limited by its piston bearing life, another key design consideration is the selection of cooler operating parameters such as speed, stroke, and moving masses to achieve a compact design with long piston bearing life. Analyses of the piston dynamics show that a lower operating speed or a shorter piston stroke, although giving rise to a lower bearing wear rate, also results in a higher piston reciprocating mass in a linear resonant compressor. The difficulty in distributing this higher moving mass along the supported length of the piston bearing is often a source of excessive rocking motion, which causes premature bearing failure.

To achieve long piston bearing life, the MX8000 is designed with low reciprocating piston mass (less than 30 grams). This is accomplished by a cycle speed of 60 Hz and a moving-coil, linear motor approach. This low mass design allows for a very simple, light weight and compact motor which requires no additional structure or guides to support the moving mass. The choice of a relatively high speed of 60 Hz also allows the design of a compact efficient linear motor and a large cooling capacity.

In order to assure commercial market acceptance of the MX8000 cooler, material, piece part and assembly costs were considered during the design phase of the project, resulting in several cost saving features. For example, in production, the motor design utilizes low cost low-carbon magnetic iron. Dual concentric compression springs, used to mechanically locate the pistons at their nominal positions, are always under compression and do not require complex and costly parts to fasten their ends to either the housing or pistons. Another cost saving feature is the housing design which is principally fabricated from thin wall stainless steel tubing.

COOLER CONFIGURATION

The MX8000 cooler operates on the Stirling Thermodynamic cycle. The compressor assembly of the MX8000 consists of two pistons, positioned co-linearly, and working in opposition against a common compression volume situated between them. The compression of the working fluid, helium, is accomplished by the reciprocating motion of the pistons which are driven by two moving-coil, linear motors. The pistons are mechanically fixed to the coil assemblies, and

positioned axially, by dual concentric compression springs already mentioned. The linear motors are composed of moving coils reciprocating at 60 Hz in a DC magnetic field. The magnetic field is furnished by permanent magnets configured in two rings which are radially magnetized in opposite directions. The magnet rings, together with the inner and outer irons, complete the magnetic circuit of the motor which is illustrated in Figure 4. To actuate the motors, an AC voltage is applied to the coils through a pair of flexible leads, which allow the coils to translate in the axial direction. The motors are wired in parallel, causing them to operate 180 degrees out of phase, or in opposition. In this way, the shaking forces generated by the moving masses balance each other providing a compressor with very low output vibration. The pistons utilize a PTFE linear bearing/clearance seal.

The expander assembly's main component is a reciprocating displacer. The displacer is located in its nominal axial position by a helical spring, which is tuned to an optimum spring rate to achieve the proper phase relationship with the compressor's operating frequency. The displacer moves linearly inside of the cold finger, riding on a PTFE bearing/clearance seal at the warm end. A regenerator which is fabricated from stacked wire meshes, resides inside of the displacer body. An annular gas to metal heat exchanger is used to reject the heat of compression from the expander's warm end to the ambient.

DESCRIPTION OF PERFORMANCE TESTS

Prototypes of MX8000 were fabricated and performance tested in an ambient of -40°C , 23°C and 70°C . The performance data including the cooldown times with a thermal mass of 250 joules, the cooling capacities, cold temperatures and AC input power were measured. Figure 5 shows the cooldown times from different soaked temperatures with maximum input power. Figure 6 (a) to (c) show the cooling capacities versus AC input power at cold temperatures of 77, 95 and 120°K respectively. The cooling capacities measured are the active resistive heater load on top of the cold finger and do not include the parasitic Dewar losses. The parasitic Dewar losses are estimated to be 50 to 60 mW.

These results show that the MX8000 cooler offers unmatched efficiencies and cooling capacities among coolers of comparable size including rotary coolers in today's market. At an ambient of 23°C , the MX8000 can produce a cooling of over 500 mW at 77°K . At an ambient of 70°C ,

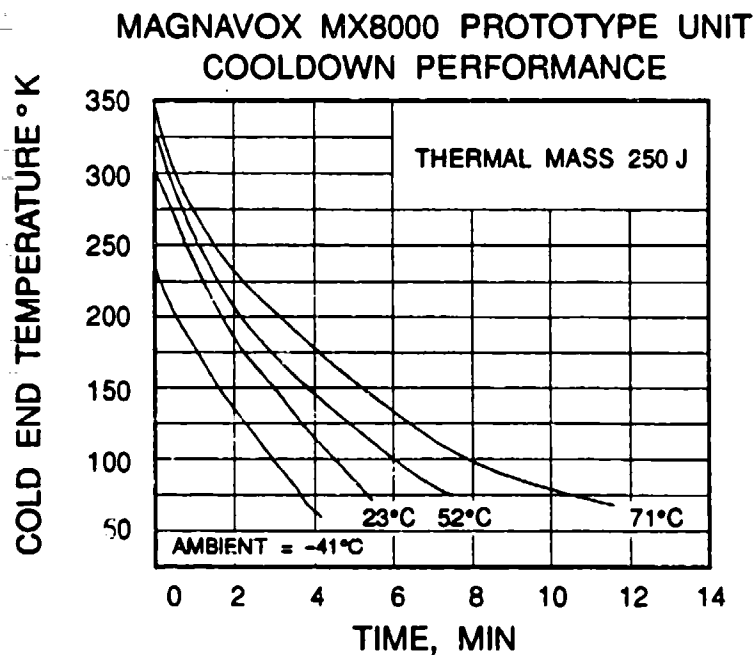


Figure 5.

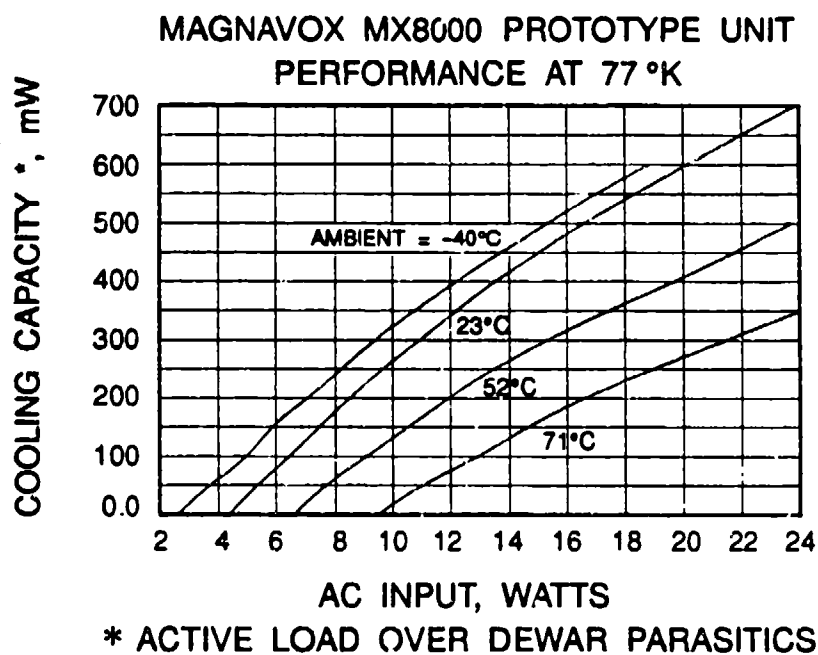


Figure 6 (a).

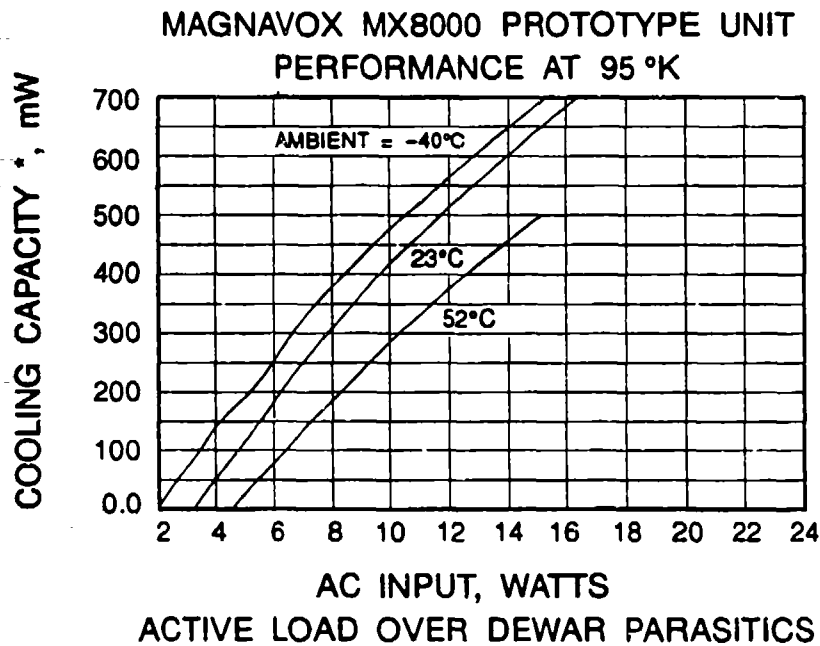


Figure 6 (b).

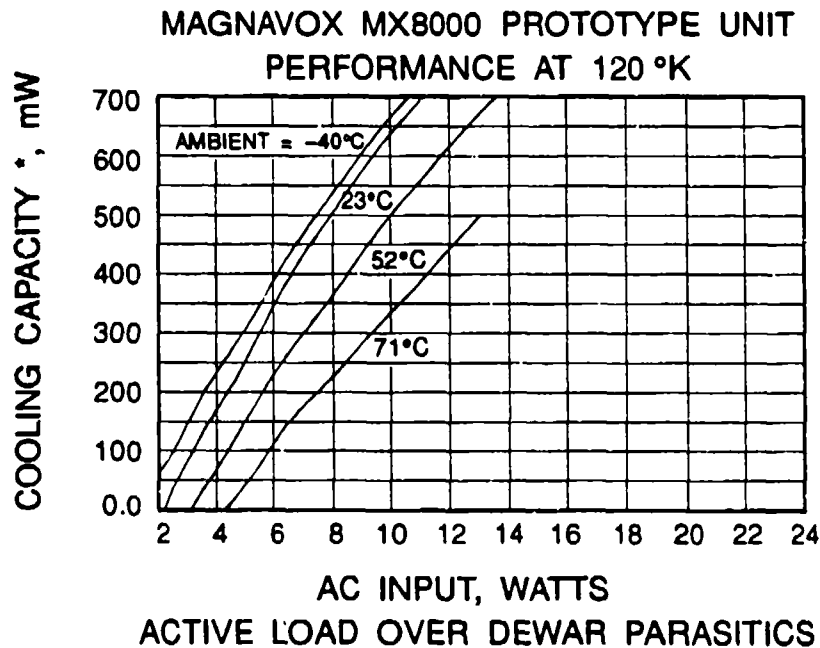


Figure 6 (c).

a cooling capacity of over 300 mW was measured. This performance exceeds the 1/4-Watt Common Module specification which has a cooler size and weight limits far above the MX8000 cooler.

A piston bearing life-test of the MX8000 is well underway at Magnavox. As of November, 1992, a total accumulation of 800 hours has been obtained. The test is run by operating a MX8000 cooler at room temperature with an AC input power of 9.4 Watts and no heat load. A performance test is performed at every 200 hours and no degradation of performance has been observed.

CONCLUSIONS

The design objectives of the Magnavox MX8000 were achieved. The MX8000 was proven to be a compact, highly efficient and reliable cryocooler with unmatched flexibility in cooling performance. The light moving mass and high cycle speed approach to achieve a long-life and compact cooler design was found to be effective and resulted in simple and low cost bearing design.

**PERFORMANCE TEST RESULTS ON A MINIATURE STIRLING
CRYOCOOLER FOR USE IN INTEGRATED DEWAR DETECTOR
ASSEMBLIES**

Philippe AB-DER-HALDEN
L'AIR LIQUIDE - D.T.A.
P.O. Box 15
38360 SASSENAGE (France)

ABSTRACT

AIR LIQUIDE - D.T.A. has introduced on the European market an Integral Stirling Microcooler, the MS.01 (formerly named MC.111) to operate with "Integrated" cooler/Dewar structures. The new designed features introduced by AIR LIQUIDE and the results of on going tests on cooler capacity, power consumption, cooldown time and endurance are presented.

INTRODUCTION AND BACKGROUND

A miniature Stirling cryocooler developed in the late 80's incorporates various innovations to improve MTTF, efficiency, manufacturability, and maintainability. Clearance seal technology is used exclusively, eliminating the deleterious effects of plastic dynamic seals. Direct integration of the detector/dewar on the cold tip of the microcooler provides a significant saving in thermal losses and consequently reduces drastically the input power, size and weight. With this design approach, for example, a common module, 250 milliwatt cryocooler can be replaced by a 100 milliwatt microcooler with IDCA construction as shown on attached sketch A.

In this paper, we provide performance data generated with the following microcooler models :

- the microcooler type MS.00 corresponding to an earlier version of the microcooler (formerly named MS.111).
Four prototypes type MS.00 have been manufactured and evaluated by AIR LIQUIDE in 1991.
- the microcooler type MS.01 incorporating advanced engineering and providing enhanced performances when compared to the earlier version type MS.00. Eighteen prototypes type MS.01 have been manufactured and evaluated by AIR LIQUIDE and various end users in 1992.

Included in this paper are data generated by the thermo-Fluid Dynamics Section of Ford Aerospace and Communication Corporation (FACC), Newport Beach, California on the earlier MC.111 version.

MICROCOOLER DESCRIPTION

AIR LIQUIDE microcoolers type MS.01 are shown on attached photograph with and without an integrated dewar. It is a small, lightweight cooler capable of achieving temperature down to around 60 K. The mass of the MS.01 with its metal dewar/detector assembly is 0.55 kg (about 1.2 pound). This cooler operates on a closed Stirling cycle using helium as the working gas. This is the most efficient thermodynamic cycle for achieving the required cryogenic temperature. Moreover, the cooler operates with moderate helium working pressure (less than 200 psi) which simplifies the compressor design.

When compared to the earlier design MS.00, the MS.01 microcooler incorporates design improvements such as :

- optimization of manufacturing tolerances and dead volumes for enhanced performances,
- development of a highly efficient Closed Cycle Temperature Control (CCTC) system in order to monitor and minimize input power requirement for a given detector temperature,
- interchangeability of the coldfinger with the compressor/displacer subassembly which greatly simplifies the detector/dewar integration and enables an easy maintainability of the microcooler,
- laser welding of coldfinger and overall use of high performance ball bearings for improved reliability.

The microcooler MS.01 can be fitted with three different types of brushless DC motor (hereafter named small, medium and large from U.S. or European origin) in order to accommodate a wide range of cooling requirements.

DEWAR ASSEMBLY

The coldfinger of the microcooler forms the inner wall of the detector's vacuum dewar, while the detector array itself is directly mounted onto the tip of the coldfinger. The outer dewar shell, lead outs, cold shielding and window complete the detector/dewar subassembly. This unit can be assembled, backed, pumped down and tested in the conventional manner prior to integration with the remainder of the cooler itself (compressor/displacer subassembly).

The compressor/displacer subassembly can be functionally checked before integration and can be mated to any detector/dewar subassembly (interchangeability). No special tools or specific expertise are required for this final assembly.

This approach drastically reduces the total heat load imposed on the cryocooler, primarily by eliminating most of the losses associated with the dewar itself. This in turn results in lower input power requirements.

DEWAR HEAT LOADS AND THERMAL MASSES

The Integrated Cooler Detector Assembly with MS.01 microcooler is presently designed and evaluated for two main applications :

- ♦ Low weight and low cost thermal camera with a small size Hg Cd Te (MCT) detector,
- ♦ High performance thermal imaging system with a large size IRCCD Focal plane arrays detector.

The performances of the microcooler have been assessed in two different test dewar which can basically be regarded as representative of the above two main applications and which can respectively be described as follows :

- ♦ A test dewar with static vacuum (welded construction) incorporating a dummy MCT detector with lead wires and connector pins.

Dewar heat load : 107 mW at 25°C ambient.

Thermal mass of dummy detector : about 10 Joules from 298 K to 77 K.

Lead wires and connector pins are attached to a resistance heater to generate an active heat load which simulates chip power dissipation.

- ♦ A test dewar with dynamic vacuum (external vacuum pump) with a copper cap of about 1.5 gramme attached on the cold tip.

Dewar heat load : 150 mW at 20°C ambient

Thermal mass of copper cap : about 155 Joules from 298 K to 77 K.

A ZN 2222 thermocouple is used to monitor the coldfinger temperature for these tests.

The dewar heat load was determined from liquid nitrogen boiloff rate measurements performed at AIR LIQUIDE. The test dewar coldfinger (without the compressor/displacer subassembly) was filled with liquid nitrogen. The measured mass loss rates near the end of boiloff gives a good approximation of the dewar heat load including the conduction down the wall of the coldfinger.

All tests have been made with a Closed Cycle Temperature Control (CCTC) system in order to maintain a constant cold tip temperature after cooldown. This CCTC system uses pulse width modulation of the input waveform, that is controlled by the output of the thermocouple on the coldfinger. By this means, the input power requirement is minimized throughout the ambient temperature range and for any dewar heat load and coldfinger steady state temperature.

COOLING CAPACITY TESTS

Figure 1 represents the input power versus ambient temperature for the earlier version MS.00 and for the dewar heat load of 107 mW. Measurement have been made over the ambient temperature range from - 49°C to + 70°C. The required input power to maintain a coldfinger temperature of 85 K is determined to be 4.5 watts, 5.9 watts and 7.0 watts for ambient temperature of respectively 20°C, 51°C and 70°C.

Figure 2 provides a direct comparison of performance between the earlier version MS.00 and the new version MS.01 equipped with a more efficient and more powerful brushless motor. In the same test conditions without active heat load (vertical axis on figure 2), the input power has been reduced to 5.1 watts and 5.65 watts for ambient temperature of respectively 51°C and 70°C. Furthermore, figure 2 shows that, with a dewar heat load of 107 mW, the new version MS.01 with medium size brushless motor can accommodate an additional detector dissipation (referred as active heat load) of 75 mW for operation up to 70°C ambient or 125 mW for operation limited to 51°C ambient with a cold tip temperature at 85 K.

The region around 77 K to 85 K is of importance to various I.R. detector materials such as Mercury Cadmium Telluride (MCT), IRCCD Focal plane arrays and especially Platinum Silicide (PtSi).

In figure 3, we show the input power needed to cool to 77 K with a dewar heat load of 150 mW. Under those test conditions, the necessary cooling capacity can be achieved with the MS.01 version equipped with the large size brushless motor and the input power do not exceed 10.0 watts for a high ambient temperature of 70°C and a supply voltage of 12.0 volts (as we will see hereafter, a supply voltage of 15.0 volts would be recommended for short cooldown time which can be reduced to 12.0 volts after cooldown for steady state operation at 77 K).

Figure 4 gives the required input power against cold end temperature for the dewar heat load of 150 mW. Minimum cold tip temperature of 73 K has been obtained at an ambient temperature of + 55°C.

COOLDOWN TESTS

Figure 5 and figure 6 provides a direct comparison of the cooldown performances obtained with the earlier version MS.00 and the new version MS.01 equipped with the medium size brushless motor.

With a dewar heat load of 107 mW and a thermal mass at cold tip of 10 Joules, the cooldown time to 85 K achieved with the new version MS.01 at ambient temperature of 20°C and 70°C are respectively 4.1 minutes and 6.5 minutes (to be compared with 6.0 minutes and 9.0 minutes for the earlier version MS.00). The maximum input power during cooldown is about 8.0 watts under those test conditions.

Figure 7 and figure 8 present the cooldown curves down to 77 K for a dewar heat load of 150 mW and a thermal mass at cold tip of 155 Joules representative of a large size Focal Plane Arrays detector. For ambient temperature of 20°C, 55°C and 70°C, the cooldown times down to less than 80 K are respectively 8.0 minutes, 11.0 minutes and 14.0 minutes for a supply voltage of 12.0 volts and 6.5 minutes, 8.2 minutes and 11.5 minutes for a supply of 15.0 volts. In those test conditions, the maximum input powers during cooldown are 10.0 watts for 12.0 volts and 13.0 watts for 15.0 volts. It may therefore be advantageous to cool down large size FPA's detector with a supply voltage of 15.0 volts and reduce this supply voltage to 12.0 volts after cooldown in order to minimize input power during steady state operation at 77 K.

ENDURANCE TEST

During summer and autumn 1992, an endurance test has been carried out with a microcooler MS.01 fixed onto a stainless steel support (no cooling fan was used). A test dewar with dynamic vacuum and heat load of 150 mW was used for this endurance test with the following operating cycles :

- cooldown to 85 K
- steady state operation at 85 K during 2.0 hours
- followed by a non operating period of 0.5 hours

Cooldown time, input power during steady state operation and acoustic noise are verified throughout the endurance test.

The cooler has presently accumulated, without any degradation of performance, 632 cycles at room ambient temperature (20°C to 32°C), therefore 632 cooldowns and 1264 hours of steady state operation at 85 K. This endurance test is still underway with

the objective of achieving a minimum of 1000 cycles (1000 cooldowns and 2000 hours of steady state operation).

An ambient temperature cycling test has been performed on another microcooler MS.01 demonstrating :

- 16 hours of storage at + 70°C ambient (and same at - 40°C ambient)
- cooldown and steady state operation during 6 hours at + 70°C ambient (and same at - 40°C ambient)

This temperature cycling test has been repeated another time without any degradation of performance.

COLDFINGER DISPLACEMENT TESTS

Measurement of cold tip displacements has been performed by the French company METRAVIB R.D.S. with a microcooler MS.01 in operating condition (dynamic test dewar) with increasing rotation speed from 2000 rpm to 4000 rpm.

Indeed, the direct integration of the detector onto the cold tip of the microcooler imposes some limitation on the displacements of the cold tip, mainly in the transverse direction :

- Axis X parallel to the movement of the compressor piston
- Axis Z parallel to the brushless motor axis

Increasing rotation speed was obtained by varying the input voltage from 10 volts to 15 volts. A laser speedometer DISA combined with an analogic integrator KHRON-HITE provides a direct record of the coldfinger displacements.

Relevant values of displacement shall be taken for rotation speeds between 2000 rpm and 2500 rpm corresponding to steady state operation. As shown in figure 9 and figure 10, the lateral displacement of the coldfinger do not exceed 3 μm in either axis X or Z, which is well within the maximum value recommended by detector manufacturers.

ACOUSTIC NOISE TESTS

Acoustic noise tests were performed at FACC in the HARM Low Cost Seeker (HLCS) anechoic chamber on the earlier version MC111. The chamber was designed to suppress radio frequency reflections, but background noise checks verified that it was also suitable for the acoustic noise tests.

Preliminary tests indicated that the cooler produced the highest noise levels when the compressor piston cover faced the sound meter. All subsequent testing was performed using this orientation.

Figure 11 presents the measured sound pressure levels compared to the U.S. Army specification levels. The results were corrected from a distance of 8.2 m to the specification distance of 10 m. They were also corrected for background noise effects. It is seen that the acoustic noise output of the cooler meets the U.S. Army requirement, except at the 2000 Hz frequency region, where it exceeds the specification by up to 4 dB for 15 V operation only. This minor increase above the specification limit can be eliminated by placing the cooler within an enclosure, which is how it is envisaged to be mounted in any similar application.

VIBRATION OUTPUT TESTS

The vibration tests were conducted in the Environmental Test Vibration Laboratory of FACC on the earlier version MC111. The housing vibration was measured with the cooler placed in a soft foam material. Since the natural frequency of the foam was much less than that of the cooler, the foam did not contribute to the measured vibration output.

A 3-axis accelerometer was epoxied to the back of the cooler as shown in figure 12. It was located on the center of the motor axis and at the intersection of the compressor piston and coldfinger axes. The accelerometer was oriented such that the X axis was along the compressor piston axis, the Y axis was down the coldfinger, and the Z axis was along the motor axis.

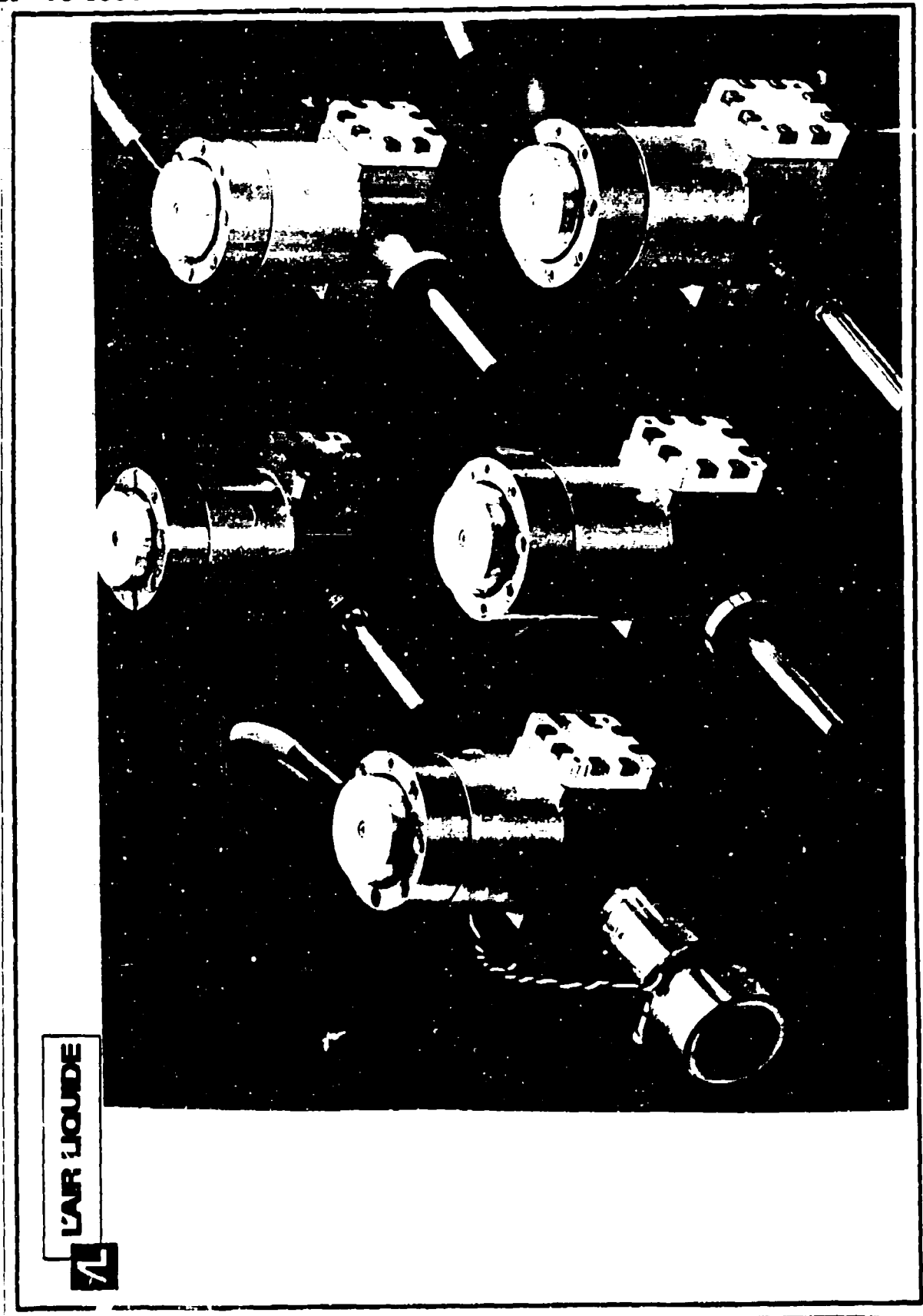
The accelerometer signals were fed into charge amplifiers whose output was displayed on a spectral analyzer. The spectral analyzer was capable of a maximum frequency range of 10 KHz with a filter bandwidth of 12.5 Hz. During the test, the ICDA was not vacuum purged.

Figure 13 shows the results for all three axes at an input voltage of 15 Vdc. The solid horizontal lines on each graph indicated the B2 specification (U.S. Army Specification B2-2303020104, Miniature Stirling Cryogenic Cooler) maximum values). It can be seen that the cooler is generally well within the specification, except for the 50 to 100 Hz bandwidth on the piston axis, and for the 60 to 80 Hz bandwidth on the coldfinger axis.

Figure 13 shows that the fundamental frequency of the cooler is between 40 and 50 Hz as indicated by the first peaks on the piston and coldfinger axis plots. The harmonics damp out around 500 Hz, and the response at higher frequencies above 1000 Hz is due to ringing of the metal housing block. The speed of the motor, along with the reciprocal motion of the pistons, contribute to this effect. The response from 8 to 10 KHz is relatively flat indicating that it will also be flat at higher frequencies.

CONCLUSION

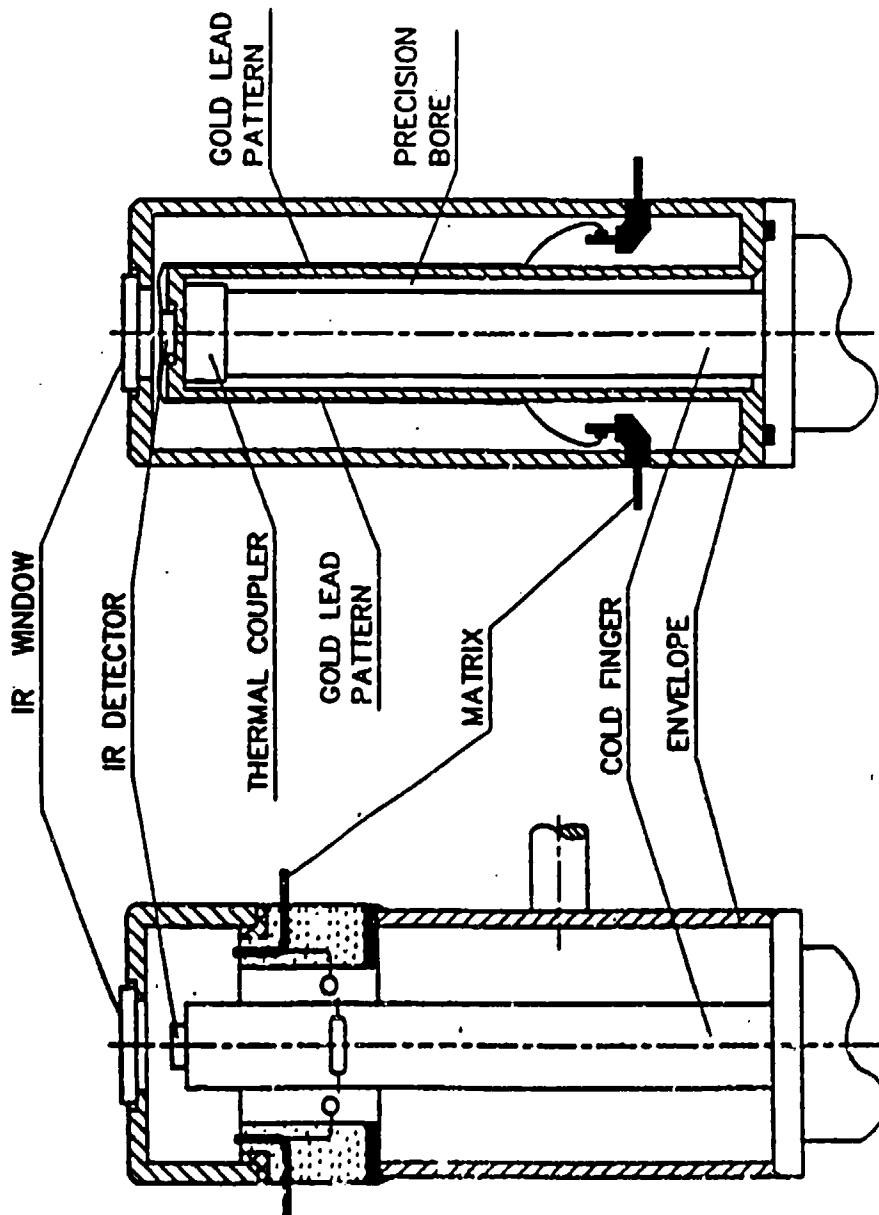
The qualification of the AIR LIQUIDE microcooler MS.01 against military environment applicable to handheld portable thermal camera is underway and will be completed in the first quarter of 1993. The in-house tests carried out by AIR LIQUIDE and the evaluation made by various customers demonstrate the high performances of the Integrated Detector Cooler Assembly (IDCA) based on the AIR LIQUIDE microcooler MS.01. Features such as compacity, low weight and low power consumption with the ability to accommodate a wide range of cooling requirements make the AIR LIQUIDE microcooler a good contender for the future thermal imaging programmes.





Division Techniques Avancées

CRYOCOOLER / DEWAR / DETECTOR STRUCTURES



COMMON MODULE

INTEGRATED DETECTOR COOLER ASSEMBLY

SKETCH A



FIGURE 1

L'AIR LIQUIDE

INPUT POWER
VS. AMBIENT TEMPERATURE

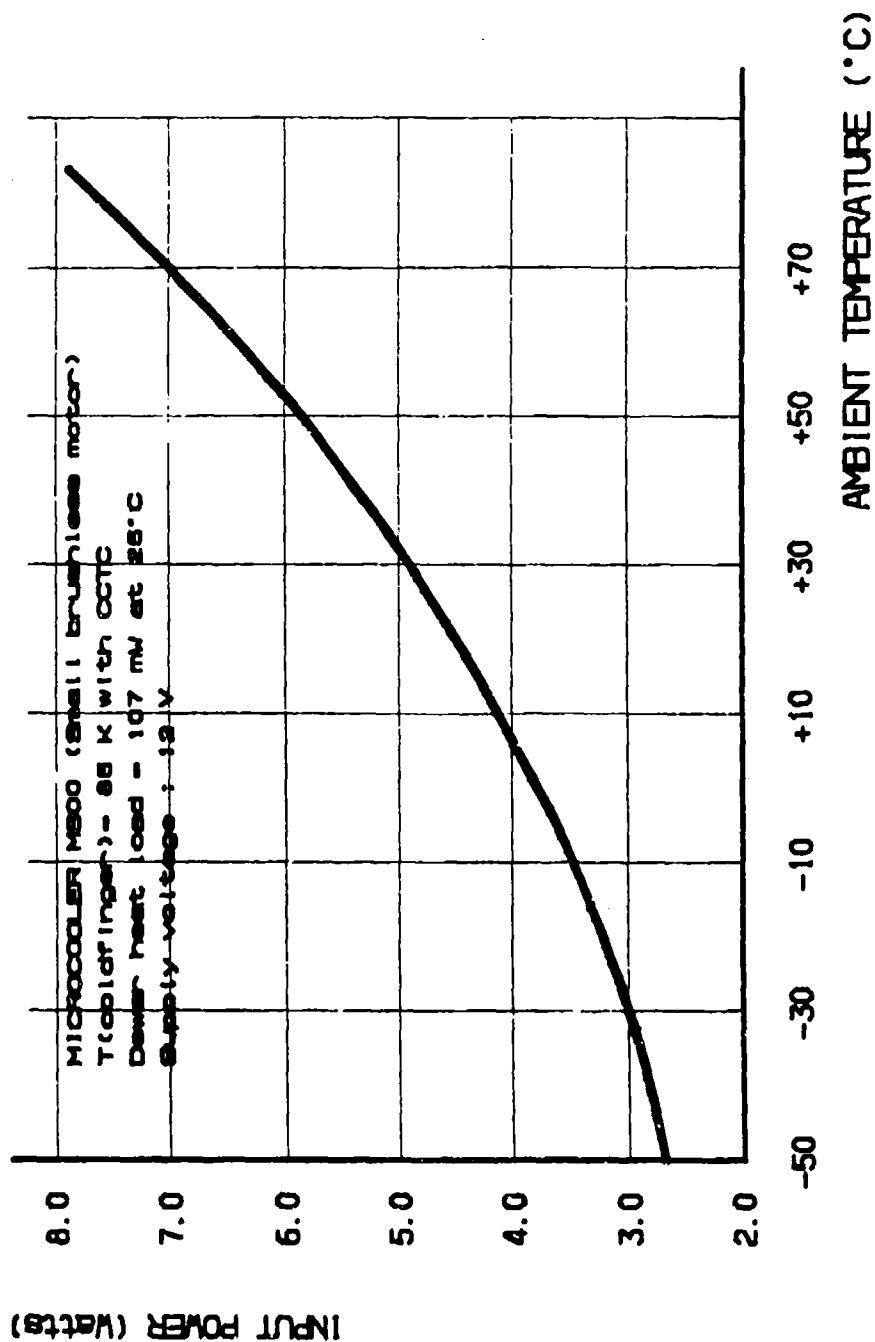
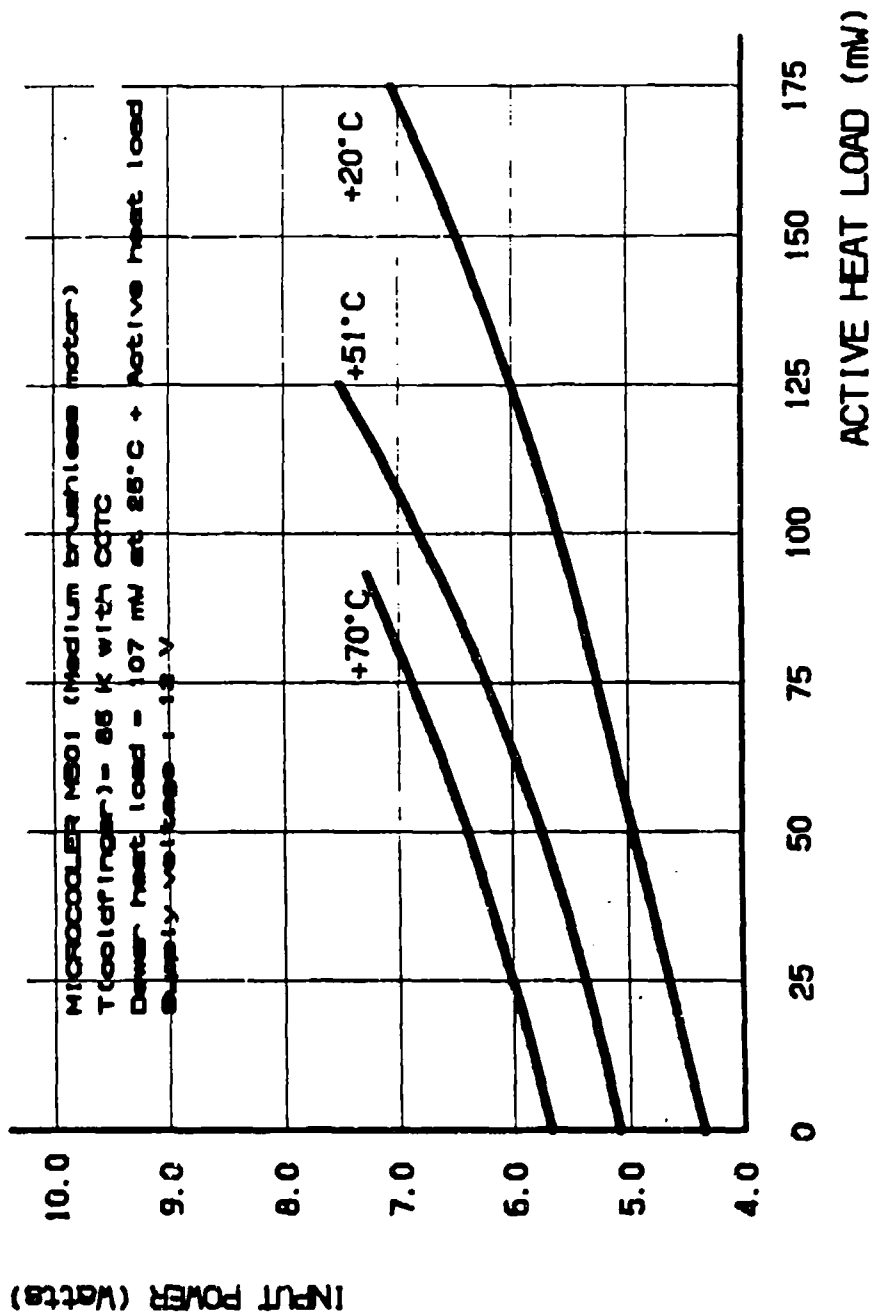


FIGURE 2

INPUT POWER
VS. ACTIVE HEAT LOAD
AT VARIOUS AMBIENT TEMPERATURES

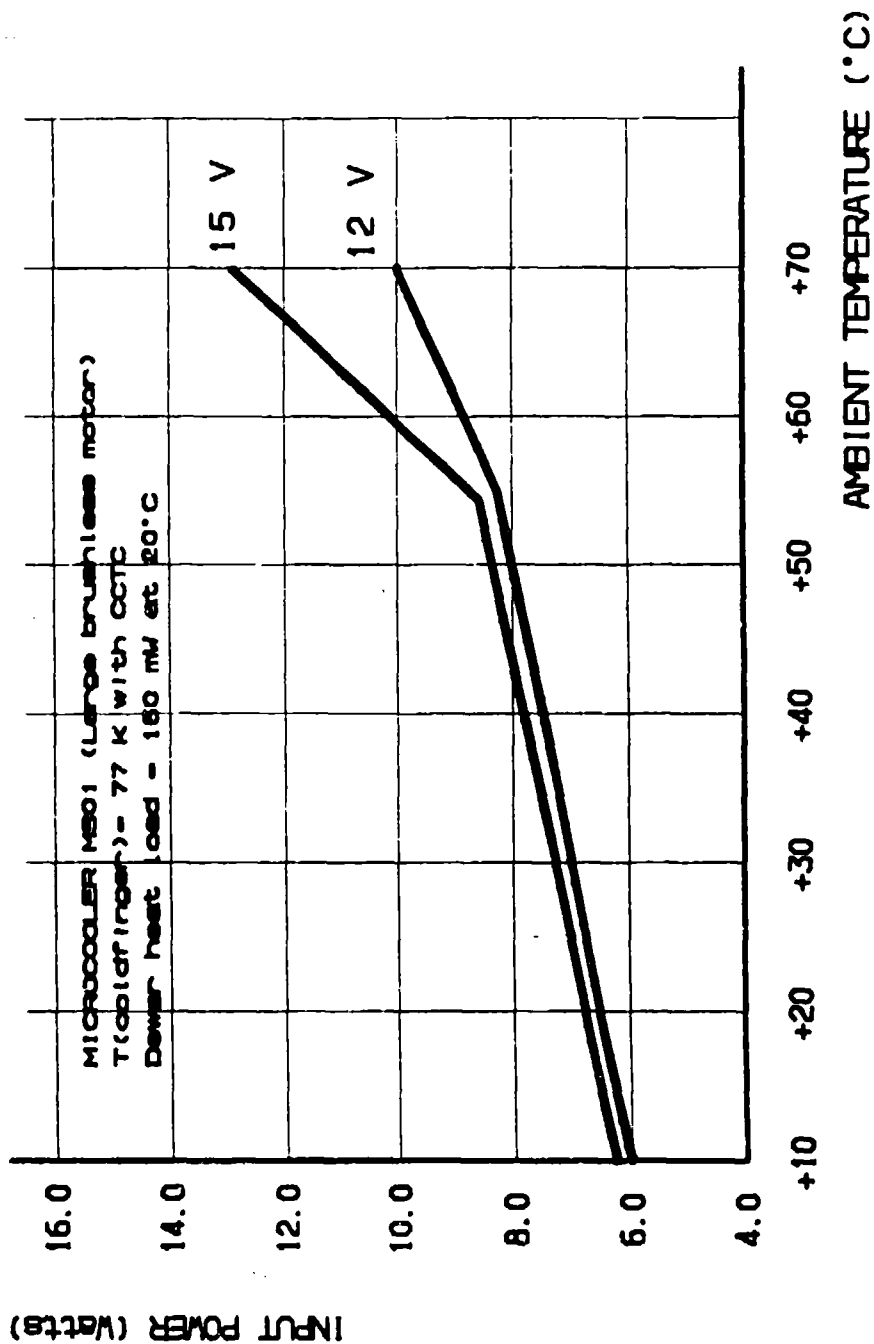


L'AIR LIQUIDE



INPUT POWER VS. AMBIENT TEMPERATURE

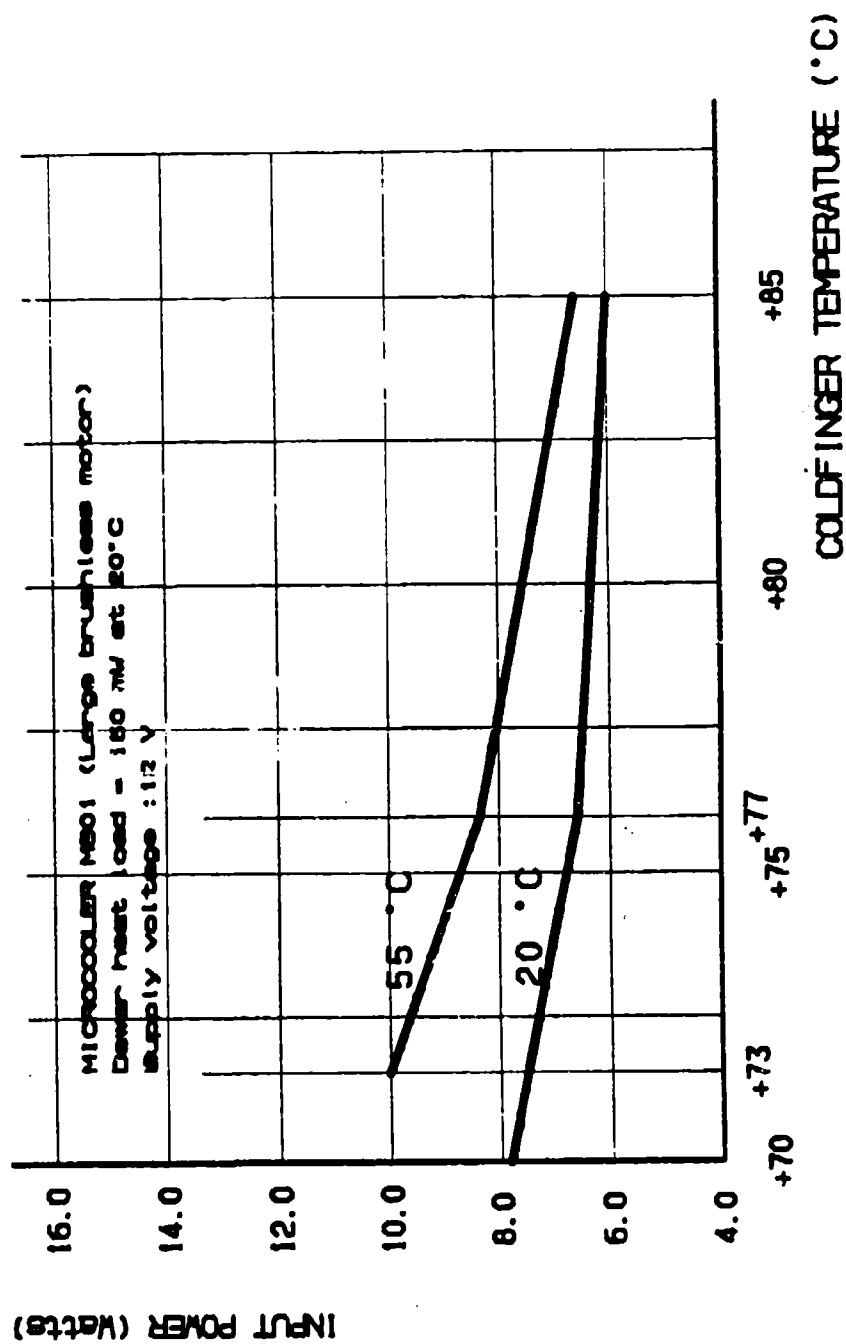
FIGURE 3



L'AIR LIQUIDE

FIGURE 4

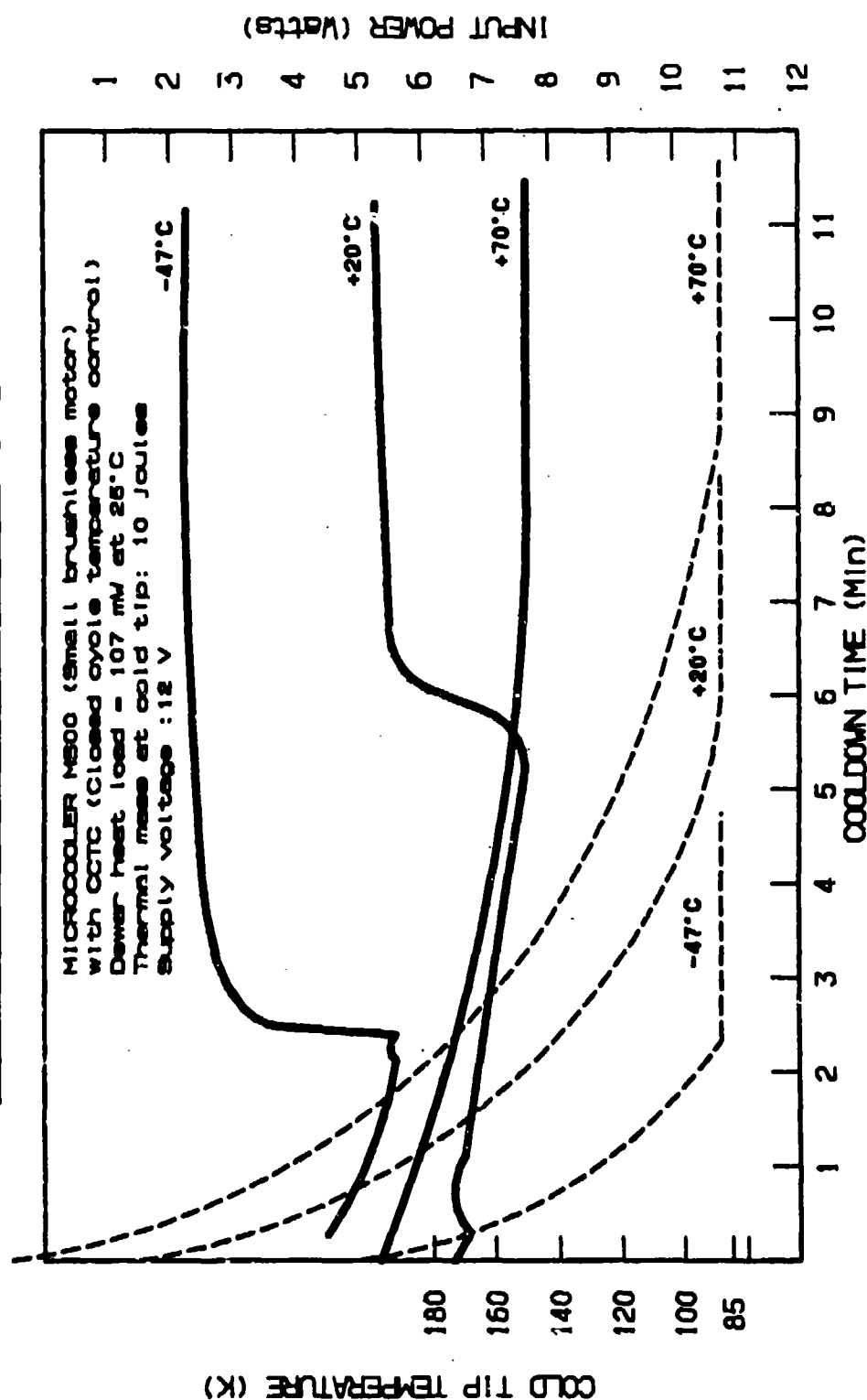
INPUT POWER
VS. COLD FINGER TEMPERATURE
AT VARIOUS AMBIENT TEMPERATURES



L'AIR LIQUIDE

COOL-DOWN TIME AND INPUT POWER AT VARIOUS AMBIENT TEMPERATURES

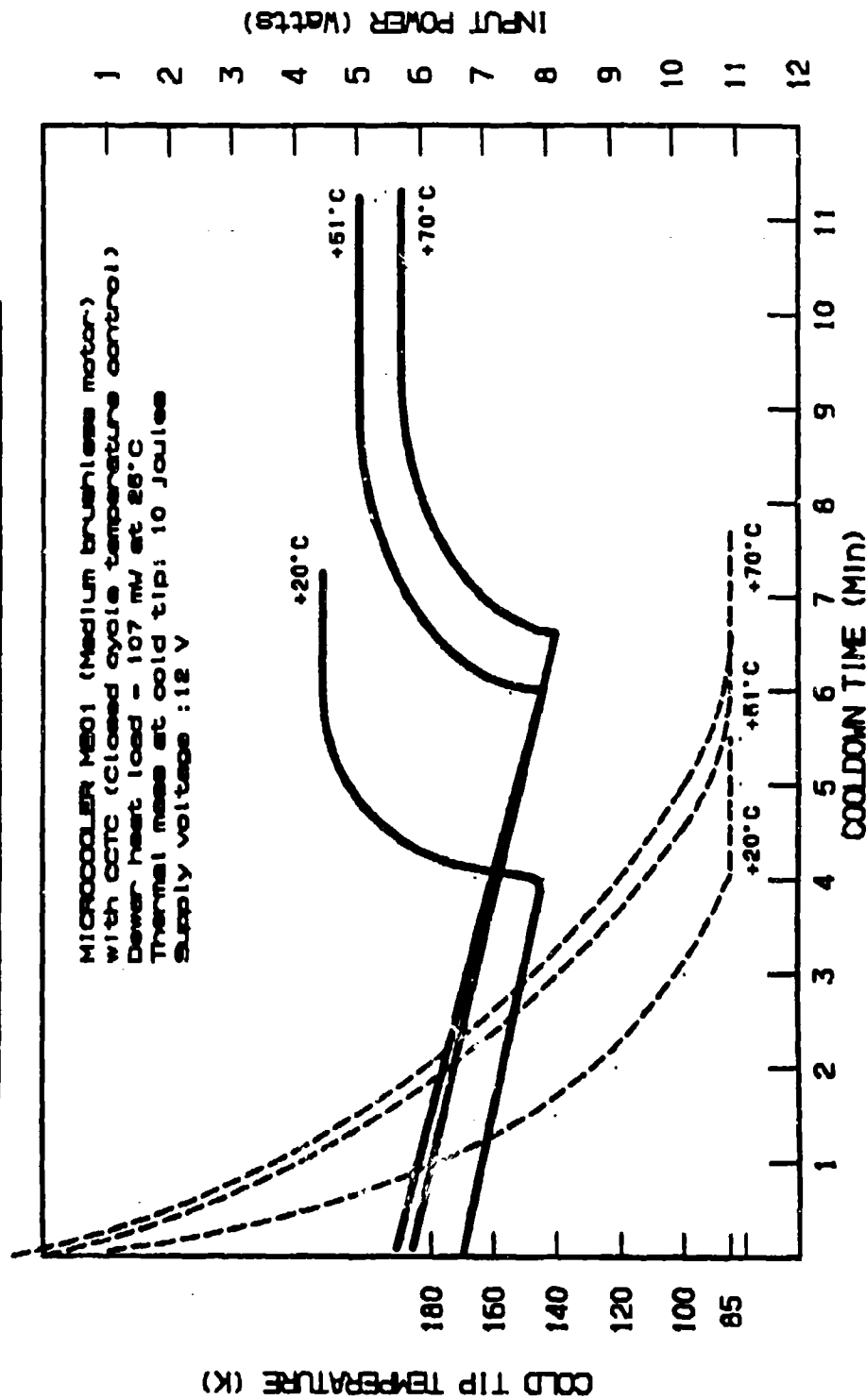
FIGURE 5



L'AIR LIQUIDE

COOL-DOWN TIME AND INPUT POWER AT VARIOUS AMBIENT TEMPERATURES

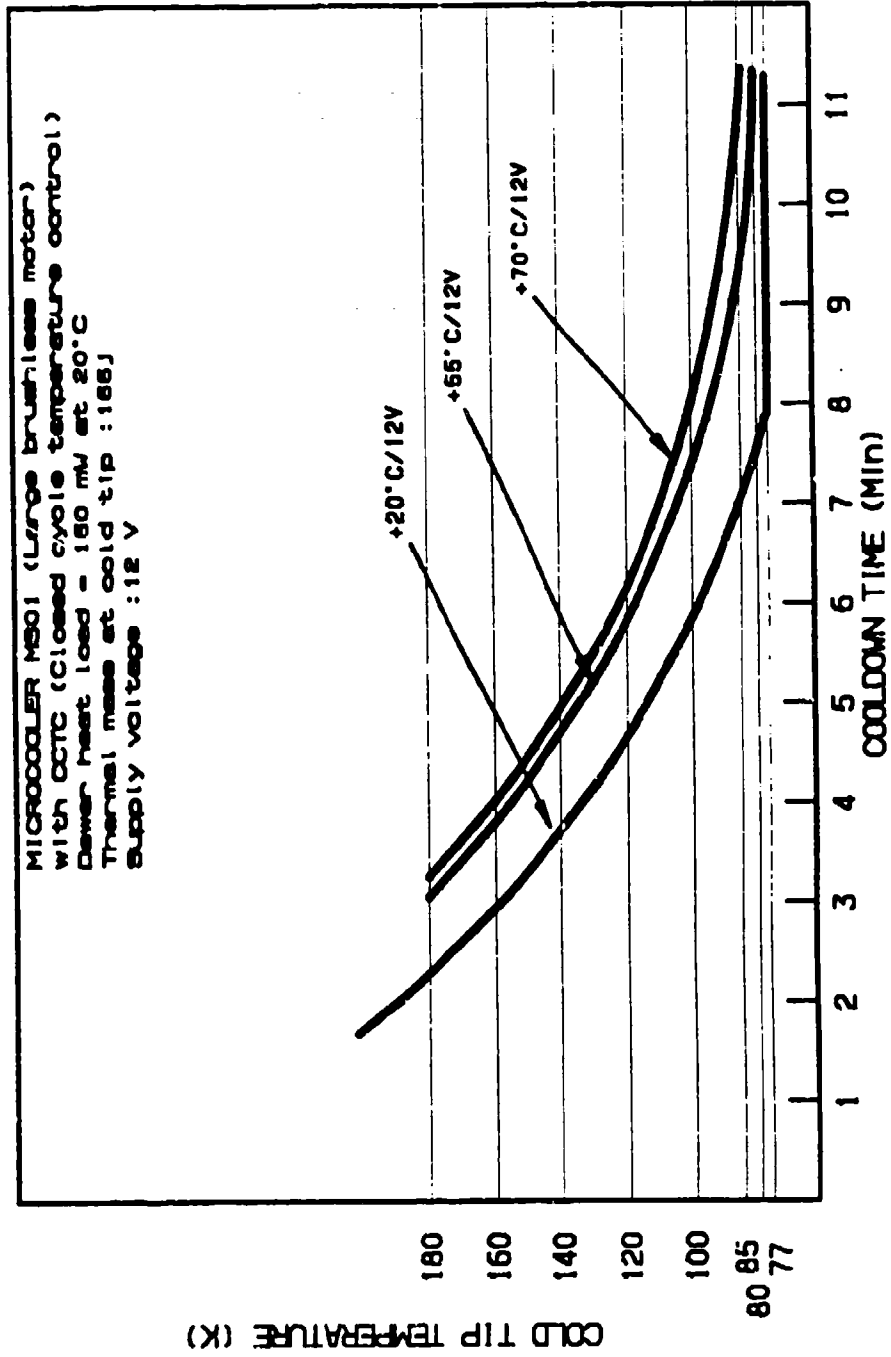
FIGURE 6





COOL-DOWN TIME AND INPUT POWER
AT VARIOUS AMBIENT TEMPERATURES

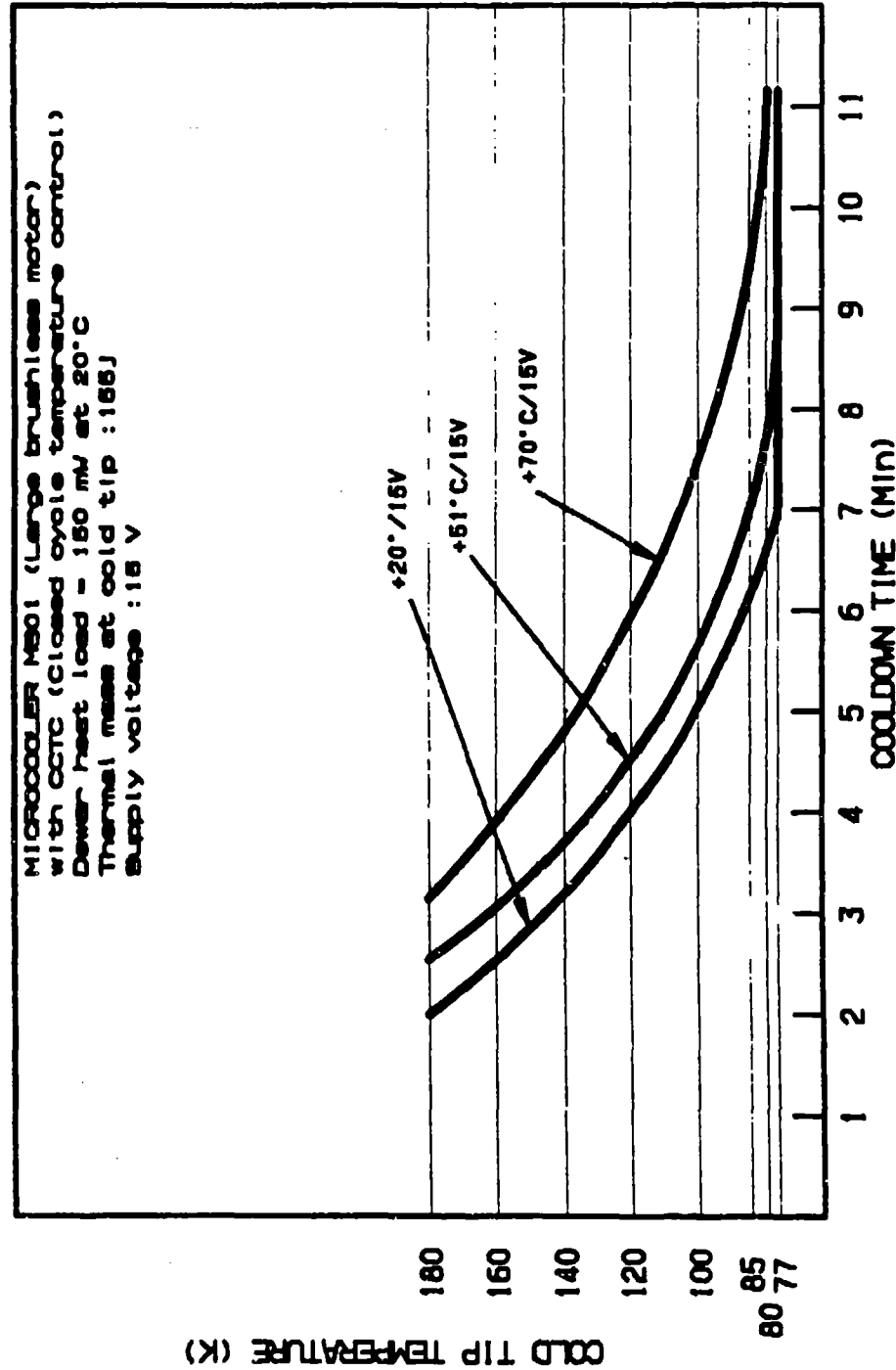
FIGURE 7



L'AIR LIQUIDE

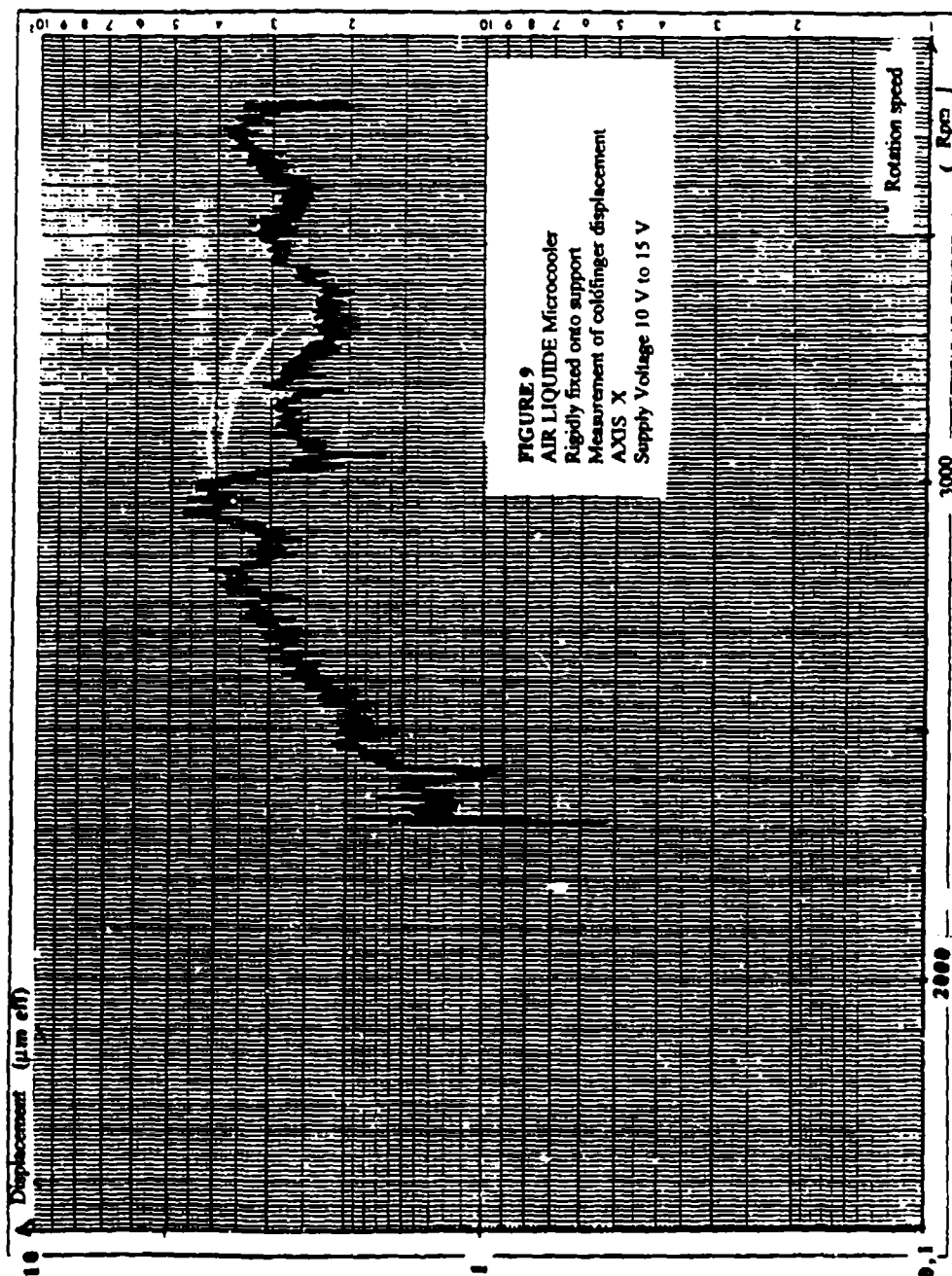
COOL-DOWN TIME AND INPUT POWER AT VARIOUS AMBIENT TEMPERATURES

FIGURE 8





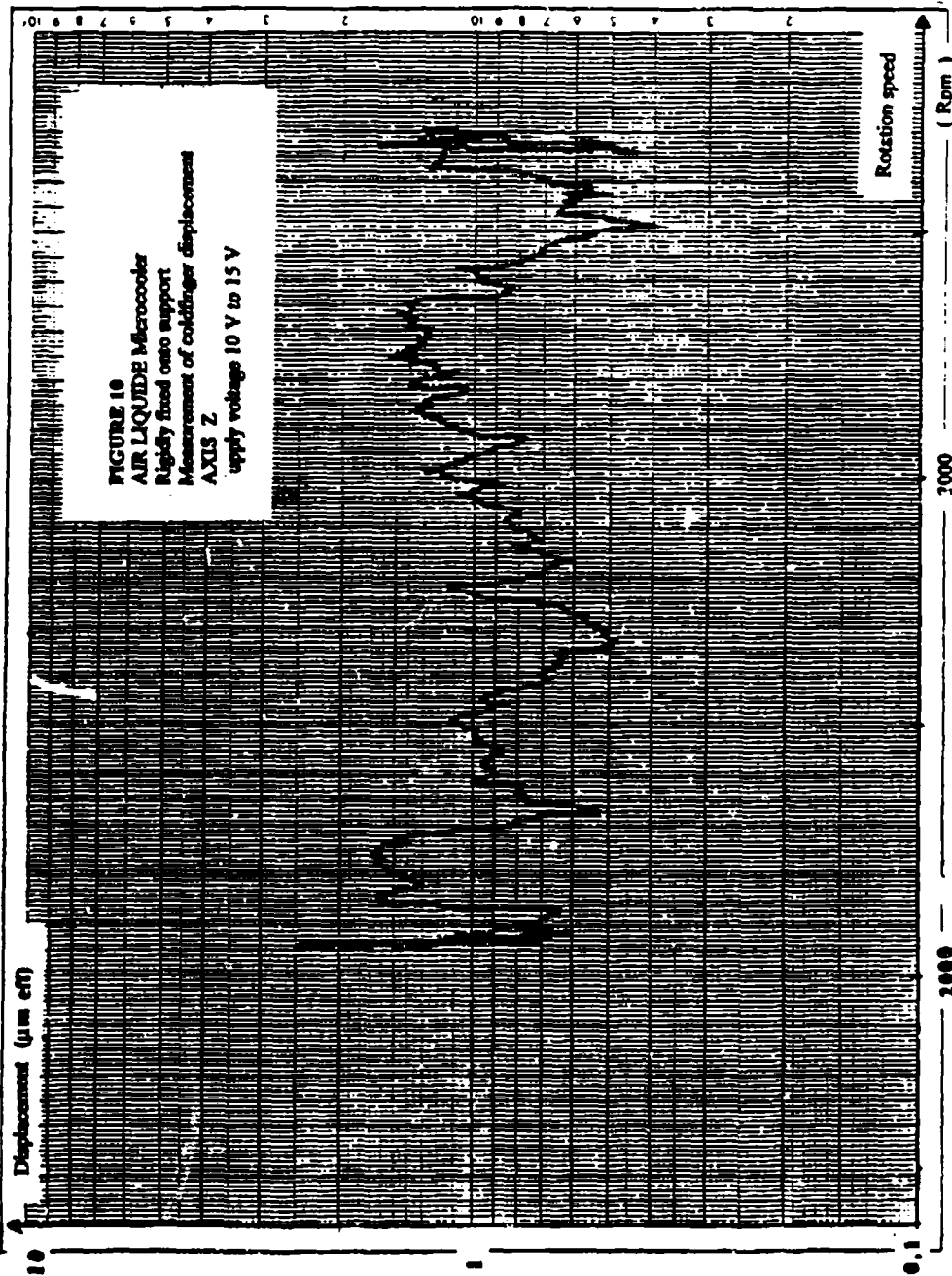
Division Techniques Armes



AIR LIQUIDE
 SAISONNIERE - FRANCE



Division Techniques Avancées



AIR LIQUIDE
 GAZES - LIQUIDES



Division Techniques Avancées

ACOUSTIC NOISE DATA AT VARYING INPUT VOLTAGES

COOLER MC111
AMBIENT TEMPERATURE = 23°C
DISTANCE = 10 M
NO ENCLOSURE AROUND COOLER

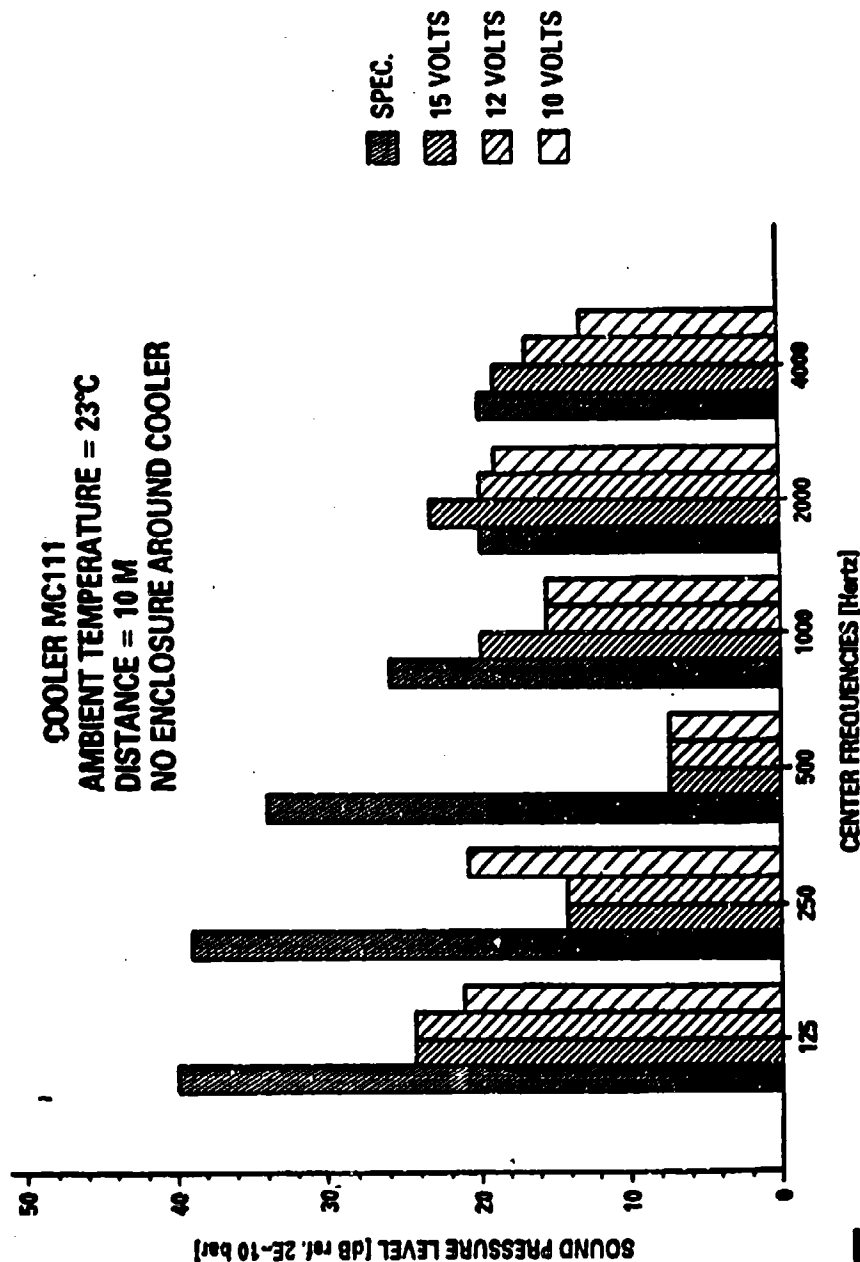


FIGURE 11

L'AIR LIQUIDE
GAS-FLUIDE - FLUIDES



AXIS ORIENTATION FOR VIBRATION TESTS

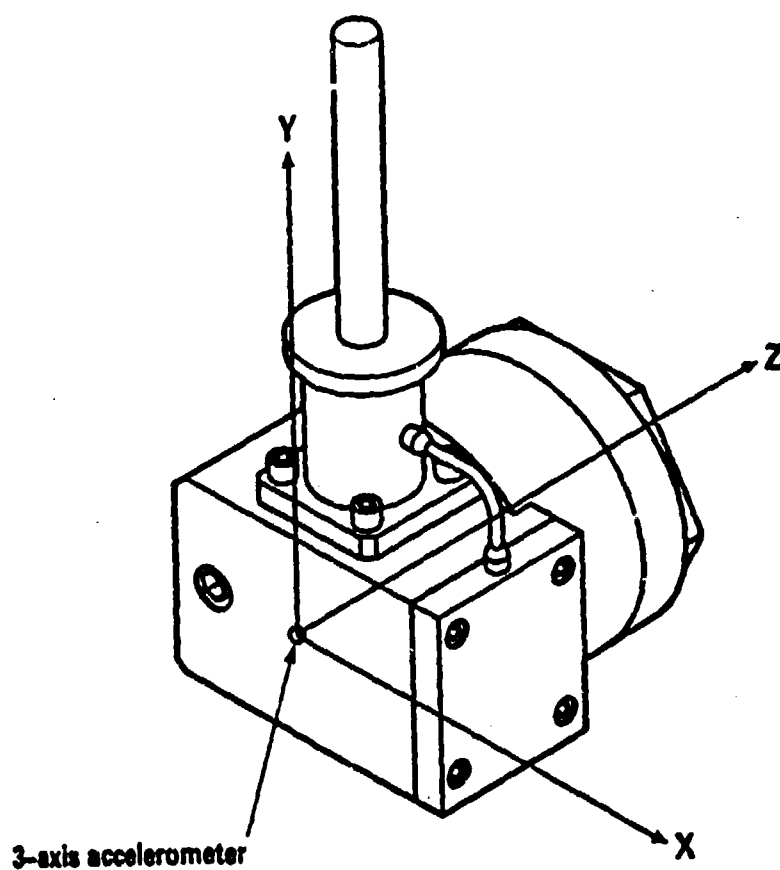


FIGURE 12

 L'AIR LIQUIDE

38360 Sassenage France



Division Techniques Avancées

MOTOR HOUSING VIBRATION RESPONSE

COOLER MC111
INPUT VOLTAGE = 15 VDC
SOFT FOAM MOUNT

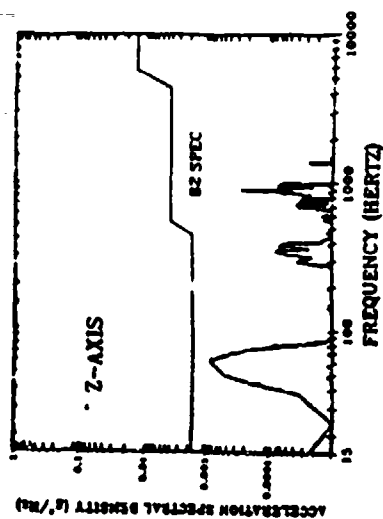
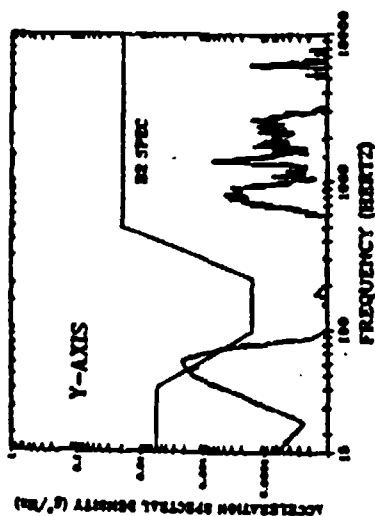
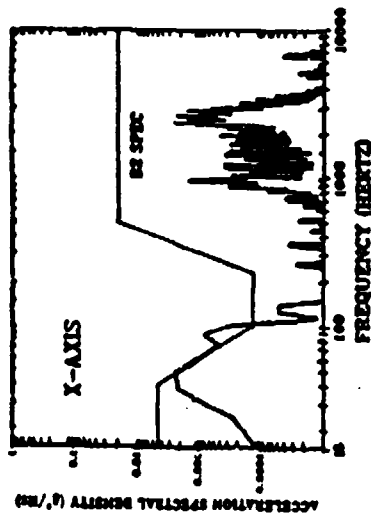


FIGURE 13

L'LAIR LIQUIDE
SAINT-GERMAIN - FRANCE

**VALIDATION OF THE STIRLING REFRIGERATOR PERFORMANCE MODEL
AGAINST THE PHILIPS/NASA MAGNETIC BEARING REFRIGERATOR**

S.W.K. Yuan and I.E. Spradley
Research and Development Division
Lockheed Missiles and Space Co.
Palo Alto, CA 94304

ABSTRACT

A third order computer program known as the Stirling Refrigerator Performance Model (SRPM) has been developed. This program has been proven to be very useful for the study and analysis of Stirling engines. It is also believed to be the only model in the literature that has been validated extensively by the experimental data of various machines. In this paper, the performance of the Philips/NASA Magnetic Bearing Refrigerator (PMBR) is compared with the prediction of SRPM. Comparison is also made with another computer code MS*2 developed by the Mitchell/Stirling Machines/System, Inc. SRPM predicts a cooling capacity of about 5 watts under normal operating conditions with an input power of 224 watts, which agrees with the experimental result obtained by Philips Lab. The effects of compressor stroke, displacer stroke, phase angle, frequency, charge pressure and cold-tip temperature on the efficiency of the refrigerator are also discussed. Considering the lack of knowledge in the exact geometry and operating conditions of the PMBR, excellent agreement was found between the prediction of SRPM and the experimental result. It can be further concluded that SRPM is a generic computer model which can be used to study any Stirling refrigerator regardless of size and cooling capacity.

INTRODUCTION

A third order computer model known as the Stirling Refrigerator Performance Model (SRPM) has been developed for the analysis and design of Stirling refrigerators. Detailed description of this model was presented elsewhere¹. SRPM was originally developed to evaluate the performance of a Lucas built Stirling refrigerator. The design of this cooler is similar to the Oxford refrigerator, with flexure bearings and close-tolerance gas seals. Validation of the SRPM against experimental data of the Lucas unit can be found in Reference 2. In the present paper, the above computer program is used to correlate the experimental data of the Philips/NASA magnetic bearing (PNMB) Stirling refrigerator. The PNMB unit is much bigger than the Lucas refrigerator with larger swept volumes and charge pressure. Since all the basic governing equations used in this computer program are based on the first principles, SRPM should be a generic model which can be used to analyze any Stirling machines regardless of their designs. The results of this paper verify this point. SRPM can also predict natural frequency of the Stirling refrigerator by calculating the gas spring and the motor forces. At the natural frequency, minimum force is exerted on the motor which results in the most efficient point for operation. The predicted natural frequency will also be compared to the experimental value. SRPM is the only model in the literature that has been validated extensively by experimental data of various machines (including: Lucas units, the Philips/NASA unit, the Oxford unit, Atmospheric Infrared Sounder Coolers: configuration A, B and C). This is the second of a series of papers to report these results.

THE PHILIPS/NASA MAGNETIC BEARING REFRIGERATOR

In 1978, Philips Laboratories proposed to design, fabricate and test a mechanical cooler for spaceborne applications, under the sponsorship of NASA Goddard Space Flight Center. This machine was successfully built and tested in

1982³⁻⁶. The refrigerator was driven by two electronically controlled linear motors. The moving elements of the refrigerator were electro-magnetically suspended in small annular gaps (25 microns), by the active magnetic reciprocating bearings. The diameter of the piston is 37 mm, with a displacer diameter of 19.6 mm. The amplitudes of the strokes in the compressor and displacer are 7.3 mm and 3 mm correspondingly. The charge pressure is 227.85 psia. The unit can produce 5 W of cooling at 65K.

MOTOR FORCES AND NATURAL FREQUENCY

The forces exerted on the compressor piston include the metal spring force, the gas spring force and the inertial force. They can be written as

$$F_{sp} = N_{sp} * K_{sp} * P_{stroke} \quad (1)$$

$$F_{gas} = \Delta P * P_{area} \quad (2)$$

$$F_{inrtl} = P_{mass} * P_{acc} \quad (3)$$

where N_{sp} and K_{sp} are the number of springs and spring constant; P_{stroke} , P_{area} , P_{mass} and P_{acc} are the piston stroke amplitude, cross-sectional area, moving mass and acceleration respectively, and ΔP is the pressure drop across the piston. Thus the total force on the motor is

$$F_{tot} = F_{sp} + F_{gas} + F_{inrtl} \quad (4)$$

In general, F_{sp} and F_{gas} act in opposite direction to the inertial force F_{inrtl} . The unbalanced force F_{tot} has to be supplied by the motor. At natural frequency, the spring forces are cancelled by the inertial force resulting in the least force F_{tot} on the motor. For this case, one can estimate the natural or resonant frequency based on the knowledge of the spring forces, the moving mass and stroke amplitude.

$$f_{\text{nat}} = [(F_{\text{sp}} + F_{\text{gas}}) / (P_{\text{mass}} \cdot P_{\text{stroke}})]^{1/2} \quad (5)$$

The Stirling Refrigerator Performance Model provides valuable information on the pressure history in the compression chamber which can be used to calculate the gas spring forces and the natural frequency.

DISCUSSION AND RESULTS

Figures 1 and 2 show the P-V diagrams in the compression and expansion space as predicted by SRPM. The P-V loop in the expansion space traverses in the

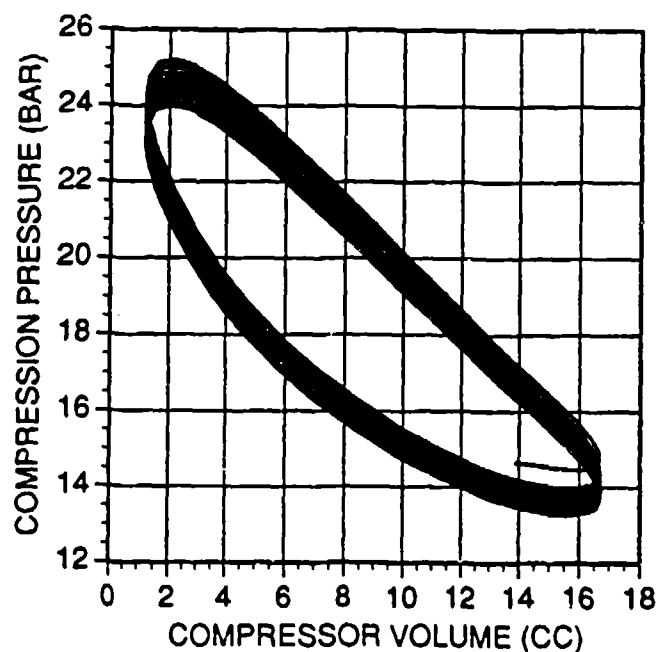


Figure 1. P-V diagram of compression space.

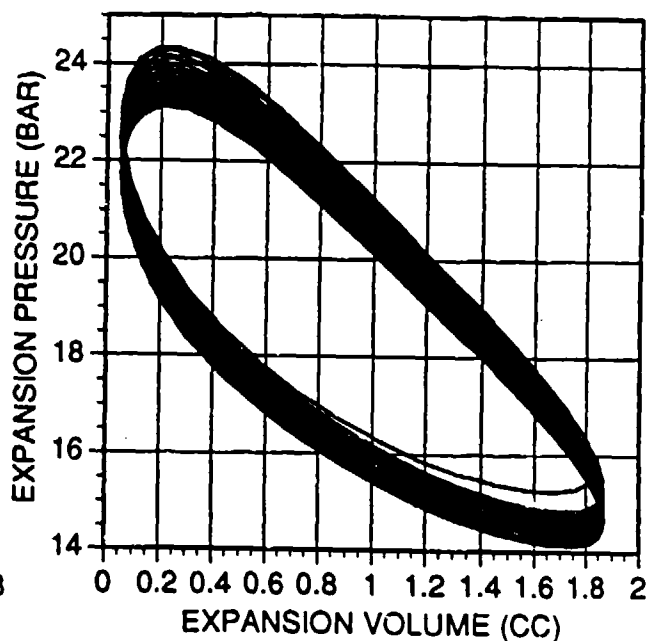


Figure 2. P-V diagram of expansion space.

clockwise direction, indicating work is done by the working fluid. The total area inside the loop times the frequency of operation gives the gross refrigeration of the cooler. The net refrigeration of the machine can be calculated by subtracting all the loss terms from the gross refrigeration. Loss terms at the cold end include

regenerator loss, blow-by loss, static (conduction) loss, etc. In the computer model, the regenerator loss is defined as the net enthalpy carried by the working gas from the hot end of the regenerator to the cold end. For a perfect regenerator, all the heat energy should be intercepted by the matrix material resulting in zero net gas enthalpy being transferred to the expansion space or no regenerator loss. Similarly, the blow-by loss is calculated as the net enthalpy carried by the gap gas to the expansion space.

The P-V loop in the compression space is also invaluable information for the evaluation of cooler performance. The curve travels in anti-clockwise direction, indicating that work is being done on the gas. The total area of the loop times the operating frequency gives the useful work for refrigeration (P-V Work). From the total motor force (Eq. 4) calculated by SRPM one can estimate the electrical current of the motor, if the motor constant is known. With the knowledge of the total resistance in the coil, the I^2R or Joule heating can be obtained. This information can thus be used to calculate the motor efficiency together with the value of the P-V Work. The motor efficiency can thus be defined as

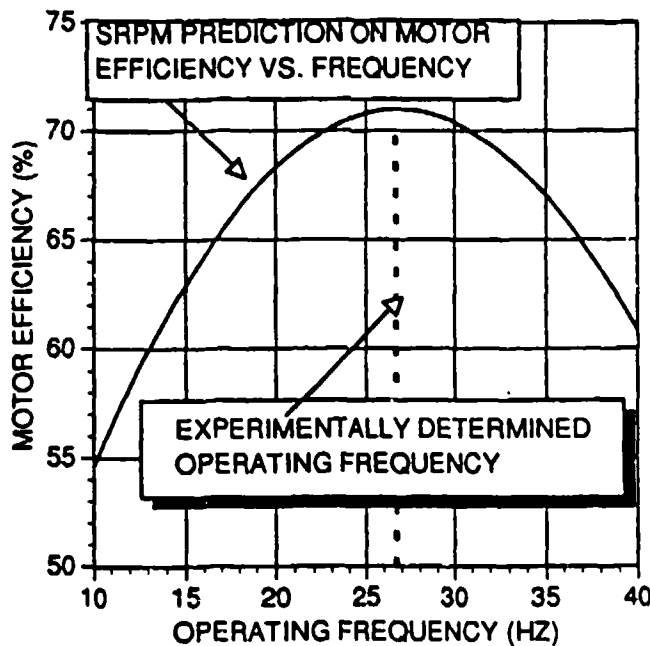


Figure 3. Motor efficiency vs. operating frequency.

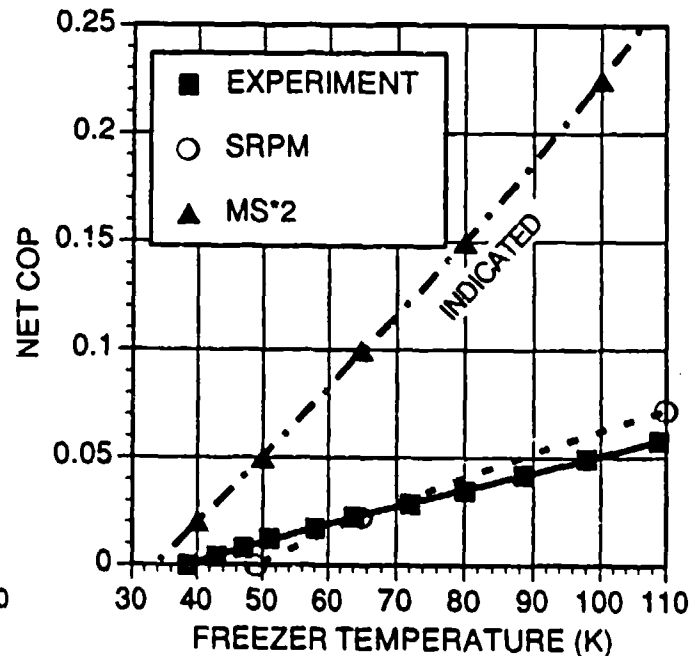


Figure 4. Net cooling vs. cold-tip temperature.

$$\eta = \text{P-V Work} / (\text{P-V Work} + I^2 R) \quad (6)$$

The motor efficiency predicted by SRPM is presented in Figure 3. Note that the experimentally determined operating frequency is 26.7 Hz, which agrees with the natural frequency estimated by the present model. If the operating frequency is lower than the natural frequency, the gas spring force is larger than the inertial force. On the other hand, for frequencies larger than the resonant value, the inertial force is dominant. In either case, the system is not operating efficiently.

The net coefficient of performance (COP) of the refrigerator is plotted as a function of cold-tip temperature in Figure 4. COP is defined as the net refrigeration over the total power input. The figure also includes data predicted by another computer model MS*2 produced by Mitchell/Stirling Machines/System Inc⁷. Note that the COPs reported in Reference 7 are indicated COPs which do not include losses external to the thermodynamic cycle of the fluid, such as mechanical losses, conduction through the mechanism, gas spring hysteresis losses and losses in the electrical drive. (MS*2 does model pressure drop losses, conduction through the

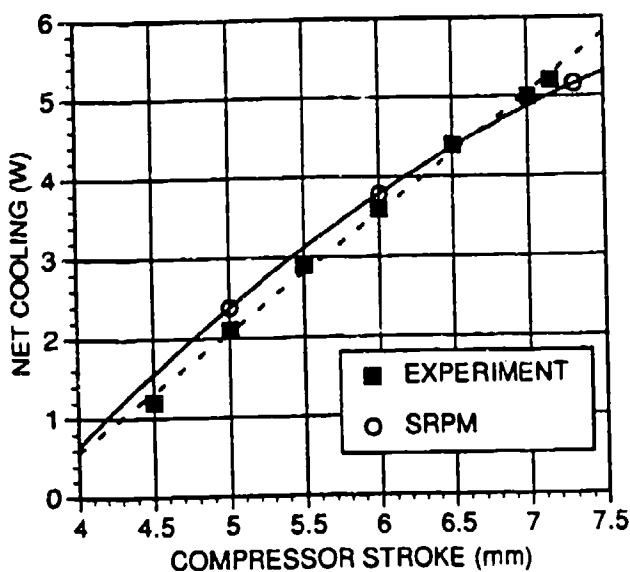


Figure 5. Net cooling vs. compressor stroke.

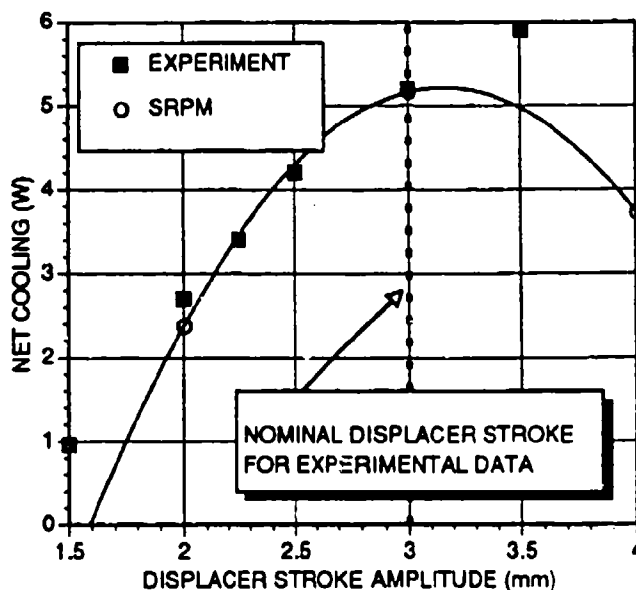


Figure 6. Net cooling vs. displacer stroke.

regenerator matrix, and irreversibilities arising from both heat transfer and cyclic variation in regenerator matrix temperature). Typical external losses at the cold end can be as large as 50% to 80%. Considering these effects, the results obtained by MS² are not inconsistent with the prediction of SRPM or the test data.

Net cooling as a function of the compressor stroke amplitudes is presented in Figures 5. The SRPM data assume that the same swept volume ratio is maintained between the compressor and displacer. Varying the compressor stroke alone result in much lower net cooling (because the optimal swept volume ratio is not maintained). The experimental data show almost a linear relationship between net cooling and compressor stroke amplitude. On the other hand the analytical data tend to indicate a slight tail-off of cooling capacity at high compressor strokes. Figure 6 shows the net cooling versus displacer amplitude. The largest displacer amplitude used in the experimental data was 3.5 mm. This might be the maximum capable stroke of the machine. The test data show an asymptotic increase in net cooling as the displacer stroke is increased. From the trend of the data, the optimal displacer amplitude might lie between 3.5 and 4 mm. SRPM predicts an optimal displacer amplitude of 3.2 mm concurring with the operating displacer amplitude of

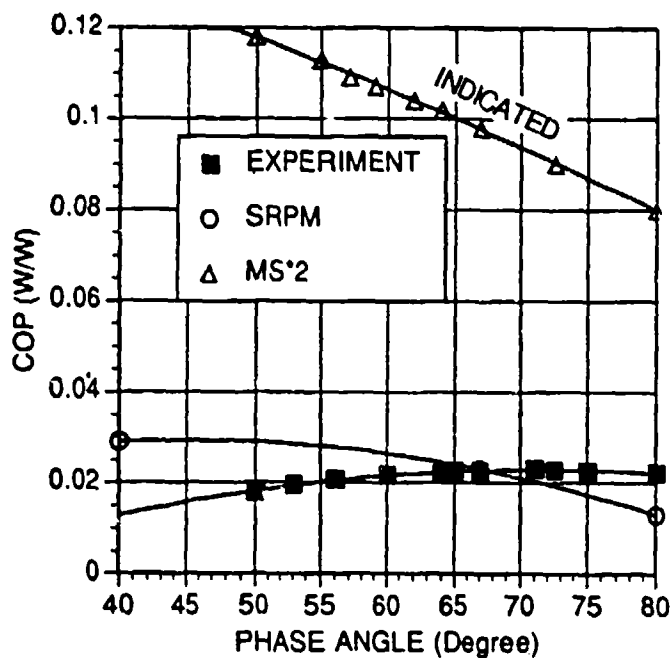


Figure 7. COP as a function of phase angle.

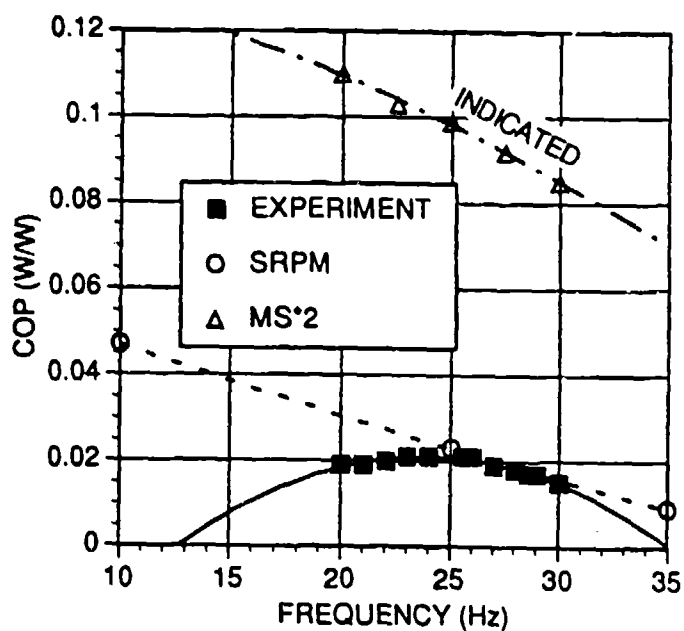


Figure 8. COP as a function of frequency.

3 mm. It was assumed that the displacer piston is not biased as the stroke is reduced. Biasing the displacer towards the cold-tip reduces void volume and results in better performance.

The coefficient of performance is plotted as functions of phase angle and operating frequency in Figure 7 and 8 respectively. While the magnitude of COP predicted by SRPM is very close to the experimental data, the optimal value for the best COP is quite different from the test data. This is true for both phase angle and frequency. Both SRPM and MS² show an increase of COP with decrease in frequency, but the test data indicate an optimal value at about 25 Hz. Possible explanations for those discrepancies include uncertainty about geometry, especially dead volumes and their distribution. It is also not clear if the operating parameters are re-optimized at various frequencies and phase angles, during collection of these experimental data. The SRPM values were obtained assuming that only one variable was varied at a time. The net cooling and input power versus mean pressure are plotted in Figure 9 and 10 respectively. Excellent agreement is found between SRPM and the experimental result. As the mean pressure of the system is

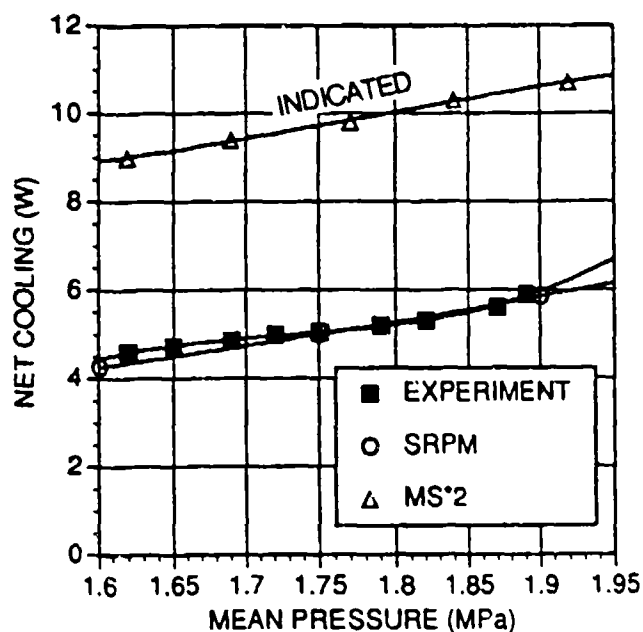


Figure 9. Net cooling vs. mean pressure.

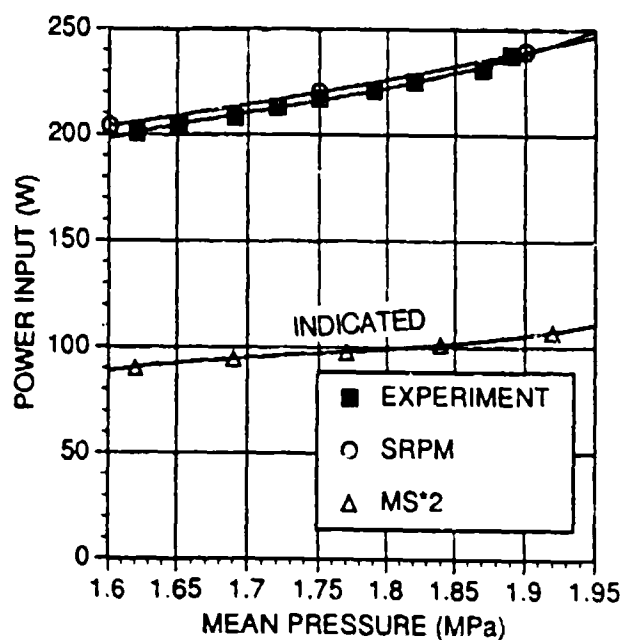


Figure 10. Power input vs. mean pressure.

increased, the total net refrigeration is larger. However, the total input power also goes up. The combination of these factors result in a coefficient of performance that is almost insensitive to the change in charge pressure (within the range of experimental data).

Table I. Summary of results predicted by SRPM and MS*2 and their comparisons with experimental data.

	EXP.	SRPM	MS*2 [@]
COLD TEMP	64.6 K	65.3 K	65.0 K
NET REFR.	5 W	4.95 W	9.8 W
POWER	220 W	224 W	105 W
NAT. FREQ	26.7 Hz	^27 Hz	-----

@ Values for MS*2 do not include certain losses

A summary of the test data and results obtained by SRPM at normal operating condition of the machine can be found in Table I (including cold-tip temperature, net refrigeration, total input power and natural frequency). SRPM predicts a cooling capacity of 5W at 65K with an input power of 224W. This agrees with the experimental data to within 2%. The prediction on natural frequency is also extremely close to the test result.

CONCLUSIONS

The Stirling Refrigerator Performance Model provides excellent prediction of cooler performance as a function of cold-tip temperature, mean pressure, compressor stroke and displacer stroke. SRPM gives the correct order of magnitude

of COP versus phase angle and frequency. Unfortunately, the prediction on optimal value for best performance is off. However this can be attributed to the uncertainty in the presence and distribution of dead volumes in the system. The model is also capable of predicting the natural frequency and motor efficiency of the refrigerator.

These results further emphasize that SRPM can be utilized as a generic computer model which can analyze any Stirling refrigerator, regardless of size or design.

ACKNOWLEDGEMENT

One of the authors SWKY would like to thank Mr. Matt Mitchell of the Mitchell/Stirling Machines/System Inc. for his discussion on the modelling of Stirling engines.

REFERENCES

- 1) Yuan,S.W.K. and Spradley,I.E., A Third Order Computer Model for Stirling Refrigerators, *Advances in Cryogenic Engineering*, Vol. 37B, p. 1055, 1992.
- 2) Yuan,S.W.K., Spradley,I.E., Yang,P.M. and Nast,T.C., Computer simulation Model for Lucas Stirling Refrigerators, *Cryogenics*, Vol. 32, No. 2, p. 143, 1992.
- 3) Stolfi,F.R., Parametric Testing of A Long Life Linearly Driven Stirling Cryogenic Refrigerator After 20,000 Hours of Operation, *Proc. of the 4th International Cryocoolers Conference*, Easton MD, Sept. 25-26, p. 241, 1986.
- 4) Daniels,A. et al., Magnetically Suspended Stirling Cryogenic Space Refrigerator: Test Results, *Advances in Cryogenic Engineering*, Vol. 29, p. 639, 1984.
- 5) Stolfi,F.R., "Final Report for Parametric Testing of Engineering Model Refrigerator", Philips Laboratories Report PL-8-CR84-0216, February 1984.
- 6) Stolfi,F.R. et al., "Design and Fabrication of a Long-Life Stirling Cycle Cooler for Space Applications", Philips Laboratories, March 1983.
- 7) Bauwens,L. and Mitchell,M.P., Regenerator Analysis: Validation of the MS*2 Stirling Cycle Code, *Proc. of the XVIIIth International Congress of Refrigeration*, August 10-17, Montreal, Canada, 1991.

THE MS*2 STIRLING CYCLE CODE

Matthew P. Mitchell
MITCHELL/STIRLING MACHINES/SYSTEMS, INC.
Berkeley, California

INTRODUCTION

The MS*2 Stirling Cycle Code models the indicated performance of all types of Stirling Cycle machinery. Unlike, for example, the Lockheed SRPM code, the MS*2 code does not attempt to model machine-specific losses such as mechanical losses, certain conduction losses, gas spring hysteresis losses or electrical losses in the drive system.

At cryocooler temperatures, the losses not modelled by the MS*2 code are large relative to the indicated refrigeration. Thus, for example, the MS*2 code predicts indicated refrigeration and COP substantially greater than the measured refrigeration and COP for the Philips 65K magnetic-bearing cryocooler.(1) That relationship is correct; a significant part of the indicated refrigeration is eaten up by losses not modelled by the MS*2 code.

Although the MS*2 code does not model machine-specific losses mentioned above, those losses can be calculated independently with relative ease. The MS*2 indicated results can then be adjusted appropriately in a spreadsheet to generate a prediction of overall, net performance for a variety of operating conditions.

Accurate calculation of indicated performance is particularly important because optimization of indicated performance offers the best hope of obtaining maximum overall, net performance after deducting the losses not modelled. Good indicated performance is the best place to start the design process. The rigorous computational scheme embodied in the MS*2 code has been reported elsewhere. (1, 2, 3)

EXPERIENCE AND VALIDATION

The MS*2 code has been under development for a number of years. (1, 2, 3). It has accumulated in excess 40,000 running hours on PCs and CRAY supercomputers. It has been validated by reference to test results of various Stirling machines, including engines as well as refrigerators. (1) Performance of the Sunpower 2A high-temperature refrigerator has recently been modelled using dimensions and operating conditions of which some were published (4) and some supplied by Sunpower, but not previously reported. The MS*2 code was run for a range of temperatures from 179 K to 241 K. The results were then adjusted for conduction losses and drive motor efficiency as reported by Sunpower as shown in Table 1.

TABLE 1

SUNPOWER REFRIGERATOR 2A

Power in: 235 W
 Th: 289 K
 Charge: 5873 g

Piston stroke: 16 mm
 Displacer stroke: 12.1 mm
 Phase angle: 60 degrees

(1)	(2)	(3)	(4)	(5)	(6)	(7)	(8)	(9)	(10)	(11)	(12)	(13)
Cold	Initial MS*2			Heat	Adjusted MS*2		Test results		SAUCE		GLIMPS	
Temp	P	Power	Refrig	Leak	Refrig	%	Refrig	%	Refrig	%	Refrig	%
(K)	(MPa)	(W)	(W)	(W)	(W)	Carnot	(W)	Carnot		Carnot		Carnot
241	1.743	219.2	239.5	8.16	249	21.1	260	28	245	26.3	135	14.5
236	1.734	221.9	228.3	9.01	233	22.2	240	29	220	26.6	115	13.9
231	1.72	229.2	223.6	9.86	219	23.4	215	29	195	26.4	95	12.8
224	1.698	239.6	216.9	11.05	202	24.9	185	30	155	24.2	70	10.9
216	1.665	247.9	205	12.41	182	26.2	170	30	130	23.7	40	7.3
209	1.644	256.2	195.2	13.6	165	26.9	145	29	90	18.6	5	1
202	1.614	263.3	184.5	14.79	150	27.5	120	27	60	13.9	-5	-1.2
195	1.592	271.5	174.5	15.98	135	27.7	95	25	30	7.8	-30	-7.8
187	1.538	276.6	160.1	17.34	119	27.5	70	21	0	0	-50	-14.7
179	1.519	284.9	148.2	18.7	104	27.1	50	17	-25	-8.3	-75	-24.8

Refrigeration is adjusted in the proportion that input power bears to 235 W.
 Conduction loss is then removed at: .17 W/K.

Unfortunately, Sunpower was unable to supply exact data on piston stroke, displacer stroke or phase angle for all temperatures measured. All of these parameters affect the predictions of the MS*2 code, and there is good reason to believe that they vary with changes in the temperature in the freezer. Accordingly, a completely satisfactory comparison is not possible. Despite this qualification, the comparison is revealing.

REFRIGERATION
 Sunpower 2A, Data Set 3/15

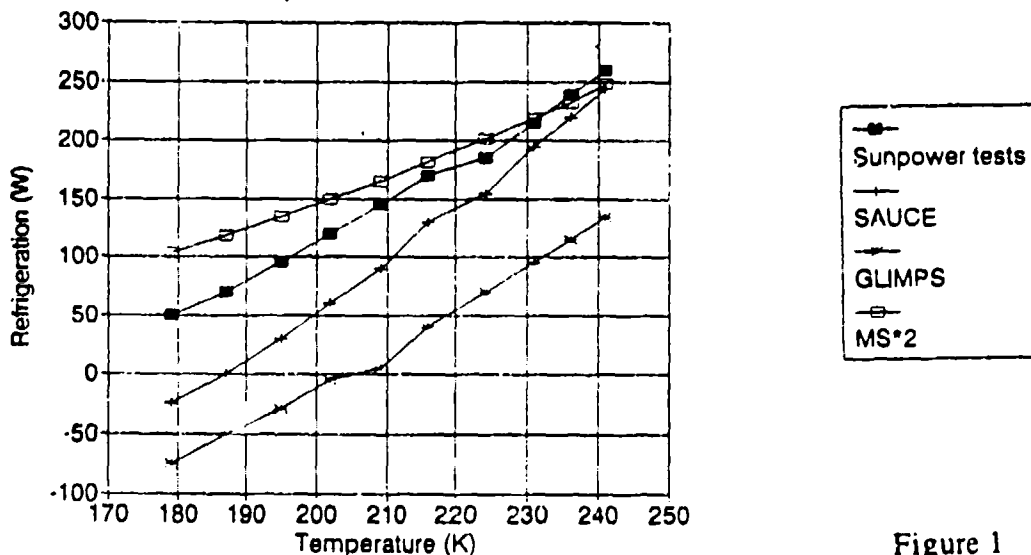


Figure 1

Figure 1 shows Sunpower's test results in terms of net refrigeration plotted against the predictions of three codes in "uncalibrated" condition. SAUCE is Sunpower's proprietary code used in designing its free-piston Stirling engines and refrigerators. GLIMPS is David Gedeon's respected Stirling cycle code. (4) The best fit appears to be the MS*2 curve.

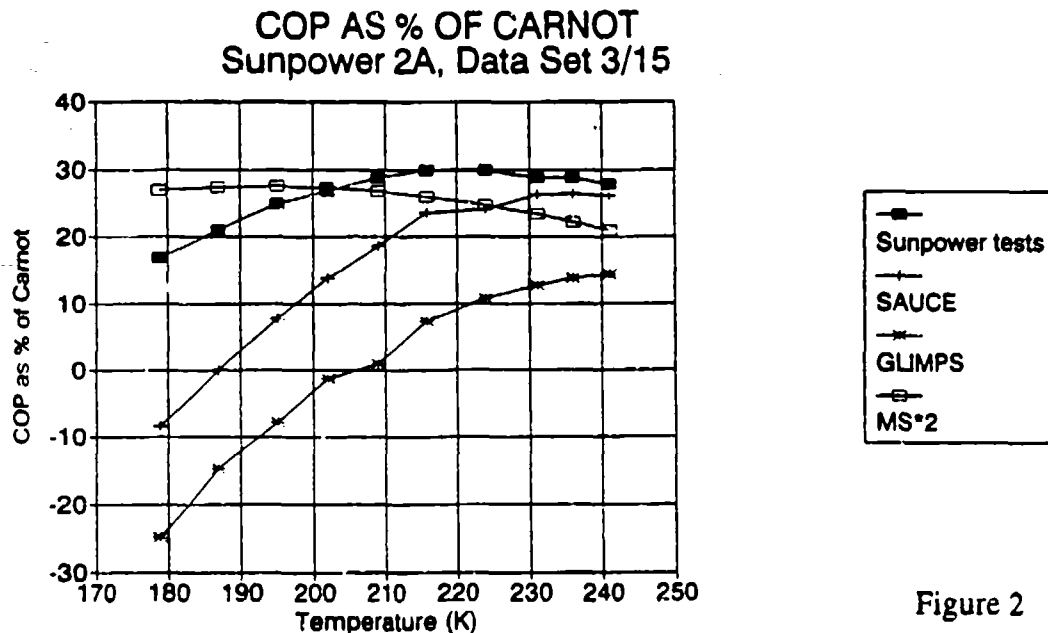


Figure 2

Figure 2 shows Sunpower's test results for COP over the same range of temperatures as shown in Figure 1. Again, the MS*2 curve fits better than either SAUCE or GLIMPS in their uncalibrated condition.

It should be noted that, once calibrated, both SAUCE and GLIMPS produced predictions that were significantly closer to the actual test results than the predictions of MS*2 (i.e. within 10% for heat lifted, PV power and % of Carnot) at the ends of the curve. However, calibration requires knowledge of the test data, which can only be obtained after a machine has been built and tested. Building and testing a machine to calibrate a code defeats a major purpose of modelling.

It seems likely that, at the lower temperatures shown in Figures 1 and 2, the strokes of both piston and displacer were shorter than at the higher temperatures. It also seems likely that the phase angle was different. Both types of changes would have reduced the refrigeration output and COP reported for the MS*2 code at those lower temperatures, improving the fit of the MS*2 curve.

CONCLUSION

While it is difficult to find test data in a form that permits exact comparison with the predictions of the MS*2 code, available data suggest that the MS*2 code, which is not "calibrated", is usefully accurate in predicting indicated performance of Stirling refrigerators in advance of their construction.

REFERENCES

1. Bauwens, L., and Mitchell, M.P., "Regenerator Analysis: Validation of the MS*2 Stirling Cycle Code". Proc. XVIIIth International Congress of Refrigeration (Montreal), 1991, Vol. III, p. 930.
2. Mitchell, M.P., Wilson, K., and Bauwens, L., "Comparative Simulation of Stirling and Sibling Cryocoolers with Two Different Codes". Proc. 24th IECEC, 1989, pp. 2205-2211.
3. Mitchell, M.P., and Bauwens, L., "Computer Simulation of Stirling and Sibling Cycle Machines". Proc. 23rd IECEC, 1988, Vol. 1, p. 59.
4. Fabien, M. J., "Evaluation of the Free Piston Stirling Cycle for Domestic Cooling Applications". Proc. XVIIIth International Congress of Refrigeration (Montreal), 1991, Vol. II, p.839.

AN INTRODUCTION TO THE LUCAS AEROSPACE
THERMODYNAMIC COMPUTER MODEL CMOD

C.S. Brice, B.Eng. (Hons), A.M.I.Mech.E.

Lucas Aerospace Limited

Engine and Electronic Systems Division

Birmingham

United Kingdom

ABSTRACT

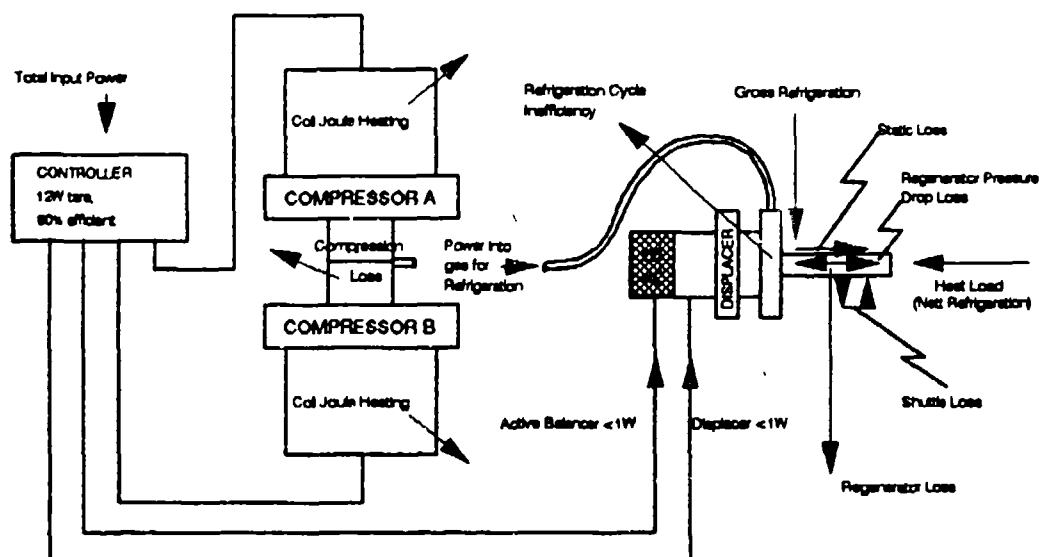
Lucas have been using and developing a combined thermodynamic, mechanical and magnetic computer model called CMOD since 1989. This model was initiated to predict of the complete range of Lucas Aerospace Cryocoolers and Configurations. CMOD is a thermodynamic model based on the Schmidt Analysis and contains empirical data from Lucas tests on both 7 and 10mm cold finger systems, as well a motor model to predict overall input powers. This paper will introduce CMOD and show how model predictions compare with test data for Lucas Cryocoolers over a range of operating conditions.

BACKGROUND

In 1988 Lucas Aerospace signed an agreement with Lockheed Missile and Space Company of Palo Alto, California. Our aim has been to jointly develop a range of low vibration mechanical Cryocoolers for a variety of Space Applications. From this a need developed to study concepts and optimise Cryocooler designs to meet an array of required parameters. CMOD has been utilised in a number of technology studies and concept designs for both European and U.S. Earth Observation and Military programmes.

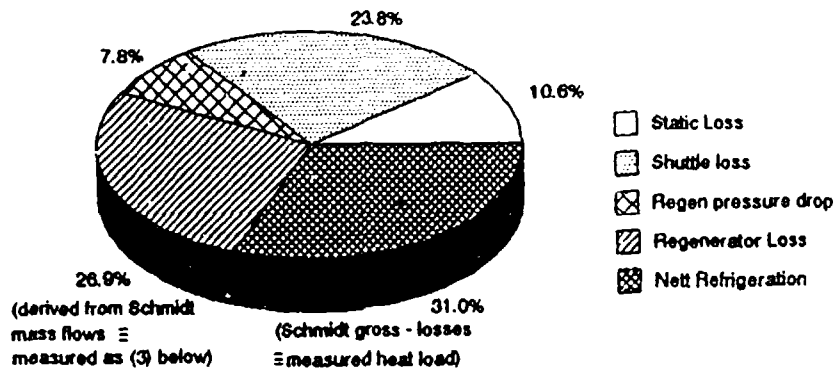
NODES OF SIMULATION

The core of the simulation is the Schmidt Analysis, a modified form of which is combined with empirical expressions for displacer losses to produce net refrigeration at various conditions. The Schmidt gross refrigeration is used to calculate pressure volume work in the compressor and when added to calculated values for Joule heating and irreversible compression loss yields total power required by the compressor.



GROSS REFRIGERATION - AN EMPIRICAL MODEL

The breakdown of gross refrigeration illustrated is typical of an 80K condition. Measured heat load on a cryocooler is represented by nett refrigeration in the model. Displacer losses are dependant on stroke, frequency and temperature and are measured with a number of empirical tests. Regenerator loss can be derived from these tests while CMOD regenerator loss depends on Schmidt mass flows and an empirically determined frequency dependance.



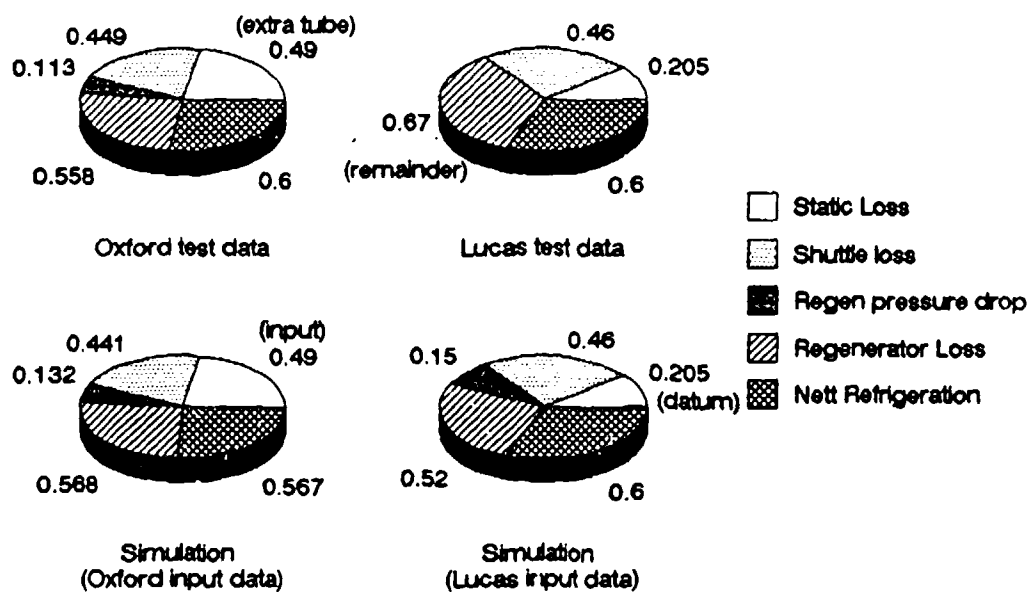
(1) Measured displacer loss =  +  + 

(2)  Shuttle loss &  Regen pressure drop measured empirically

(3)  Regenerator Loss = (1) - (2) (deduced)

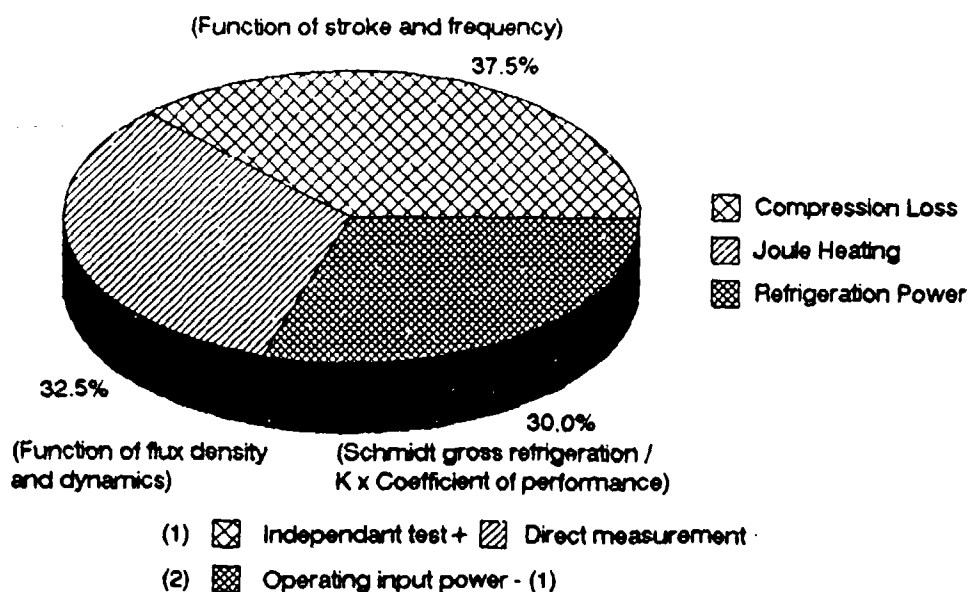
SIMULATION OF OXFORD 20/10 & LUCAS 17/7 DISPLACERS

The original CMOD simulation was a forced fit to two different cryocoolers at different conditions. The objective was to create a set of algorithms which showed a very good agreement of all the independent variables at the different conditions. This was achieved satisfactorily with two minor exceptions. Static loss on the Oxford 20/10 was much greater due to a second thin walled tube in the regenerator, and the Lucas 17/7 regenerator pressure drop measurements were so small as to be indistinguishable from experimental error.



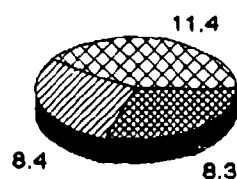
COMPRESSOR POWER - AN EMPIRICAL MODEL

Around 70% of power into a compressor results in heat due to irreversible compression loss and Joule heating in the motor coil. The remaining 30% can contribute to useful refrigeration.

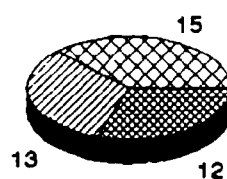


SIMULATION OF OXFORD 20/10 AND LUCAS 17/7 COMPRESSORS




A similar strategy was adopted for the compressor simulation. This gave very satisfactory agreement with the two compressors operating at two different conditions. This was achieved notwithstanding the fact that the Oxford motor had at least three times the magnet volume in a much different configuration to the Lucas compressor motor.

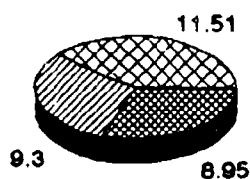
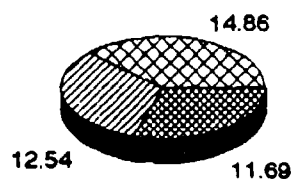


Oxford test data



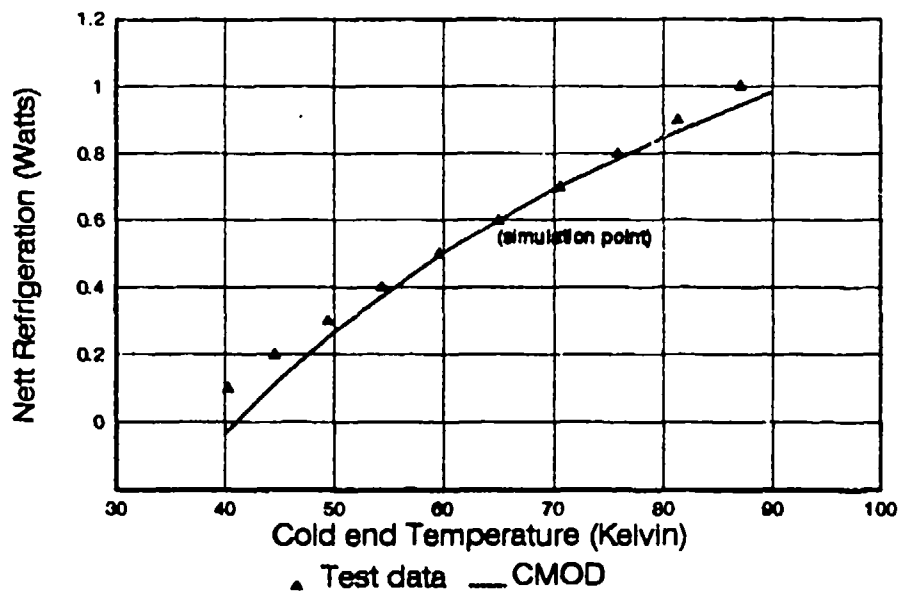
Lucas test data

 Compression Loss
 Joule Heating
 Refrigeration Power

Simulation
(Oxford input data)Simulation
(Lucas input data)

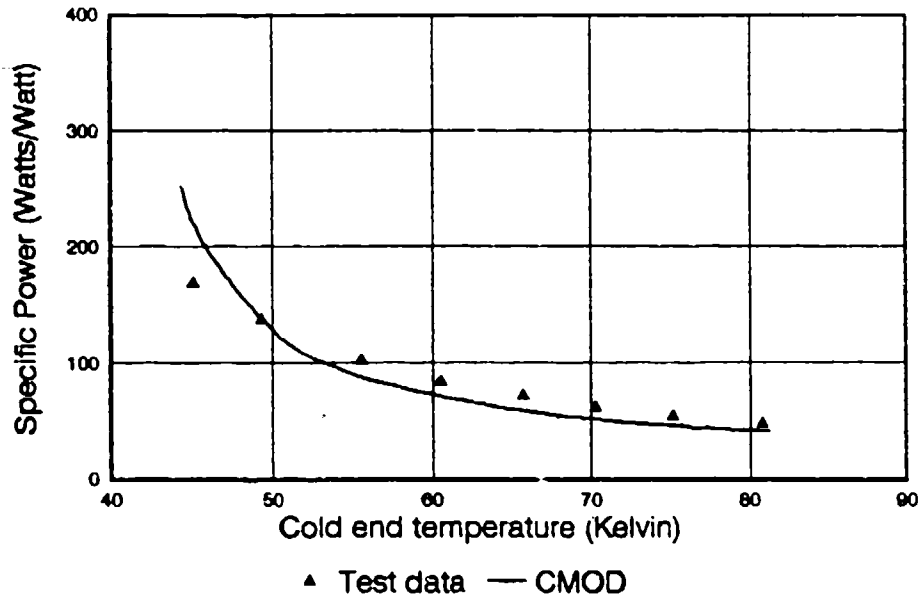
SYSTEM IV/5, (17/7), NO FORCED COOLING, FLANGE 67°C

A nett refrigeration of 0.6 watts at 65K was the point of simulation for the model. Varying the heat load on the cryocooler results in a different cold end temperature to which the model agrees very well. It can also be seen that a single 17/7 unit can easily achieve 0.8 watts at 80K although at non ideal conditions.



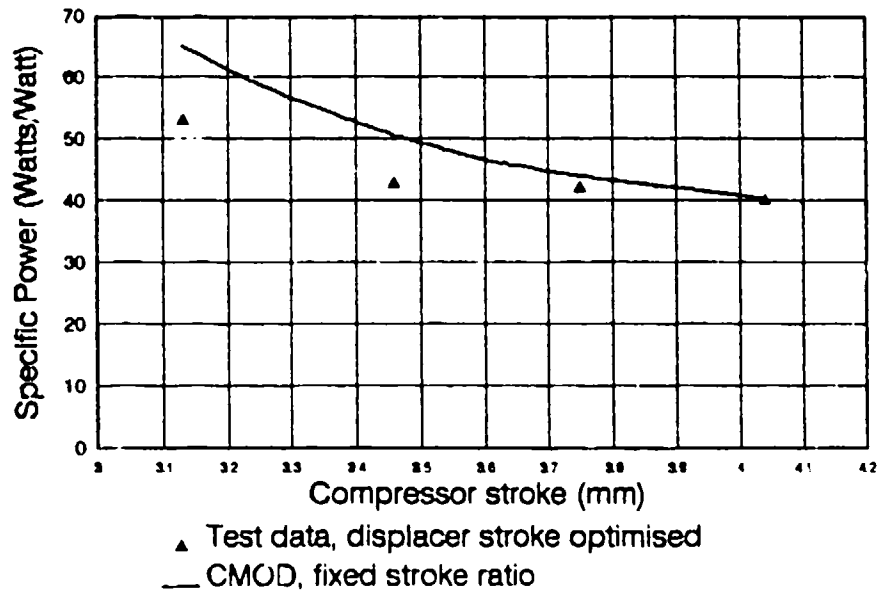
SYSTEM IV/5, (17/7), FORCED COOLED TO A LOWER FLANGE TEMPERATURE

Changing the flange temperature conditions the model shows very good agreement with test data between 50 and 80K.



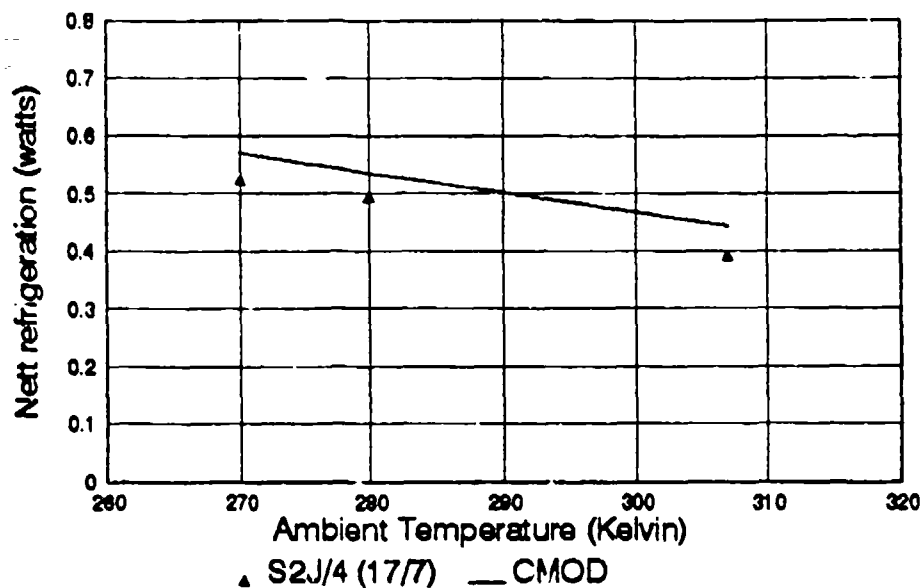
SYSTEM IV/5, (17/7), AT 80K, FLANGE FORCED COOLED TO BELOW AMBIENT

Lowering the flange temperature still further the model concurs very well with specific power at low compressor strokes.

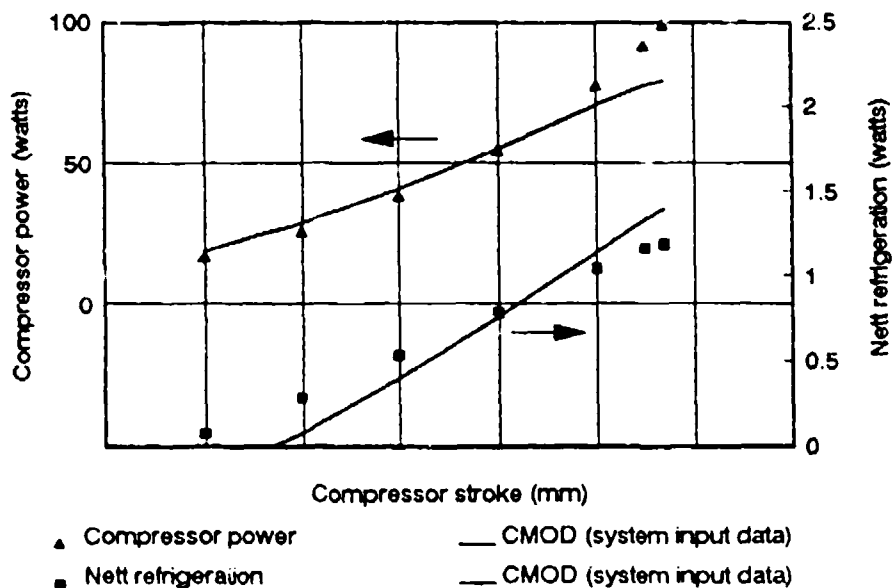


NETT REFRIGERATION VS AMBIENT TEMPERATURE

CMOD shows very good agreement with another 17/7 cryocooler. (S2J/4), over a range of flange temperatures.

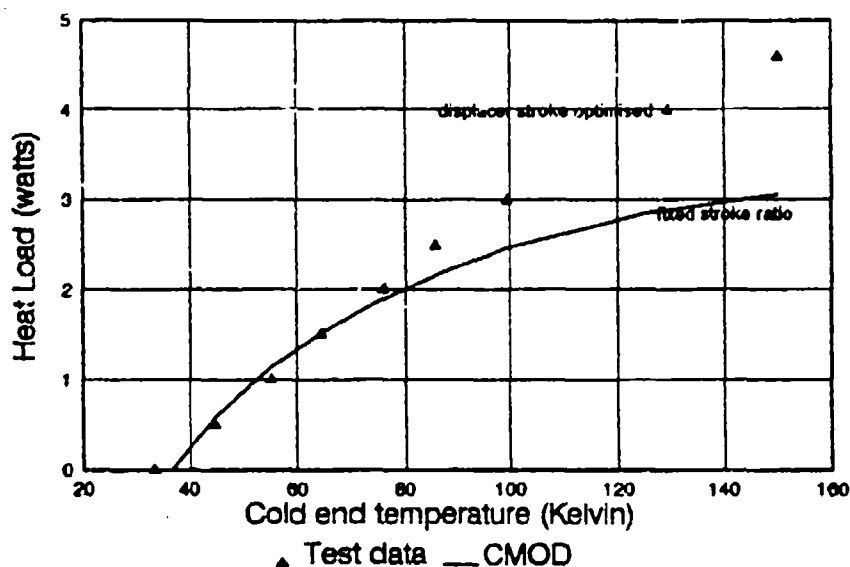
20/10 SYSTEM, COMPRESSOR STROKE VS POWER AND NETT REFRIGERATION

Up to a certain stroke the model shows very good agreement, but the power noticeably increases above this condition. We believe this is due to a gas flow limit with the resulting pressure drop reducing potential nett refrigeration.

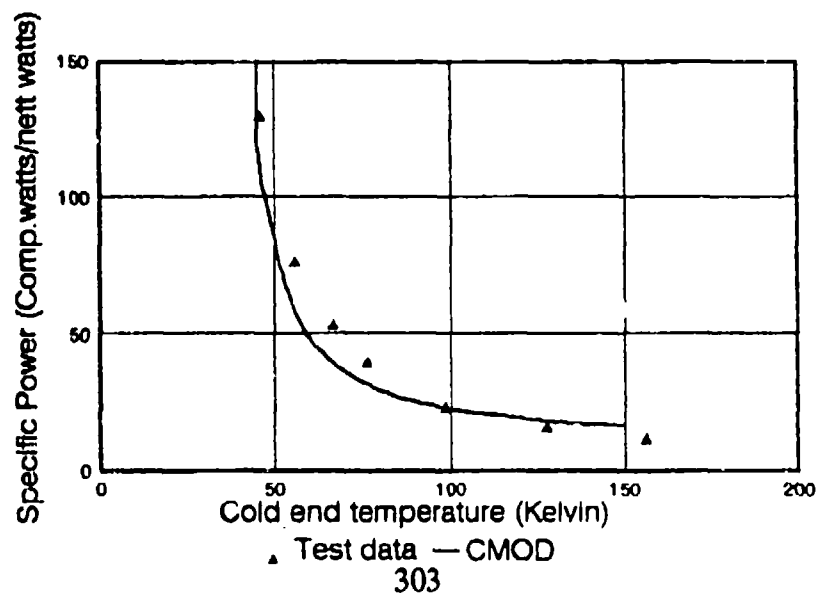


20/10 SYSTEM, NETT REFRIGERATION VS COLD END TEMPERATURE

CMOD shows very good agreement between 40 and 80K. Beyond this the test data reflects an optimised stroke ratio where CMOD was a fixed ratio. Running the model the optimised displacer stroke is in accordance with the actual test.

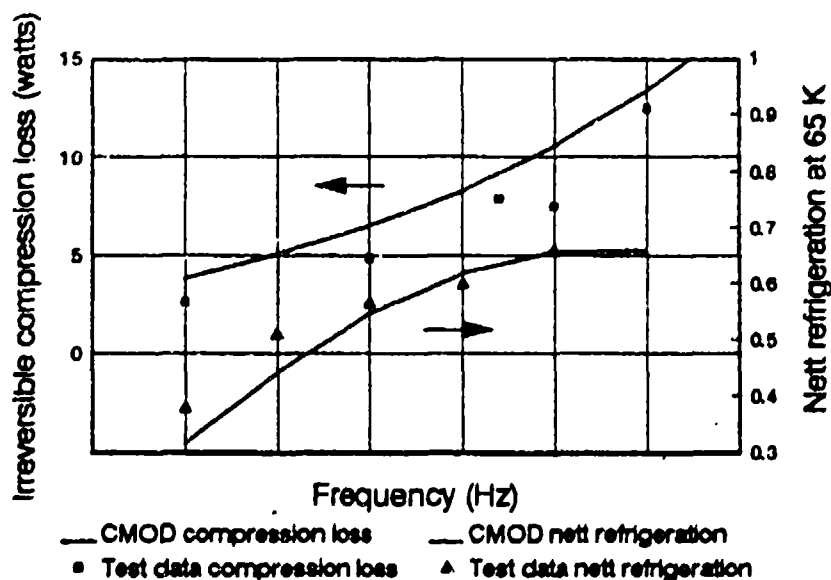
20/10 SYSTEM, SPECIFIC POWER VS COLD END TEMPERATURE

CMOD shows very good agreement of compressor power in proportion to nett refrigeration when compared to a 20/10 cryocooler.



CRYOCOOLER OPERATING FREQUENCY

All cryocooler configuration trade studies are performed at an optimum operating frequency. As the rate of growth of nett refrigeration declines with increasing frequency, predominant compressor losses further reduce efficiency. CMOD is in very good agreement with this effect.



CONCLUSION

In conclusion Lucas Aerospace has a cryocooler model which has been verified against a range of coolers over a variety of conditions. This model gives Lucas the capability and flexibility to respond rapidly to customer requirements and enquiries in the range of 50 to 150 Kelvin. CMOD is also extremely valuable in optimising to design characteristics to match the varied performance requirements of our many customers including NASA, USAF, JPL, MBB and Aerospatiale.